UNIVERSITÀ DEGLI STUDI DI SALERNO

Dipartimento di Farmacia

PhD Program

in **Drug Discovery and Development**

XXX Cycle — Academic Year 2017/2018

PhD Thesis in

Modulators of protein-protein interactions with anticancer activity

Candidate   Supervisor

Paola Galatello   Prof. *Anna Ramunno*

PhD Program Coordinator: Prof. Dr. *Gianluca Sbardella*

Preface

My PhD project in Drug Discovery and Development at the Department of Pharmacy, University of Salerno, under the supervision of Prof. Anna Ramunno, focused on the development of new inhibitors of the p53/MDM2/MDM4 interaction and new modulators of tubulin polymerization (Chapters 1-5).

During my PhD experience, I was also involved in the synthesis of dual hAK/hGSK-3β inhibitors; the results of this study have been published (Eur. J. Med. Chem, 2017, 138, 438-457), and are summarized in Chapter 6 of this thesis.

As a part of my PhD program, I spent six months (from September 2016 to February 2017), in Prof. Alexander Domling's research group (Department of Drug Design, University of Groningen, NL), working on the development of new modulators of the IL17A/IL17RA interaction. In particular, a series of new IL17A/IL17RA inhibitors was designed using the pharmacophore based virtual screening platform ANCHOR.QUERY, and synthesized employing multicomponent reactions. All compounds were evaluated by Differential Scanning Fluorimetry (DSF), and two of them were selected for further biological investigation. The results of this study have not been reported in this thesis because a patent application is in progress.

Publications

- Brogi, S.; Ramunno, A.; Savi, L.; Chemi, G.; Alfano, G.; Pecorelli, A.; Pambianchi, E.; **Galatello, P**.; Compagnoni, G.; Focher, F.; Biamonti, G.; Valacchi, G.; Butini, S.; Gemma, S.; Campiani, G.; Brindisi, M. First dual AK/GSK-3beta inhibitors endowed with antioxidant properties as multifunctional, potential neuroprotective agents. *Eur. J. Med. Chem.* **2017**, *138*, 438-457.

Conference Proceedings

- 2th-6th July 2017: *Development of small molecules inhibitors of protein-protein interactions with antiproliferative activity*. **P. Galatello**, ESMEC 2017 Urbino (PU).

- 10th-14th September: *Development of small modulators of protein-protein interactions endowed with anticancer activity*. **P. Galatello**, A. Ramunno, M. Persico, N. Orteca, C. Irace, M. Piccolo, M. Varra, C. Fattorusso, SCI 2017, Paestum (SA).

Abstract

The identification of small molecules targeting specific protein-protein interactions (PPIs) involved in the regulation of the cell cycle is a recent and promising approach for the development of new anticancer agents. Targeting PPIs has long been viewed as a very challenging task because protein-protein interfaces tend to be large and flat. However, the discovery of so-called "hot spots" supported the hypothesis that many PPIs are "druggable" by small molecules.

This PhD thesis describes the development of new modulators of the p53/MDM2/MDM4 interaction, and new microtubules targeting agents.

The p53 protein is a transcription factor with a critical role in safeguarding genome integrity by activation of cell cycle checkpoints. Many different types of cancer show a high incidence of TP53 mutations, leading to the expression of mutant p53 proteins, which can promote cancer progression both by loss of their tumor-suppressor function, or acquisition of pro-oncogenic properties. However, human cancers retaining wild-type p53 frequently show overexpression of MDM2 and/or MDM4 proteins. MDM2 and MDM4 are negative regulators of the p53 protein, and their overexpression compromise p53 transcriptional activity. Thus, in these cases, inhibition of the p53/MDM2 (and/or p53/MDM4) interaction by small molecules is a promising anticancer strategy.

Recently, biological and computational studies supported the hypothesis that a tetrasubstituted pyrrole derivative (4-benzoyl-5-methyl-1-(4-methylbenzylbenzyl)-1H-pyrrole-2 carboxylic acid 3-chlorobenzylamide, **1**) is a modulator of p53/MDM2 interaction. In this thesis, the design and synthesis of new pyrrole derivatives analogues of **1** were described. The antiproliferative activity of some of them was investigated *in vitro* on three cell lines: the A375 human melanoma cell line, the HCT-116 colon cancer cell line as well as on the HaCaT human keratinocyte cell line. Among all tested compounds, 1-(4-amino-benzyl)-4-benzoyl-5-methyl-1H-pyrrole-2-carboxylic acid 3-chloro-benzylamide was found to be the most active pyrrole derivative, with IC_{50} values in a micromolar range.

Microtubules constitute a well-validated cancer drug target because of their central role in cell division. Many microtubule targeting agents (MTAs) currently

in clinical use (e.g. taxol, vinca alkaloids) have shown several limitations (i.e. resistance, severe toxic side effects and low oral bioavailability), therefore innovative MTAs are needed.

Pyrrolo-1,5-benzoxazepine (PBOX) compounds have been reported as tubulin-targeting agents. In particular, PBOX-6 (namely 7-[(dimethylcarbamoyl) oxy]-6-(2-naphthyl)pyrrolo-[2,1-*d*][1,5]benzoxazepine potently induces apoptotic cell death in a variety of human cancer cell lines, indicating its potential in the treatment of both solid tumors and tumors derived from the hematopoietic system. However, recent studies revealed PBOX resistance, mainly related to autophagy induction. In this project, PBOX-6 was chosen as a starting point for chemical modifications in order to improve its pharmacological profile and extend SAR analysis of this class of compounds. A small set of PBOX-6 analogues was generated by introducing substituents with different lipophilic, steric and electronic properties on the benzo-fused ring of our lead. Furthermore, their ability to affect the cell cycle and induce apoptosis on the HL60 (human promyelocytic leukemia) cell line was determined by flow cytometric analysis.

TABLE OF CONTENTS

Chapter 1
Introduction

Hot Spot Identification

Small Molecule Inhibitors

Protein- Protein Interaction

1.1 Protein-protein interactions (PPIs) as drug target

Pivotal processes in living cells such as intracellular signal transduction, maintenance of cytoskeletal architecture, cell recognition and transcription process, are largely controlled by proteins, sometimes alone, but more often in concert with protein partners in a large complex network [1].

It has been estimated that there are approximatively 650,000 significant protein-protein interactions (PPIs) in the cell [1]. Understanding the dynamics related to these networks and their perturbations if a mutation occurs in a given protein of them, is a big challenge in chemical biology, with practical implications for the discovery of new drugs and biological probes.

In particular, targeting aberrant PPIs with small molecules can offer new opportunities for the treatment of complex diseases such as cancer [2].

The druggability of a specific PPI has long been considered very difficult if not impossible because of the generally large and noncontiguous nature of PPI surfaces [3-5]. It has to be noted that the binding sites available at protein-protein interfaces to bind small molecules are different from those seen in traditional drug target proteins (e.g. enzymes, receptors) [6-8]. In fact, the latter have one or two binding sites for their endogenous ligands with an average volume of 260 Å^3, while PPIs typically occur over a relatively large contact surfaces (1500-3000 Å^2), that tend to be relatively flat and may lack binding sites for small molecules [7-9].

However, for a molecule targeting a specific PPIs through competitive binding it is not necessary to cover the entire protein-protein interface. In this regard, it must be emphasized that only few point mutations of interfacial residues have destabilizing effects and severely disrupt protein-protein interactions [10-12].

Residues whose mutation has destabilizing effects are called "*hot spot*" residues (Figure 1.1). Alanine scanning technique has been one of the most frequently used approaches to identify hot spot residues, leading to a definition of a hot spot as '*a residue that, when mutated to alanine, gives a distinct drop in the binding constant, typically ten-fold or higher*' [13, 14].

Hot spot residues can be identified also by phage display technology, yeast two-hybrid system, ubiquitin-based split-protein sensor, protein microarrays, Fluorescence Resonance Energy Transfer (FRET) microscopy and mass

spectrometry-based methods (i.e. Hydrogen/Deuterium Exchange Mass Spectrometry, DXMS) [15-20].

   More recently, many computational approaches also proved to be accurate in predictions of hot spot residues, with the advantage to be less costly and time consuming compared to experimental methods [21, 22].
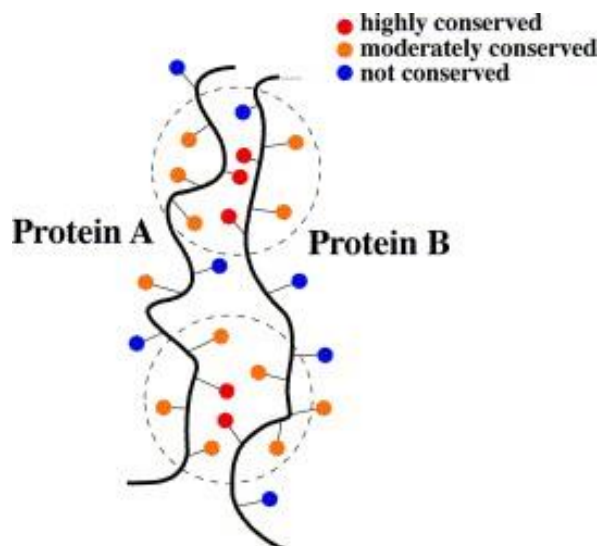
Figure 1.1 *Hot spot residues [23]*

   In general, hot-spot residues act as binding site anchors, and stabilize the protein-protein complex contributing in more than 1 or 2 kcal/mol to its total binding energy [21]. Of consequence, the highly conserved hot spot residues directly involved in inappropriate PPIs can be the target for drug design of specific inhibitors. In these cases, a small molecule endowed with chemical and structural features correctly mimicking the topography and nature of the side chains of hot spots residues of one specific protein, can be competitive in the binding of the protein partner.

Noteworthy, such hot spots tend to be clustered in densely packed regions at the center of small to medium size binding interfaces; however, in larger protein-protein interfaces, they can be more distributed and distanciated along the binding interface, and in general show a more complex combination of chemical functions. Then, in these cases, it can be a very difficult challenge to find a molecule interfering with all of them [23, 24].

The most frequent hot-spot residues include Tyr, Arg and Trp, which share the ability to form multiple interactions [24-29]. They are often surrounded by a set of residues forming a hydrophobic O-ring responsible to occlude hot spots from water molecules. Trp can give aromatic π-interactions and act as H-bond donor; further, it has a large hydrophobic surface, and can protect hydrogen bonds from water. Trp mutation to Ala generates a large cavity and produces a strong destabilizing effect [25]. Tyr has a 4-OH-phenyl group in side chain and can establish both aromatic-π interactions and H-bonds. Arg is able to form H-bonds and a salt-bridge with its positive charged guanidinium motif. Moreover, the electron delocalization of the guanidinium π-system has a pseudo-aromatic character [25]. Leu, Ser, Thr, and Val residues are disfavored and essentially absent as hot spot residues; Asp and Asn are favored over Glu and Gln, probably due to differences in side-chain conformational entropy [25].

Interestingly, the same hot-spot residues can be arranged in different conformations and adapted in different structural contexts [30, 31]. This high functional and structural adaptivity justifies how a given protein molecule, employing the same crucial recognition elements, may bind to different protein interaction partners.

1.2   The cell cycle: an overview

The cell cycle is a complex process by which a parent cell divides into two genetically identical daughter cells. It is composed of two processes: *interphase* and *mitosis* [32, 33].

During *interphase* the cell grows and ultimately DNA replication occurs. Within the human cell cycle, it generally needs at least 12 to 20 hours to complete and includes three sub-phases: Gap 1 (G_1), Synthesis (S) and Gap 2 (G_2) (Figure 1.2).

During G_1, the cell grows, copies organelles, makes the molecular building blocks it will need in later steps (including the building blocks of chromosomal DNA and associated proteins). At the end of this phase there is the first checkpoint (G_1/S checkpoint): the cell checks whether all conditions (e.g. nutrients, enzymes, DNA integrity etc.) are optimal to support DNA replication before entry into S phase [32].

If intracellular and extracellular conditions are favorable for a successful cell division, the cell, stimulated by appropriate external growth factors, passes the G_1 checkpoint and enters the next phase of interphase called S phase [34].

G_1/S checkpoint is particularly important to provide cell with time to repair damaged DNA. However, if the DNA cannot be repaired cell undergoes apoptosis or may initiate senescence (growth arrest) [35].

In some cases, the cell may leave the cell cycle and enters in a quiescent or resting phase called G_0. Some cells (that have reach the end stage of development and will no longer divide) stay permanently in G_0 (e.g. human neurons). In other cases, cells stay in G_0 phase for days, weeks, or even years, and can resume dividing only in response to appropriate stimuli and in presence of favorable conditions [34, 35].
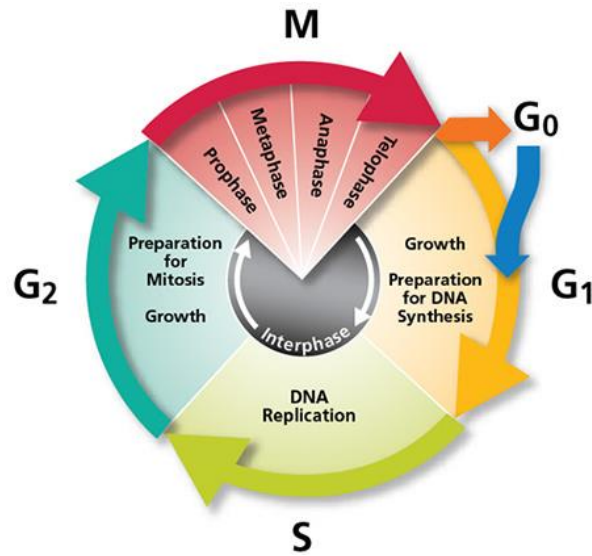
Figure 1.2 *Phases of the cell cycle*

In the S phase, chromosomes are replicated, resulting in the formation of identical pairs of DNA molecules (*sister chromatids*), that are attached to each other at a specific region called *centromere* (Figure 1.3) [36].

In this phase also a microtubule-organizing structure, called *centrosome*, is duplicated. Cell growth continues through S phase, as does the rate of synthesis of a number of proteins and enzymes that are involved in DNA synthesis.
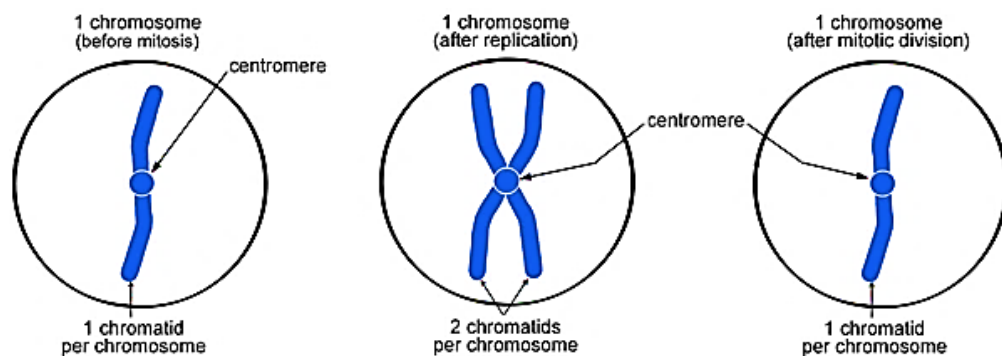
Figure 1.3 *The two chromatids of a duplicated chromosome are held together at a region of DNA called the centromere.*

An intra-S phase checkpoint takes place to control if DNA is properly replicated during this critical phase, in which many types of errors and lesions can occur spontaneously or in response to diverse genotoxic stresses (i.e. ROS, chemicals, UV or IR radiation).

If DNA damage occurs and is excessive to be repaired, the cell cycle will exit S phase and arrest later when reaching the next checkpoint [36].

Once DNA replication is complete, the cell contains twice its normal number of chromosomes and becomes ready to enter the phase called G_2 [37].

G_2 phase is a period of rapid cell growth and protein synthesis, during which the cell reorganizes its contents in preparation for mitosis, and ascertains (G_2/M checkpoint) if the DNA has been faithfully replicated [38].

Interphase is followed by the *mitotic phase* (or M phase), which last approximately 1-2 hours, and includes *mitosis* and *cytokinesis* [33, 34].

Mitosis (also called *karyokinesis*) is the process of chromosome segregation and nuclear division. This process assures that each daughter nucleus receives a complete copy of the organism's genome.

Mitosis is divided into several stages: *prophase*, *prometaphase*, *metaphase*, *anaphase*, and *telophase* (Figure 1.4) [32].
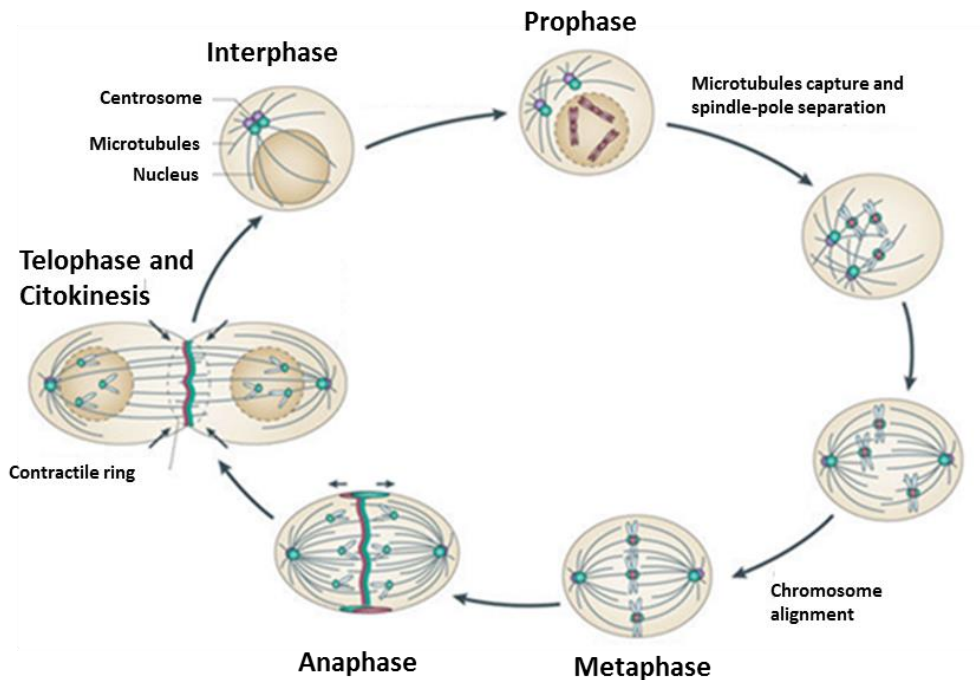
Figure 1.4 *Stages of mitosis.*

During *prophase*, chromatin is compacted into visible chromosomes; each chromosome (that was duplicated during S-phase) consists of two genetically

identical sister chromatids attached at centromere, and appears as X-shaped structure when viewed under a microscope (Figure 1.3).

During this phase, the cytoskeleton reorganizes to form the mitotic spindle. In particular, two centrioles, mainly composed of tubulin, serve as a type of anchor, and begin recruiting microtubules to form a mitotic spindle between them.

By recruiting more microtubules, therefore increasing the length of the spindle, the centrioles push apart to opposite ends of the cell nucleus (Figure 1.4) [33].

Following completion of prophase, the cell enters *prometaphase*: the nuclear membrane breaks down into small vesicles, and the microtubules of the mitotic spindle enter the nuclear region.

Some microtubules attach to the *kinetochore*, a specialized region composed of a number of protein complexes located on the centromeres of chromosomes (Figure 1.5).
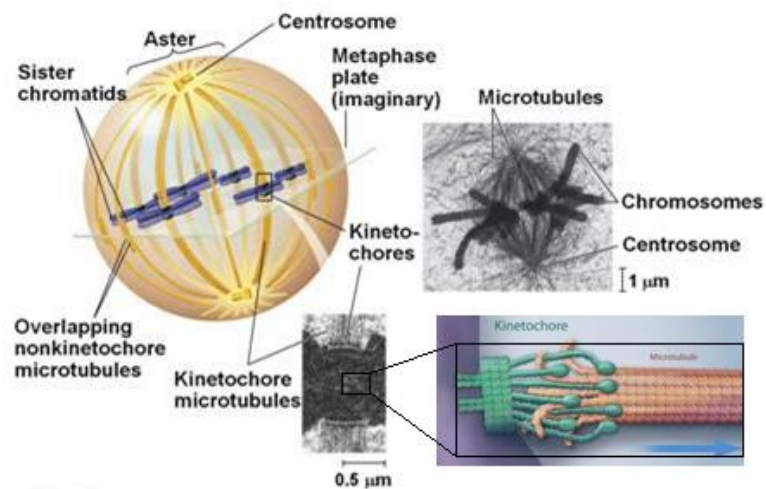
Figure 1.5 *Kinetochore's structure and function.*

Then, kinetochore fibers and microtubules work together to separate chromosomes during cell division [39, 40].

In particular, the kinetochores of sister chromatids are oriented on opposite sites of the chromosome, and then attach to microtubules emanating from opposite poles of the spindle. The chromosomes shuffle back and forth, and at the end of prometaphase move toward the center of the cell. Microtubule structure allows

them to be dynamic molecules: the α,β-tubulin heterodimers (the basic building blocks of microtubules) are constantly added to one end and removed from the opposite end of microtubules leading to a state of head-to-tail polymerization or *"treadmilling"* [40, 41]. In addition, microtubules interact with motor proteins and non-motor proteins; thus, there is also a complex network of PPIs to properly drive chromosomes movements on the spindle.

Metaphase is marked by the alignment of chromosomes at the center of the cell; at this point, they no longer move back and forth. It is thought that unattached kinetochores control this process by generating a signal, referred to as the mitotic spindle checkpoint (or M-checkpoint), that delays anaphase onset until all sister chromatids are correctly attached to the mitotic spindle [42].

During *anaphase* sister chromatids separate from each other and move to opposite poles of the spindle; upon separation, every chromatid becomes an independent chromosome. This phase is relatively short (usually only lasting a few minutes), and leads to *telophase*, that is marked by the reforming of the nuclear envelope around each group of chromosomes. Then two nuclei are present in the same cell, and the chromosomes are unfolded to form the chromatin.

Following the exit from telophase, the cell undergoes *cytokinesis* that finally splits the parent cell into two identical daughter cells. After the completion of the cytokinesis, each daughter cell enters the interphase of the cell cycle [32, 33].

1.3 Cell cycle regulation

Cell cycle progression is strictly monitored to ensure the order, integrity, and fidelity of the major events of the cell cycle, and then is of utmost importance to prevent growth abnormalities and cancer development [43, 44].

The control of each stage of the cell cycle is accomplished by a family of serine/threonine protein kinases called *cyclin dependent kinases* (CDKs) [44, 45]. These enzymes phosphorylate key substrates to promote DNA synthesis and mitotic progression. CDKs themselves are activated by forming complexes with cyclins, another group of regulatory proteins (Figure 1.7) [44, 45].

Cyclins undergo a constant cycle of synthesis and degradation and are present only for short periods during cell division; on the contrary, CDK protein levels

remain stable during the cell cycle. In addition to cyclin binding, CDK activity is also regulated by phosphorylation on conserved threonine and tyrosine residues; this phosphorylation induces conformational changes and enhances the binding of cyclins.

When cyclin degrades, deactivation of CDK occurs. However, CDK activity can also be negatively regulated by the binding of small inhibitory proteins, the CKIs, which bind to CDK alone or to the CDK-cyclin complex [44, 45].

Two distinct families of CDK inhibitors have been identified so far in mammalian cells: the INK4 family, that includes $p15^{INK4b}$, $p16^{INK4a}$, $p18^{INK4c}$ and $p19^{INK4d}$ and the CIP/KIP family that is made up of three proteins: $p21^{cip1 / waf1}$, $p27^{kip1}$ and $p57^{kip2}$ [44-52].

The members of the INK4 family form stable complexes with the CDK4/6 enzymes before cyclin binding, preventing association with cyclin D, while the members of the CIP/KIP family inhibit cyclin E/A-CDK2 complexes, and to a lesser extent, CDK1-cyclin B complex (Figure 1.6) [44].

CKIs are regulated both by internal and external signals. For example, the expression and activation of, respectively, p15 and p27, increase in response to transforming growth factor β (TGF–β), while the expression of p21 is under transcriptional control of the p53 tumour suppressor gene [44].
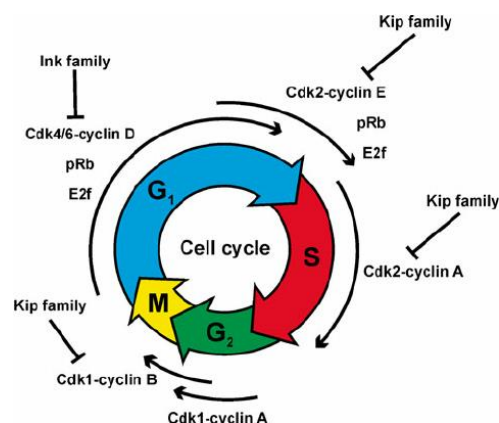

Figure 1.6 *Cyclins and CDKs involved in cell cycle (adapted from [51])*

CDK-cyclin complexes regulate cell cycle progression by phosphorylation of their targets. For example, CDK4/6-cyclin D phosphorylates the retinoblastoma protein (pRb) (Figure 1.7). Retinoblastoma is a sporadic or hereditary retinal

tumor caused by the mutation of a suppressor gene known as Rb expressing a mutated dysfunctional protein (pRb), that has also been reported in other cancers (bladder, breast and lung cancer) [34, 53, 54].

The main function of pRb is the inhibition of the cell cycle at the restriction point at the end of G1 phase, temporarily preventing the cells progression into the S phase.

pRb promotes the cell cycle when it is phosphorylated while, when it is dephosphorylated, inhibits it. Phosphorylation is catalyzed at the end of G1 phase by a CDK2/4/6/cyclin D complex; the phosphorylated form of pRb releases a transcription factor known as E2F, which positively regulate the transcription of genes allowing the cell to progress from the G1 phase into the S phase of the cell cycle (Figure 1.4) [34, 53]. Other CDK substrates include: NPAT (nuclear protein mapped to the ATM locus), histone H1, DNA polymerase alpha primase, Wee1 and Cdc25 as well as nuclear lamins, microtubules and vimentin, which are required for correct mitosis [44].
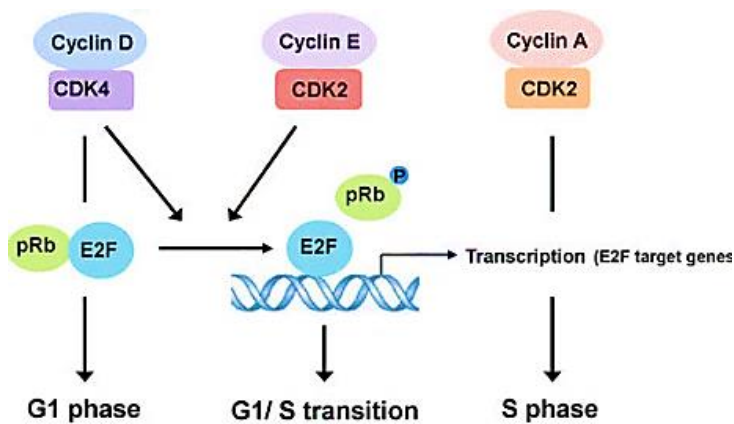
Figure 1.7 *Schematic drawing of activation of E2F by CDK-cyclin complexes (from ref [52])*

1.4 Cell cycle analysis

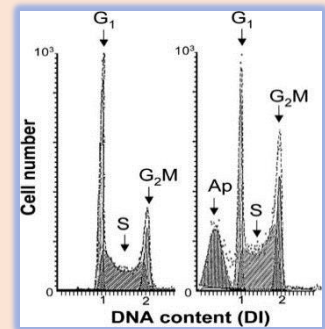Assessing cell cycle distribution and cell proliferation is important for evaluating therapeutic efficacy of anticancer drugs. In general, analysis of the cell cycle requires identification of cells at the different stages of the cycle (G_1, S, and G_2) by biochemical criteria. Cells in S phase can be readily identified by autoradiography because they incorporate radioactive thymidine, which is used

exclusively for DNA synthesis [33, 50, 51]. Alternatively, bromodeoxyuridine (BrdU) can be used; it is a thymidine analogue, specifically incorporated into DNA during the S-phase of the cell cycle, and can be detected using anti-BrdU antibodies. Cells at different stages of the cell cycle can also be distinguished by their DNA content, using a general DNA intercalating fluorescent dye that binds to DNA stoichiometrically (for example propidium iodide (PI), 7-aminoactinomycin-D (7-AAD), Hoechst 33342, 33258 and S769121, TO-PRO-3, 4'6'-diamidino-2-phenylindole (DAPI), DRAQ5™ and DRAQ7™) [55-63] (Figure 1.8, Box-1).

BOX-1

Experimentally, a population of cells is labeled with a fluorescent dye that binds to DNA; in most cases, cells must be permeabilized (most often by detergent or hypotonic treatment or by solvents (e.g. ethanol) to allow entry of the dye which is otherwise actively pumped out by living cells. The cells are then passed through a flow cytometer, which measures the fluorescence intensity of individual cells. The data are plotted as cell number versus fluorescence intensity, which is proportional to DNA content (Figure 1.8). Cells in G_0/G_1 phase are diploid (2N), while cells in G_2 and M are tetraploid (4N). The amount of DNA increases from 2N to 4N during S phase, and decreases to 2N after cytokinesis. The DNA content

Figure 1.8 *Determination of DNA content (from ref. [64])*

measured by flow cytometry is defined as DNA index (DI); for normal cells in G_0/G_1 phase, DI is 1.0, whereas cells in G2/M phase have DI= 2.0 and cells in S-phase are characterized by $1.0 < DI < 2.0$. In Figure 1.8 is also reported the "sub-G_1" peak referred to apoptotic cells, which are characterized by fractional DNA content (DI < 1.0) [64]. Other flow-cytometry-based approaches have been reported enabling to distinguish resting/quiescent cells (G_0) from G_1 phase cells, identify mitotic cells, or relate expression of intracellular proteins to the cell cycle position [58].

1.5 Apoptosis: an overview

Apoptosis, also known as *programmed cell death*, is a homeostatic mechanism to maintain cell populations in tissues as well as a response to cell stress [65]. The mechanisms of apoptosis are highly complex, however two major pathways can be distinguished: the *extrinsic* and the *intrinsic* pathway, which lead to caspases activation (Figure 1.9). Caspases are cysteine proteases and cleave proteins at aspartic acid residues; they exist as latent precursors (or procaspases), and once

activated, can activate other caspases, amplifying the apoptotic signaling pathway [65]. Then a rapid cell death occurs as a consequence of the degradation of key cellular components (DNA, proteins, cytoskeletal etc.) and activation of a number of factors that damage the cells. Caspases are commonly distinguished into three groups: *initiator caspases* (caspase-2,-8,-9,-10), *effector or executioner caspases* (caspase-3,-6,-7), and *inflammatory caspases* (caspase-1,-4,-5) [65, 66].

The *extrinsic* pathway involves death receptors (DR) and their corresponding ligands (Figure 1.9). Death receptors are members of the tumor necrosis factor (TNF) receptor gene superfamily and some of them have been well characterized including:

- FASR (also known as CD95 and APO1)
- TRAILR1, (Tumour necrosis factor (TNF)-Related Apoptosis-Inducing Ligand Receptor 1, also known as DR4 and TNFRSF10A)
- TRAILR2 (also known as DR5, TNFRSF10B and KILLER)
- TNFR1 (TNF receptor 1, also known as TNFRSF1A)
- DR3 (also know as APO-3, SWL-1 and TRAMP)

whose ligands are FASL, APO2L, APO2L, TNF-α and APO3L respectively [68].

In all cases, a death receptor ligand promotes oligomerization of its own receptor, which in turn promotes the recruitment of specialized adaptor proteins and activation of caspase cascades.

For example, binding of FASL to FASR, induces FASR trimerization, followed by binding of the adaptor protein FADD and activation of caspase-8, which in turn activates caspase-3 [65-68].

In particular, death receptor FASR has an intracytoplasmic death domain (DD) through which interacts with the DD of FADD.
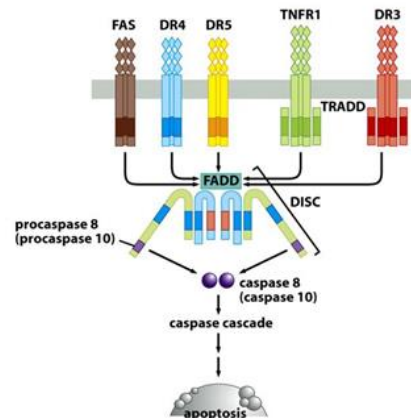
This latter has also another domain called the death effector domain (DED) which allows it to bind the DED domain of procaspase-8.
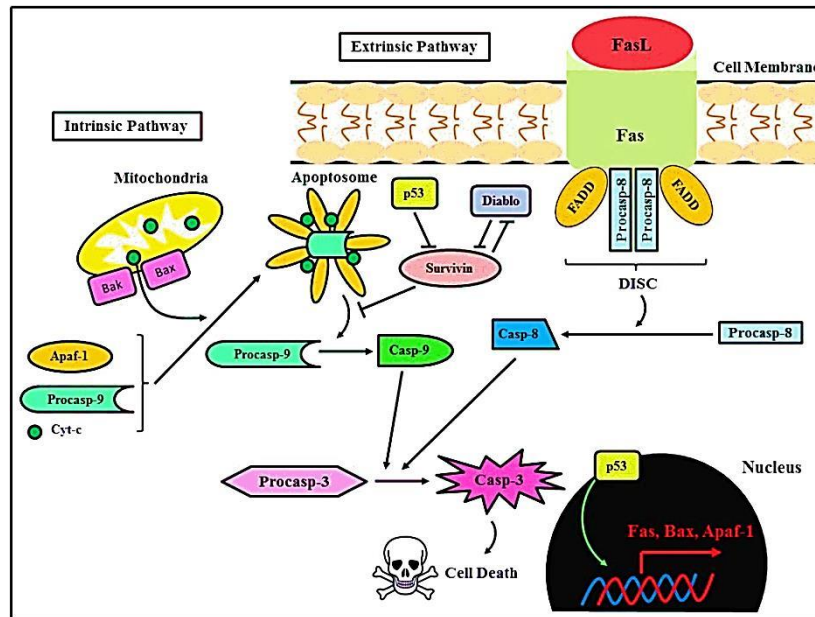
Figure 1.9 *Extrinsic and intrinsic apoptosis pathways (from ref. [67])*

The resulting complex is termed the *death-inducing signaling complex* (DISC) [68-70] (Figure 1.10).

Figure 1.9 *Death receptors (from ref. [70])*

The *intrinsic* signaling pathway is characterized by mitochondrial release of pro-apoptotic proteins into the cytoplasm, and is promoted by various pro-apoptotic stimuli (e.g. radiation, ROS, toxins, hypoxia, hyperthermia, viral infections) as well as in the absence of anti-apoptotic factors (i.e. certain growth factors, hormones and cytokines) [65].

Mitochondrial pro-apoptotic proteins include: cytochrome *c*, Smac/DIABLO, HtrA2/Om, AIF, endonuclease G and CAD.

Once in the cytoplasm, *cytochrome c* activates a caspase-dependent apoptosis with the recruitment of Apaf-1 (protease-activating factor 1) and procaspase-9 to form the so-called *apoptosome*, which in turn activates effector caspases, that induce cell death by proteolytic cleavage of downstream target proteins.

Smac/DIABLO and HtrA2/Omi are reported to promote apoptosis by inhibiting IAPs (inhibitors of apoptosis proteins) activity. Eight IAP family members have been found in humans including XIAP, cIAP1, cIAP2, NAIP, survivin, BRUCE (Apollon), ILP2 and ML-IAP. All of them have one or more BIR domains, and most of them have also a RING domain that allows them to act as E3 ubiquitin ligases. XIAP is the most potent caspase inhibitor in the IAP family; it inhibits caspases- 3, -7 and -9, directly binding target proteins by its BIR domain, and is overexpressed in many cancers [71].

AIF, endonuclease G and CAD, once released into the cytoplasm, translocate to the nucleus where cause DNA fragmentation. AIF and endonuclease G function in a caspase-independent manner, while CAD needs to be activated by caspase-3 [65].

The control and regulation of the intrinsic apoptotic pathway occur through members of the Bcl-2 family which can be either anti apoptotic (i.e. BCL-2, BCL-XL, BCL-W, A1 and MCL-1) or pro-apoptotic (i.e. BAX, BAK, BID, BIM, BAD, BIK, BMF, HRK, NOXA and PUMA) [72].

It is thought that the main mechanism of action of the Bcl-2 family proteins is the regulation of *cytochrome c* release from the mitochondria via alteration of mitochondrial outer membrane permeability (MOMP).

BAX and BAK are "*effector proteins*": they can be activated by BID and BIM (classified as "*direct activators*") as well as by non-protein factors (e.g., mild heat, detergents, and high pH); once activated, they homo-oligomerize into proteolipid pores within the outer mitochondrial membrane and promote MOMP [72].

All other pro-apoptotic members (BAD, BIK, BMF etc) can act either as "*sensitizers*" or "*derepressors*"; further, they function predominantly by binding

to the anti-apoptotic Bcl-2 family members (and not by directly activating BAK or BAX) [72].

The extrinsic and intrinsic pathways cross-talk through caspase-8 cleavage: in fact, caspase-8 (activated by the extrinsic apoptotic pathway) cleaves BID to give truncated BID (tBID), which in turn triggers MOMP [65, 72].

Finally, cell death can still occur even when the caspase cascade is blocked, providing evidence for a *caspase-independent cell death pathway* (CICD) [71-75]. AIF (*A*poptosis-*I*nducing *F*actor) is the most important caspase-independent death effector [73].

This factor is transcribed and translated in a 67 kDa precursor protein, then is imported into mitochondria, where is processed to a mature form of 62 kDa by a mitochondrial endopeptidase. Upon an apoptotic insult, cysteine proteases such as calpains (cytosolic and/or mitochondrial) and cathepsins cleave AIF, yielding the truncated form of the protein, tAIF (57 kDa). Moreover, different proteins, such as BAX and BID, regulate tAIF release through the formation of the outer mitochondrial membrane pores. AIF is then released from mitochondria to the cytosol where interacts with different targets (e.g. iFE3g); further, it can translocate to the nucleus, where it promotes chromatolysis [73-75].

Other factors involved in CICD include:

- EndoG, a sequence-unspecific DNase, which upon apoptotic stimuli translocates from mitochondria to nucleus, where extensively degrades nuclear DNA into oligonucleosomal fragments;
- Omi/HtrA2, a mitochondrial protein which partecipates not only in the caspase-dependent pathway (through interaction with IAPs), but also in the CICD via its serine protease activity [73-75].

Moreover, several studies have shown that death receptor activation can also trigger a form of CICD termed *necroptosis*. In particular, it has been reported that when caspase activity is blocked, activation of death receptor TNFR1 can drive necroptosis through the upregulation of PLA2 which, in turn, increases ROS production. On the other hand, FASL can induce FASR trimerization, followed by binding of the adaptor proteins FADD and RIP-1 (*R*eceptor-*I*nteracting *P*rotein-1).

RIP-1 is a kinase and can induce necroptosis probably by directly acting upon mitochondrial function or, perhaps, by affecting autophagy [74, 75].

An additional apoptotic pathway is the perforin/granzyme pathway that is used by cytotoxic T lymphocytes (CTLs) and natural killer (NK) cells to eliminate harmful target cells [65, 76, 77].

CTLs and NK cells induce apoptosis in their targets through the concerted action of effector molecules contained in their cytolytic granules (i.e. granzyme B, granzyme A, perforin). Perforin is a pore-forming protein, whereas granzyme A and granzyme B are serine proteases. Although granzymes can get access to target cells independent of perforin, their delivery to the cytosol and/or nucleus, is strictly dependent on this protein [65, 76]. In the cytoplasm granzyme B activates pro-apoptotic BID and cleaves the anti-apoptotic MCL-1 [77]. Furthermore, it can activate caspase 3 either directly or indirectly (through activation of caspase 8). On the contrary, granzyme A activates caspase independent pathway, cleaving the SET complex, which normally inhibits the cancer suppressor gene NM23-H1 and is involved in maintenance of chromatin integrity [65].

References

[1] Stumpf, M. P.; Thorne, T.; de Silva, E.; Stewart, R.; An, H. J.; Lappe, M.; Wiuf, C. Estimating the size of the human interactome. *Proc. Natl. Acad. Sci. U. S. A.* **2008**, *105* (19), 6959-64.

[2] Yin, H.; Hamilton, A. D. Strategies for targeting protein-protein interactions with synthetic agents. *Angew. Chem. Int. Ed. Engl.* **2005**, *44* (27), 4130-63.

[3] Wanner, J.; Fry, D. C.; Peng, Z.; Roberts, J. Druggability assessment of protein-protein interfaces. *Future Med. Chem.* **2011**, *3* (16), 2021-38.

[4] London, N.; Raveh, B.; Schueler-Furman, O. Druggable protein-protein interactions-from hot spots to hot segments. *Curr. Opin. Chem. Biol.* **2013**, *17* (6), 952-9.

[5] Jubb, H.; Blundell, T. L.; Ascher, D. B. Flexibility and small pockets at protein-protein interfaces: New insights into druggability. *Prog. Biophys. Mol. Biol.* **2015**, *119* (1), 2-9.

[6] Fauman, E. B.; Rai, B. K.; Huang, E. S. Structure-based druggability assessment-identifying suitable targets for small molecule therapeutics. *Curr. Opin. Chem. Biol.* **2011**, *15* (4), 463-8.

[7] Che, Y.; Brooks, B. R.; Marshall, G. R. Development of small molecules designed to modulate protein-protein interactions. *J. Comput. Aided Mol. Des*. **2006**, *20* (2), 109-30.

[8] Smith, M. C.; Gestwicki, J. E. Features of protein-protein interactions that translate into potent inhibitors: topology, surface area and affinity. *Expert Rev. Mol. Med.* **2012**, *14*, e16.

[9] Guo, W.; Wisniewski, J. A.; Ji, H. Hot spot-based design of small-molecule inhibitors for protein-protein interactions. *Bioorg. Med. Chem. Lett.* **2014**, *24* (11), 2546-54.

[10] Schreiber, G.; Fersht, A. R. Energetics of protein-protein interactions: analysis of the barnase-barstar interface by single mutations and double mutant cycles. *J. Mol. Biol.* **1995**, *248* (2), 478-86.

[11] Jones, S.; Thornton, J. M. Principles of protein-protein interactions. *Proc. Natl. Acad. Sci. U. S. A.* **1996**, *93* (1), 13-20.

[12] Clackson, T.; Wells, J. A. A hot spot of binding energy in a hormone-receptor interface. *Science* **1995**, *267* (5196), 383-6.

[13] White, A. W.; Westwell, A. D.; Brahemi, G. Protein-protein interactions as targets for small-molecule therapeutics in cancer. *Expert. Rev. Mol. Med.* **2008**, *10*, e8.

[14] DeLano, W. L. Unraveling hot spots in binding interfaces: progress and challenges. *Curr. Opin. Struct. Biol.* **2002**, *12* (1), 14-20.

[15] Goodyear, C. S.; Silverman, G. J. Phage-display methodology for the study of protein-protein interactions: overview. *CSH protoc.* **2008**, pdb top48.

[16] Causier, B.; Davies, B. *Analysing protein-protein interactions with the yeast* two-hybrid system. *Plant. Mol. Biol.* **2002**, *50* (6), 855-70.

[17] Dunkler, A.; Muller, J.; Johnsson, N. Detecting protein-protein interactions with the Split-Ubiquitin sensor. *Methods Mol. Biol.* **2012**, *786*, 115-30.

[18] Kukar, T.; Eckenrode, S.; Gu, Y.; Lian, W.; Megginson, M.; She, J. X.; Wu, D. Protein microarrays to detect protein-protein interactions using red and green fluorescent proteins. *Anal. Biochem.* **2002**, *306* (1), 50-4.

[19] Kenworthy, A. K. Imaging protein-protein interactions using fluorescence resonance energy transfer microscopy. *Methods* **2001**, *24* (3), 289-96.

[20] Percy, A. J.; Rey, M.; Burns, K. M.; Schriemer, D. C. Probing protein interactions with hydrogen/deuterium exchange and mass spectrometry-a review. *Anal. Chim. Acta* **2012**, *721*, 7-21.

[21] Grosdidier, S.; Fernandez-Recio, J. Identification of hot-spot residues in protein-protein interactions by computational docking. *BMC Bioinformatics* **2008**, *9*, 447.

[22] Morrow, J. K.; Zhang, S. Computational prediction of protein hot spot residues. *Curr. Pharm. Des.* **2012**, *18* (9), 1255-65.

[23] Keskin, O.; Ma, B.; Nussinov, R. Hot regions in protein-protein interactions: the organization and contribution of structurally conserved hot spot residues. *J. Mol.Biol.* **2005**, *345* (5), 1281-94.

[24] Bakail, M.; Ochsenbein, F. Targeting proteine-protein interactions, a wide open field for drug design. *C. R. Chim.* **2016**, *19*, 19e27.

[25] Bogan, A. A.; Thorn, K. S. Anatomy of hot spots in protein interfaces. *J. Mol. Biol.* **1998**, *280* (1), 1-9.

[26] Moreira, I. S.; Fernandes, P. A.; Ramos, M. J. Hot spots-a review of the protein-protein interface determinant amino-acid residues. *Proteins* **2007**, *68* (4), 803-12.

[27] Samanta, U.; Pal, D.; Chakrabarti, P. Environment of tryptophan side chains in proteins. *Proteins* **2000**, *38* (3), 288-300.

[28] Fernandez, A. Desolvation shell of hydrogen bonds in folded proteins, protein complexes and folding pathways. *FEBS Lett.* **2002**, *527* (1-3), 166-70.

[29] Lee, K. H.; Xie, D.; Freire, E.; Amzel, L. M. Estimation of changes in side chain configurational entropy in binding and folding: general methods and application to helix formation. *Proteins* **1994**, *20* (1), 68-84.

[30] Arkin, M. R.; Wells, J. A. Small-molecule inhibitors of protein-protein interactions: progressing towards the dream. *Nat. Rev. Drug Disc.* **2004**, *3* (4), 301-17.

[31] Cukuroglu, E.; Engin, H. B.; Gursoy, A.; Keskin, O. Hot spots in protein-protein interfaces: towards drug discovery. *Prog. Biophys. Mol. Biol.* **2014**, *116* (2-3), 165-73.

[32] Schafer, K. A. The cell cycle: a review. *Vet. Pathol.* **1998**, *35* (6), 461-78.

[33] Cooper G. M. The Cell Cycle. *The Cell: A Molecular Approach*. 2nd Ed., **2000**, Chapter 14.

[34] Barnum, K. J.; O'Connell, M. J. Cell cycle regulation by checkpoints. *Methods Mol. Biol.* **2014**, *1170*, 29-40.

[35] Kaufmann, W. K. Cell cycle checkpoints and DNA repair preserve the stability of the human genome. *Cancer Metastasis Rev.* **1995**, *14* (1), 31-41

[36] Bailis, J. M.; Forsburg, S. L. S phase assembly of centromeric heterochromatin and cohesion. *Cell cycle* **2004**, *3* (4), 416-8.

[37] O'Connell, M. J.; Walworth, N. C.; Carr, A. M. The G2-phase DNA-damage checkpoint. *Trends Cell Biol.* **2000**, *10* (7), 296-303.

[38] O'Connell, M. J.; Cimprich, K. A. G2 damage checkpoints: what is the turn-on? *J. Cell Sci.* **2005**, *118* (Pt 1), 1-6.

[39] Hauf, S.; Watanabe, Y. Kinetochore orientation in mitosis and meiosis. *Cell* **2004**, *119* (3), 317-27.

[40] Lodish, H. F.; Berk, A.; Kaiser, C. A.; Krieger, M.; Scott, M. P. Microtubule Dynamics and Motor Proteins during Mitosis. *Mol. Cell Biol.* 4th Ed. **2000**, Section 19.5.

[41] Waterman-Storer, C. M.; Salmon, E. D. Microtubule dynamics: treadmilling comes around again. *Curr. Biol.* **1997**, *7* (6), R369-72.

[42] Nurse, P. Universal control mechanism regulating onset of M-phase. *Nature* **1990**, *344* (6266), 503-8.

[43] Malumbres, M. Cyclin-dependent kinases. *Genome Biol.* **2014**, *15* (6), 122.

[44] Vermeulen, K.; Van Bockstaele D. R.; Berneman Z. N. The cell cycle: a review of regulation, deregulation and therapeutic targets in cancer. *Cell Prolif.* **2003**, *36*, 131-149.

[45] Lim, S.; Kaldis P. Cdks, cyclins and CKIs: roles beyond cell cycle regulation. *Development* **2013**, *140*, 3079-3093.

[46] Schwaller, J.; Pabst, T.; Koeffler, H. P.; Niklaus, G.; Loetscher, P.; Fey, M. F.; Tobler, A. Expression and regulation of G1 cell-cycle inhibitors (p16INK4A, p15INK4B, p18INK4C, p19INK4D) in human acute myeloid leukemia and normal myeloid cells. *Leukemia* **1997**, *11* (1), 54-63..

[47] Orlow, I.; Iavarone, A.; Crider-Miller, S. J.; Bonilla, F.; Latres, E.; Lee, M. H.; Gerald, W. L.; Massague, J.; Weissman, B. E.; Cordon-Cardo, C. Cyclin-dependent kinase inhibitor p57KIP2 in soft tissue sarcomas and Wilms tumors. *Cancer Res.* **1996**, *56* (6), 1219-21.

[48] Cerqueira, A.; Martin, A.; Symonds, C. E.; Odajima, J.; Dubus, P.; Barbacid, M.; Santamaria, D. Genetic characterization of the role of the Cip/Kip family of proteins as cyclin-dependent kinase inhibitors and assembly factors. *Mol. Cell. Biol.* **2014**, *34* (8), 1452-9.

[49] Warner, B. J.; Blain, S. W.; Seoane, J.; Massague, J. Myc downregulation by transforming growth factor beta required for activation of the p15(Ink4b) G(1) arrest pathway. *Mol. Cell. Biol.* **1999**, *19* (9), 5913-22.

[50] El-Deiry, W. S.; Tokino, T.; Velculescu, V. E.; Levy, D. B.; Parsons, R.; Trent, J. M.; Lin, D.; Mercer, W. E.; Kinzler, K. W.; Vogelstein, B. WAF1, a potential mediator of p53 tumor suppression. *Cell* **1993**, *75* (4), 817-25.

[51] Cheffer, A.; Tarnok, A.; Ulrich, H. Cell cycle regulation during neurogenesis in the embryonic and adult brain. *Stem Cell Rev.* **2013**, *9* (6), 794-805.

[52] Wu, J.; Lv, Q.; He, J.; Zhang, H.; Mei, X.; Cui, K.; Huang, N.; Xie, W.; Xu, N.; Zhang, Y. MicroRNA-188 suppresses G1/S transition by targeting multiple cyclin/CDK complexes. *Cell Commun. Signal.* **2014**, *12*, 66.

[53] Lees, J. A.; Saito, M.; Vidal, M.; Valentine, M.; Look, T.; Harlow, E.; Dyson, N.; Helin, K. The retinoblastoma protein binds to a family of E2F transcription factors. *Mol. Cell Biol.* **1993**, *13* (12), 7813-25.

[54] Sengupta, S.; Henry, R. W. Regulation of the retinoblastoma-E2F pathway by the ubiquitin-proteasome system. *Biochim. Biophys. Acta, Gene Regul. Mech.* **2015**, *1849* (10), 1289-1297.

[55] Cavanagh, B. L.; Walker, T.; Norazit, A.; Meedeniya, A. C. Thymidine analogues for tracking DNA synthesis. *Molecules* **2011**, *16* (9), 7980-93.

[56] Tobey, R. A.; Crissman, H. A. Use of flow microfluorometry in detailed analysis of effects of chemical agents on cell cycle progression. *Cancer Res.* **1972**, *32* (12), 2726-32.

[57] Darzynkiewicz, Z.; Juan, G.; Bedner, E. Determining cell cycle stages by flow cytometry. *Curr. Protoc. Cell. Biol.* **2001**, *Chapter 8*, Unit 8 4.

[58] Kim, K. H.; Sederstrom, J. M. Assaying Cell Cycle Status Using Flow Cytometry. *Curr. Protoc. Mol. Biol.* **2015**, *111*, 28 6 1-11.

[59] Schmid, I.; Cole, S. W.; Korin, Y. D.; Zack, J. A.; Giorgi, J. V. Detection of cell cycle subcompartments by flow cytometric estimation of DNA-RNA content in combination with dual-color immunofluorescence. *Cytometry* **2000**, *39* (2), 108-16.

[60] Ciancio, G.; Pollack, A.; Taupier, M. A.; Block, N. L.; Irvin, G. L. 3rd. Measurement of cell-cycle phase-specific cell death using Hoechst 33342 and propidium iodide: preservation by ethanol fixation. *J. Histochem. Cytochem.* **1988**, *36* (9), 1147-52.

[61] Tavecchio, M.; Simone, M.; Bernasconi, S.; Tognon, G.; Mazzini, G.; Erba, E. Multi-parametric flow cytometric cell cycle analysis using TO-PRO-3 iodide (TP3): detailed protocols. *Acta Histochem.* **2008**, *110* (3), 232-44.

[62] Pozarowski, P.; Darzynkiewicz, Z. Analysis of cell cycle by flow cytometry. *Methods Mol. Biol.* **2004**, *281*, 301-11.

[63] Nunez, R. DNA measurement and cell cycle analysis by flow cytometry. *Curr. Issues. Mol. Biol.* **2001**, *3* (3), 67-70.

[64] Darzynkiewicz, Z.; Halicka, H. D.; Zhao, H. Analysis of Cellular DNA Content by flow and laser scanning cytometry. *Adv. Exp. Med. Biol.* **2010**, *676*, 137–147.

[65] Elmore, S. Apoptosis: a review of programmed cell death. *Toxicol. Pathol.* **2007**, *35* (4), 495-516.

[66] Friedlander, R. M. Apoptosis and caspases in neurodegenerative diseases. *N. Engl. J. Med.* **2003**, *348* (14), 1365-75.

[67] Malherbe, J. A. J.; Fuller, K. A.; Mirzai, B.; Kavanagh, S.; So C.-C.; Ip, H.-W.; Guo, B. B.; Forsyth, C.; Howman, R.; Erber, W. N. Dysregulation of the intrinsic apoptotic pathway mediates megakaryocytic hyperplasia in myeloproliferative neoplasms. *J. Clin. Pathol.* **2016**, *0*, 1-8.

[68] Ichim, G.; Tait, S. W. A fate worse than death: apoptosis as an oncogenic process. *Nat. Rev. Cancer* **2016**, *16* (8), 539-48.

[69] Riley, J. S.; Malik, A.; Holohan, C.; Longley, D. B. DED or alive: assembly and regulation of the death effector domain complexes. *Cell Death Dis.* **2015**, *6*(8), e1866.

[70] Weinberg, R. A. P53 and apoptosis: master guardian and executioners. *The Biology of Cancer* 2nd Ed. **2013**, Chapter 9, Garland Science.

[71] Nomura, T.; Satoh, F.; Yamasaki, M.; Mimata H. IAP as a new diagnostic and effective therapeutic target molecule for prostate cancer. *Gene Ther. Mol. Biol.* **2007**, *11*, 103-112.

[72] Chipuk, J. E.; Moldoveanu, T.; Llambi, F.; Parsons, M. J.; Green, D. R. The BCL-2 family reunion. *Mol. Cell* **2010**, *37* (3), 299-310.

[73] Delavallee, L.; Cabon, L.; Galan-Malo, P.; Lorenzo, H. K.; Susin, S. A. AIF-mediated caspase-independent necroptosis: a new chance for targeted therapeutics. *IUBMB Life* **2011**, *63* (4), 221-32.

[74] Lorenzo, H. K.; Susin, S. A. Mitochondrial effectors in caspase-independent cell death. *FEBS Letters* **2004**, *557* (1-3), 14-20.

[75] Tait, S. W.; Green, D. R. Caspase-independent cell death: leaving the set without the final cut. *Oncogene* **2008**, *27* (50), 6452-61.

[76] Pardo, J.; Bosque, A.; Brehm, R.; Wallich, R.; Naval, J.; Mullbacher, A.; Anel, A.; Simon, M. M. Apoptotic pathways are selectively activated by granzyme A and/or granzyme B in CTL-mediated target cell lysis. *J. Cell Biol.* **2004**, *167* (3), 457-68.

[77] Han, J.; Goldstein, L. A.; Gastman, B. R.; Rabinovitz, A.; Rabinowich, H. Disruption of Mcl-1.Bim complex in granzyme B-mediated mitochondrial apoptosis. *J. Biol. Chem.* **2005**, *280* (16), 16383-92.

Chapter 2

p53/MDM2/MDM4 Interactions as Target in Anticancer Therapy
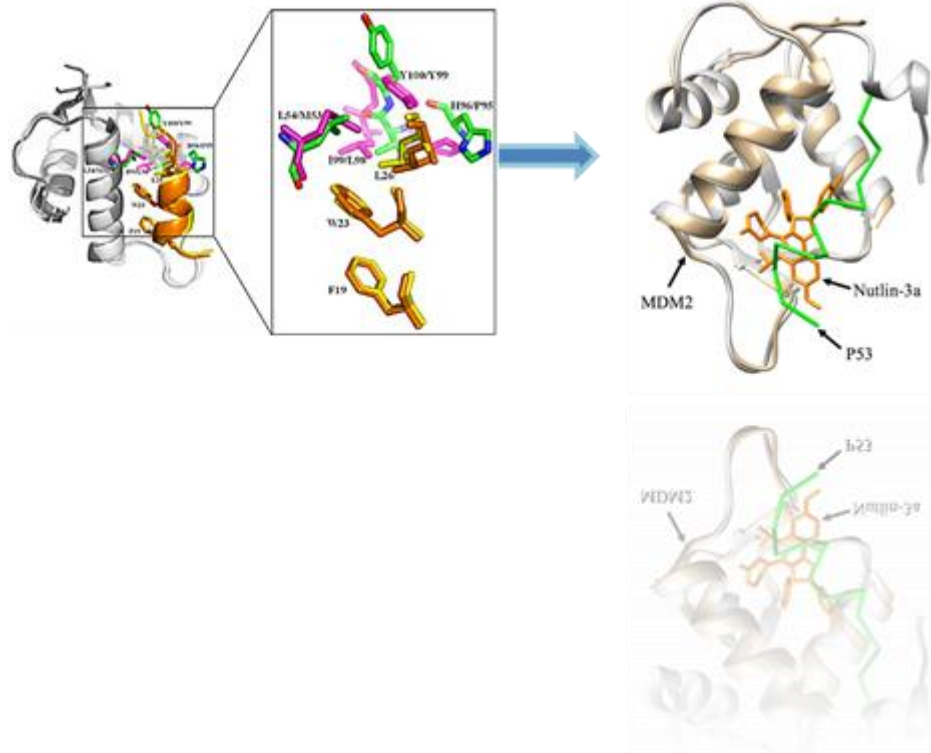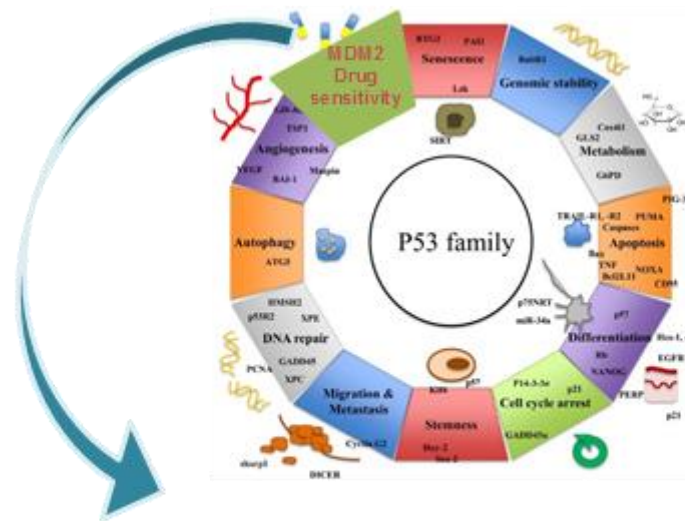
2.1   p53 protein: "the guardian of the genome"

The p53 protein is a transcription factor also known as the "guardian of the genome". In fact, its function is to activate the transcriptional expression of downstream target genes whose protein products induce cell growth arrest, apoptosis or senescence in response to stress signals such as DNA damage (induced by UV, gamma or X radiation, bulky carcinogens, alkylating agents, mycotoxins, inhibitors of topoisomerases, etc), hypoxia, depletion of ribonucleotides, disruption of cell adhesion or aberrant oncogene expression [1, 2] (Figure 2.1).

These signals activate p53 through several pathways, leading to variable speed or level of p53 activation, depending on the nature of the stress, its intensity and the sensitivity of the cell type considered [3] (Figure 2.1).
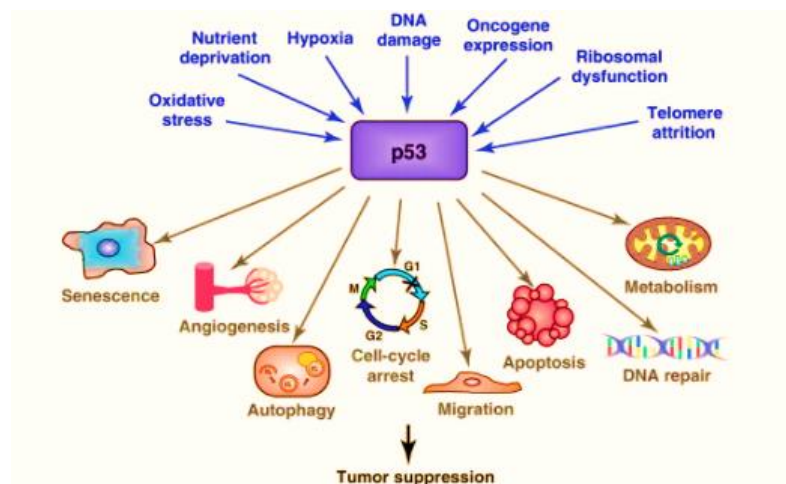
Figure 2.1. *p53 pathways (from ref. [2])*

In general, severe stresses induce more extreme and irreversible responses, whereas milder stresses lead to a transient growth arrest coupled with an attempt to repair the damage caused [4]. However, there is no uniform "p53 response", and the exact criteria that influence p53 to stimulate cell cycle arrest or apoptosis are not well understood.

The p53 can activate both extrinsic and intrinsic apoptotic pathways [5-7]. In particular, it is able to control the transcription of proapoptotic members of the Bcl-2 family (e.g. BAX, PUMA, NOXA, BID), and can promote the activation of

caspases (including caspase-8 and caspase-3) through engagement of "death receptors".

Furthermore, it can transactivate several components of the apoptotic effector machinery, including the gene encoding Apaf-1 which acts as a coactivator of caspase-9 [7].

p53 regulates both G1/S and G2/M checkpoints upon physiological stress (Figure 2.2); moreover, several reports have argued that this protein is also involved in activation of the S-phase checkpoint and mitotic spindle checkpoint [8].
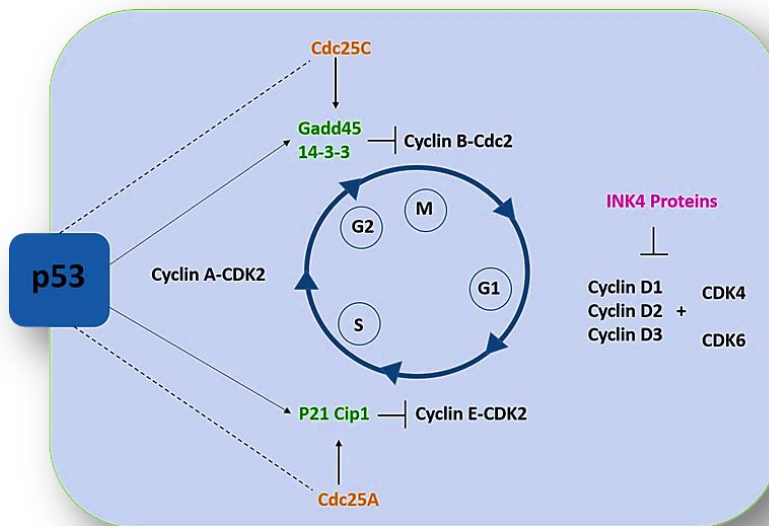
Figure 2.2. *The role of p53 in cell cycle regulation*

p21 is the most famous p53-induced cell cycle inhibitory gene. In particular, p21 protein can induce both G_1 and G_2 arrest by inhibiting cyclin E/CDK2 and cyclin B/CDK1 respectively. In addition, p21 is also involved in activation of the pRb tumor suppressor pathway [9, 10].

pRb is inactivated through hyperphosphorylation mediated by cyclin/CDKs during cell cycle process. Upon induction, p21 inhibits cyclin E/CDK2 causing hypophosphorylation of pRb, that interacts with E2F to inhibits E2F-mediated transcription of cell cycle genes [11]. Another p53-induced target, 14-3-3σ,

belongs to a family of proteins that regulate cellular activity by binding and sequestering phosphorylated proteins.

14-3-3σ inactivates Cdc25 (which is necessary for activation of CDK1) and CDK1 by sequestering them to the cytoplasm to trigger pre-mitotic G_2/M block upon DNA damage [11, 12].

2.2 p53 structure

The p53 protein consists of 393 amino acid residues; in its active conformation, it is tetrameric and each monomer is organized in several functional domains including [13-15] (Figure 2.3):

- an *N-terminal transactivation domain* (TAD), where is located the binding site of some of its regulatory proteins such as MDM2, MDM4 and p300/CPB;

- a *proline rich domain* (PRR), involved in the induction of p53-dependent apoptosis as well as in DNA binding, inhibition of cell growth, and suppression of cell transformation;

- a central *DNA binding domain* (DBD), required for sequence-specific DNA binding;

- a *nuclear localization signal* (NLS), essential for the translocation of p53 into the nucleus;

- a *tetramerization domain* (TET), which permits the oligomerization of the protein;

- a *nuclear export signal* (NES), which mediates the subcellular localization and nuclear-cytoplasmic shuttling of p53;

- a *C-terminal regulatory domain* (REG), which is extensively post-translationally modified with a regulatory effect on p53 activity.

In general, all above mentioned p53 domains can be extensively modified with post-translational modifications which modulate p53 stability and activity [16, 17].
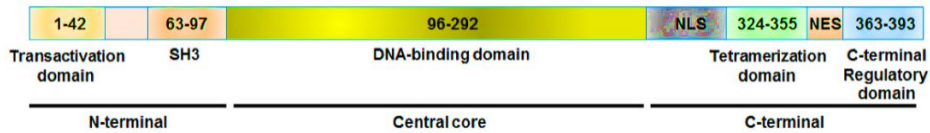
Figure 2.3 *p53 protein structure (from ref. [18])*

2.3 p53 regulation

In normal cells, p53 function is tightly regulated by a variety of positive and negative regulators, often creating feedback loops. This regulation can be achieved through three major mechanisms: a) regulation of p53 protein levels; b) control of the subcellular localization of the p53 protein, and c) modulation of the activity of p53, particularly its ability to function as a sequence specific transcription factor [18-21].

The cellular level of p53 protein is usually kept low by ubiquitination at its *N*-terminal transactivation domain, followed by rapid protein degradation in cellular proteasomes [22].

Ubiquitination is the addition of ubiquitin (a small regulatory protein) to a substrate protein. This reaction requires the sequential actions of three enzymes: E1, E2 and E3. E1 activating enzyme forms a thioester between the C-terminal glycine of ubiquitin and its own active site cysteine [23]. Ubiquitin is then transferred to the active site cysteine of an E2 conjugating enzyme. An E3 ubiquitin ligase facilitates the transfer of ubiquitin to the protein substrate, resulting in its rapid proteasome degradation [23].

The murine double minute 2 (MDM2; HDM2 in humans) is recognized as the principal physiological E3 ubiquitin ligase of p53 [24, 25].

This protein can induce both monoubiquitination and polyubiquitination of p53 protein [22, 24]. In general, low levels of MDM2 activity induce monoubiquitination and nuclear export of p53, which allows p53 degradation in cytoplasmic proteasomes, whereas high levels of MDM2 promote p53 polyubiquitination and degradation in the nucleus [22, 24].

p53 and MDM2 form an autoregulatory feedback loop. In fact, p53 stimulates the expression of the MDM2 protein, which in turn inhibits p53. MDM2 acts negatively on p53 also by binding to its transactivation domain, inhibiting its transcriptional activity [24, 25].

Finally, p53's activity and stability are regulated by other mechanisms including: phosphorylation, acetylation, methylation, sumoylation (i.e. attachment of *S*mall *U*biquitin-like *Mo*difier or *SUMO* proteins) and neddylation (i.e. conjugation of ubiquitin-like protein NEDD8) [26, 27].

MDM4 (also known as MDMX, and human versions as HDM4, and HDMX) is a protein structurally related to MDM2 but it does not possess intrinsic E3-ligase activity [28].

MDM4 can hetero-oligomerize with MDM2 protein and stabilize it (by interfering with MDM2 auto-ubiquitination), increasing ubiquitinylation of p53 [29]. MDM4 also inhibits p53 transcriptional activity via binding to its transactivation domain. This association of MDM4 with p53 transactivation domain also reduces p53 acetylation by p300/CBP, and this effect further inhibits p53 activity [30].
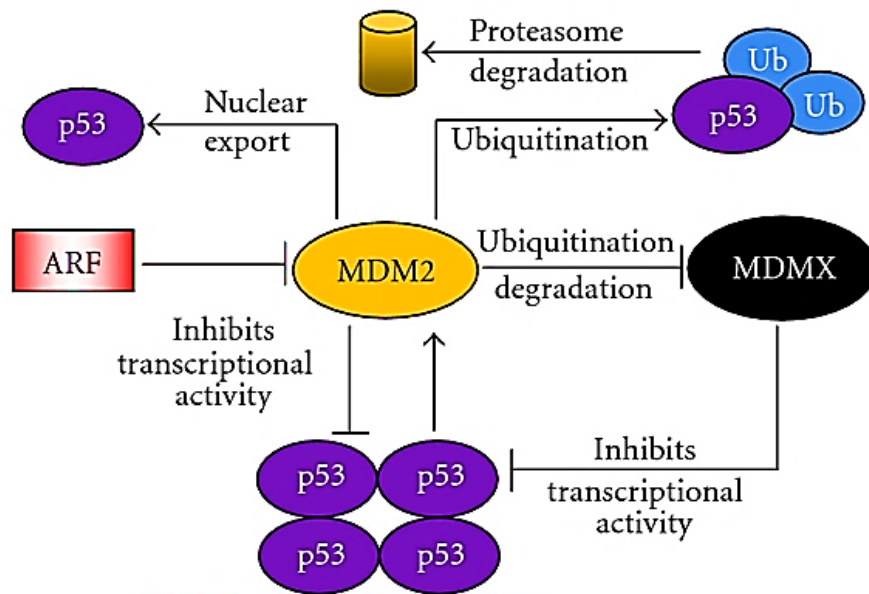
Figure 2.4. *Regulation of p53 by MDM2 and MDM4 (from ref. [31]).*

Apart MDM4, other proteins can associate with the tumor suppressor protein p53 without having enzymatic activity [4, 32]. Their modulator activity can occur by association with the *N*-terminal transactivation domain or the DNA binding domain, which leads to enhance or reduce the association of p53 with co-activators or modifying enzymes. In other cases, these interaction partners can impinge on p53 tetramerization [32].

2.4 p53 and cancer

Many different types of cancer show a high incidence of *TP*53 mutations, leading to the expression of mutant p53 proteins, that in most cases have not only lost wild-type p53 tumor suppressor activity, but also gained pro-oncogenic properties [33-37].

Most of these mutations (95%) lies in the core DNA-binding domain, and 75% of them occur as single missense mutations rather than deletions, insertions or frameshifts [36]. Of the mutations in this domain, about 30% fall within six hot spot residues (R175, G245, R248, R249, R273, and R282), and are frequent in almost all types of cancer [37].

It is worth of note that the core DNA-binding domain of human p53 has low intrinsic thermodynamic stability, and its melting temperature is only slightly above body temperature. Hence, even weakly destabilizing mutations can have a detrimental effect and result in a large population of unfolded proteins under physiological conditions [36]. Thermodynamic studies on a wide range of p53 core domain mutations indicate three broad phenotypes:

- mutations that cause loss of DNA contacts (e.g. R273H), with little or no effect on folding and on the overall stability of the protein;
- mutations that disrupt local structure and destabilize the core domain by < 2 kcal/mol (e.g. G245S and R249S);
- mutations that are highly destabilizing (> 3 kcal/mol) and result in global unfolding of the protein at body temperature [36].

In different types of tumors p53 inactivity is a consequence of overexpression of its negative regulators MDM2 and/or MDM4 [38-42].

For example, glioblastoma multiformis, one of the most common and aggressive primary brain tumors in humans, has been well established as a tumor with cells highly overexpressing MDM2 protein, causing a severe decrease in p53 expression [39].

Overexpression of MDM2 has been observed also in soft tissue tumors, osteosarcomas, esophageal carcinomas, testicular germ cell cancers and neuro-blastomas [40, 41].

Similarly to MDM2, MDM4 can be overexpressed in different types of cancers retaining wild-type p53 including gliomas, a number of pre-B acute lymphoblastic leukemias, and some primary tumors including breast tumors, head and neck squamous cell carcinomas, and retinoblastomas [41, 42].

Of consequence, in these cases agents preventing the MDM2/MDM4-mediated inactivation of p53 should promote the activation of p53 wild type and show anticancer activity.

2.5 MDM2 and MDM4: structure and function

MDM2 is a protein of 491 amino acids with four well-conserved domains [43-45] (Figure 2.4):

- an *N-terminal domain*, important for binding to the *N*-terminal part of p53;

- an *acidic domain*, necessary for MDM2's interaction with ribosomal proteins L5, L11, L23, S14 and ARF; in addition, this domain is also important for efficient degradation of p53, and is a site for interaction with p300/CBP, which cooperates with MDM2 to target p53 for degradation;

- a *Zinc-finger domain*, whose function remains largely unknown;

- a *C-terminal RING-finger domain* (RING = *R*eally *I*nteresting *N*ew *G*ene), which has intrinsic E3 ligase activity allowing MDM2 to monoubiquitinate and polyubiquitinate itself, p53 and several other targets. Moreover, the RING domain is the site through which MDM2 can bind to its homolog, MDM4, via RING-RING interaction, and is required to transport p53 out of the nucleus [44, 45];

- a *nuclear localization sequence (NLS)* and a *nuclear export sequence (NES)*, through which MDM2 can translocate between the cytoplasm and the nucleus.

MDM4 is a protein of 490 amino acid, structurally related to MDM2 [46-50]. The greatest similarity between the two proteins is at the *N*-terminus (between amino acids 24-108), where the residues required for interaction with p53 are strictly conserved in both MDM2 and MDM4 proteins (G58, D68, V75, C77 in MDM2 corresponding to MDM4 G57, D67, V74, C76) [51].

The other region with high similarity between MDM4 and MDM2 is the *C*-terminus containing the *RING finger motif* (aa 437-477) which, however, in

MDM4 lacks intrinsic ubiquitin-ligase activity, in contrast to RING domain in MDM2 [51]. MDM4 contains also a *zinc-finger domain* (aa 300 and 328), the function of which is largely unknown; close to this domain there is a tetrapeptide (aa 357-361, DVPD), that represents a canonical caspase cleavage signal. The caspase cleavage of MDM4 at this site has been shown to affect protein stability [50].Another difference between MDM2 and MDM4 lies in the acidic domain (Figure 2.5); so far no specific activities have been attributed to this portion of the MDM4 protein. Further, MDM4 has neither nuclear localization nor nuclear export sequences (Figure 2.5).

The binding of the wild-type p53 based peptides to MDM2 and MDM4 has been well established by X-ray crystallography [52-56]. These crystallographic studies evidenced that the same residues in p53 (Trp23, Leu26, and Phe19) are required for both MDM2-p53 and MDM4-p53 interactions. In addition, binding poses of these three key residues of p53 peptide in the two co-crystal structures are very similar [53, 54].

The p53 residues 15-29 do not appear to adopt a stably folded structure in solution, but form an α-helix when bound to MDM2 [55]. MDM2 has a deep and structured binding pocket for p53, that is only 18 Å along the long edge [57]. Notably, formation of the MDM2-based binding pocket is induced upon p53 interaction; in fact, the NMR structure of apo-MDM2 does not show any pocket, except a small indent anticipatory of the future [p53]Trp23 binding site (PDB ID: 1Z1M) [55].

In p53/MDM2 complex, the indole nitrogen of p53 Trp23 forms a hydrogen bond with Leu54 of MDM2, while p53 residues F19 and W23 are located face to face on the same side of the α-helix and, together with p53 L26, they point toward a cleft at the surface of the MDM2 protein, where they are surrounded by hydrophobic MDM2 residues L54, L57, I61, M62, Y67, Q72, V75, F86, F91, V93, H96, I99, Y100 and I101 (Figure 2.6) [55].
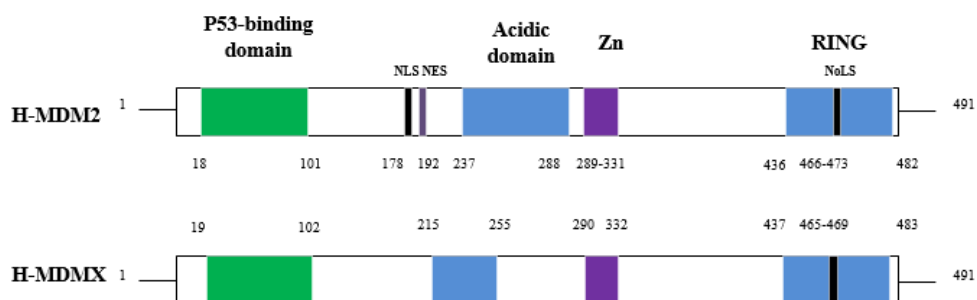
Figure 2.5 *Comparison of the MDM2 and MDMX primary structures*

Importantly, 10 out of these 14 residues of the *N*-terminal domain of MDM2 are conserved in the *N*-terminal domain of MDM4. Thus, the cleft at the surface of MDM4 is similar to, but not identical with, that of MDM2 [55, 58].

In particular, some residues around the Leu26 pocket are different (Figure 2.6), leading to changes in the shape and size of the MDM4 groove as compared to the MDM2 groove. These include Met53 (Leu54 in MDM2), Leu98 (Ile99 in MDM2), Leu102 (Ile103 in MDM2), and Pro95 (His96 in MDM2), which result in a shallower and smaller binding groove in MDM4 compared to that in MDM2. Additionally, around the Trp23 pocket, the Leu85 residue in MDM4 is aligned with the Phe86 residue in MDM2 [58].

Overall, the binding groove in MDM2 is compact and well-defined, as is, to a lesser extent, the groove in MDM4. The well-defined binding grooves in MDM2 and MDM4 suggest the feasibility of designing small-molecule inhibitors of the MDM2-p53 interaction and/or the MDM4-p53 interaction [59, 60]. Noticeably, in MDM4 a secondary hydrophobic area is next to the Leu26 binding site, and is formed by Leu33, Val52, and Leu106. This binding site is separated from the Leu26 binding site by Met53 and Leu102 side chains and could play a critical role in the discovery of selective MDM4 ligands [57].

MDM2 activity and stability are strictly regulated in order to inhibit p53 under non-stressed cell conditions or stop the inhibition of p53 in the case of cellular stress that elicits a p53 response.

Like p53, MDM2 is subjected to intensive posttranslational modifications including phosphorylation, ubiquitination, acetylation and sumoylation. Further, it can be degraded by ubiquitination by other ligases as well as by auto-

ubiquitination [32, 61, 62]. For example, when a DNA damage occurs, MDM2 is directly phosphorylated by ATM kinase at S395, which lies within the RING domain. This modification alters the MDM2 ligase activity to stop p53 degradation and export [32]. ATM also indirectly causes phosphorylation of MDM2 by the c-Abl kinase at Y394 which allows for p53 activation of apoptosis [32, 61]. Another kinase in the DNA damage cascade, DNA-PK (DNA-activated Protein Kinase) has been shown to phosphorylate MDM2 within its p53-binding domain at S17, decreasing the affinity of MDM2 for p53 [61].

Modifications to MDM2 after DNA damage not only stop MDM2 from ubiquitinating p53, but actually change the affinity of MDM2 so that it tags its stabilizing binding partner MDM4 for degradation, which in turn destabilizes and leads to degradation of MDM2. This process leads to a rapid decrease in MDM2 and MDM4 after DNA damage. Due to the aforementioned negative feedback loop, activation of p53 also causes an increase in MDM2 protein production. Therefore, once the DNA damage is repaired and signals no longer demand stabilization of p53, changes in modifications of MDM2 allow it to return to inhibiting p53 so that the cell cycle can proceed [61]. The protein ARF (*A*lternate open *R*eading *F*ame of locus p16INK4a), activated under oncogenic stress, is another important MDM2 regulator and acts through different mechanisms. In fact, it can sequester MDM2 in the nucleolus, thereby preventing MDM2 from interacting with and inhibiting p53; ARF can also inhibit MDM2 by promoting its sumoylation [61].

Finally, in the event of ribosomal stress, ribosomal proteins as L5, L12, L23 and S7 can bind to and inhibit MDM2, allowing for p53 activation [61]. Post translational modifications also affect MDM4 function and stability [61-65].

As previously described, MDM4 shares a high degree of homology with MDM2, largely in its p53-binding domain and in its RING domain and, unlike MDM2, has not E3 ligase activity. In addition, MDM4 lacks both nuclear localization and nuclear export sequences, and then this protein is intrinsically a cytoplasmic protein. In particular, MDM4 itself cannot cause degradation or nuclear export of p53 in the absence of MDM2 [66-70].

MDM2 shuttles MDM4 into the nucleus where the MDM2-MDM4 complex can interact with and suppress p53 in a RING-RING interaction-dependent manner [68, 69]. MDM2 and MDM4 are non-redundant proteins despite their high level of homology. [71]. To date it is not clear why both MDM2 and MDM4 are required for survival. In this regard, some evidence suggests that while MDM2 inhibits the apoptotic activity of p53, MDM4 may inhibit the ability of p53 to induce cell cycle arrest. However, it has been reported that the intrinsic ligase activity of MDM2 without MDM4 is not sufficient, and that the MDM2-MDM4 heterocomplex itself should be considered the E3 ligase of p53 [61].
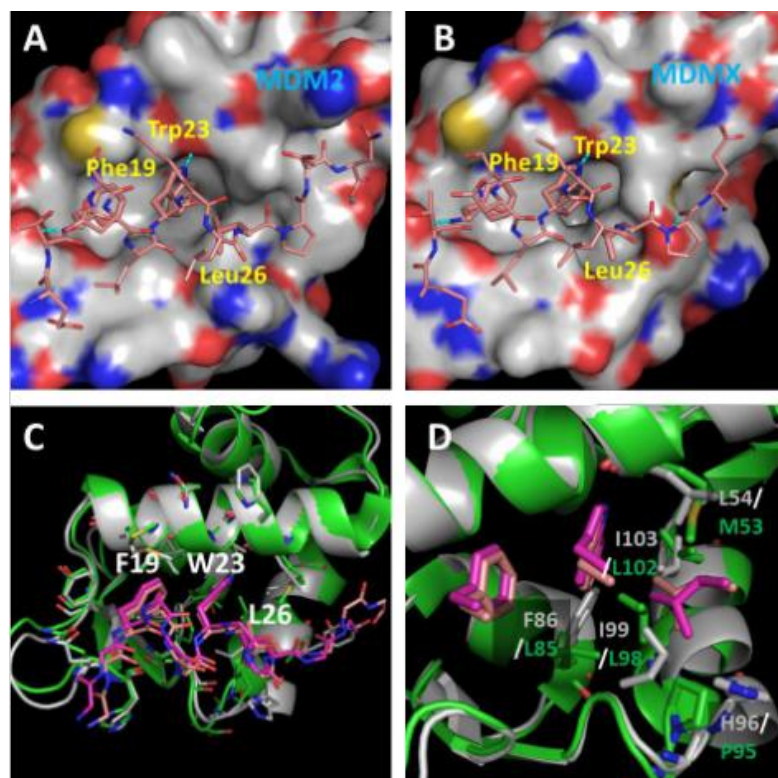
Figure 2.6 A*) MDM2 (surface)-p53 (line and sticks) complex (PDB ID: 1YCR), B) MDMX (surface)-p53 (line and sticks) complex (PDB ID: 3DAB), C and D) Superimposition of the two complexes. MDM2 is in grey, MDM4 is in green, and p53 are in pink and magenta respectively (from ref. [72]).*

2.6 p53/MDM2/MDM4 inhibitors

Designing small molecules to block the MDM2-p53 and/or MDM4-p53 interaction and then reactivate the p53 function is one of the most promising therapeutic strategy for the treatment of cancers retaining wild-type p53 [72, 73].

Alternative approaches to activate the p53 pathway in tumors via inhibition of the MDM2 protein include: decreasing the cellular concentration of MDM2 with antisense oligodeoxynucleotides, blocking the MDM2-mediated ubiquitination of p53; mimicking of p14ARF, a negative regulator of MDM2.

A prerequisite for high affinity MDM2 and/or MDM4 antagonists is that certain moieties of the molecule must mimic the three amino acids of p53 hot spot triad Trp23, Leu26, and Phe19.

Amongst the three buried hydrophobic side chains, Trp23 contributes most to the interaction energy and thus must be closely mimicked in terms of hydrophobicity and shape, to ensure sufficient affinity of the inhibitors.

In addition, the challenge to design druglike p53/MDM2 and/or p53/MDM4 inhibitors rests with balancing the lipophilic interactions required for binding affinity to the target, with the need to maintain acceptable physicochemical properties (i.e. MW, cLogP, solubility etc.) in a single compound [74-80].

Thus far, many synthetic low molecular weight inhibitors of the p53-MDM2 have been reported in literature, and seven of them are advanced into clinical trials for treatment of human cancers [72]. These compounds have different molecular scaffold and include a cis-diphenyl substituted imidazoline (RG7112 or RO5045337), a pyrrolidine derivative (RG7388 or RO5503781), two spiro-oxindole derivatives (MI-77301 or SAR405838), two piperidin-2-one derivatives (AMG 232 and DS-3032b), a dihydroisoquinolinone derivative (NVP-CGM097) and a pyrimidinone derivative (MK-8242 or SCH 900242) (Figure 2.7) [72].

As the importance of MDM4 in the negative regulation of p53 has become increasingly apparent, many efforts have been made to develop selective inhibitors of MDM4.

Recently, SJ-172550 was identified in a high-throughput screen as p53/MDM4 inhibitor (Figure 2.8) [81].

This compound causes p53 dependent cell death of retinoblastoma cells, in which the expression of MDM4 is amplified, and its effect is additive when combined with an MDM2 inhibitor (e.g. nutlin-3a). However, further studies evidenced that SJ-172550 forms a covalent but reversible complex with MDM4 and locks MDM4 into a conformation that is unable to bind p53. The relative

stability of this complex is influenced by many factors that complicate the interpretation of biological results, hampering further development of SJ-172550 as a selective MDM4 inhibitor [82].

The p53/MDM4 inhibitor NSC207895 (Figure 2.7), a benzofuroxan derivative, promotes p53 in MCF-7 cells, resulting in elevated expression of proapoptotic genes (e.g. PUMA, BAX, and PIG3), and acts additively with nutlin-3a [83].

The small molecule, WK298, has a moderate MDM4 binding affinity (K_i= 11 μM) and a higher affinity for MDM2 (K_i= 109 nM). This compound has been co-crystallized with MDM4 (PDB: 3LBJ). A co-crystal structure of MDM2 and WK23 (PDB: 3LBK), an analogue of WK298, was also determined at a resolution of 2.3 Å and this facilitated analysis of the differences between MDM2-p53 and MDM4-p53 [54]. In particular, this study indicated that Leu26 pocket is less open to solvent in the case of MDM2 and this may explain why WK23 and WK298 bind to MDM2 with much higher affinities than to MDM4 [54].

With the recent *in vitro* and *in vivo* evidence emphasizing the importance of the MDM2-MDM4 complex, it has been encouraged the development of dual MDM2/MDM4 inhibitors as they should activate p53 more significantly than agents targeting only MDM2 or MDM4.
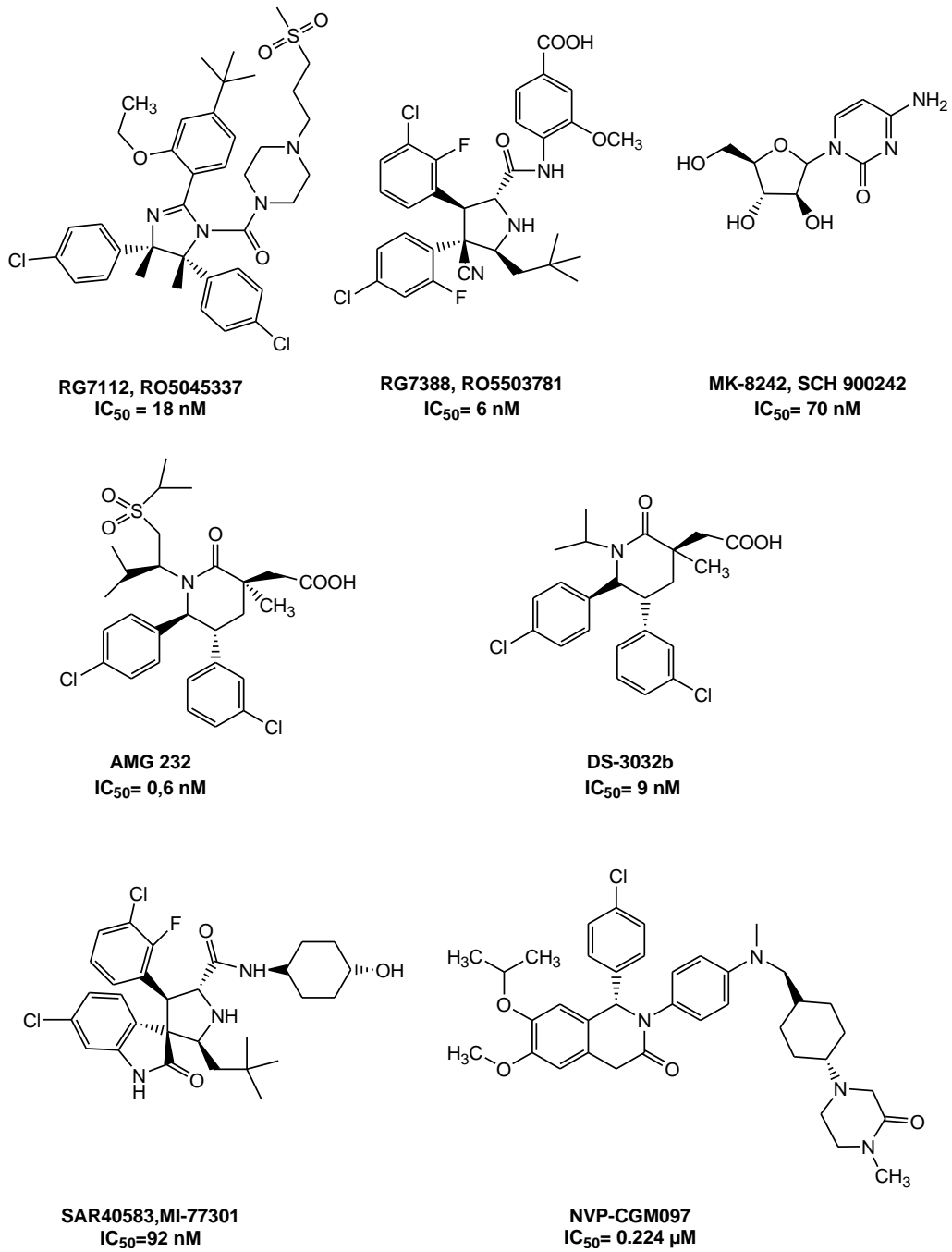
Figure 2.7 *MDM2 inhibitors*
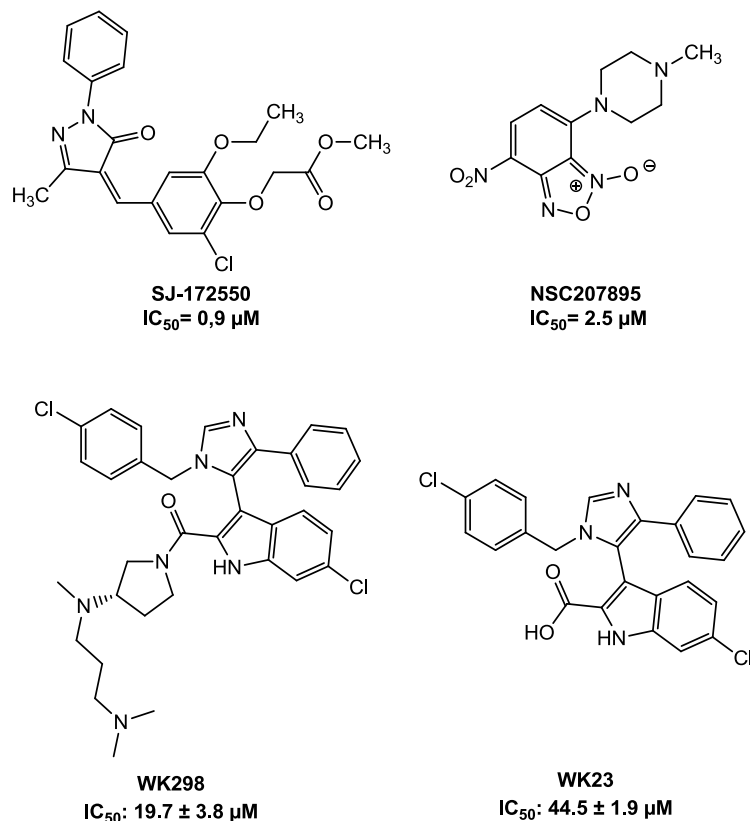
Figure 2.8 *MDM4 inhibitors*

2.7 p53-based cyclotherapy

The purpose of the chemotherapy is to selectively kill tumour cells. Standard chemotherapy preferentially target rapidly dividing cells, giving rise to unwanted side effects. In addition, most classic chemotherapeutics are highly mutagenic and can lead to an increased risk of the formation of new tumors as well as further dedifferentiation of existing tumor cells [84].

Cyclotherapy is a promising therapeutic strategy to protect normal tissues from the side effects of standard chemotherapy. This therapeutic approach exploits the differences between the cell cycle controls that regulate normal cells (where normal checkpoints are in place) and those that regulate cancer cells (where checkpoint function is frequently lost) [85].

The *p53* protein is known to regulate G1 checkpoint, which can induce G1 arrest (if DNA damage can be repaired) or initiate apoptosis (if DNA damage is too

severe and cannot be repaired); however in many different cancers the p53 protein is mutated and cannot act as a tumor suppressor.

Two different studies showed that pretreatment with a p53 activating drug (e.g. nutlin-3a) for 24h halts the cell cycle in G1/G2 only in normal cells carrying wild-type p53, whereas p53-mutant cancer cells continue cycling into S and M phase (Figure 2.9) [86-88].

Subsequent treatment for additional 48h with an anti-S phase (e.g. gemcitabine) or antimitotic drug (e.g. paclitaxel.) then kills the tumor cells but not the normal cells. (Figure 2.9).

Therefore, p53 stabilising agents may be utilised to arrest normal cells (with wild-type p53) in the G1/G2-phase of the cell cycle, protecting them from the effects of subsequent administration of cell cycle specific (anti-S or anti-M) cytotoxic agents.
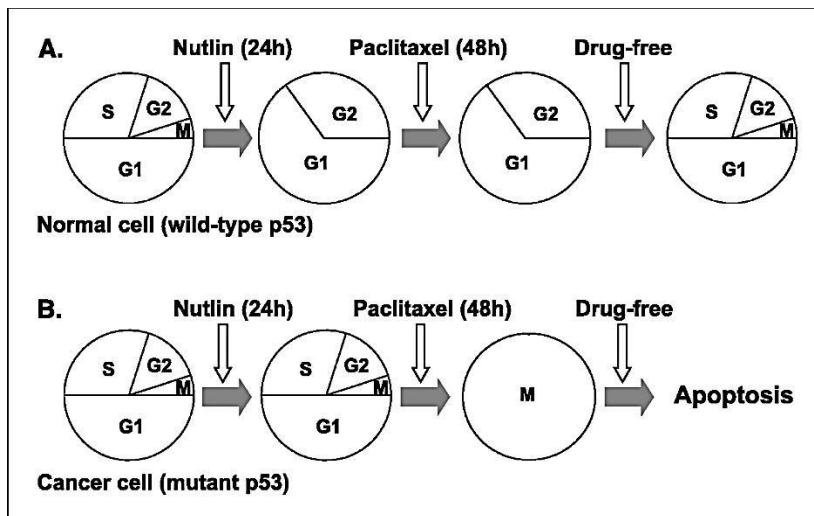
Figure 2.9. *p53-based cycloterapy (from ref. [86]).*

References

[1] Rozan, L. M.; El-Deiry, W. S. p53 downstream target genes and tumor suppression: a classical view in evolution. *Cell Death Differ.* **2007**, *14* (1), 3-9.

[2] Bieging, K. T.; Attardi, L. D. Deconstructing p53 transcriptional networks in tumor suppression. *Trends Genet.* **2012**, *22* (2), 97-106.

[3] Szymañska, K.; Hainaut P. TP53 and mutations in human cancer. *Acta Biochim. Pol.* **2003**, *50*, 231-238.

[4] Nag, S.; Qin, J.; Srivenugopal, K. S.; Wang, M.; Zhang, R. The MDM2-p53 pathway revisited. *J. Biomed. Res.* **2013**, 27, 1-18.

[5] Schuler, M.; Bossy-Wetzel, E.; Goldstein, J. C.; Fitzgerald, P.; Green, D. R. p53 induces apoptosis by caspase activation through mitochondrial cytochrome c release. *J. Biol. Chem.* **2000**, *275* (10), 7337-42.

[6] Nikoletopoulou, V.; Markaki, M.; Palikaras, K.; Tavernarakis, N. Crosstalk between apoptosis, necrosis and autophagy. *Biochim. Biophys. Acta* **2013**, *1833* (12), 3448-3459.

[7] Fridman, J. S.; Lowe, S. W. Control of apoptosis by p53. *Oncogene* **2003**, *22* (56), 9030-40.

[8] Giono, L. E.; Manfredi, J. J. The p53 tumor suppressor participates in multiple cell cycle checkpoints. *J. Cell. Physiol.* **2006**, *209* (1), 13-20.

[9] Abbas, T.; Dutta, A. p21 in cancer: intricate networks and multiple activities. *Nat. Rev. Cancer* **2009**, *9* (6), 400-14.

[10] Peyressatre, M.; Prevel, C.; Pellerano, M.; Morris, M. C. Targeting cyclin-dependent kinases in human cancers: from small molecules to Peptide inhibitors. *Cancers* **2015**, *7* (1), 179-237.

[11] Pucci, B.; Kasten, M.; Giordano, A. Cell Cycle and Apoptosis. *Neoplasia* **2000**, *2* (4), 291–299.

[12] Fischer, M. Census and evaluation of p53 target genes. *Oncogene* **2017**, *36* (28), 3943-3956.

[13] Joerger, A. C.; Fersht A. R. Structure–function–rescue: the diverse nature of common p53 cancer mutants. *Oncogene* **2007**, *26*, 2226–2242.

[14] Joerger, A. C.; Fersht, A. R. Structural biology of the tumor suppressor p53. *Annu. Rev. Biochem.* **2008**, *77*, 557-82.

[15] Joerger, A. C.; Fersht, A. R. The tumor suppressor p53: from structures to drug discovery. *Cold Spring Harb. Perspect. Biol.* **2010**, *2* (6), a000919.

[16] Dai, C.; Gu, W. p53 post-translational modification: deregulated in tumorigenesis. *Trends Mol. Med.* **2010**, *16* (11), 528-36.

[17] Taira, N.; Yoshida, K. Post-translational modifications of p53 tumor suppressor: determinants of its functional targets. *Histol. Histopathol.* **2012**, *27* (4), 437-43.

[18] Kruse, J.-P.; Gu, W. Modes of p53 Regulation. *Cell* **2009**, *137* (4), 609-622.

[19] O'Brate, A.; Giannakakou, P. The importance of p53 location: nuclear or cytoplasmic zip code? *Drug Resist. Updat.* **2003**, *6* (6), 313-22.

[20] Ashcroft, M.; Vousden, K. H. Regulation of p53 stability. *Oncogene* **1999**, *18* (53), 7637-43.

[21] Liu, G.; Chen, X. Regulation of the p53 transcriptional activity. *J. Cell. Biochem.* **2006**, *97* (3), 448-58.

[22] Brooks, C. L.; Gu, W. p53 ubiquitination: Mdm2 and beyond. *Mol. Cell.* **2006**, *21* (3), 307-15.

[23] *Wilkinson, K. D.* The discovery of ubiquitin-dependent proteolysis. *Proc. Natl. Acad. Sci. U.S.A.* **2005***, 102 (43), 15280-2.*

[24] Li, M.; Brooks, C. L.; Wu-Baer, F.; Chen, D.; Baer, R.; Gu, W. Mono-versus polyubiquitination: differential control of p53 fate by Mdm2. *Science* **2003**, *302* (5652), 1972-5.

[25] O'Keefe, K.; Li, H.; Zhang, Y. Nucleocytoplasmic shuttling of p53 is essential for MDM2-mediated cytoplasmic degradation but not ubiquitination. *Mol. Cell. Biol.* **2003**, *23* (18), 6396-405.

[26] Xu, Y. Regulation of p53 responses by post-translational modifications. *Cell. Death Differ.* **2003**, *10* (4), 400-3.

[27] Meek, D. W.; Anderson, C. W. Posttranslational modification of p53: cooperative integrators of function. *Cold Spring Harb. Perspect. Biol.* **2009**, *1* (6), a000950.

[28] Marine, J. C.; Dyer, M. A.; Jochemsen, A. G. MDMX: from bench to bedside. *J. Cell Sci.* **2007**, *120* (Pt 3), 371-8.

[29] Leslie, P. L.; Ke, H.; Zhang, Y. The MDM2 RING domain and central acidic domain play distinct roles in MDM2 protein homodimerization and MDM2-MDMX protein heterodimerization. *J. Biol. Chem.* **2015**, *290* (20), 12941-50.

[30] Reed, S. M.; Quelle, D. E. p53 Acetylation: Regulation and Consequences. *Cancers* **2014**, *7* (1), 30-69.

[31] Denaro, N.; Lo Nigro, C.; Natoli, G.; Russi, E. G.; Adamo, V.; Merlano, M. C. The Role of p53 and MDM2 in Head and Neck Cancer. *ISRN Otolaryngol.* **2011**, *2011*, 8.

[32] Boehme, K. A.; Blattne, C. Regulation of p53-insights into a complex process. *Crit. Rev. Biochem. Mol. Biol.* **2009**, *44* (6), 367-392.

[33] Muller, P. A.; Vousden, K. H. p53 mutations in cancer. *Nat. Cell. Biol.* **2013**, *15* (1), 2-8.

[34] Wright, J. D.; Noskov, S. Y.; Lim, C. Factors governing loss and rescue of DNA binding upon single and double mutations in the p53 core domain. *Nucleic Acids Res.* **2002**, *30* (7), 1563-74.

[35] Ang, H. C.; Joerger, A. C.; Mayer, S.; Fersht, A. R. Effects of common cancer mutations on stability and DNA binding of full-length p53 compared with isolated core domains. *J. Biol. Chem.* **2006**, *281* (31), 21934-41.

[36] Bullock, A. N.; Fersht, A. R. Rescuing the function of mutant p53. *Nat. Rev.Canc.* **2001**, *1*, 68-76.

[37] Rivlin, N.; Brosh, R.; Oren, M.; Rotter, V. Mutations in the p53 Tumor Suppressor Gene. *Genes Cancer* **2011**, *2* (4), 466–474.

[38] Momand, J.; Jung, D.; Wilczynski, S.; Niland, J. The MDM2 gene amplification database. *Nucleic Acids Res.* **1998**, *26* (15), 3453-9.

[39] Costa, B.; Bendinelli, S.; Gabelloni, P.; Da Pozzo, E.; Daniele, S.; Scatena, F.; Vanacore, R.; Campiglia, P.; Bertamino, A.; Gomez-Monterrey, I.; Sorriento, D.; Del Giudice, C.; Iaccarino, G.; Novellino, E.; Martini, C. Human glioblastoma multiforme: p53 reactivation by a novel MDM2 inhibitor. *PLoS One* **2013**, *8* (8), e72281.

[40] Onel, K.; Cordon-Cardo, C. MDM2 and prognosis. *Mol. Cancer Res.* **2004**, *2* (1), 1-8.

[41] Danovi, D.; Meulmeester, E.; Pasini, D.; Migliorini, D.; Capra, M.; Frenk, R.; de Graaf, P.; Francoz, S.; Gasparini, P.; Gobbi, A.; Helin, K.; Pelicci, P. G.; Jochemsen, A. G.; Marine, J. C. Amplification of Mdmx (or Mdm4) directly contributes to tumor formation by inhibiting p53 tumor suppressor activity. *Mol. Cell. Biol.* **2004**, *24* (13), 5835-43.

[42] Pant, V.; Larsson, C. A.; Aryal, N.; Xiong, S.; You, M. J.; Quintas-Cardama, A.; Lozano, G. Tumorigenesis promotes Mdm4-S overexpression. *Oncotarget* **2017**, *8* (16), 25837-25847.

[43] Kussie, P. H.; Gorina, S.; Marechal, V.; Elenbaas, B.; Moreau, J.; Levine, A. J.; Pavletich, N. P. Structure of the MDM2 oncoprotein bound to the p53 tumor suppressor transactivation domain. *Science* **1996**, *274* (5289), 948-53.

[44] Geyer, R. K.; Yu, Z. K.; Maki, C. G. The MDM2 RING-finger domain is required to promote p53 nuclear export. *Nat. Cell Biol.* **2000**, *2* (9), 569-73.

[45] Boyd, S. D.; Tsai, K. Y.; Jacks, T. An intact HDM2 RING-finger domain is required for nuclear exclusion of p53. *Nat. Cell Biol.* **2000**, *2* (9), 563-8.

[46] Popowicz, G. M.; Czarna, A.; Holak, T. A. Structure of the human Mdmx protein bound to the p53 tumor suppressor transactivation domain. *Cell Cycle* **2008**, *7* (15), 2441-3.

[47] Bottger, V.; Bottger, A.; Garcia-Echeverria, C.; Ramos, Y. F.; van der Eb, A. J.; Jochemsen, A. G.; Lane, D. P. Comparative study of the p53-mdm2 and p53-MDMX interfaces. *Oncogene* **1999**, *18* (1), 189-99.

[48] Shvarts, A.; Steegenga, W. T.; Riteco, N.; van Laar, T.; Dekker, P.; Bazuine, M.; van Ham, R. C.; van der Houven van Oordt, W.; Hateboer, G.; van der Eb, A. J.; Jochemsen, A. G. MDMX: a novel p53-binding protein with some functional properties of MDM2. *EMBO J.* **1996**, *15* (19), 5349-57.

[49] LeBron, C.; Chen, L.; Gilkes, D. M.; Chen, J. Regulation of MDMX nuclear import and degradation by Chk2 and 14-3-3. *EMBO J.* **2006**, *25* (6), 1196-206.

[50] Gentiletti, F.; Mancini, F.; D'Angelo, M.; Sacchi, A.; Pontecorvi, A.; Jochemsen, A. G.; Moretti, F. MDMX stability is regulated by p53-induced caspase cleavage in NIH3T3 mouse fibroblasts. *Oncogene* **2002**, *21* (6), 867-77.

[51] Mancini, F.; Di Conza, G.; Moretti F. MDM4 (MDMX) and its Transcript Variants. *Curr. Genomics* **2009**, *10,* 42-50

[52] Chi, S. W.; Lee, S. H.; Kim, D. H.; Ahn, M. J.; Kim, J. S.; Woo, J. Y.; Torizawa, T.; Kainosho, M.; Han, K. H. Structural details on mdm2-p53 interaction. *J. Biol Chem.* **2005**, *280* (46), 38795-802.

[53] Chene, P. Inhibition of the p53-MDM2 interaction: targeting a protein-protein interface. *Mol. Cancer Res.* **2004**, *2* (1), 20-8.

[54] Popowicz, G. M.; Czarna, A.; Wolf, S.; Wang, K.; Wang, W.; Domling, A.; Holak, T. A. Structures of low molecular weight inhibitors bound to MDMX and MDM2 reveal new approaches for p53-MDMX/MDM2 antagonist drug discovery. *Cell Cycle* **2010**, *9* (6), 1104-11.

[55] Toledo, F.; Wahl G. M. MDM2 and MDM4: p53 regulators as targets in anticancer therapy. *Int. J. Biochem. Cell Biol*. **2007**, *39* (7-8), 1476-1482.

[56] Khourya, K.; Popowicz, G. M., Holakb, T. A.; Dömling, A. The p53-MDM2/MDMX axis-A chemotype perspective. *Med. Chem. Comm.* **2011**, *2*, 246–260.

[57] Popowicz, G. M.; Domling, A.; Holak, T. A. The structure-based design of Mdm2/Mdmx-p53 inhibitors gets serious. *Angew. Chem.* **2011**, *50* (12), 2680-8.

[58] Estrada-Ortiza, N.; Neochoritisa, C. G.; Dömling, A. How to Design a Successful p53-MDM2/X interaction inhibitor: a thorough overview based on crystal structures. *Chem. Med. Chem.* **2016**, *11* (8), 757-772.

[59] Uhrinova, S.; Uhrin, D.; Powers, H.; Watt, K.; Zheleva, D.; Fischer, P.; McInnes, C.; Barlow, P. N. Structure of free MDM2 N-terminal domain reveals conformational adjustments that accompany p53-binding. *J. Mol. Biol.* **2005**, *350* (3), 587-98.

[60] Pazgier, M.; Liu, M.; Zou, G.; Yuan, W.; Li, C.; Li, C.; Li, J.; Monbo, J.; Zella, D.; Tarasov, S. G.; Lu, W. Structural basis for high-affinity peptide inhibition of p53 interactions with MDM2 and MDMX. *Proc. Natl. Acad. Sci. U. S. A.* **2009**, *106* (12), 4665-70.

[61] Shadfan, M.; Lopez-Pajares, V.; Yuan Z.-M. MDM2 and MDMX: alone and together in regulation of p53. *Transl. Cancer Res.* **2012**, *1* (2): 88-89.

[62] Meek, D. W.; Knippschild, U. Posttranslational modification of MDM2. *Mol. Cancer Res.* **2003**, *1* (14), 1017-26.

[63] Pan, Y.; Chen, J. Modification of MDMX by sumoylation. *Biochem. Biophys. Res. Commun.* **2005**, *332* (3), 702-9.

[64] Elias, B.; Laine, A.; Ronai, Z. Phosphorylation of MdmX by CDK2/Cdc2(p34) is required for nuclear export of Mdm2. *Oncogene* **2005**, *24* (15), 2574-9.

[65] Lopez-Pajares, V.; Kim, M. M.; Yuan, Z. M. Phosphorylation of MDMX mediated by Akt leads to stabilization and induces 14-3-3 binding. *J. Biol. Chem.* **2008**, *283* (20), 13707-13.

[66] Marine, J. C.; Jochemsen, A. G. Mdmx as an essential regulator of p53 activity. *Biochem. Biophys. Res. Commun.* **2005**, *331* (3), 750-60.

[67] Pei, D.; Zhang, Y.; Zheng, J. Regulation of p53: a collaboration between Mdm2 and Mdmx. *Oncotarget* **2012**, *3* (3), 228-35.

[68] Linke, K.; Mace, P. D.; Smith, C. A.; Vaux, D. L.; Silke, J.; Day, C. L. Structure of the MDM2/MDMX RING domain heterodimer reveals dimerization is required for their ubiquitylation in trans. *Cell Death Differ.* **2008**, *15* (5), 841-8.

[69] Poyurovsky, M. V.; Priest, C.; Kentsis, A.; Borden, K. L.; Pan, Z. Q.; Pavletich, N.; Prives, C. The Mdm2 RING domain C-terminus is required for supramolecular assembly and ubiquitin ligase activity. *The EMBO journal* **2007**, *26* (1), 90-101.

[70] Uldrijan, S.; Pannekoek, W. J.; Vousden, K. H. An essential function of the extreme C-terminus of MDM2 can be provided by MDMX. *EMBO J.* **2007**, *26* (1), 102-12.

[71] Marine J.-C.; Jochemsen, A. G. Mdmx and Mdm2 brothers in arms? *Cell Cycle* **2004**, *3* (7), 900-904.

[72] Zhao, Y.; Aguilar, A.; Bernard, D.; Wang, S. Small-molecule inhibitors of the MDM2-p53 protein-protein interaction (MDM2 Inhibitors) in clinical trials for cancer treatment. *J. Med. Chem.* **2015**, *58* (3), 1038-52.

[73] Shangary, S.; Wang, S. Small-molecule inhibitors of the MDM2-p53 protein-protein interaction to reactivate p53 function: a novel approach for cancer therapy. *Annu. Rev. Pharmacol Toxicol* **2009**, *49*, 223-41.

[74] Veber, D. F.; Johnson, S. R.; Cheng, H. Y.; Smith, B. R.; Ward, K. W.; Kopple, K. D. Molecular properties that influence the oral bioavailability of drug candidates. *J. Med. Chem.* **2002**, *45* (12), 2615-23.

[75] Lipinski, C. A.; Lombardo, F.; Dominy, B. W.; Feeney, P. J. Experimental and computational approaches to estimate solubility and permeability in drug discovery and development settings. *Adv. Drug Deliv. Rev.* **2001**, *46* (1-3), 3-26.

[76] Hughes, J. D.; Blagg, J.; Price, D. A.; Bailey, S.; Decrescenzo, G. A.; Devraj, R. V.; Ellsworth, E.; Fobian, Y. M.; Gibbs, M. E.; Gilles, R. W.; Greene, N.; Huang, E.; Krieger-Burke, T.; Loesel, J.; Wager, T.; Whiteley, L.; Zhang, Y. Physiochemical drug properties associated with in vivo toxicological outcomes. *Bioorg. Med. Chem. Lett.* **2008**, *18* (17), 4872-5.

[77] Ritchie, T. J.; Macdonald, S. J. The impact of aromatic ring count on compound developability-are too many aromatic rings a liability in drug design? *Drug Discov. Today* **2009**, *14* (21-22), 1011-20.

[78] Lovering, F.; Bikker, J.; Humblet, C. Escape from flatland: increasing saturation as an approach to improving clinical success. *J. Med. Chem.* **2009**, *52* (21), 6752-6.

[79] Rauch, C. Toward a mechanical control of drug delivery. On the relationship between Lipinski's 2nd rule and cytosolic pH changes in doxorubicin resistance levels in cancer cells: a comparison to published data. *Eur. Biophys. J.* **2009**, *38* (7), 829-46.

[80] Congreve, M.; Carr, R.; Murray, C.; Jhoti, H. A 'rule of three' for fragment-based lead discovery? *Drug Discov. Today* **2003**, *8* (19), 876-7.

[81] Reed, D.; Shen, Y.; Shelat, A. A.; Arnold, L. A.; Ferreira, A. M.; Zhu, F.; Mills, N.; Smithson, D. C.; Regni, C. A.; Bashford, D.; Cicero, S. A.; Schulman, B. A.; Jochemsen, A. G.; Guy, R. K.; Dyer, M. A. Identification and characterization of the first small molecule inhibitor of MDMX. *J. Biol. Chem.* **2010**, *285* (14), 10786-96.

[82] Bista, M.; Smithson, D.; Pecak, A.; Salinas, G.; Pustelny, K.; Min, J.; Pirog, A.; Finch, K.; Zdzalik, M.; Waddell, B.; Wladyka, B.; Kedracka-Krok, S.; Dyer, M. A.; Dubin, G.; Guy, R. K. On the mechanism of action of SJ-172550 in inhibiting the interaction of MDM4 and p53. *PLoS One* **2012**, *7* (6), e37518.

[83] Wang, H.; Ma, X.; Ren, S.; Buolamwini, J. K.; Yan, C. A small-molecule inhibitor of MDMX activates p53 and induces apoptosis. *Mol. Cancer. Ther.* **2011**, *10* (1), 69-79.

[84] Rao, B.; Lain, S.; Thompson, A. M. p53-Based cyclotherapy: exploiting the 'guardian of the genome to protect normal cells from cytotoxic therapy. *Br. J. Cancer* **2013**, *109* (12), 2954-8.

[85] Choong, M. L.; Yang, H.; Lee, M. A.; Lane, D. P. Specific activation of the p53 pathway by low dose actinomycin D: a new route to p53 based cyclotherapy. *Cell Cycle* **2009**, *8* (17), 2810-8.

[86] Carvajal, D.; Tovar, C.; Yang, H.; Vu, B. T.; Heimbrook, D. C.; Vassilev, L. T. Activation of p53 by MDM2 antagonists can protect proliferating cells from mitotic inhibitors. *Cancer Res.* **2005**, *65* (5), 1918-24.

[87] Kranz, D.; Dobbelstein, M. Nongenotoxic p53 activation protects cells against S-phase-specific chemotherapy. *Cancer Res.* **2006**, *66* (21), 10274-80.

[88] Van Leeuwen, I. M.; Rao, B.; Sachweh, M. C.; Lain, S. An evaluation of small-molecule p53 activators as chemoprotectants ameliorating adverse effects of anticancer drugs in normal cells. *Cell Cycle* **2012**, *11* (9), 1851-61.

Chapter 3
Development of New
p53/MDM2/MDM4 Inhibitors
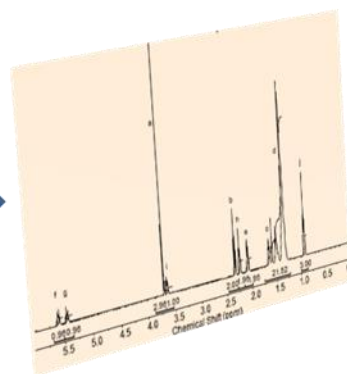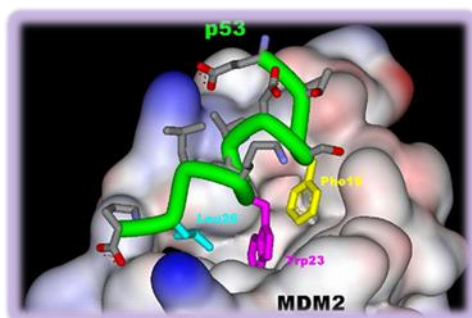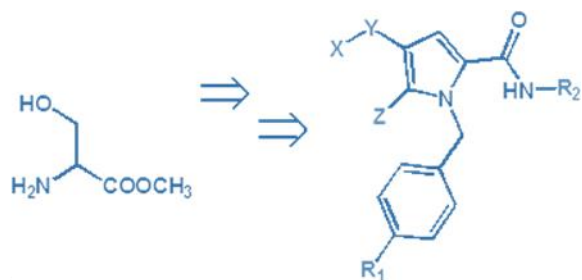
3.1 Background

A large body of evidence has established that LxxLL is one of the most representative binding motifs involved in protein-protein interactions associated with different aspects of transcriptional regulation [1]. LxxLL binding motif is characterized by the presence of three residues of leucine, highly conserved in the positions 1 (residue *i*), 4 (residue *i + 3*) and 5 (residue *i +4*) in an α-helical conformation. Its interaction properties are also shared by LxxLL-like and LxxLLxxL-like binding motifs, in which the leucine residues are replaced by aromatic amino acids [2].

^{19}FxxL^{23}Wxx^{26}L is a LxxLL-like binding motif and is related to "*hot spot triad*" of the p53 protein that is recognized by its protein partners MDM2/MDM4.

Until now many compounds with structurally distinct scaffolds have been reported as mimics of this binding motif (see Chapter 2, *sec. 2.6*).

More in general, the design of new p53/MDM2 and/or MDM4 inhibitors should take account of the following features:

- introduction of at least three hydrophobic groups mimicking p53's Phe19, Trp23, Leu26;

- a synthetic strategy easily enabling a pharmacokinetic and/or pharmacodynamic lead optimization;

- a low molecular weight scaffold amenable to chemical modifications to extend structure-activity relationships (SAR), and insure drug-like properties according to highly predictive rules of drug-likeness, widely used in preclinical drug discovery (e.g. Lipinski's rule of five, Veber's rule) [3, 4];

- the possibility to mimic other interactions between p53 and MDM2/MDM4.

For example, Leu22 (p53) is part of the p53 binding motif ^{19}Fxx^{22}**L**^{23}Wxx^{26}L; this residue interacts with Gln72 (MDM2), and is partially exposed to solvent. In a lead optimization process it could be advantageous to introduce a polar moiety on a chosen scaffold not only to mimic the interaction of p53's Leu22 to MDM2, but also to improve both pharmacodynamics and physiochemical properties (such as water solubility) of the compounds [5].

Recently, a tetrasubstituted pyrrole derivative, namely 4-benzoyl-*N*-[(3-chlorophenyl)methyl]-5-methyl-1-[(4-methylphenyl)methyl]-1H-pyrrole-2-carboxamide (**1,** Figure 3.1), has been identified by our research group as putative p53/MDM2 inhibitor [6].
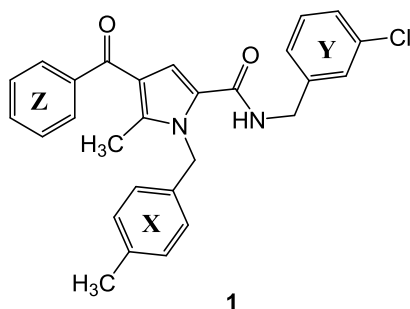
Figure 3.1 *Structure of 4-benzoyl-N-[(3-chlorophenyl)methyl]-5-methyl-1-[(4-methylphenyl)methyl]-1H-pyrrole-2-carboxamide* (**1**)

This compound was investigated on different cell lines (M14, MCF7, Huh-7, Jurkat) as well as on mouse monocyte macrophages Raw 264-7 by MTT assay, and showed a selective cytotoxicity against M14 melanoma cells at low micromolar concentration ($IC_{50}= 2.5 \pm 0.1$ μM). Compound **1** induced cellular accumulation in S phase after 24h of treatment as well as an increase in the expression of cyclin A, that promotes cell entry into S phase. A deeper biological investigation evidenced an enhancement of p53's expression in M14 cells at 24h (an effect that disappeared after 48h of incubation), but not in Huh7 cells, that contain a missense mutation in p53 gene and are not sensitive to compound **1** [6]. Finally, it was observed that accumulation of p53 in the nuclear fraction increased in cells treated for 24h compared with control cells, an effect that disappeared after 48h of incubation.

The putative ability of compound **1** to disrupt the p53-MDM2 interaction was investigated by NMR analysis. The method employed, named AIDA (for *A*ntagonist *I*nduced *D*issociation *A*ssay), provides information on whether an antagonist of a protein-protein interaction is strong enough to dissociate the complex, and whether its mode of action is modulated by denaturation, precipitation, or release of a protein in its functional folded state [7, 8].

The 1D proton NMR version of AIDA monitors the NMR signal of NH side chain ($^NH^\varepsilon$) of W23 and W53 present in the *N*-terminal domain of p53. Tryptophan is the only amino acid whose NH indole side chain ($^NH^\varepsilon$) gives a NMR signal at around 10 ppm at physiological pH, far away from the bulk amide protons region, and then it can be easily monitored. In the free p53 1D proton spectrum, side chains of W23 and W53 produce two sharp lines; instead, in the 1D NMR spectrum of the p53/MDM2 complex, only W53 is observable (Figure 3.2, a), whereas W23 signal disappears since this residue is one of p53's hot spot residues and interacts with a deep cleft on the MDM2 surface. Addition of nutlin-3a (0.1 mM) to the p53-MDM2 complex disrupts the MDM2/p53 interaction, causing a complete p53 release, as evidenced by W23 $^NH^\varepsilon$ side chains signal in the 1D NMR spectrum (Figure 3.2, c). On the contrary, the addition of **1** from a stock DMSO solution (0.1 mM formal final concentration) to the p53-MDM2 complex caused sample precipitation. The full 1D proton NMR spectrum of the supernatant solution did not change compared to that acquired before **1** addition, indicating that only **1** precipitated after its addition (Figure 3.2, b). In particular, the W23 peak was still not observable indicating that the p53-MDM2 complex was not dissociated [6]. However, it is important to emphasize that the experimental conditions needed for NMR analysis allows the detection of only very soluble inhibitors. Then, because of the poor solubility of **1**, NMR analysis did not provide a conclusive evidence of its mechanism of action [6].
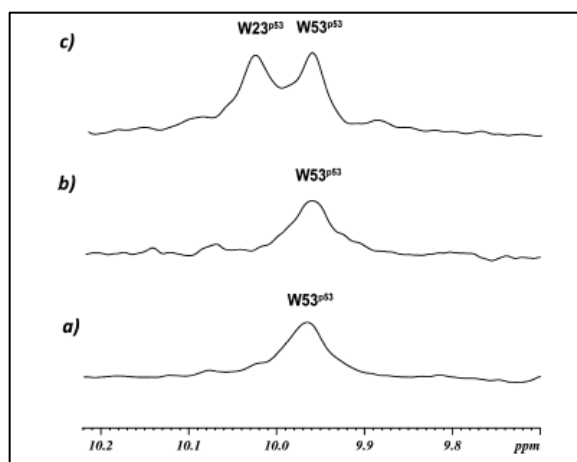
Figure 3.2 *One-dimensional proton spectra of the side chains of tryptophans (W) of: (a) p53−MDM2 complex; (b) after addition of **1**, and (c) after addition of nutlin-3a.*

A conformational analysis indicated that some low energy conformers of **1** (i. e. within 5 kcal/mol from the global minimum energy value ($\Delta E_{GM} \leq 5$ kcal/mol) are able to reproduce the *i, i + 3, i + 4* as well as the *i, i + 3, i + 7* residues of LxxLL-like motifs [6].

To further investigate the molecular mechanism of action of **1**, a pharmacophore model was generated for each conformational subfamily of **1**, i.e. for each set of pharmacophoric distances (Figure 3.3 and Figure 3.4).

The three phenyl rings (X, Y, and Z, Figure 3.1) and the halogen atom on ring Y of **1** were selected as pharmacophore fragments. The generated pharmacophore models were then employed to perform as many 3D database searches in molecular databases [6].

The resulting 1529 hits were analysed and filtered on the basis of the compatibility of their reported biological activity with the activity profile of **1**. First, only compounds whose biological activity on M14 cells has been explored were taken into consideration. This reduced the number of hits to 189.

Among them, only 19 were reported to be active in the micromolar range (<10 µM) on M14 cells. Two of them ***NSC671136*** (pubchem.ncbi.nlm.nih.gov/assay/assay.cgi?cid=383092) and ***NSC659611*** (http://pubchem.ncbi.nlm.nih.gov/assay/assay.cgi?cid=6712209), presented the same pharmacological profile as **1**, being active on M14 and not on MCF7 cells.

Compounds ***NSC659611*** and ***NSC671136*** fit the pharmacophore models of conformers CCC-II, TCT-II, TCC-I, and TTC-II of **1** (Figure 3.3 and Figure 3.4). While for ***NSC659611*** only growth inhibition assays are reported, several possible molecular targets are indicated for ***NSC671136***, and all of them are involved in protein-protein interactions regulating DNA transcription. In particular, the ability of ***NSC671136*** to inhibit MDM2-MDM4 heterodimer formation has also been proven.
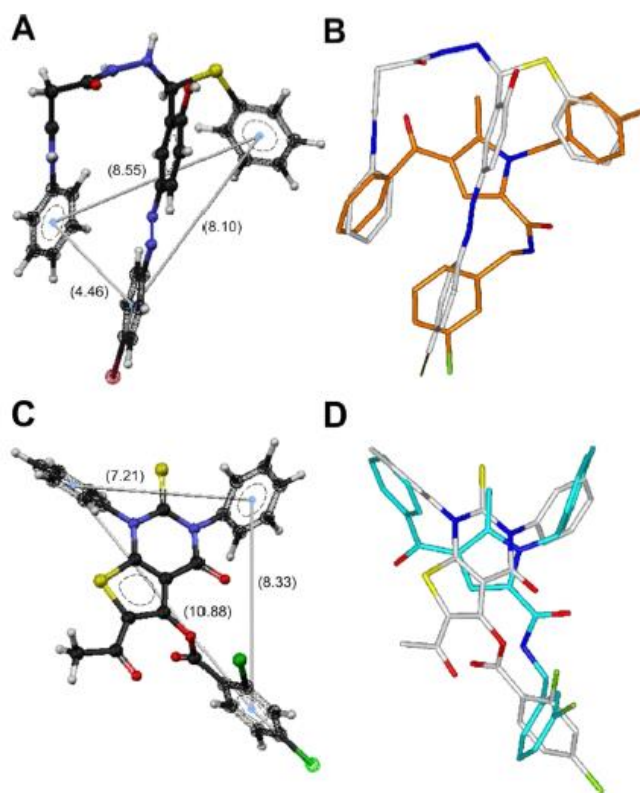
Figure 3.3 *(A) NSC659611 low energy conformer resulting from 3D database pharmacophore search, where matching distances are indicated. (B) Superimposition of CCC II lowest energy conformer of **1** (carbons, orange) on NSC659611 (carbons, white). (C) NSC671136 low energy conformer resulting from 3D database pharmacophore search, where matching distances are indicated. (D) Superimposition of TCT II lowest energy conformer of **1** (carbons, cyan) on NSC671136 (carbons, white). Hydrogens are omitted for clarity. Heteroatoms are colored by atom type: O, red; N, blue; S, yellow; Cl, light green.*
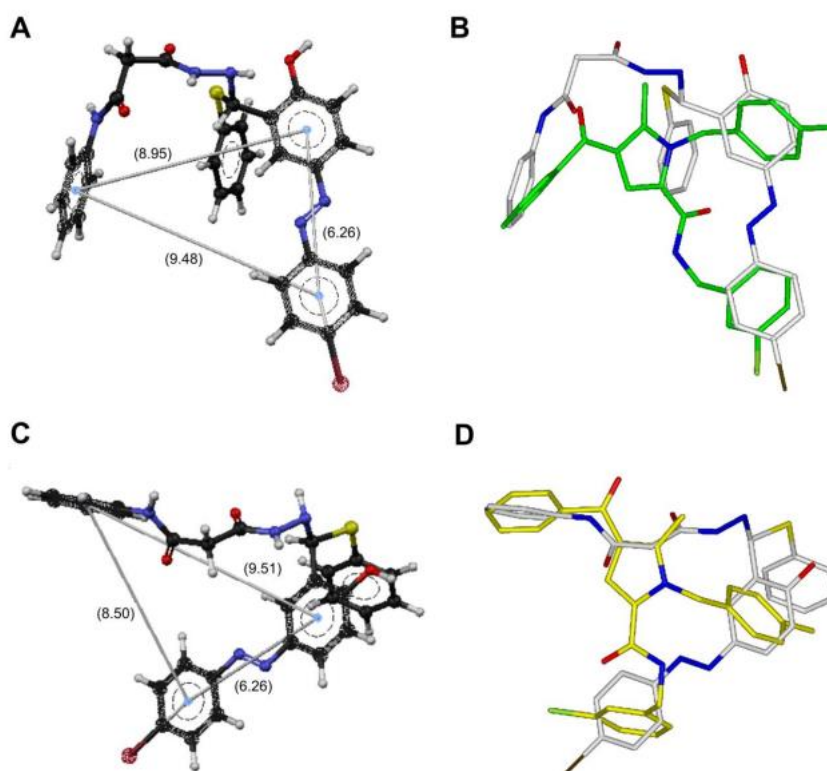
Figure 3.4. *(A, C) NSC659611 low energy conformers resulting from 3D database pharmacophore search; matching distances are indicated. Superimposition of (B) TCC-I (carbon: green) and (D) TTC-II (carbons: yellow) lowest energy conformers of 1 on NSC659611 (carbons: white). Hydrogens are omitted for clarity. Heteroatoms are colored by atom type: O, red; N, blue; S, yellow; Cl, light green.*
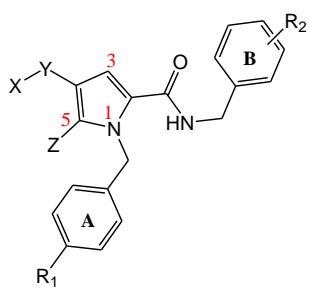
3.2 Aim of the work

The aim of this PhD project was to extend the structure activity relationships (SARs) investigation of a series of compounds typified by **1** in order to optimize the interaction with the hypothesized target and shed light on their mechanism of action.

A first series of tetrasubstituted pyrrole analogues of **1** (Table I) was synthesized in order to:

- evaluate the effects of different substituents (R_2= Cl, OCH_3, F, NO_2, NH_2) at the meta position of ring B (compounds **9a-d**, **9l**) in place of the methyl group present in **1**;

- evaluate the effects of shifting the ring B substituent from position 3 to position 4 (**9e** *vs* **1** and **9f** *vs* **9a**);

- evaluate the combination of an unsubstituted benzyl group (ring A) at the position 1 of the pyrrole ring with a *meta*-CF$_3$ substituent on ring B (**9g**);

- evaluate the introduction of an additional aromatic ring at the position 5 of the pyrrole ring in place of the methyl group present in **1** (**9k**);

- investigate the effects of the isomeric replacement of the CH$_3$/phenyl groups at the position 4/5 of the pyrrole ring (compound **9h**);

- evaluate the effects of the introduction of a *para*-substituted aromatic ring at the position 4 of the pyrrole ring (**9i**, X= (4-CH$_3$)C$_6$H$_4$, **9j**, X= (4-OCH$_3$)C$_6$H$_4$) (Table I);

- evaluate the effects of the reduction of the carbonyl group at the position 4 of the pyrrole ring (±**9m**).

Table I. *Structure of Compounds* **1, 9a-m**

Cpd	X	Y	Z	R$_1$	R$_2$
1	C$_6$H$_5$	C=O	CH$_3$	CH$_3$	3-Cl
9a	C$_6$H$_5$	C=O	CH$_3$	Cl	3-Cl
9b	C$_6$H$_5$	C=O	CH$_3$	OCH$_3$	3-Cl
9c	C$_6$H$_5$	C=O	CH$_3$	F	3-Cl
9d	C$_6$H$_5$	C=O	CH$_3$	NO$_2$	3-Cl
9e	C$_6$H$_5$	C=O	CH$_3$	CH$_3$	4-Cl
9f	C$_6$H$_5$	C=O	CH$_3$	Cl	4-Cl
9g	C$_6$H$_5$	C=O	CH$_3$	H	3-CF$_3$
9h	CH$_3$	C=O	C$_6$H$_5$	CH$_3$	3-Br
9i	(4-CH$_3$)C$_6$H$_4$	C=O	CH$_3$	CH$_3$	3-Cl
9j	(4-OCH$_3$)C$_6$H$_4$	C=O	CH$_3$	CH$_3$	3-Cl
9k	C$_6$H$_5$	C=O	C$_6$H$_5$	H	3-Cl
9l	C$_6$H$_5$	C=O	CH$_3$	NH$_2$	3-Cl
(±)9m	C$_6$H$_5$	CHOH	CH$_3$	CH$_3$	3-Cl

3.3 Synthesis of 1, 9a-m

The synthetic route of the title compounds **1**, **9a-m** is outlined in Scheme 3.1. In detail, reaction of (±)-serine methyl ester hydrochloride **2** with *p*-toluenesulfonyl chloride afforded the derivative **3** which in turn was reacted with tert-butyl pyrocarbonate, (Boc)$_2$O, and a catalytic amount of 4-dimethylaminopyridine (DMAP) to give the dehydroalanine derivative **4** [6, 9]. Then the intermediate **4** was reacted with the appropriate β-diketone **5a-d**, using Cs$_2$CO$_3$ as a base, and the crude mixture was treated with 10% TFA in dichloromethane at room temperature to yield the pyrrole derivatives **6a**, its regioisomer **6b**, and **6c-e** (Scheme 3.1, Table II).

N-benzylation of **6a-e** with commercially available benzyl bromides afforded the esters **7a-j**, which in turn were hydrolyzed with 2M NaOH at room temperature.

The corresponding acids **8a-j** were precipitated by adding 2M HCl and subjected to a coupling reaction with an appropriate amine using 1-hydroxybenzotriazole (HOBT) and O-benzotriazol-1-yl-*N,N,N′,N′*-tetramethyluronium-hexafluorophosphate (HBTU) as coupling reagents in the presence of *N*-methylmorpholine (NMM) in DMF to provide the final compounds **1**, **9a-k** (Table I) in good yields. Compounds **9l** and (±)**9m** were obtained by reduction of **9d** (with Fe/NH$_4$Cl) and **1** (with NaBH$_4$) respectively.

Compounds 1-(4-methylphenyl)butane-1,3-dione **5b** and 1-(4-methoxyphenyl)butane-1,3-dione **5c** are not commercially available, and were synthesized as reported in Scheme 3.2, by condensation of 4-methylacetophenone **10a** and 4-methoxyacetophenone **10b** respectively in the presence of dry ethyl acetate and NaH (60% dispersion in mineral oil) [10].

Scheme 3.1

5a, R$_1$= H, R$_2$= CH$_3$
5b, R$_1$= R$_2$= CH$_3$
5c, R$_1$= OCH$_3$, R$_2$= CH$_3$
5d, R$_1$= H, R$_2$= phenyl

6a-e   **7a-j**   **8a-j**

1, 9a-k

h
(from 9d)

i
(from 1)

9l

9m
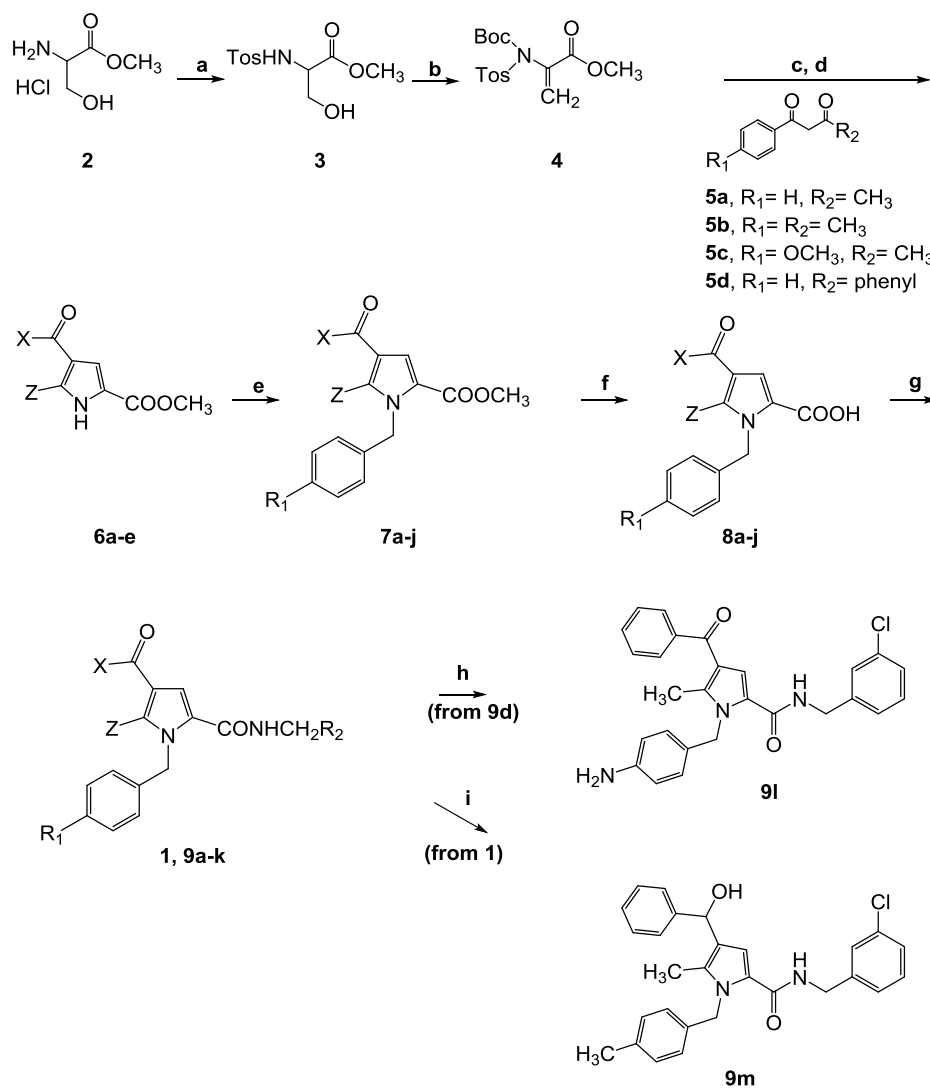
Reagents and conditions: *a) TsCl, TEA, DCM, rt, 12h; b) (Boc)$_2$O, DMAP; CH$_3$CN, rt, 3h; c) Cs$_2$CO$_3$, dry CH$_3$CN, 12h, rt; d) TFA, DCM, rt; e) 4X-BnBr, NaOH (50% w/v), TBAH, DCM, from 0° C to rt, 18h; f) NaOH 2M, MeOH, 70 °C, 2h; g) HOBT, HBTU, NMM, DMF, rt, 12h; h) Fe/NH$_4$Cl/THF, 100 °C; i) NaBH$_4$, EtOH, 80 °C, 4h.*

Table II. *Chemical structure of* **6a-e**, **7a-j** *and* **8a-j**

| | 6a-e | | | | | 7a-j, 8a-j | | | |
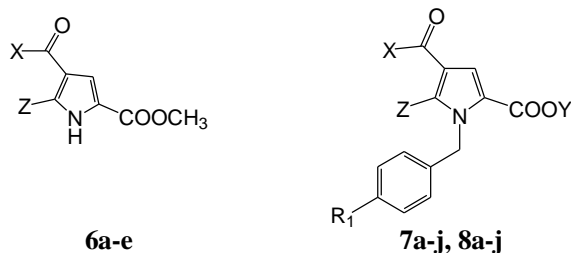
Cmps	X	Z	R_1	Y	Cmps	X	Z	R_1	Y
6a	C_6H_5	CH_3	-	-	7i	$(4\text{-}OCH_3)C_6H_4$	CH_3	CH_3	CH_3
6b	CH_3	C_6H_5	-	-	7j	C_6H_5	C_6H_5	H	CH_3
6c	$(4\text{-}CH_3)C_6H_5$	CH_3	-	-	8a	C_6H_5	CH_3	CH_3	H
6d	$(4\text{-}OCH_3)C_6H_5$	CH_3	-	-	8b	C_6H_5	CH_3	Cl	H
6e	C_6H_5	C_6H_5	-	-	8c	C_6H_5	CH_3	OCH_3	H
7a	C_6H_5	CH_3	CH_3	CH_3	8d	C_6H_5	CH_3	F	H
7b	C_6H_5	CH_3	Cl	CH_3	8e	C_6H_5	CH_3	NO_2	H
7c	C_6H_5	CH_3	OCH_3	CH_3	8f	C_6H_5	CH_3	H	H
7d	C_6H_5	CH_3	F	CH_3	8g	CH_3	C_6H_5	CH_3	H
7e	C_6H_5	CH_3	NO_2	CH_3	8h	$(4\text{-}CH_3)C_6H_4$	C_6H_5	CH_3	H
7f	C_6H_5	CH_3	H	CH_3	8i	$(4\text{-}OCH_3)C_6H_4$	CH_3	CH_3	H
7g	CH_3	C_6H_5	CH_3	CH_3	8j	C_6H_5	C_6H_5	H	H
7h	$(4\text{-}CH_3)C_6H_4$	CH_3	Cl	CH_3					

Scheme 3.2
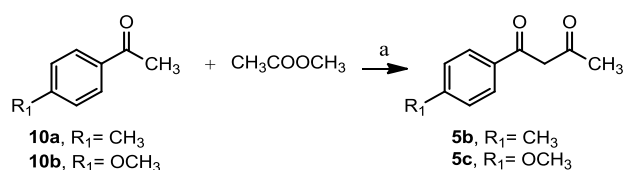
Reagents and conditions: *a) NaH (60 % dispersion in mineral oil), DMF dry, rt, 18h.*

3.4 Biological evaluation

In the first instance this small library of synthesized compounds was submitted to NHI/NCI (Bethesda, USA) for evaluation against the NCI-60 human cancer cell line panel. This panel is organized into subpanels representing leukemia, melanoma and cancers of lung, colon, kidney, ovary, breast, prostate and central

nervous system. Only two compounds **9a** (Exp ID: 1506OS04, NSC: D-784846/1) and **9k** (Exp ID: 1506OS04, NSC: D-784845/1) were selected and tested following the NCI protocol.

The standard NCI protocol provides for an initial assessment of the antiproliferative activity of submitted compounds at a single high concentration (10^{-5} M) (sulforhodamine, SRB, assay). Then, only compounds which satisfy pre-determined threshold inhibition criteria in a minimum number of cell lines progress to the full 5-concentration assay. The threshold inhibition criteria for progression to the 5-concentration screen is selected to efficiently capture compounds with anti-proliferative activity based on the analysis of historical NCI DTP database.

Compound **9a** showed a good antiproliferative activity on a prostate tumor cell line (PC-3), and on two colon cancer lines (HCT-116 and HCT-15), with percent growth (*PG*) of treated cells of 25.20%, 32.47%, and 34.06% respectively at the tested concentration of 10^{-5} M following 48 h incubation (Table III). Moreover, a percent growth of treated cells of ~ 40% was reported on a leukemia (SR, *PG*= 41.70%), two non-small cell lung cancer (HOP-92, *PG*= 42.59% and NCI-H522, *PG*= 42.24%), and on a CNS cancer (U251, *PG*= 42.73%) cell lines. Overall, compound **9k** was less active than **9a**; however a weak antiproliferative activity was reported on the following cancer cell lines: PC-3 (*PG*= 44.66%), HOP-92 (PG= 54.45%), NCI-H522 (*PG*= 52.85%) (Table III). Both **9a** and **9k** were not screened at concentrations below 10 μM because, according to the NCI standard procedure, this is provided only for the compounds which have a high growth inhibition activity against majority of tested cell lines.

All synthesized compounds **1**, **9a-c, 9e-m** were later investigated on three cell lines (MTT assay, see *Experimental Section, sec. 3.7.2*): HCT-116 (colon cancer), A375 (melanoma) and HaCat (immortalized human keratinocytes), using nutlin-3a (a well know p53/MDM2 inhibitor) as reference anticancer molecule (Table IV) (prof. C. Irace, University of Naples "Federico II").

In general, compared to A375 and HaCat cell lines, colon cancer line HCT-116 was less sensitive to tested compounds, with IC_{50} values ranging from 25 to 56 μM (**1**, **9a-c**, **9e-i**, **9k-m**), with the exception of **9j** whose IC_{50} value was >100

μM. Then, the introduction of a 4-methoxyphenyl group at the position 4 of the pyrrole ring was detrimental for activity against colon cancer line HCT-116 (**9j** *vs* **1**, **9i**). On the contrary, reduction of the carbonyl group at position 4 as in (±)**9m** improved the activity with respect to its oxidized counterpart **1** ((±)**9m**, IC$_{50}$= 25 ± 5 μM *vs* **1**, IC$_{50}$= 41.4 ± 6 μM), suggesting that the change of hybridization (i.e. from sp2 to sp3) as well as the introduction of an H-bond donor in this position can increase the antiproliferative activity against this cancer cell line.

On A375 cell line not significant difference in IC$_{50}$ values were observed among newly synthesized pyrrole derivatives compared to lead **1**, with the exception of **9c** bearing a strong electron-withdrawing fluorine atom at the *para* position on ring A (IC$_{50}$ = 12.9 ± 4 μM), and **9l**, bearing a 4-amino group in the same position (IC$_{50}$= 9.8 ± 4 μM) (Table IV). In particular, compound **9l** was the most active pyrrole derivative among tested compounds, resulting slightly more active than the reference compound nutlin-3a (Table IV), probably due to its better water solubility.

HaCat cell line is considered representative of a very early stage in skin tumorigenesis [11-13]. In general, on this cell line, tested compounds showed IC$_{50}$ values comparable than those reported on A375 cell line with some exceptions. In particular, compound **9e** (IC$_{50}$= 33 ± 7 μM) was twice less potent than its 3-chloro analogue **1** (IC$_{50}$= 16.9 ± 5 μM) evidencing that against this cancer line cell shifting chlorine atom from 3 to 4 position on ring B appreciably modify the antiproliferative activity. On the other hand, the introduction of a trifluoromethyl group on ring B and the presence of an unsubstituted benzyl group in position 1 of the pyrrole ring as in **9g** led to an increased activity on HaCat cell line compared to A375 and HCT-116 cell lines (Table IV). Moreover, CH$_3$/phenyl isomeric replacement in position 4/5 as in **9h** reduced twice the antiproliferative activity compared to led **1**, whereas the introduction of a phenyl group at the 5 position of the pyrrole ring was disfavored (**9k** *vs* **9g**). Finally, **9l** was confirmed as the most active pyrrole derivative of this series also against HaCat cell line, showing an IC$_{50}$ value of 10 ± 5 μM, and resulting slightly more active than reference compound nutlin-3a, evidencing that water solubility plays a key role in the antiproliferative activity of this series of compounds (Table IV).

For this pyrrole derivative a more deeper investigation is currently in progress in order to assess its apoptotic activity.

Table III. *Percent growth of compounds* **9a** *and* **9k**

	HCT-116	HCT-15	SR	PC-3	HOP-92	U251	NCI-H522
9a	**32.47**	**34.06**	**41.70**	**25.20**	**42.59**	**42.73**	62.20
9k	71.50	79.51	83.91	**44.66**	**54.45**	78.66	**52.85**

Table IV. *Inhibitory activity of compounds* **1**, **9a-m** *against HCT116, A375 and HaCat cell lines (IC$_{50}$, μM).*

Cpd	X	Y	Z	R$_1$	R$_2$	HCT-116 IC$_{50}$ (μM)^a	A375 IC$_{50}$ (μM)^a	HaCat IC$_{50}$ (μM)^a
1	C$_6$H$_5$	C=O	CH$_3$	CH$_3$	3-Cl	41.4±6	20 ± 4	16.9 ± 5
9a	C$_6$H$_5$	C=O	CH$_3$	Cl	3-Cl	36.4 ± 8	18 ± 4	18.8 ± 5
9b	C$_6$H$_5$	C=O	CH$_3$	OCH$_3$	3-Cl	46± 18	24± 14	20 ± 6
9c	C$_6$H$_5$	C=O	CH$_3$	F	3-Cl	55.9 ± 7	12.9 ± 4	20.6 ± 6
9d	C$_6$H$_5$	C=O	CH$_3$	NO$_2$	3-Cl	NT^b	NT^b	NT^b
9e	C$_6$H$_5$	C=O	CH$_3$	CH$_3$	4-Cl	35.4 ± 6	15 ± 5	33 ± 7
9f	C$_6$H$_5$	C=O	CH$_3$	Cl	4-Cl	34.6 ± 6	23 ± 6	21.4 ± 5
9g	C$_6$H$_5$	C=O	CH$_3$	H	3-CF$_3$	28.4 ± 7	26.9 ± 8	16.3 ± 6
9h	CH$_3$	C=O	C$_6$H$_5$	CH$_3$	3-Br	34 ± 6	18.4 ± 5	28.7 ± 6
9i	(4-CH$_3$)C$_6$H$_4$	C=O	CH$_3$	CH$_3$	3-Cl	56.3± 15	24 ± 6	23.5 ± 7
9j	(4-OCH$_3$)C$_6$H$_4$	C=O	CH$_3$	CH$_3$	3-Cl	167.6 ± 9	15.8 ±6	23.4 ± 6
9k	C$_6$H$_5$	C=O	C$_6$H$_5$	H	3-Cl	33.6 ± 5	22 ± 6	26.2 ± 4
9l	C$_6$H$_5$	C=O	CH$_3$	NH$_2$	3-Cl	41.3 ± 6	9.8 ± 4	10 ± 5
(±) 9m	C$_6$H$_5$	CHOH	CH$_3$	CH$_3$	3-Cl	25 ± 5	15 ± 5	23.9 ± 5
Nut-3a	-	-	-	-	-	12.5± 5	14.6± 3	12.7± 2

(a) IC$_{50}$ values are expressed as mean values ± SEM of three independent experiments; (b) NT, not tested.

3.5 Rational design of new analogues of 1

In general, achieving good water solubility is particularly challenging in the case of p53/MDM2 inhibitors, because of the hydrophobic nature of the p53 binding pocket in MDM2. The poor water solubility of many *in vitro* potent MDM2 (and/or MDM4) inhibitors often not allowed for a meaningful assessment of their cellular activity, because lack cellular permeability [14].

The solubility of all newly synthesized pyrrole derivatives **1**, **9a-c, 9e-m** was evaluated in the PBS (phosphate-buffered saline) solution (pH = 7.4) by Lipinski approach [3] (*sec. 3.7.3*); (±)**9m** was the most soluble derivative (10 μM), while **9a-c**, **9e-l** were less soluble, with values of solubility ranging from 1.4 to 2.6 μM, very close to that reported for **1** (2.3 μM).

Thus, in order to improve both pharmacodynamics and physiochemical properties, a second series of pyrroles analogues of **1** was designed, in which a polar substituent on **1** should be able to mimic the interaction of Leu22$_{(p53)}$ with Gln72$_{(MDM2)}$. As previously reported in this Chapter (*sec. 3.1*), Leu22 is part of the p53 binding motif ^{19}Fxx^{22}**L**^{23}Wxx^{26}L, and is located in a much more polar environment with respect to the crucial "*hot spot triad*" Phe19, Trp23 and Leu26.

With this in mind, the replacement of the carbonyl group with a polar substituent in position 4 of compound **1** was evaluated. In this regard, it is worth of note that a previously reported conformational analysis performed on the X-ray structure of the ^{19}FxxLWxxL^{26} motif of p53 in complex with HDM2 protein (PDB code 1YCR) evidenced that in CCC-III conformer rings X, Y and Z of **1** overlay *i*, *i+4* and *i+7* residues, while a substituent in position 4 could overlay *i+3* residue (that is Leu22 in p53 binding motif) (Figure 3.4) [6].

Unfortunately, all synthetic approaches evaluated to introduce a polar group at the position 4 of the pyrrole ring to test our hypothesis were unsuccessful (compounds **1a-d**, Scheme 3.3).

Figure 3.4 *Superimposition of CCC-III conformer of **1** on the i, i+ 4, i + 7 residues of*
[19]FxxLWxxL[26] motif in the 1YCR structure (carbons in pink). The motif backbone and interacting
amino acids are displayed as stick. Heteroatoms are colored by atom type: O, red; N, blue; Cl,
light green. Hydrogens are omitted for clarity. At the bottom: intramolecular distances (Å) of the
*conformational subfamily TCC-III of **1** considering the PM7 conformities within 5 kcal / mol from*
the global minimum

Distance (Å)						
Motif	**PDB ID**	*i, i+3*	*i, i+4*	*i, i+7*	*i+3, i+4*	*i+3, i+7*	*i+4, i+7*
[19]FxxLWxxL[26]	1YCR	**7.8**	**5.3**	**8.2**	**10.2**	**9.7**	**4.3**
Fam		d2 (Z-K)	d1 (Y-Z)	d3 (X-Z)	d4 (Y-K)	d6 (X-K)	d5 (X-Y)
TCC III		**-**	**5.6-**	**8.6**	**-**	**-**	**4.8**

Scheme 3.3
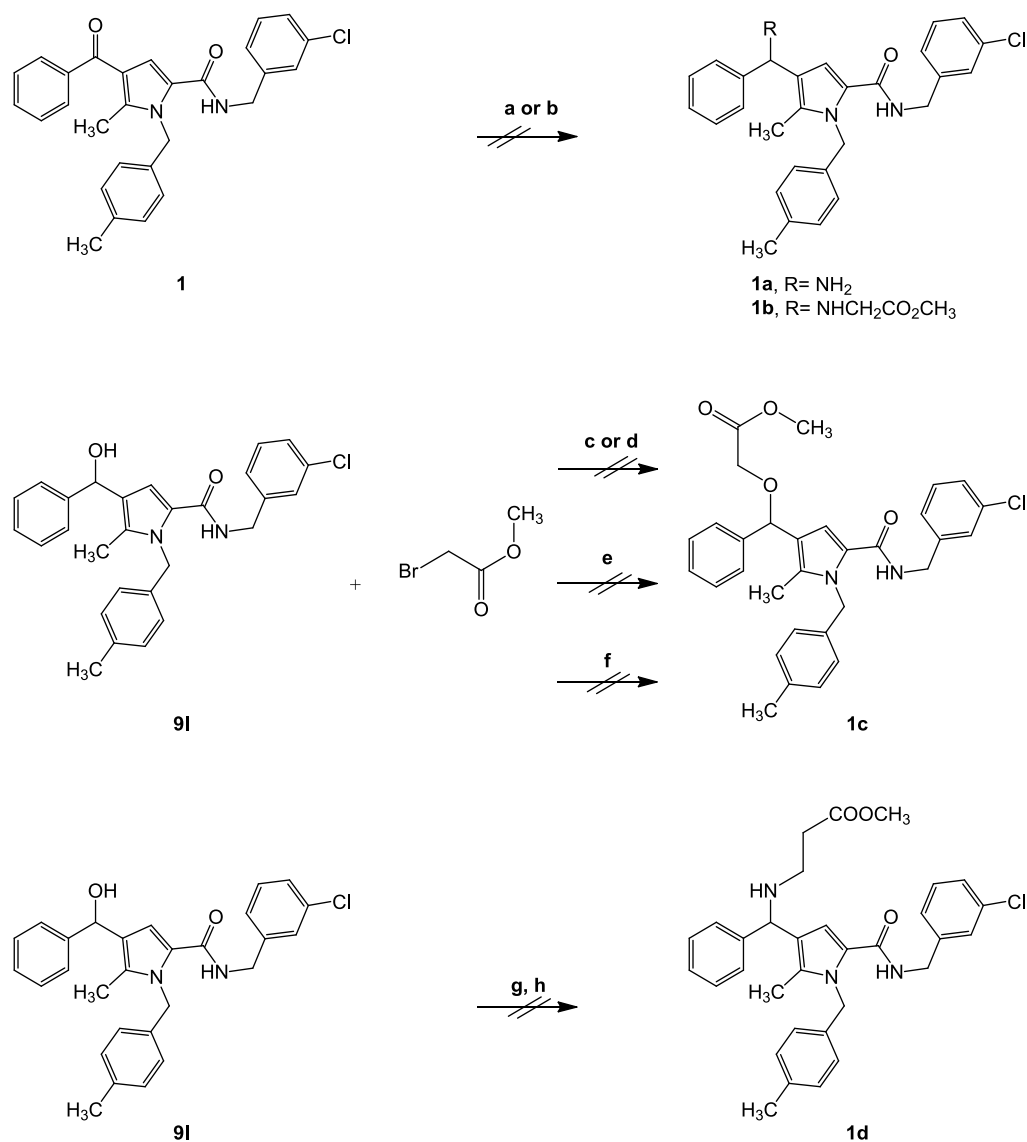
Reagents and conditions: *a) CH₃COONH₄, NaBH₃CN, EtOH, 130 °C, MW* [15]; *b) NH₂CH₂CO₂CH₃, NaBH₄, CH₃CN, rt; c) NaH (60% dispersion in mineral oil), dry DMF, rt, 12h; d) NaH (60% dispersion in mineral oil), dry DMF, rt, 12h, and then 4h, 70 °C; e) K₂CO₃, DMF, 12h, rt; f) TBAH, NaOH (50% w/v), DCM, 12h, rt; g) cyanuric chloride (NCCl)₃* [16]; *h) β-alanine, TEA, dry DMF, 12h.*

Thus, the design of the new series shifted to a synthetically affordable modification of the chemical skeleton of **1**. Accordingly, the hydrophilic moiety was introduced at the position 2 of the pyrrole ring; in addition, to guarantee the presence of the three aromatic moieties supposed to mimic the *hot-spot* residues, the methyl substituent at the position 5 of the pyrrole ring of **1** was replaced by an additional phenyl ring, as in compound **9k**.

In this regard, in the superimposition of TCC-II conformer of **9k** (Figures 3.5) rings X, Z and K can mimic the *i*, *i+4* and *i+7* residues of the [19]FxxLWxxL[26] motif of p53, while the ring Y overlays the *i+3* residue (i. e. p53's Leu22).
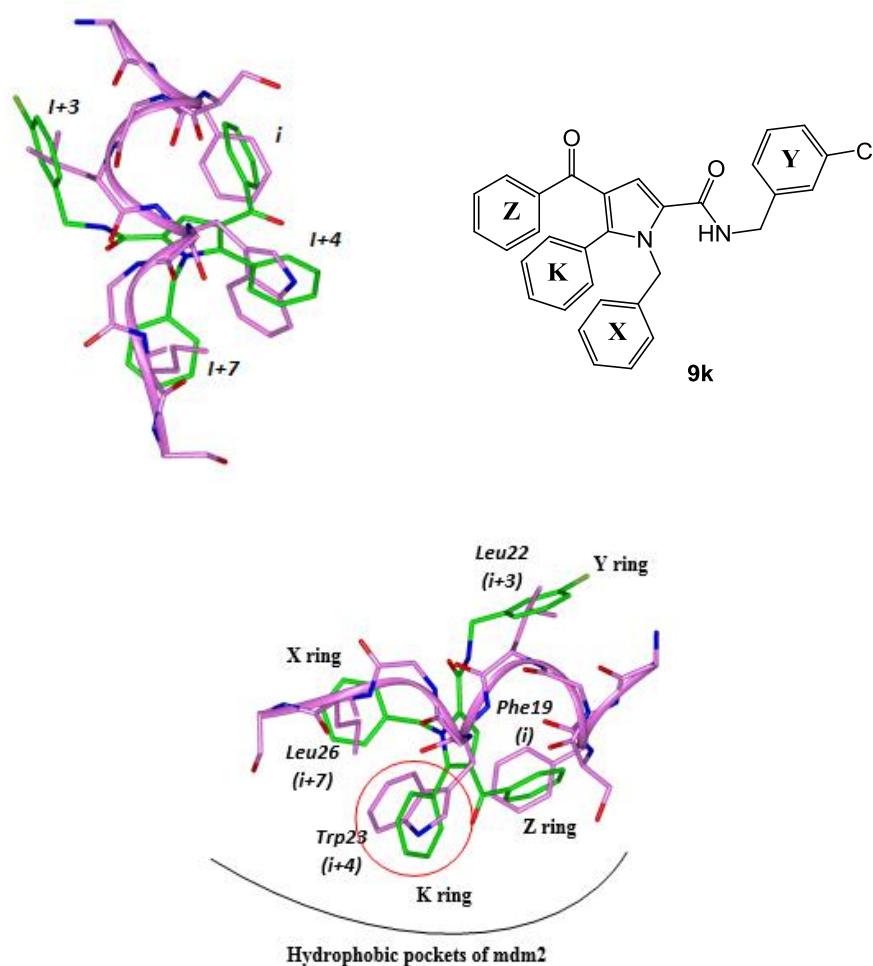
,

Distance (Å)							%
Motif	**PDB ID**	*i, i+3*	*i, i+4*	*i, i+7*	*i+3, i+4*	*i+3, i+7*	*i+4,i+7*	
[19]FxxLWxxL[26]	1YCR	**7.8**	**5.3**	**8.2**	**10.2**	**9.7**	**4.3**	
Fam		d2 (Z-K)	d1 (Y-Z)	d3 (X-Z)	d4 (Y-K)	d6 (X-K)	d5 (X-Y)	15.0
TCC II		8.0	7.0	9.0	10.3	8.8	5.4	

Figure 3.5 *Superimposition of TCC-II conformer of **9k** on the i, i+ 4, i + 7 residues of* *[19]FxxLWxxL[26] motif in the 1YCR structure (carbons in pink). The motif backbone and interacting amino acids are displayed as stick. Heteroatoms are colored by atom type: O, red; N, blue; Cl, light green. Hydrogens are omitted for clarity. At the bottom, intramolecular distances (Å) of the conformational subfamily TCC III of **9k** considering the PM7 conformities within 5 kcal/mol from the global minimum.*

The second series of pyrroles derivatives was designed and synthetized, in which the 3-chlorobenzyl moiety of **9k** was replaced by a more polar substituent (compounds **11a-n**, Table V, Scheme 3.4), with calculated $LogD_{7.2}$ values ranging from 0.7 to 5.6.

For all synthesized compounds a biological investigation is currently in progress in order to assess their antiproliferative activity.

Table V. *Compounds* **11a-n**
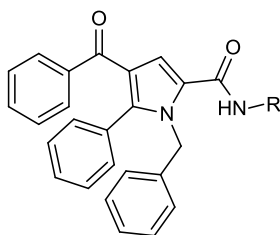
Cmp	R	$LogD_{7.2}$	Cmp	R	$LogD_{7.2}$
11a		5.2	11h		2.5
11b		3.6	11i		3.1
11c		3.6	11j		4.4
11d		4.8	11k		4.6
11e		4.9	11l		0.7
11f		1.1	11m		4.2
11g		5.6	11n		4.6

3.6 Synthesis of 11a-n

The synthesis of the amides **11a-n** is described in Scheme 3.4. Briefly, commercially available amines were coupled with **8j** employing 1-hydroxybenzotriazole (HOBT) and *O*-benzotriazol-1-yl-*N,N,N′,N′*-tetramethyluronium-hexafluorophosphate (HBTU) as coupling reagents in the presence of *N*-methylmorpholine (NMM) to give **11a-g**. The synthesis of pyrrole derivatives **11h,i** was accomplished in two steps, starting from **8j** which was coupled with *N*-Boc-1,2-ethylenediamine and *N*-Boc-1,3-propanediamine respectively employing HOBT/HBTU as coupling reagents. The corresponding amides **12a,b** were treated with TFA/DCM (1:1) to give the title compounds **11h,i** respectively in good yields.

The reaction of **11h,i** with methanesulfonyl chloride gave the corresponding methanesulfonyl amides **11j,k**.

The synthesis of **11l** was accomplished by reaction of **8j** with L-serine methyl ester to give **12c**, which in turn was hydrolyzed with 2M LiOH at room temperature.

The coupling of **8j** with 3-(aminomethyl)benzoic acid methyl ester **16** furnished the pyrrole intermediate **13** which in turn was hydrolyzed to the corresponding acid **11m**.

Then **11m** was converted to the corresponding amide **11n** by reaction with 1,1′-carbonyldiimidazole, [Bmim]BF_4 and CH_3COONH_4 [17].

The 3-(aminomethyl)benzoic acid methyl ester **16** was not commercially available, and then was synthesized starting from methyl 3-(bromomethyl)benzoate **14** which was converted in methyl 3-(azidomethyl)benzoate **15** by treatment with NaN_3. Then reduction of **15** with Zn/$HCOONH_4$ gave **16** in good yield [18].

Scheme 4

8j

11a-g
12a, R= CH$_2$CH$_2$NHBoc
12b, R= CH$_2$CH$_2$CH$_2$NHBoc
12c, R= CH(COOCH$_3$)(CH$_2$OH)

11h, n= 1, R= H
11i, n= 2, R= H
11j, n= 1, R= SO$_2$CH$_3$
11k, n= 2, R= SO$_2$CH$_3$
11l, R= CH(COOH)(CH$_2$OH)

13

11m, X= OH
11n, X= NH$_2$

14

15

16
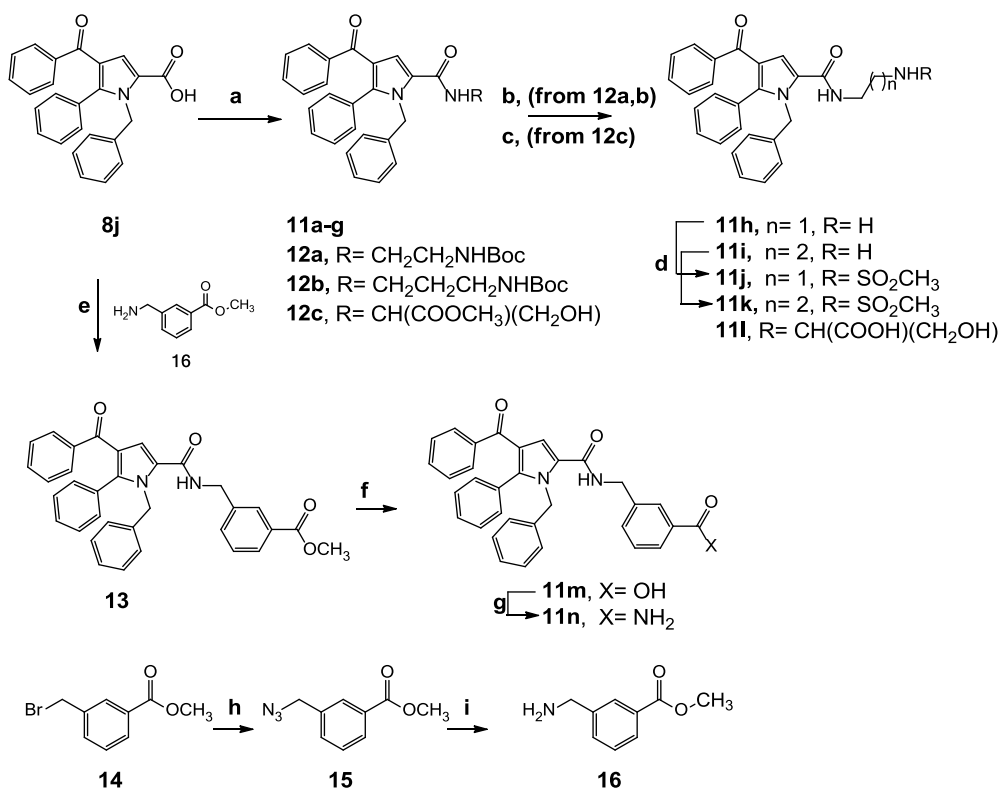
Reagents and conditions*: a) appropriate R-NH$_2$ (for **11a-g**), NH$_2$CH$_2$CH$_2$NHBoc (for **12a**), NH$_2$CH$_2$CH$_2$CH$_2$NHBoc (for **12b**), L-Ser(OCH$_3$) (for **12c**), HBTU, HOBT, DMF, NMM, 12h, rt; b) TFA, DMC, rt; c) LiOH, MeOH, rt; d) CH$_3$SO$_2$Cl, TEA, DCM; e) HBTU, HOBT, DMF, NMM, 12h, rt; f) NaOH 4N, MeOH, 80 °C; g) 1,1'-carbonyldiimidazole, [Bmim]BF$_4$, CH$_3$COONH$_4$, TEA, 80 °C, 12h; h) NaN$_3$, DMF, 80 °C; i) Zn/HCOONH$_4$, THF, 80 °C, 12h.*

3.7 Experimental Section

3.7.1 General

Melting points were taken on a Gallenkamp melting point apparatus. ^{1}H and ^{13}C NMR spectra were recorded at 300 and 75 MHz respectively, using a Bruker Avance 300 MHz spectrometer. Splitting patterns are described as singlet (s), doublet (d), triplet (t), quartet (q), quintuplet (qt), and broad (br). Mass spectra were obtained by electrospray ionization (ESIMS) using a Thermo Finningan LCQ Deca XP Max ion-trap mass spectrometer equipped with Xcalibur software and an LTQ Orbitrap XL mass spectrometer (Thermo FisherScientific, San Jose, CA, USA) operated in positive ion mode. The Orbitrap mass analyzer was calibrated according to the manufacturer's directions using a mixture of caffeine, methionine, arginine, phenylalanine and alanine-acetate (MRFA), and Ultramark 1621 in a solution of acetonitrile, methanol, and acetic acid. Chromatographic separations were performed on silica gel (Kieselgel 40, 0.040−0.063 mm, Merck). Reactions and product mixtures were routinely monitored by thin-layer chromatography (TLC) on Merck 0.2 mm precoated silica (60 F254) aluminum sheets, with visualization by irradiation with a UV lamp. All starting materials, reagents, and solvents (reagent grade) were purchased from Sigma-Aldrich and used without further purification.

Methyl 3-hydroxy-2-(4methylphenylsulfonamido)propanoate **3**
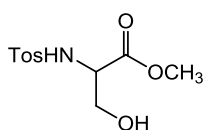
To a suspension of H-Ser-OMe-HCl (3.00 g, 19.3 mmol) in dichloromethane (40 mL) at 0°C, were added triethylamine (5.40 mL, 38.6 mmol), and then a solution of *p*-toluenesulfonyl chloride (3.68 g, 19.3 mmol) in dichloromethane. The reaction mixture was allowed to warm to room temperature, and stirred in these conditions overnight. The solvent was removed under reduced pressure, and the residue was taken up in ethyl acetate and washed with 1M KHSO$_4$, 1M NaHCO$_3$ and brine. Then the organic phase was dried (MgSO$_4$), filtered and solvent was

removed under vacuum. The resulting residue was crystallized by EtOAc/*n*-hexane (1:1) to give the title compound as a white powder.

Yield: 83%. ^{1}H NMR (CDCl$_3$) δ: 2.47 (s, 3H), 3.63 (s, 3H), 3.98 (s, 2H), 3.99-4.03 (m, 1H), 5.74 (d, 1H, *J*= 7.2 Hz), 7.32 (d, 2H, *J*= 8.1 Hz), 7.76 (d, 2H, *J*= 8.1 Hz).

Methyl 2-(N-(tert-butoxycarbonyl)-4-methylphenyl-sulfonamido)acrylate **4**
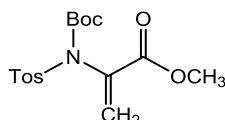
To a solution of Tos-Ser-OMe **3** in dry acetonitrile (10 mL), DMAP (0.09 g, 0.732 mmol) was added followed by (BOC)$_2$O (2.0 g, 9.15 mmol). The resulting mixture was vigorously stirred at room temperature for 6h. Then the solvent was removed under vacuum, and the resulting residue was taken up in EtOAc, and washed with 1M KHSO$_4$, 1M NaHCO$_3$ and brine. After crystallization by Et$_2$O/*n*-hexane the title compound was obtained as a white powder.

Yield: 85%. ^{1}H NMR (CDCl$_3$) δ: 1.32 (s, 9H), 2.45 (s, 3H), 3.78 (s, 3H), 6.06 (s, 1H), 6.59 (s, 1H), 7.32 (d, 2H, *J*= 8.1 Hz), 7.95 (d, 2H, *J*= 8.1 Hz).

Methyl 4-benzoyl-5-methyl-1H-pyrrole-2-carboxylate **6a**
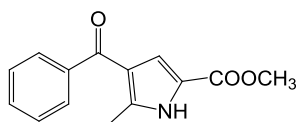
To a suspension of methyl 2-(*N*-(tert-butoxycarbonyl)-4-methylphenyl-sulfonamido)acrylate (**4**) in dry CH$_3$CN (10 mL), 1-phenyl-1,3-butanedione **5a** (0.46 g, 2.81 mmol) and Cs$_2$CO$_3$ (1.38 g, 4.22 mmol) were added and the resulting mixture was stirred at room temperature overnight. Then the solvent was removed under reduced pressure, and the resulting residue was dissolved in EtOAc, and washed with H$_2$O. The organic phase was dried (Na$_2$SO$_4$), filtered, and the solvent was removed under vacuum. The resulting residue was dissolved in DCM (10 mL), and TFA (2.1 mL) was added. After 12h the organic phase was washed with 1M NaOH and brine, dried (Na$_2$SO$_4$), filtered, and the solvent was removed under vacuum. The resulting residue was purified by flash column chromatography

(SiO$_2$, EtOAc/petroleum ether, 40−60 °C, 1:1 v/v) to give the title compound as a white powder.

Yield: 78%. ^{1}H NMR (CDCl$_3$) δ: 2.64 (s, 3H), 3.86 (s, 3H), 7.09 (d, 1H, *J*= 2.5 Hz), 7.44-7.57 (m, 3H), 7.79 (d, 2H, *J*= 7.1 Hz), 9.36 (brs, 1H).

Methyl 4-acetyl-5-phenyl-1H-pyrrole-2-carboxylate **6b**
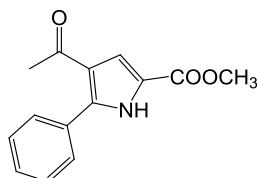
The title compound was a by-product of the reaction reported for **6a** and was obtained as a white powder.

Yield: 11%. ^{1}H NMR (CDCl$_3$) δ: 2.40 (s, 3H), 3.87 (s, 3H), 7.39 (m, 1H), 7.47 (m, 3H), 7.61 (m, 2H), 7.59 (brs, 1H).

Methyl 5-methyl-4-(4-methylbenzoyl)-1H-pyrrole-2-carboxylate **6c**
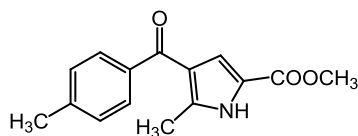
Starting from 1-(*p*-tolyl)butane-1,3-dione **5b** and following the same procedure described for **6a** the title compound was obtained as a white powder.

Yield: 65%. ^{1}H NMR (CDCl$_3$) δ: 2.45 (s, 3H), 2.65 (s, 3H), 3.87 (s, 3H), 7.11 (s, 1H), 7.28 (d, 2H, *J*= 7.6 Hz), 7.73 (d, 2H, *J*= 7.9 Hz), 9.56 (brs, 1H).

Methyl 4-(4-methoxybenzoyl)-5-methyl-1H-pyrrole-2-carboxylate **6d**
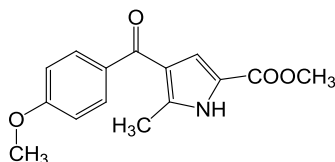
Starting from 1-(4-methoxyphenyl)butane-1,3-dione **5c** and following the same procedure described for **6a** the title compound was obtained as a white powder.

Yield: 58%. ^{1}H NMR (CDCl$_3$) δ: 2.64 (s, 3H), 3.88 (s, 3H), 3.90 (s, 3H), 6.98 (d, 2H, *J*= 8.7 Hz), 7.12 (s, 1H), 7.85 (d, 2H, *J*= 8.7 Hz), 9.52 (brs, 1H).

Methyl 4-benzoyl-5-phenyl-1H-pyrrole-2-carboxylate **6e**
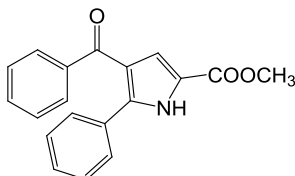
Starting from 1,3-diphenylpropane-1,3-dione **5d** and following the same procedure described for **6a** the title compound was obtained as a white powder.

Yield: 63%. ^{1}H NMR (CDCl$_3$) δ: 3.85 (s, 3H), 7.24 (m, 1H), 7.36-7.42 (m, 5H), 7.48-7.56 (m, 3H), 7.82 (d, 2H, *J*= 7.1 Hz), 9.76 (s, 1H); ^{13}C NMR (CDCl$_3$) δ: 51.9, 119.5, 121.8, 121.9, 128.1, 128.4, 128.8, 128.9, 129.6, 130.7, 132.1, 138.9, 140.8, 161.6, 191.6.

3.7.1.1 General Procedure for the Synthesis of Diketone Derivates **5b**, **c**

To a solution of the ketone **10a,b** (1 mmol) and dry ethyl acetate (1.2 mmol) in dry DMF (3 mL), NaH (60% w/w oil suspension, 1 mmol) was added. The reaction mixture was stirred at room temperature until no starting material was detected by TLC (*n*-hexane/AcOEt 7:3 as eluent, ca 4h). After cooling to 0 °C, the reaction mixture was acidified with 3M HCl to give a solid product which was washed with H$_2$O and recrystallized (H$_2$O/EtOH) to give the titles compounds **5b, c** in good yields.

1-(p-Tolyl)butan-1,3-dione **5b**
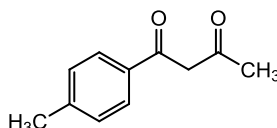
White powder.

Yield: 73%. ^{1}H NMR (CDCl$_3$) δ: 2.22 (s, 3H), 2.44 (s, 3H), 6.19 (s, 1H), 7.28 (d, 2H, *J*= 8.0 Hz), 7.81 (d, 2H, *J*= 8.0 Hz).

1-(4-Methoxyphenyl)butane-1,3-dione **5c**
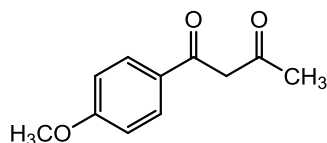
White powder.

Yield: 68%. ^{1}H NMR (CDCl$_3$) δ: 2.19 (s, 3H), 3.88 (s, 3H), 6.13 (s,1H), 6.97 (d, 2H, *J*= 5.4 Hz), 7.89 (d, 2H, *J*= 5.4) 16.31 (s, 1H).

3.7.1.2 General Procedure for the Synthesis of Esters **7a-j**

Sodium hydroxide (8 mL, 50% w/v) and tetra-*n*-butylammonium hydroxide (TBAH) (0.1 mL, 40% w/v) were added to a stirred mixture of esters **6a-e** (1 mmol) in dichloromethane (10 mL) at 0 °C. After 15 min, a solution of the appropriate aryl bromide (1.5 mmol) in dichloromethane (5 mL) was added dropwise.

The resulting mixture was allowed to warm to room temperature, stirred in these conditions overnight, and then neutralized with 2M HCl.

The organic phase was washed with brine, dried (Na$_2$SO$_4$), filtered, and the solvent was removed under vacuum. The resulting residue was purified by flash chromatography (SiO$_2$, EtOAc/*n*-hexane, 1:4 v/v).

Methyl 4-benzoyl-5-methyl-1-(4-methylbenzyl)-1H-pyrrole-2-carboxylate **7a**
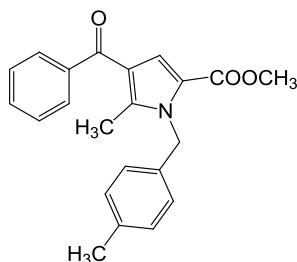
White powder. Yield: 86%, mp: 98-100 °C. ^{1}H NMR (CDCl$_3$) δ: 2.34 (s, 3H), 2.59 (s, 3H), 3.77 (s, 3H), 5.69 (s, 2H), 6.92 (d, 2H, *J*= 7.9 Hz), 7.14 (d, 2H, *J*= 7.9 Hz), 7.26 (s, 1H), 7.48-7.60 (m, 3H), 7.83 (d, 2H, *J*= 6.9 Hz).

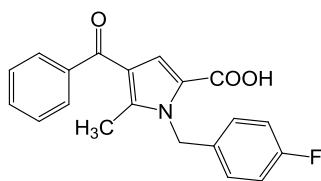*Methyl 4-benzoyl-1-(4-chlorobenzyl)-5-methyl-1H-pyrrole-2-carboxylate* **7b**
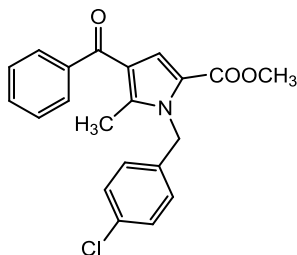
White powder. Yield: 67%. ^{1}H NMR (CDCl$_3$) δ: 2.58 (s, 3H), 3.77 (s, 3H), 5.69 (s, 2H), 6.96 (d, 2H, J = 8.2 Hz), 7.26-7.32 (m, 3H), 7.48-7.61 (m, 3H), 7.83 (d, 2H, J= 7.1 Hz).

Methyl 4-benzoyl-1-(4-methoxybenzyl)-5-methyl-1H-pyrrole-2-carboxylate **7c**
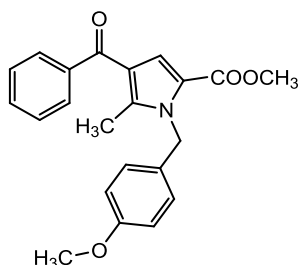
White powder. Yield: 74%. ^{1}H NMR (CDCl$_3$) δ: 2.62 (s, 3H), 3.80 (s, 3H), 3.82 (s, 3H), 5.68 (s, 2H), 6.88 (d, 2H, J= 8.7 Hz), 7.00 (d, 2H, J= 8.7 Hz), 7.26 (s, 1H), 7.49-7.61 (m, 3H), 7.84 (d, 2H, J= 8.4 Hz).

*Methyl 4-benzoyl-1-(4-fluorobenzyl)-5-methyl-1H-pyrrole-2-carboxylate* **7d**
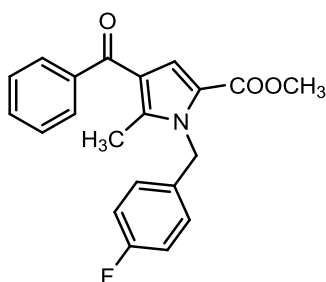
White solid. Yield: 66%, mp: 87-89 °C. ^{1}H NMR (CDCl$_3$) δ: 2.58 (s, 3H), 3.77 (s, 3H), 5.68 (s, 2H), 7.01 (m, 4H), 7.26 (s, 1H), 7.46-7.57 (m, 3H), 7.82 (d, 2H, J= 6.8 Hz).

Methyl 4-benzoyl-5-methyl-1-(4-nitrobenzyl)-1H-pyrrole-2-carboxylate **7e**
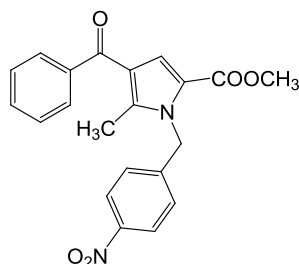
White solid. Yield: 68%, mp: 164-166 °C. ^{1}H NMR (CDCl$_3$) δ: 2.58 (s, 3H), 3.77 (s, 3H), 5.81 (s, 2H), 7.17 (d, 2H, *J*= 8.4 Hz), 7.30 (s, 1H), 7.49-7.62 (m, 3H), 7.84 (d, 2H, *J* = 7.1 Hz), 8.22 (d, 2H, *J*= 8.5 Hz).

Methyl 4-benzoyl-1-benzyl-5-methyl-1H-pyrrole-2-carboxylate **7f**
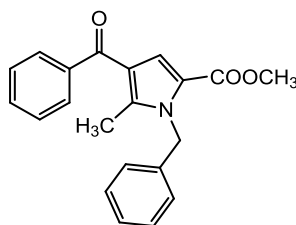
White solid. Yield: 89%, mp: 93−95 °C. ^{1}HNMR (CDCl$_3$) δ: 2.59 (s, 3H), 3.77 (s, 3H), 5.74 (s, 2H), 7.02 (d, 2H, *J*= 7.5 Hz), 7.27-7.36 (m, 4H), 7.48-7.58 (m, 3H), 7.84 (d, 2H, *J*= 7.8 Hz).

Methyl-4-acetyl-1-(4-methylbenzyl)-5-phenyl-1H-pyrrole-2-carboxylate **7g**
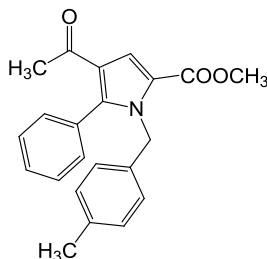
White solid. Yield: 77%, mp: 116-118 °C. ^{1}H NMR (CDCl$_3$) δ: 2.30 (s, 3H), 3.81 (s, 3H), 5.39 (s, 2H), 6.68 (d, 2H, *J*= 8.0 Hz), 7.03 (d, 2H, *J*= 8.0 Hz), 7.23 (d, 2H, *J*= 8.0 Hz), 7.37-7.47 (m, 4H).

Methyl 5-methyl-4-(4-methylbenzoyl)-1-(4-methylbenzyl)-1H-pyrrole-2-carboxylate **7h**
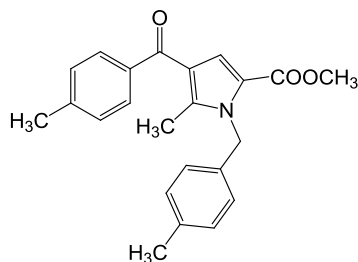
White solid. Yield: 73%, mp: 110-112 °C. ^{1}H NMR (CDCl$_3$) δ: 2.33 (s, 3H), 2.45 (s, 3H), 2.57 (s, 3H), 3.77 (s, 3H), 5.68 (s, 2H), 6.91 (d, 2H, *J*= 7.5 Hz), 7.13 (d, 2H, *J*= 7.5 Hz), 7.26-7.31 (m, 3H), 7.75 (d, 2H, *J*= 7.8 Hz).

Methyl 4-(4-methoxybenzoyl)-5-methyl-1-(4-methylbenzyl)-1H-pyrrole-2-carboxylate **7i**
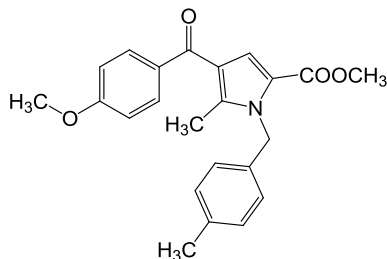
White solid. Yield: 79%, mp: 129-132 °C. ^{1}H NMR (CDCl$_3$) δ: 2.33 (s, 3H), 2.54 (s, 3H), 3.77 (s, 3H), 3.90 (s, 3H), 5.67 (s, 2H), 6.91 (d, 2H, *J*= 7.5 Hz), 6.98 (d, 2H, *J*= 7.9 Hz), 7.13 (d, 2H, *J*= 7.8 Hz), 7.27 (s, 1H), 7.86 (d, 2H, *J*= 7.2 Hz).

*Methyl 4-benzoyl-1-benzyl-5-phenyl-1H-pyrrole-2-carboxylate* **7j**
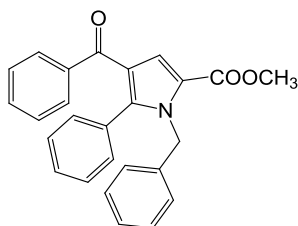
White solid. Yield: 79%, mp: 117-120 °C. ^{1}H NMR (CDCl$_3$) δ: 3.81 (s, 3H), 5.59 (s, 2H) 6.89 (d, 2H, *J*= 6.3 Hz), 7.25-7.52 (m, 3H) 7.80 (d, 2H, *J*= 7.0 Hz); ^{13}C NMR (CDCl$_3$) δ 49.2, 51.4, 121.2, 122.1 (2C), 125.9, 127.1, 128.0, 128.2, 128.5, 129.0, 129.4, 130.3, 130.5, 131.8, 138.1, 138.9, 144.7, 161.1, 190.9.

3.7.1.3 General Procedure for the Synthesis of Acids **8a-j**

To a solution of esters **7a-j** (1 mmol) in methanol (10 mL) 2M NaOH (5 mmol) was added, and the resulting mixture was refluxed until no starting material was detected by TLC (DCM as eluent). The solvent was removed under reduced pressure, then the residue was acidified with 2M HCl (pH ∼ 3), and extracted with EtOAc. The organic phase was dried (Na_2SO_4), filtered, and the solvent was removed under vacuum. The resulting residue was purified by flash chromatography (SiO_2, EtOAc/EtOH, 9:1 v/v, as eluent) and recrystallized from ethyl ether/petroleum ether (40−60 °C).

4-Benzoyl-5-methyl-1-(4-methylbenzyl)-1H-pyrrole-2-carboxylic acid **8a**
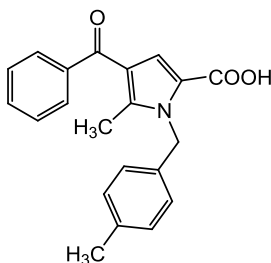
White solid. Yield: 97%, mp: 158-160 °C. ^{1}H NMR ($CDCl_3$) δ: 2.34 (s, 3H), 2.59 (s, 3H), 5.66 (s, 2H), 6.91 (d, 2H, *J*= 8.0 Hz), 7.13 (d, 2H, *J*= 7.9 Hz), 7.38 (s, 1H), 7.46-7.60 (m, 3H), 7.83 (d, 2H, *J*= 6.9 Hz).

4-Benzoyl-1-(4-chlorobenzyl)-5-methyl-1H-pyrrole-2-carboxylic acid **8b**
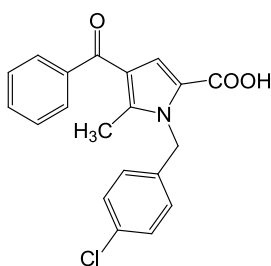
White solid. Yield: 95%, mp: 163-165 °C. ^{1}H NMR ($CDCl_3$) δ: 2.45 (s, 3H), 5.73 (s, 2H), 7.02 (s, 1H), 7.05 (s, 2H), 7.40 (d, 2H, *J*= 8.4 Hz), 7.51-7.65 (m, 3H), 7.72 (d, 2H, *J*= 6.8 Hz).

4-Benzoyl-1-(4-methoxybenzyl)-5-methyl-1H-pyrrole-2-carboxylic acid **8c**
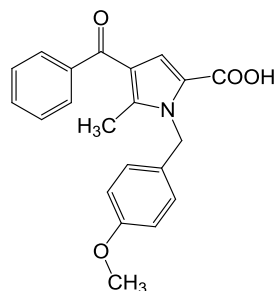
White solid. Yield: 97%. ^{1}H NMR (CDCl$_3$) δ: 2.61 (s, 3H), 3.81 (s, 3H), 5.64 (s, 2H), 6.87 (d, 2H, *J*= 8.6 Hz), 6.99 (d, 2H, *J*= 8.5 Hz), 7.40 (s, 1H), 7.48-7.61 (m, 3H), 7.84 (d, 2H, *J*= 7.2 Hz).

4-Benzoyl-1-(4-fluorobenzyl)-5-methyl-1H-pyrrole-2-carboxylic acid **8d**

White solid. Yield: 96%, mp: 187-188 °C. ^{1}H NMR (DMSO*d$_6$*) δ: 2.50 (s, 3H), 5.73 (s, 2H), 7.07 (m, 3H), 7.18 (m, 2H), 7.51-7.64 (m, 3H), 7.72 (d, 2H, *J*= 7.2 Hz).

4-Benzoyl-5-methyl-1-(4-nitrobenzyl)-1H-pyrrole-2-carboxylic acid **8e**
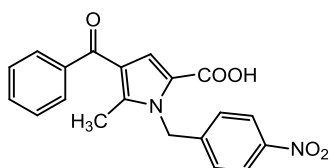
White solid. Yield: 93%, mp: 219-220 °C. ^{1}H NMR (DMSO-*d$_6$*) δ: 2.45 (s, 3H), 5.88 (s, 2H), 7.07 (s, 1H), 7.25 (d, 2H, *J*= 8.4 Hz), 7.52-7.66 (m, 3H), 7.74 (d, 2H, *J*= 7.1 Hz), 8.22 (d, 2H, *J*= 8.5 Hz).

4-Benzoyl-1-benzyl-5-methyl-1H-pyrrole-2-carboxylic acid **8f**
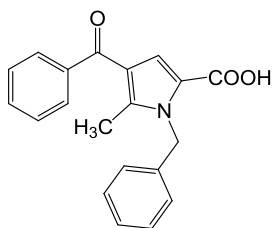
White solid. Yield: 97%, mp: 186-187 °C. ^{1}H NMR (CDCl$_3$) δ: 2.61 (s, 3H), 3.81 (s, 3H), 5.64 (s, 2H), 6.87 (d, 2H, *J*= 8.6 Hz), 6.99 (d, 2H, *J*= 8.5 Hz), 7.40 (s, 1H), 7.48-7.61 (m, 3H), 7.84 (d, 2H, *J*= 7.2 Hz).

4-Acetyl-1-(4-methylbenzyl)-5-phenyl-1H-pyrrole-2-carboxylic acid **8g**
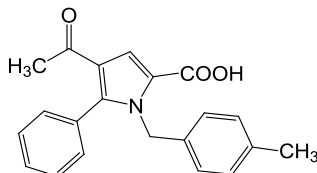
White solid. Yield: 78%, mp: 173-175 °C. ^{1}H NMR (CDCl$_3$) δ: 2.14 (s, 3H), 2.30 (s, 3H), 5.37 (s, 2H), 6.68 (d, 2H, *J*=7.7 Hz), 7.03 (d, 2H, *J*=7.7 Hz), 7.38-7.49 (m, 3H), 7.69 (s, 1H).

5-Methyl-4-(4-methylbenzoyl)-1-(4-methylbenzyl)-1H-pyrrole-2-carboxylic acid **8h**
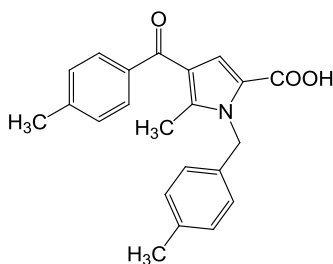
White solid. Yield: 93%, mp: 193-195 °C. ^{1}H NMR (CDCl$_3$) δ: 2.33 (s, 3H), 2.45 (s, 3H), 2.56 (s, 3H), 5.65 (s, 2H), 6.91 (d, 2H, *J*= 7.2 Hz), 7.13 (d, 2H, *J*= 7.2 Hz), 7.28 (d, 2H, *J*= 7.5 Hz), 7.38 (s, 1H), 7.74 (d, 2H, *J*= 7.8 Hz).

4-(4-Methoxybenzoyl)-5-methyl-1-(4-methylbenzyl)-1H-pyrrole-2-carboxylic acid **8i**
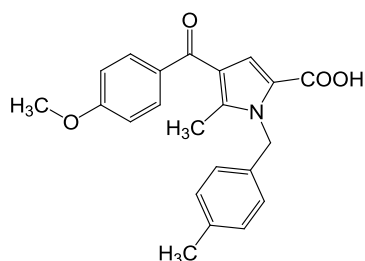
White solid. Yield: 93%, mp: 202-204 °C. ^{1}H NMR (CDCl$_3$) δ: 2.33(s, 3H), 2.54 (s, 3H), 3.90 (s, 3H), 5.65 (s, 2H), 6.91 (d, 2H, *J*=7.6 Hz), 6.98 (d, 2H, *J*=8.4 Hz), 7.12 (d, 2H, *J*= 7.7 Hz), 7.39 (s, 1H), 7.85 (d, 2H, *J*= 8.4 Hz).

4-Benzoyl-1-benzyl-5-phenyl-1H-pyrrole-2-carboxylic acid **8j**
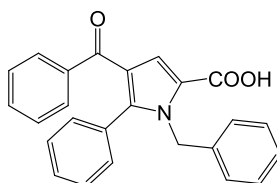
White solid. Yield: 89%, mp: 181-183 °C. ^{1}H NMR (DMSO-d_6) δ: 5.54 (s, 2H), 6.77 (d, 2H, *J*= 6.9 Hz), 7.16-7.54 (m, 12H), 7.65 (d, 2H, *J*= 7.0 Hz); ^{13}C NMR (CDCl$_3$) δ: 49.3, 121.2, 122.5, 123.2, 125.9, 127.3, 128.1, 128.3, 128.5, 129.2, 129.4, 130.1, 130.4, 131.5, 137.8, 138.8, 145.8, 164.9, 190.8.

3.7.1.4 General Procedure for the Synthesis of Compounds **1, 9a-k, 11a-l** *and* **13**

To a solution of the acids **8a**-**j** (1 mmol) in DMF (5 mL) HOBT (2.5 mmol) and HBTU (2.5 mmol) were added, and the resulting mixture was stirred for 20 min at room temperature. Then *N*-methylmorpholine (NMM) (5 mmol) and the appropriate amine (2.5 mmol) were added, and the resulting mixture was stirred at room temperature overnight. The solvent was removed under reduced pressure, and the resulting residue was taken up in EtOAc and washed successively with 2M KHSO$_4$, saturated solution of NaHCO$_3$, and brine. The organic phase was dried (Na$_2$SO$_4$), filtered, and concentrated under reduced pressure. The residue was purified by flash chromatography (SiO$_2$, EtOAc/petroleum ether (40-60 °C)

1:1 v/v as eluent) and recrystallized from EtOAc/*n*-hexane to give the title compounds **1, 9a-k, 11a-l** and **13** in good yields.

4-Benzoyl-5-methyl-1-(4-methyl-benzyl)-1H-pyrrole-2-carboxylic acid 3-chloro-benzylamide **1**
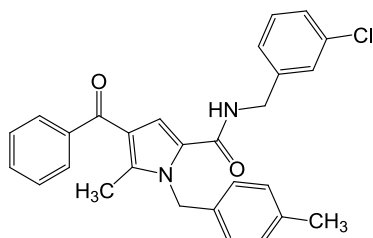
White solid. Yield: 71%, mp: 167-168 °C. ^{1}H NMR (CDCl$_3$) δ: 2.35 (s, 3H), 2.56 (s, 3H), 4.47 (d, 2H, *J*= 5.9 Hz); 5.70 (s, 2H), 6.13 (brt, 1H, *J*= 5.6 Hz), 6.80 (s, 1H), 6.92 (d, 3H, *J*= 7.9 Hz), 7.11-7.27 (m, 3H), 7.45-7.58 (m, 3H), 7.78 (d, 2H, *J*= 6.9 Hz); ^{13}C NMR δ: 11.9, 21.1, 42.6, 47.9, 115.1, 119.9, 124.7, 126.2, 128.3, 128.8, 129.0, 129.1, 129.4, 131.6, 133.2, 134.2, 136.8, 137.0, 140.1, 141.9, 161.4, 192.0. HRMS (ESI) *m/z* 457.1663 [M+H]$^+$ (calcd. for [C$_{28}$H$_{26}$ClN$_2$O$_2$]$^+$ 457.1683).

4-Benzoyl-1-(4-chloro-benzyl)-5-methyl-1H-pyrrole-2-carboxylic acid 3-chloro-benzylamide **9a**
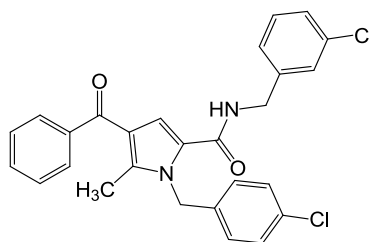
White solid. Yield: 89%, mp: 117-119 °C. ^{1}H NMR (CDCl$_3$) δ: 2.55 (s, 3H), 4.49 (d, 2H, *J*=6.0 Hz), 5.72 (s, 2H), 6.17 (brt, 1H, *J*= 3.4 Hz), 6.84 (s, 1H), 6.99 (d, 2H, *J*= 8.4 Hz), 7.07 (d, 1H, *J*= 6.0 Hz), 7.24-7.32 (m, 5H), 7.47-7.59 (m, 3H), 7.79 (d, 2H, *J*= 8.4Hz); ^{13}C NMR δ: 11.8, 42.7, 47.6, 115.3, 124.4, 125.6, 127.6, 127.7 (2C), 129.0, 129.1, 130.0, 131.8, 133.2, 134.5, 135.8, 139.9, 140.3, 141.8, 161.2, 192.0. HRMS (ESI) *m/z* 477.1126 [M+H]$^+$ (calcd. for [C$_{27}$H$_{23}$O$_2$N$_2$Cl$_2$]$^+$ 477.1137).

4-Benzoyl-1-(4-methoxy-benzyl)-5-methyl-1H-pyrrole-2-carboxylic acid 3-chloro-benzylamide **9b**
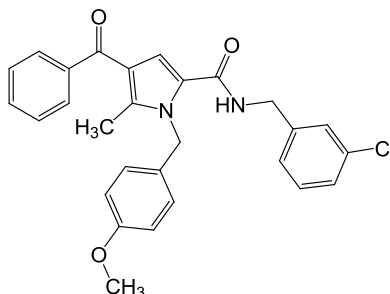
White solid. Yield: 81%, mp: 137-138 °C. ^{1}H NMR CDCl$_3$ δ: 2.57 (s, 3H), 3.80 (s, 3H), 4.49 (d, 2H, *J*= 5.9 Hz), 5.67 (s, 2H), 6.15 (brt, 1H, *J*= 5.4 Hz), 6.81 (s, 1H), 6.85 (d, 2H, *J*= 7.6 Hz), 7.04 (d, 2H, *J*= 8.3 Hz), 7.08 (d, 1H, *J*= 4.8 Hz), 7.25 (m, 3H), 7.45- 7.58 (m, 3H), 7.78 (d, 2H, *J*= 7.9 Hz); ^{13}C NMR (CDCl$_3$) δ:12.0, 42.7, 47.6, 55.3, 90.0, 114.2, 115.2, 120.0, 124.5, 125.8, 127.7 (2C), 128.3, 129.1, 129.3, 130.0, 131.6, 134.6, 140.0, 140.3, 142.9, 158.8, 161.4, 192.0. HRMS (ESI) *m/z* 458.1624 [M+H]$^+$ (calc. for [C$_{27}$H$_{25}$ClN$_3$O$_2$]$^+$ 473.1052).

4-Benzoyl-1-(4-fluoro-benzyl)-5-methyl-1H-pyrrole-2-carboxylic acid 3-chloro-benzylamide **9c**
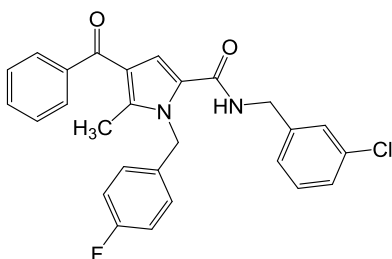
White solid. Yield: 69%, mp: 130-132 °C. ^{1}H NMR (CDCl$_3$) δ: 2.54 (s, 3H), 4.48 (d, 2H, *J*= 6.0 Hz), 5.70 (s, 2H), 6.24 (brt, 1H, *J*= 5.4 Hz), 6.84 (s, 1H), 6.26-7.09 (m, 5H), 7.23 (m, 3H), 7.45-7.58 (m, 3H), 7.78 (d, 2H, *J*= 8.4 Hz); ^{13}C NMR (CDCl$_3$) δ: 11.9, 42.7, 47.5, 115.3, 115.7 (^{2}d, *J*$_{CF}$= 21.6 Hz), 120.1, 124.4, 125.7, 127.7 (^{4}d, *J*$_{CF}$ = 3.1 Hz), 128.0 (^{3}d, *J*$_{CF}$= 8.1 Hz), 128.3, 129.1, 130.0, 131.7, 132.9, 133.0, 134.6, 139.9, 140.3, 141.7, 161.3, 162.0 (^{1}d, *J*$_{CF}$ = 245.8 Hz), 192.0. HRMS (ESI) *m/z* 461.1422 [M+H]$^+$ (calcd. for [C$_{27}$H$_{23}$O$_2$N$_2$ClF]$^+$, 461.1432).

4-Benzoyl-5-methyl-1-(4-nitro-benzyl)-1H-pyrrole-2-carboxylic acid 3-chloro-benzylamide **9d**
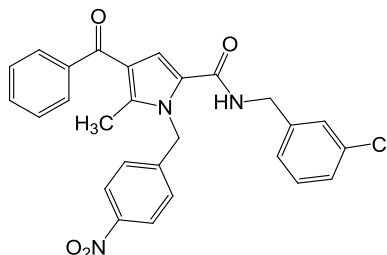
White solid. Yield: 87%. ^{1}H NMR (CDCl$_3$) δ: 2.54 (s, 3H), 4.47 (d, 2H, *J*= 6.0 Hz), 5.85 (s, 2H), 6.25 (brt, 1H, *J*= 5.4 Hz), 6.89 (s, 1H), 7.10 (d, 1H, *J*= 5.0 Hz), 7.19-7.28 (m, 5H), 7.47-7.60 (m, 3H), 7.80 (d, 2H, *J*= 7.7 Hz), 8.20 (d, 2H, *J*= 8.2 Hz); ^{13}C NMR (CDCl$_3$) δ: 11.6, 42.6, 47.8, 115.4, 120.4, 123.9, 124.3, 125.6, 126.8, 127.5, 127.5, 128.2, 128.9, 129.8, 131.7, 134.4, 139.6, 140.3, 141.3, 144.7, 147.2, 161.1, 191.7. ESIMS *m/z* 489.1 [M + H]$^+$.

4-Benzoyl-5-methyl-1-(4-methyl-benzyl)-1H-pyrrole-2-carboxylic acid 4-chloro-benzylamide **9e**
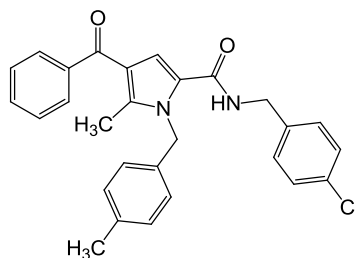
White solid. Yield: 90%, mp: 154-156 °C. ^{1}H NMR (CDCl$_3$) δ: 2.34 (s, 3H), 2.55 (s, 3H), 4.49 (d, 2H, *J*= 5.9 Hz), 5.71 (s, 2H), 6.19 (brt, 1H, *J*= 5.5 Hz), 6.82 (s, 1H), 6.94 (d, 2H, *J*= 7.7 Hz), 7.08-7.24 (m, 6H), 7.45-7.55 (m, 3H), 7.79 (d, 2H, *J*= 7.8 Hz); ^{13}C NMR(CDCl$_3$) δ: 11.9, 21.1, 42.7, 47.9 115.2, 120.0, 124.7, 125.7, 126.2, 127.6, 127.7, 128.2, 129.0, 129.4, 129.9, 131.5, 134.2, 134.5, 137.0, 140.1, 140.4, 141.8, 161.4, 191.9. HRMS (ESI) *m/z* 457.1669 [M+H]$^+$ (calcd. for [C$_{28}$H$_{26}$O$_2$N$_2$Cl]$^+$, 457.1683).

4-Benzoyl-1-(4-chloro-benzyl)-5-methyl-1H-pyrrole-2-carboxylic acid 4-chloro-benzylamide **9f**
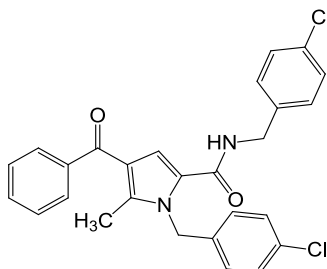
White solid. Yield: 68%, mp: 147-149 °C. ^{1}H NMR (CDCl$_3$) δ: 2.54 (s, 3H), 4.46 (d, 2H, *J*= 5.9 Hz), 5.70 (s, 2H), 6.16 (brt, 1H, *J*= 5.4 Hz), 6.82 (s, 1H), 6.98 (d, 2H, *J*= 8.4 Hz), 7.12 (d, 2H, *J*= 8.4 Hz), 7.26-7.31 (m, 4H), 7.46-7.59 (m, 3H), 7.78 (d, 2H, *J*= 6.9 Hz); ^{13}C NMR (CDCl$_3$): 11.8, 42.6, 47.6, 115.2, 120.1, 124.5, 127.7, 128.3, 128.8, 129.0 (2C), 128.1, 131.7, 133.2, 133.4, 135.8, 136.6, 139.9, 141.7, 161.2, 192.0. HRMS (ESI) *m/z* 477.1122 [M+H]$^+$ (calcd. for [C$_{27}$H$_{23}$O$_2$N$_2$Cl$_2$]$^+$ 477.1137).

4-Benzoyl-1-benzyl-5-methyl-1H-pyrrole-2-carboxylic acid 3-trifluoromethyl-benzylamide **9g**
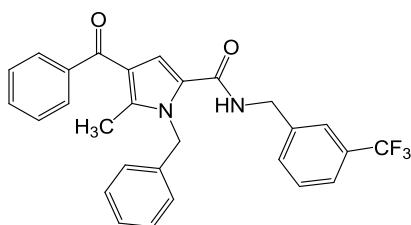
White solid. Yield: 87%, mp: 139-141 °C. ^{1}H NMR (CDCl$_3$) δ: 2.55 (s, 3H), 4.57 (d, 2H, *J*= 6.1 Hz), 5.77 (s, 2H), 6.21 (brt, 1H, *J*= 5.5 Hz), 6.85 (s, 1H), 7.04 (d, 2H, *J*= 6.5 Hz), 7.29-7.56 (m, 10H), 7.79 (d, 2H, *J* = 6.9 Hz); ^{13}C NMR (CDCl$_3$) δ: 11.9, 42.8, 48.1, 115.4, 120.0, 124.2 (2C), 124.3 (2C), 124.4, 124.5, 127.4, 128.3, 128.8, 129.1, 129.2, 131.0, 131.7, 137.2, 139.4, 140.0, 142.0, 161.4. HRMS (ESI) *m/z* 477,1767 [M+H]$^+$ (calcd. for [C$_{28}$H$_{23}$F$_3$N$_2$O$_2$]$^+$ 477.1790).

4-Acetyl-1-(4-methyl-benzyl)-5-phenyl-1H-pyrrole-2-carboxylic acid 3-bromo-benzylamide **9h**
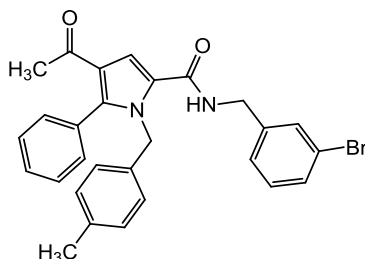
White solid. Yield: 74%, mp: 157-159 °C. ^{1}H NMR (CDCl$_3$) δ: 2.54 (s, 3H), 4.48 (d, 2H, *J*= 6.0 Hz), 5.76 (s, 2H), 6.20 (brt, 1H, *J*= 5.8 Hz), 7.03 (s, 1H), 7.05-7.56 (m, 8H), 7.79 (d, 2H, *J*= 6.8Hz); ^{13}C NMR δ (CDCl$_3$) δ: 21.2, 29.1, 42.7, 48.7 (2C), 113.1, 122.3, 123.6, 126.1, 126.2, 128.7, 129.1, 129.6, 130.2, 130.5, 130.5,

130.6, 131.1, 135.1, 136.8, 140.6, 142.7, 161.5, 194.1. HRMS (ESI) *m/z* 501.1159 [M+H]$^+$ (calcd. for [C$_{28}$H$_{26}$BrN$_2$O$_2$]$^+$ 501.1178).

*5-Methyl-4-(4-methyl-benzoyl)-1-(4-methyl-benzyl)-1H-pyrrole-2-carboxylic acid 3-chloro-benzylamide* **9i**
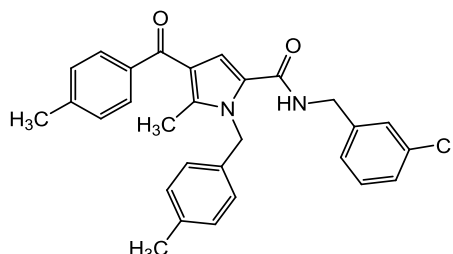
White solid. Yield: 78%, mp: 134-136 °C. ^{1}H NMR (CDCl$_3$) δ: 2.34 (s, 3H), 2.44 (s, 3H), 2.54 (s, 3H), 4.49 (d, 2H, *J*= 5.8 Hz), 5.70 (s, 2H), 6.13 (brt, 1H, *J*= 6.2 Hz), 6.82 (s, 1H), 6.93 (d, 2H, *J*= 7.5 Hz), 7.24-7.28 (m, 5H), 7.71 (d, 2H, *J*= 8.0 Hz); ^{13}C NMR (CDCl$_3$) δ: 11.9, 21.1, 21.6, 42.7, 47.9, 115.2, 120.1, 124.4, 125.8, 126.2, 127.6, 127.7, 128.9, 129.3, 129.46, 130.0 ,134.2, 134.5, 137.0, 137.3, 140.4, 141.7, 142.3, 161.4, 191.8. HRMS (ESI) *m/z* 471.1821 [M+H]$^+$ (calcd. for [C$_{29}$H$_{28}$O$_2$N$_2$Cl]$^+$ 471.1839).

4-(4-Methoxy-benzoyl)-5-methyl-1-(4-methyl-benzyl)-1H-pyrrole-2-carboxylic acid 3-chloro-benzylamide **9j**
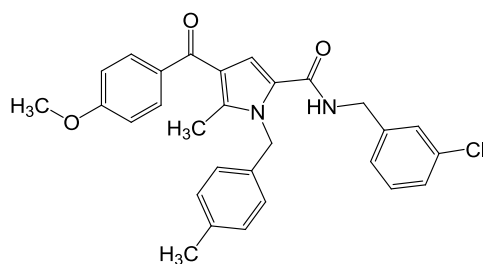
White solid. Yield: 69%, mp: 136-138 °C. ^{1}H NMR (CDCl$_3$) δ: 2.34 (s, 3H), 2.51 (s, 3H), 3.89 (s, 3H), 4.49 (d, 2H, *J*= 5.9 Hz), 5.70 (s, 1H), 6.19 (brt, 1H, *J*= 5.7 Hz), 6.84 (s, 1H), 6.92-6.98 (m, 4H), 7.08-7.14 (m, 3H), 7.19-7.24 (m, 4H), 7.81 (d, 2H, *J*=8.7Hz); ^{13}C NMR (CDCl$_3$) δ: 11.8, 21.1, 42.7, 47.9, 55.5, 113.5, 115.0, 120.2, 124.4, 125.76, 126.2, 127.6, 127.7, 129.4, 130.0, 131.5, 132.5, 134.3, 134.5, 137.0, 140.4, 141.3, 161.5, 162.6. HRMS (ESI) *m/z* 487.1770 [M+H]$^+$ (calcd. for [C$_{29}$H$_{28}$O$_3$N$_2$Cl]$^+$ 487.1788).

4-Benzoyl-1-benzyl-5-phenyl-1H-pyrrole-2-carboxylic acid 3-chloro-benzylamide **9k**
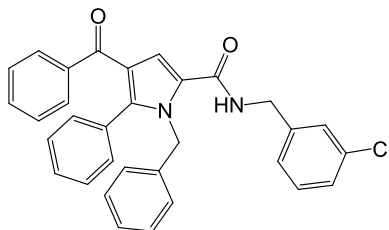
White solid. Yield: 76%, mp: 110-112 °C. ^{1}H NMR (CDCl$_3$) δ: 4.48 (d, 2H, *J*= 6.0 Hz), 5.61 (s, 2H), 6.35 (brs, 1H), 6.85 (m, 2H), 6.98 (d, 1H, *J*= 6.6 Hz), 7.09 (s, 1H), 7.21-7.28 (m, 13H), 7.38 (t, 1H; *J*= 7.3 Hz), 7.64 (d, 2H, *J*= 7.6 Hz); ^{13}C NMR (CDCl$_3$) δ: 42.7, 49.0, 115.2, 121.9, 125.6, 126.2, 126.4, 127.3, 127.6 (2C), 127.9, 128.2, 128.5, 128.9, 129.3, 129.9, 130.3, 130.7, 131.7, 134.4, 138.1, 138.9, 140.3, 143.6, 161.5, 191.7. HRMS (ESI) *m/z* 505.1664 [M+H]$^+$ (calcd. for [C$_{32}$H$_{26}$O$_2$N$_2$Cl]$^+$ 505.1683).

1-(4-Amino-benzyl)-4-benzoyl-5-methyl-1H-pyrrole-2-carboxylic acid 3-chloro-benzylamide **9l**
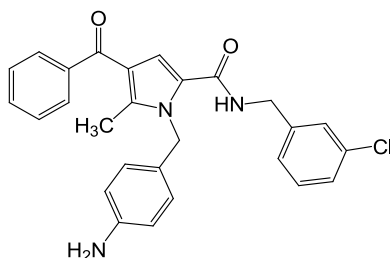
To a solution of EtOH (30 mL), THF (7 mL), and saturated solution of NH$_4$Cl (7 mL), **9d** (0.200 g, 0.628 mmol) and iron powder (0.513 g, 9.20 mmol) were added, and the resulting mixture was stirred for 2h at 100 °C. After cooling to room temperature, the reaction mixture was diluted with EtOH and filtered on a celite pad. The organic solvents were removed under vacuum and the residue was taken up in AcOEt and washed with brine, dried (Na$_2$SO$_4$) and filtered. The organic solvent was removed under reduced pressure, and the residue was purified by flash chromatography (SiO$_2$) using AcOEt/petroleum ether (40-60 °C)/DCM (7: 1.5: 1.5) as eluent to give the title compound as a white solid.

Yield: 81%, mp: 129-131 °C. ^{1}H NMR (CDCl$_3$) δ: 2.58 (s, 3H), 3.67 (brs, 1H), 4.50 (d, 2H, = 6.0 Hz), 5.61 (s, 1H), 6.15 (brt, 1H, *J*= 6.0 Hz), 6.63 (d, 2H, *J*= 8.2

Hz), 6.79 (s, 1H), 6.88 (d, 2H, *J*= 8.2 Hz), 7.24 (m, 4H), 7.45-7.57 (m, 3H), 7.78 (d, 2H, *J*= 7.7 Hz); ^{13}C NMR (CDCl$_3$) δ: 12.0, 42.7, 47.7, 115.3 (2C), 119.9, 124.6, 125.8, 127.1, 127.7 (2C), 127.8, 128.2, 129.1, 130.0, 131.6, 140.1, 140.4, 141.9, 145.7, 158.4, 161.5. HRMS (ESI) *m/z* 458.1624 [M+H]$^+$ (calcd. for [C$_{27}$H$_{25}$ClN$_3$O$_2$]$^+$ 458.1635).

(±) 4-(Hydroxy-phenyl-methyl)-5-methyl-1-(4-methyl-benzyl)-1H-pyrrole-2-carboxylic acid 3-chloro-benzylamide **9m**
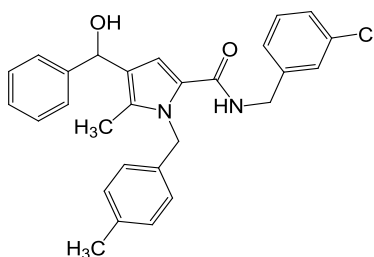
To a solution of **1** (0.657 mmol, 0.3g) in EtOH/H$_2$O (10:1.5) NaBH$_4$ (0.723 mmol, 0.027g) was added over 20 minutes. The reaction mixture was stirred at 50 °C for 18 hours. After cooling to room temperature, the reaction mixture was taken up in AcOEt, and washed with a 1N HCl. The organic phase was filtered, dried (Na$_2$SO$_4$), and solvent was removed under vacuum. The resulting residue was purified by flash chromatography on silica gel using petroleum ether (40-60 °C)/AcOEt (7: 3) as eluent to give the title compound as a white solid.

Yield: 78%, mp: 107-109 °C. ^{1}H NMR (CDCl$_3$) δ: 2.03 (d, 1H, *J*= 3.3 Hz), 2.21 (s, 3H), 4.38-4.53 (m, 2H), 5.63 (q, 2H, *J*=16.0 Hz), 5.85 (d, 1H, *J*= 3.3 Hz), 6.09 (brt, 1H, *J*= 5.6 Hz), 6.43 (s, 1H), 6.88 (d, 2H, *J*= 7.8 Hz), 7.10 (d, 3H, *J*= 7.5 Hz), 7.21-7.43 (m, 8H); ^{13}C NMR (CDCl$_3$) δ: 10.4, 21.1, 42.5, 47.9, 69.6, 110.4, 123.5, 124.3, 125.7, 126.1, 126.2, 127.3, 127.5, 127.6, 128.4, 129.3, 129.9, 132.9, 134.4, 135.4, 136.6, 140.8, 143.9, 161.7.

*4-Benzoyl-1-benzyl-N-(2-morpholinoethyl)-5-phenyl-1H-pyrrole-2-carboxamide* **11a**
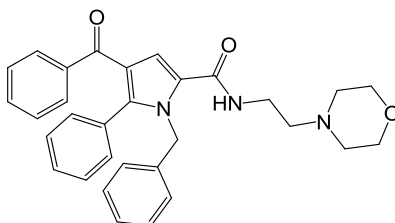
The title compound was obtained according to the procedure described for **9a-k**. After purification by flash chromatography (SiO$_2$, EtOAc/MeOH/NH$_4$OH 9/0.5/0.2 as eluent) **11a** was obtained as a white solid.

Yield: 84%. ^{1}H NMR (CDCl$_3$) δ: 2.42 (t, *J*= 4.6 Hz, 4H), 2.48 (t, *J*= 6.0 Hz, 2H), 3.69 (t, *J*= 4.6 Hz, 4H), 5.59 (s, 2H), 6.52 (t, *J*= 5.0 Hz, 1H), 6.80-6.87 (m, 2H), 7.06 (s, 1H), 7.12-7.31 (m, 9H), 7.38 (t, *J*= 7.4 Hz, 1H), 7.65 (d, *J*= 7.6 Hz, 2H); ^{13}C NMR (CDCl$_3$) δ: 35.7, 48.9, 53.3, 56.9, 66.9, 114.7, 121.9, 126.4, 127.0, 127.1, 127.8, 128.1, 128.3, 128.8, 129.3, 130.4, 130.8, 131.6, 138.3, 139.0, 143.1, 161.8, 191.8. HRMS (ESI) *m/z* 515.1952 [M+H]$^+$. (calcd. for [C$_{31}$H$_{31}$O$_3$N$_3$Na]$^+$ 515.1823).

4-Benzoyl-1-benzyl-N-(3-(diethylamino)propyl)-5-phenyl-1H-pyrrole-2-carboxamide **11b**
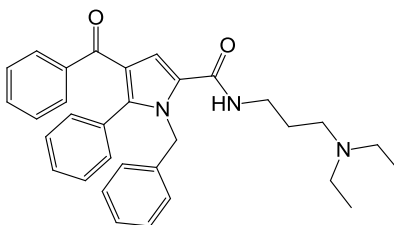
The title compound was obtained according to the procedure described in *sec. 3.7.1.4*. After purification by column chromatography (SiO$_2$, EtOAc/MeOH/NH$_4$OH 4/1/0.15 as eluent) **11b** was obtained as a white solid.

Yield: 82%. ^{1}H NMR (DMSO-*d$_6$*) δ: 1.13 (t, *J*= 7.3 Hz, 6H), 1.76 (d, *J*= 8.4 Hz, 2H), 2.99 (d, *J*= 24.4 Hz, 6H), 3.23 (q, *J*= 6.3 Hz, 2H), 5.59 (s, 2H), 6.75 (d, *J*= 7.4 Hz, 2H), 7.16 – 7.34 (m, 9H), 7.39 (t, *J*= 7.5 Hz, 2H), 7.51 (t, *J*= 7.4 Hz, 1H), 7.64 (d, *J*= 7.6 Hz, 2H), 8.48 (t, *J*= 5.9 Hz, 1H), 9.04 (s, 1H); ^{13}C NMR (DMSO-*d$_6$*) δ: 9.2, 24.4, 36.4, 46.8, 48.5, 49.3, 115.9, 121.4, 126.1, 126.2, 127.3, 128.5 (2C), 128.8, 129.1, 129.3, 130.8, 131.0, 132.2, 139.0, 139.3, 142.7, 161.5, 190.8. HRMS (ESI) *m/z* 494.2788 [M+H]$^+$ (calcd. for [C$_{32}$H$_{36}$O$_2$N$_3$]$^+$ 494.2808).
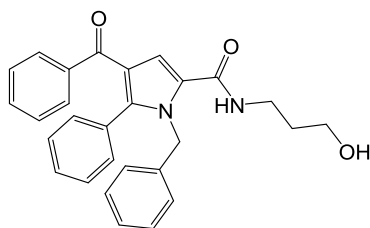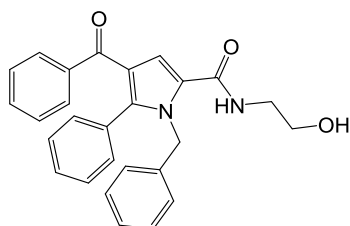
4-Benzoyl-1-benzyl-N-(2-(4-methylpiperazin-1-yl)ethyl)-5-phenyl-1H-pyrrole-2-carboxamide **11c**
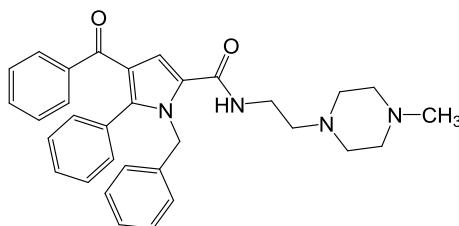
The title compound was obtained according to the procedure described in *sec. 3.7.1.4*. After purification by column chromatography (SiO$_2$, and EtOAC/MeOH/NH$_4$OH 8/2/0.2 as eluent) **11c** was obtained as a white solid.

Yield: 75%. ^{1}H NMR (CDCl$_3$) δ: 0.87 (t, *J*= 6.4 Hz, 2H), 1.27 (t, 2H), 2.33 (s, 3H), 2.49 (t, 6H), 3.40 (q, *J*= 5.6 Hz, 2H), 5.58 (s, 2H), 6.59 (t, *J*= 5.1 Hz, 1H), 6.83 (dd, *J*= 7.2, 2.2 Hz, 2H), 7.06 (s, 1H), 7.13-7.32 (m, 10H), 7.38 (t, *J*= 7.4 Hz, 1H), 7.62-7.73 (m, 2H); ^{13}C NMR (CDCl$_3$) δ: 35.9, 45.8, 48.9, 52.6, 55.0, 56.2, 114.7, 121.8, 126.4, 126.9, 127.1, 127.8, 128.1, 128.3, 128.7, 129.3, 130.4, 130.8, 131.5, 138.2, 138.9, 143.1, 161.7, 191.8. HRMS (ESI) *m/z* 507.2755 [M+H]$^+$ (calcd. for [C$_{32}$H$_{35}$O$_2$N$_4$]$^+$ 507.2760).

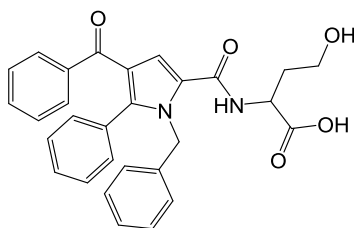*4-Benzoyl-1-benzyl-N-(3-hydroxypropyl)-5-phenyl-1H-pyrrole-2-carboxamide*
11d

The title compound was obtained according to the procedure described in *sec. 3.7.1.4*. After purification by column chromatography (SiO$_2$, DCM/EtOAc 5/5 as eluent), **11d** was obtained as a white solid.

Yield: 83%. ^{1}H NMR (CDCl$_3$) δ: 1.61 (p, *J*= 5.8 Hz, 2H), 2.37 (s, H), 3.45 (q, *J*= 6.2 Hz, 2H), 5.58 (s, 2H), 5.59 (s, 2H), 6.35 (s, 1H), 6.84 (d, *J*= 7.1 Hz, 1H), 7.07 (s, 1H), 7.15-7.29 (m, 1H), 7.34-7.45 (m, 1H), 7.65 (d, *J*= 8.0 Hz, 2H); ^{13}C NMR (CDCl$_3$) δ: 32.2, 36.0, 49.0, 58.7, 115.2, 121.8, 126.2, 126.3, 127.2, 127.8, 128.2, 128.5, 128.9, 129.3, 130.3, 130.8, 131.6, 138.1, 138.9, 143.6, 162.7, 191.7. HRMS (ESI) *m/z* 439.2020 [M+H]$^+$ (calcd. for [C$_{28}$H$_{26}$O$_3$N$_2$]$^+$ 439.2022).

4-Benzoyl-1-benzyl-N-(2-hydroxyethyl)-5-phenyl-1H-pyrrole-2-carboxamide **11e**

93

The title compound was obtained according to the procedure described in *sec. 3.7.1.4*. After purification by column chromatography (SiO$_2$, DCM/EtOAc 5/5 as eluent), **11e** was obtained as a white solid.

Yield: 81%. ^{1}H NMR (CDCl$_3$) δ: 3.04 (broad-s, 1H), 3.45 (t, *J*= 4.9 Hz, 2H), 3.65 (t, *J*= 4.9 Hz, 2H), 5.55 (s, 2H), 6.62 (broad-s, 1H), 6.84 (d, 2H), 7.10 (s, 1H), 7.17-7.32 (m, 10H), 7,35-7.44 (m, 1H), 7.64 (d, *J*= 7.4 Hz, 2H).^{13}C NMR (CDCl$_3$) δ: 42.36, 49.05, 62.11, 115.34, 121.79, 126.38, 126.40, 127.17, 127.86, 128.17, 128.41, 128.46, 128.82, 129.29, 130.33, 130.75, 131.69, 138.20, 138.84, 143.53, 162.58, 192.00; ^{13}C NMR (CDCl$_3$) δ: 42.4, 49.1, 62.1, 115.3, 121.8, 126.4 (2C), 127.2, 127.9, 128.2, 128.4, 128.8, 129.3, 130.3, 130.8, 131.7, 138.2, 138.8, 143.5, 162.6, 192.0. HRMS (ESI) *m/z* 413,2649 [M+H]$^+$, *m/z* 447.1664 [M+Na]$^+$ (calcd. for [C$_{27}$H$_{24}$O$_3$N$_2$Na]$^+$ 447.1865).

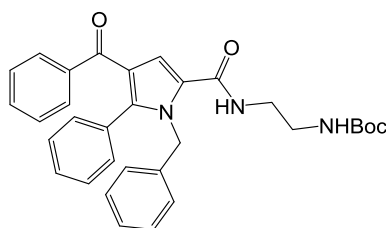*2-(4-Benzoyl-1-benzyl-5-phenyl-1H-pyrrole-2-carboxamido)-4-hydroxybutanoic acid* **11f**

The title compound was obtained according to the procedure described in *sec. 3.7.1.4*. After purification by column chromatography (SiO$_2$, DCM/EtOAc 5/5 as eluent) **11f** was obtained as a white solid.

Yield: 77%. ^{1}H NMR (CDCl$_3$) δ: 7.69 (d, 2H), 7.43 (t, 1H), 7.39-7.18 (m, 10H), 6.85 (d, 2H), 6.41 (d, *J*= 5.7 Hz, 1H), 5.59 (q, 2H), 4.63-4.54 (m, 1H), 4.48 (t, *J*= 9.1, 1.2 Hz, 1H), 4.33-4.25 (m, 1H), 2.89-2.78 (m, 1H), 2.22-2.03 (m, 1H); ^{13}C NMR (CDCl$_3$) δ: 30.4, 49.1, 49.3, 66.0, 116.1, 122.0, 124.9, 126.3, 127.2, 128.0, 128.2, 128.4, 129.0, 129.3, 130.2, 130.7, 131.7, 138.0, 138.9, 144.0, 161.7, 175.1, 191.4. HRMS (ESI) *m/z* 465.1801 [M-H$_2$O]$^+$ (calcd. for [C$_{29}$H$_{26}$O$_5$N$_2$]$^+$ 465.1920).

4-Benzoyl-1-benzyl-N-((1r,4r)-4-hydroxycyclohexyl)-5-phenyl-1H-pyrrole-2-carboxamide **11g**
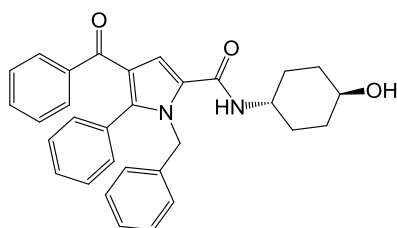
The title compound was obtained according to the procedure described in *sec. 3.7.1.4*. After purification by column chromatography (SiO$_2$, petroleum ether (40-60 °C)/EtOAc 2/8 as eluent) **11g** was obtained as a white solid.

Yield: 98%. ^{1}H NMR (CDCl$_3$) δ: 1.05-1.57 (m, 4H), 1.91-2.03 (m, 4H), 2.54 (s, 1H), 3.51-3.69 (m, 1H), 3.71-3.86 (m, 1H), 5.54 (s, 2H), 5.84 (s, 1H), 6.83 (d, *J*= 4.6 Hz, 2H), 7.01 (s, 1H), 7.14-7.32 (m, 10H), 7.38 (t, *J*= 7.4 Hz, 1H), 7.62 (d, *J*= 8.0 Hz, 2H); ^{13}C NMR (CDCl$_3$) δ: 30.6, 33.7, 47.7, 49.0, 69.8, 114.7, 121.7, 126.4, 126.9, 127.2, 127.8, 128.2, 128.4, 128.8, 129.3, 130.3, 130.8, 131.6, 138.1, 138.8, 143.3, 161.2, 192.0. HRMS (ESI) *m/z* 479.2335 [M+H]$^+$ (calcd. for [C$_{31}$H$_{30}$O$_3$N$_2$]$^+$ 479.2335).

Tert-Butyl(2-(4-benzoyl-1-benzyl-5-phenyl-1H-pyrrole-2-(carboxamido)ethyl) carbamate **12a**

The title compound was obtained according to the procedure described in *sec. 3.7.1.4*. After purification by flash chromatography (SiO$_2$, petroleum ether (40-60 °C)/AcOEt 7:3 as eluent, **12a** was obtained as a white solid.

Yield: 98%. ^{1}H NMR (CDCl$_3$) δ: 1.39 (s, 9H), 3.25 (s, 2H), 3.40 (q, *J*= 5.3 Hz, 2H), 4.75 (s, 1H), 5.59 (s, 2H), 6.81-6.88 (m, 2H), 7.07 (s, 1H), 7.17-7.35 (m, 12H), 7.38-7.46 (m, 1H), 7.67-7.76 (m, 2H).

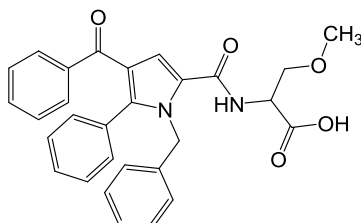*Tert-Butyl(3-(4-benzoyl-1-benzyl-5-phenyl-1H-pyrrole-2-carboxamido)propyl) carbamate* **12b**
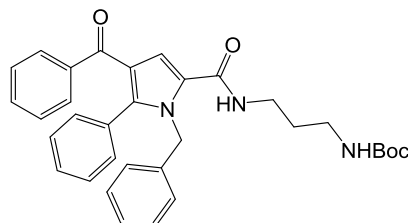
The title compound was obtained according to the procedure described in *sec. 3.7.1.4*. After purification by column chromatography (SiO$_2$, petroleum ether (40-60 °C)/AcOEt 7: 3 as eluent, **12b** was obtained as a white solid.

Yield:81%. ^{1}H NMR (CDCl$_3$) δ: 1.44 (s, 9H), 1.55 (t, *J*= 6.2 Hz, 2H), 2.99 (t, *J*= 6.1 Hz, 2H), 3.34 (q, 2H), 5.58 (s, 2H), 6.85 (d, *J*= 7.2 Hz, 2H), 7.13 (d, *J*= 2.2 Hz, 1H), 7.15-7.36 (m, 10H), 7.41 (t, 2H), 7.71 (d, 2H).

2-(4-Benzoyl-1-benzyl-5-phenyl-1H-pyrrole-2-carboxamido)-3-methoxypropanoic acid **12c**

The title compound was obtained according to the procedure described in *sec. 3.7.1.4*. After purification by column chromatography (SiO$_2$, DCM /EtOAc 5:5 as eluent, **12c** was obtained as a white solid.

Yield: 80%. ^{1}H NMR (CDCl$_3$) δ: 3.79 (s, 3H), 3.81-4.01 (m, 2H), 4.70 (dt, *J*= 7.1, 3.5 Hz, 1H), 5.57 (q, 2H), 6.80 (d, *J*= 7.3 Hz, 1H), 6.85 (d, *J*= 7.2, 2.1 Hz, 2H), 7.14-7.35 (m, 11H), 7.42 (t, 1H), 7.68 (d, 2H).

N-(2-Aminoethyl)-4-benzoyl-1-benzyl-5-phenyl-1H-pyrrole-2-carboxamide **11h**
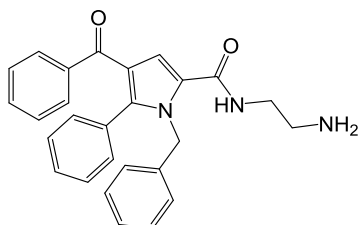

To a solution of **12a** (1.2 mmol, 0.6523 g) in DCM (2 mL), TFA (1 mL) was added, and the reaction mixture was stirred at room temperature for 2h. Then DCM (10 mL) was added and the mixture was washed with a 1N HCl solution. The organic phase was dried (Na$_2$SO$_4$), filtered and solvent was removed under vacuum. After purification by column chromatography (SiO$_2$, EtOAc/MeOH 8/2 as eluent) **11h** was obtained as a white solid.

Yield: 98%. ^{1}H NMR (CDCl$_3$) δ: 2.90 (s, 2H), 3.44 (q, *J*= 5.9 Hz, 2H), 3.99 (s, 2H), 5.52 (s, 2H), 6.77-6.86 (m, 2H), 7.21 (dtd, *J*= 23.2, 15.8, 13.7, 8.1 Hz, 12H),

7.57 (d, *J*= 7.6 Hz, 2H). HRMS (ESI) *m/z* 424.2003 [M+H]$^+$ (calcd. for [C$_{27}$H$_{26}$O$_2$N$_3$]$^+$ 424.2025).

N-(3-aminopropyl)-4-benzoyl-1-benzyl-5-phenyl-1H-pyrrole-2-carboxamide **11i**
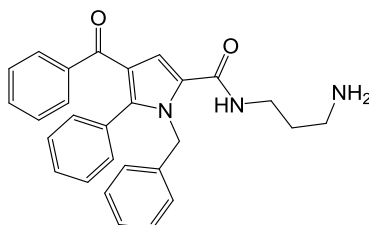
Starting from **12b** the title compound was obtained according to the procedure described for **11h**. After purification by column chromatography (SiO$_2$, EtOAC/MeOH 8/2 as eluent) **11i** was obtained as a white solid.

Yield: 98%. ^{1}H NMR (CDCl$_3$) δ: 1.64 (p, *J*= 6.2 Hz, 2H), 2.73 (t, *J*= 6.2 Hz, 2H), 3.44 (q, *J*= 5.9 Hz, 2H), 5.59 (s, 2H), 6.84 (dd, *J*= 7.4, 2.0 Hz, 2H), 7.08 (s, 1H), 7.13-7.29 (m, 8H), 7.31-7.43 (m, 2H), 7.61-7.66 (m, 3H). HRMS (ESI) *m/z* 438.2171[M+H]$^+$ (calcd. for [C$_{28}$H$_{29}$O$_2$N$_3$]$^+$ 438.2182).

*4-Benzoyl-1-benzyl-N-(2-(methylsulfonamido)ethyl)-5-phenyl-1H-pyrrole-2-carboxamide* **11j**
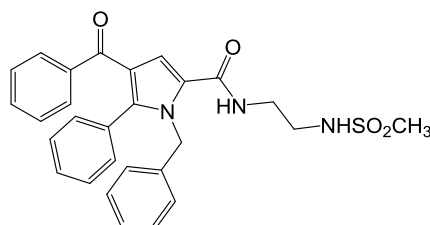
To a solution of the amine **11h** (0.312g, 7mmol) and triethylamine (0.172 g, 1.7 mmol) in DCM (5 ml) at 0 °C was added methanesulfonyl chloride (1.7 mmol, 0.200 g) over a period of 5-10 min, and the resulting mixture was stirred for 12h a room temperature. Then the solvent was removed under vacuum and the mixture is solubilized in ethyl acetate and washed with saturated sodium bicarbonate solution and brine, filtered and dried over sodium sulphate. The solvent was removed under reduced pressure, and the residue was purified by flash chromatography (SiO$_2$, EtOAc/MeOH 9/1) to give **11j** as a white solid.

Yield: 62%. ^{1}H NMR (CDCl$_3$) δ: 2.86 (s, 3H), 3.20 (t, *J*= 5.4 Hz, 2H), 3.44 (t, *J*= 5.6 Hz, 2H), 5.56 (s, 2H), 6.74 (s, 1H), 6.84 (dd, *J*= 2.1, 7.4 Hz, 2H), 7.09-7.35 (m, 11H), 7.34-7.43 (m, 1H), 7.64 (d, *J*= 8.2 Hz, 2H); ^{13}C NMR (CDCl$_3$) δ: 39.9,

40.2, 43.2, 49.1, 115.6, 121.8, 125.9, 126.2, 127.2, 127.9, 128.2, 128.5, 128.9, 129.3, 130.2, 130.7, 131.7, 138.32, 138.78, 143.7, 162.4, 191.8. HRMS (ESI) *m/z* 502.1781 [M+H]$^+$ (calcd. for [C$_{28}$H$_{27}$O$_4$N$_3$S]$^+$ 502.1801).

4-Benzoyl-1-benzyl-N-(3-(methylsulfonamido)propyl)-5-phenyl-1H-pyrrole-2-carboxamide **11k**
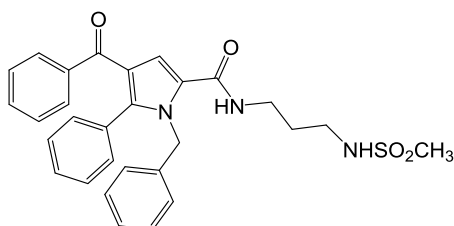
The title compound was obtained according to the procedure described for **11j**. After purification by flash chromatography (SiO$_2$, EtOAc/MeOH 9/1) **11k** was obtained as a white solid.

Yield: 63%. ^{1}H NMR (CDCl$_3$) δ: 1.66 (d, *J*= 6.0 Hz, 1H), 2.84 (s, 3H), 2.89 (d, *J*= 6.1 Hz, 2H), 3.44 (q, *J*= 6.2 Hz, 2H), 5.33 (t, *J*= 6.7 Hz, 1H), 5.59 (s, 2H), 6.42 (t, *J*= 6.6 Hz, 1H), 6.84 (d, *J*= 7.0 Hz, 2H), 7.12 (s, 1H), 7.16-7.34 (m, 10H), 7.40 (t, *J*= 7.4 Hz, 1H), 7.66 (d, *J*= 7.6 Hz, 2H); ^{13}C NMR (CDCl$_3$) δ 30.6, 35.5, 39.4, 40.4, 48.9, 115.2, 121.8, 126.0, 126.1, 127.1, 127.9, 128.2, 128.5, 128.9, 129.3, 130.2, 130.7, 131.7, 138.4, 138.9, 143.6, 162.4, 191.6. HRMS (ESI) *m/z* 516.1934 [M+H]$^+$ (calcd. for [C$_{29}$H$_{30}$O$_4$N$_3$S]$^+$ 516.1957).

*2-(4-Benzoyl-1-benzyl-5-phenyl-1H-pyrrole-2-carboxamido)-3-hydroxypropanoic acid* **11l**
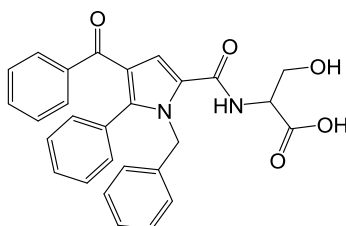
To a solution of **12c** (0.64 mmol, 0.3122 g) in methanol (10 mL), 2M LiOH (0.902 mmol, 0.042 g) was added, and the resulting mixture was refluxed until no starting material was detected by TLC (AcOEt as eluent). The solvent was removed under reduced pressure, then the residue was acidified with 2M HCl (pH~3) and extracted with AcOEt. The organic phase was dried (Na$_2$SO$_4$),

filtered, and the solvent was removed under vacuum. The resulting residue was purified by flash chromatography (SiO$_2$, EtOAc/MeOH, 9:1 as eluent) to give **11l** as a white solid.

Yield: 98%. ^{1}H NMR (DMSO-d_6) δ; 3.50-3.66 (m, 3H), 4.14 (s, 1H), 5.58 (s, 2H), 6.75 (d, *J*= 7.2 Hz, 2H), 7.18 (dt, *J*= 10.3, 4.8 Hz, 5H), 7.24-7.33 (m, 3H), 7.40 (t, *J*= 7.5 Hz, 2H), 7.51 (t, *J*= 7.4 Hz, 1H), 7.66 (d, *J*= 7.6 Hz, 2H), 8.04 (s, 1H). HRMS (ESI) *m/z* 469.1754 [M+H]$^+$ (calcd. for [C$_{28}$H$_{26}$O$_5$N$_2$]$^+$ 469.1756).

Methyl-3-((4-benzoyl-1-benzyl-5-phenyl-1H-pyrrole-2-carboxamido)methyl) benzoate **13**
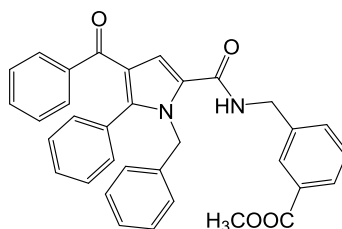
The title compound was obtained according to the procedure described in *sec. 3.7.1.4*. After purification by flash chromatography (SiO$_2$, petroleum ether (40-60 °C)/ AcOEt 5:5 as eluent), **13** was obtained as a white solid.

Yield: 98%. ^{1}H NMR (CDCl$_3$) δ: 3.94 (s, 3H), 4.57 (d, *J*= 6.0 Hz, 2H), 5.62 (s, 2H), 6.30 (t, *J*= 6.0 Hz, 1H), 6.83-6.87 (m, 2H), 7.06 (s, 1H), 7.18-7.30 (m, 10H), 7.38 (dt, *J*= 11.8, 7.5 Hz, 2H), 7.63-7.68 (m, 2H), 7.95 (d, 2H).

*3-((4-Benzoyl-1-benzyl-5-phenyl-1H-pyrrole-2-carboxamido)methyl)benzoic acid* **11m**
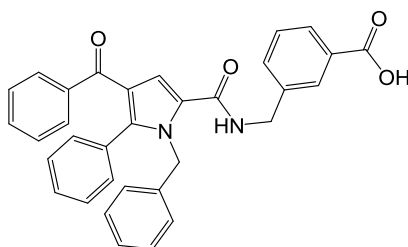
To a solution of ester **13** (0.818 g, 1.55 mmol) in methanol (20 mL) was added 2M NaOH (1.93 mL, 7.75 mmol), and the resulting mixture was refluxed until no starting material was detected by TLC (DCM as eluent). The solvent was removed under reduced pressure. Then the residue was acidified with 2M HCl (pH~3) and extracted with EtOAc. The organic phase was dried (Na$_2$SO$_4$), filtered, and the

solvent was removed under vacuum. The resulting residue was purified by flash chromatography (SiO$_2$, EtOAc/MeOH, 9:1 v/v, as eluent) and recrystallized from ethyl ether/petroleum ether (40-60 °C).

Yield: 80%. ^{1}H NMR (DMSO-d_6) δ: 3.38 (s, 1H), 4.42 (d, J= 6.0 Hz, 2H), 5.60 (s, 2H), 6.74 (d, J= 5.7 Hz, 2H), 7.14-7.44 (m, 14H), 7.50 (t, J= 7.4 Hz, 1H), 7.66 (d, J= 6.9 Hz, 1H), 7.77-7.85 (m, 1H), 7.88 (d, J= 2.0 Hz, 1H), 8.99 (t, J= 6.1 Hz, 1H); ^{13}C NMR (DMSO-d_6) δ: 42.2, 48.5, 116.1, 121.4, 126.1, 126.4, 127.4, 128.1, 128.4, 128.5 (2C), 128.8, 128.9, 129.0, 129.4, 130.9, 131.1, 131.8, 132.1, 138.8, 139.3, 140.5, 142.8, 161.3, 168.0, 190.7. HRMS (ESI) *m/z* 515.1952 [M+H]$^+$ (calcd. for [C$_{33}$H$_{27}$O$_4$N$_2$]$^+$ 515.1917).

*3-((4-Benzoyl-1-benzyl-5-phenyl-1H-pyrrole-2-carboxamido)methyl)benzoic acid* **11n**
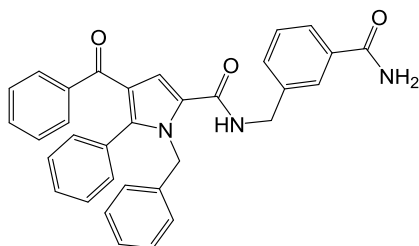
N,N'-carbonyldiimizole (0.128 g, 0.78 mmol) was added to a solution of **11m** (0.270 g, 0.52 mmol) in [bmim]BF$_4$ (1.05 mL). The resulting mixture was stirred at 80 °C for 2h, then ammonium acetate (0.202 g, 2.6 mmol) and TEA (0.212 g, 2.1 mmol) were added. The reaction was stirred at 80 °C for 3h, then was allowed to room temperature. Ethyl acetate was added and the resulting mixture was washed with 0.1N HCl, filtered and dried (MgSO$_4$). The solvent was removed in *vacuo*, and the crude product was purified by flash chromatography (SiO$_2$, EtOAc/MeOH/NH$_4$OH 4.5/0.5/0.05 as eluent) to give the title compound as a white solid.

Yield: 52%. ^{1}H NMR (DMSO-d_6) δ: 4.40 (d, J= 6.0 Hz, 2H), 5.60 (s, 2H), 6.74 (d, J= 5.8 Hz, 2H), 7.15-7.44 (m, 14H), 7.50 (t, J= 7.4 Hz, 1H), 7.66 (d, J= 6.7 Hz, 1H), 7.73 (d, J= 6.5 Hz, 1H), 7.80 (s, 1H), 7.94 (s, 1H), 8.95 (t, J= 6.1 Hz, 1H); ^{13}C NMR (DMSO-d_6) δ: 42.3, 48.5, 116.1, 121.4, 126.1 (2C), 126.4, 127.0, 127.4, 128.5 (2C), 128.6, 128.8, 129.0, 129.4, 130.3, 130.9, 131.1, 132.1, 134.8, 138.9,

139.3, 140.2, 142.7, 161.3, 168.3, 190.7. HRMS (ESI) *m/z* 514.2136 [M+H]$^+$ (calcd. for [C$_{33}$H$_{28}$O$_3$N$_3$]$^+$ 513.2052).

Methyl 3-(azidomethyl)benzoate **15**
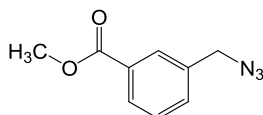
To a solution of methyl 3-(bromomethyl)benzoate **14** (4.0 mmol, 1.04 g) in DMF (2 mL), NaN$_3$ (2.56 mmol, 0.5101 g) was added, and the resulting mixture was stirred at room temperature for 4h. The organic solvent was removed under reduced pressure and the residue was purified by flash column chromatography (SiO$_2$, *n*-hexane/AcOEt, 99:1 as eluent) to give **15** as a colourless oil.

Yield: 98%. ^{1}H NMR (DMSO-*d$_6$*) δ: 3.88 (s, 3H), 4.58 (s, 2H), 7.57 (t, *J*= 7.7 Hz, 1H), 7.67 (dd, *J*= 7.8, 1.6 Hz, 1H), 7.95 (d, *J*= 7.7, 1.4 Hz, 1H), 7.98 (s, 1H).

Methyl 3-(aminomethyl)benzoate **16**
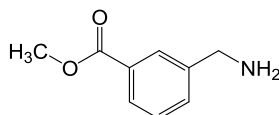
A suspension of azide **15** (0.43 mmol, 0.837 g), ammonium formate (10.9 mmol, 0.69 g), and zinc powder (10.9 mmol, 0.69 g) in MeOH (5 mL) was stirred at room temperature, under nitrogen condition until completion of the reaction (monitored by TLC, AcOEt). Then, the reaction mixture was filtered through a celite pad, and the filtrate was concentrated under vacuum. The residue was taken up in DCM, washed with brine and water. The organic phase was dried (Na$_2$SO$_4$), filtered and the solvent was removed under vacuum. After purification by flash chromatography (SiO$_2$, EtOAc as eluent) **16** was obtained as a brown solid.

Yield: 80%. ^{1}H NMR (CDCl$_3$) δ: 3.94 (s, 3H), 3.96 (s, 2H), 7.43 (t, *J*= 7.7 Hz, 1H), 7.55 (d, 1H), 7.94 (d, *J*= 7.8, 1.5 Hz, 1H).

3.7.2 *In vitro* bioscreen

Cells were inoculated in 96-microwell culture plates at a density of 10^4 cells/well, and allowed to grow for 24h. The medium was then replaced with fresh medium and cells were treated for further 48 h with a range of concentrations ($1\rightarrow$ 1000 μM) of tested compounds **1**, **9a-c**, **9e-m**.

Using the same experimental procedure, cell cultures were also incubated with nutlin-3a as a positive control for cytotoxic effects.

Cell viability was evaluated using the MTT assay procedure, which measures the level of mitochondrial dehydrogenase activity using the yellow 3-(4,5-dimethyl-2-thiazolyl)-2,5-diphenyl-2H-tetrazolium bromide (MTT, Sigma) as substrate. The assay is based on the redox ability of living mitochondria to convert dissolved MTT into insoluble purple formazan. Briefly, after the treatments, the medium was removed and the cells were incubated with 20μl/well of a MTT solution (5mg/mL) for 1h in a humidified 5% CO_2 incubator at 37 °C. The incubation was stopped by removing the MTT solution and by adding 100 μl/well of DMSO to solubilize the obtained formazan. Finally, the absorbance was monitored at 550nm using a microplate reader (iMark microplate reader, Bio-Rad, Milan, Italy). Cell number was determined by TC10 automated cell counter (Bio-Rad, Milan, Italy), providing an accurate and reproducible total count of cells and a live/dead ratio in one step by a specific dye (trypan blue) exclusion assay. Bio-Rad's TC10 automated cell counter uses disposable slides, TC10 trypan blue dye (0.4% trypan blue dye w/v in 0.81% sodium chloride and 0.06% potassium phosphate dibasic solution) and a CCD camera to count cells based on the analyses of captured images. Once the loaded slide is inserted into the slide port, the TC10 automatically focuses on the cells, detects the presence of trypan blue dye and provides the count. When cells are damaged or dead, trypan blue can enter the cell allowing living cells to be counted. Operationally, after treatments in 96-microwell culture plates, the medium was removed and the cells were collected. Ten microliters of cell suspension, mixed with 0.4% trypan blue solution at 1:1 ratio, were loaded into the chambers of disposable slides. The results are expressed in terms of total cell count (number of cells per mL). If trypan blue is detected, the instrument also accounts for the dilution and shows

live cell count and percent viability. Total counts and live/dead ratio from random samples for each cell line were subjected to comparisons with manual hemocytometers in control experiments. The calculation of the concentration required to inhibit the net increase in the cell number and viability by 50% (IC_{50}) is based on plots of data (n= 3 for each experiment) and repeated five times (total n= 9). IC_{50} values were obtained by means of a concentration response curve by nonlinear regression using a curve fitting program, GraphPad Prism 5.0, and are expressed as mean values±SEM (n=9) of three independent experiments.

3.7.3 Solubility assay

The solubility of the compound **1**, **9a-c**, **9e-m** was measured in a PBS buffer solution (pH =7.4) adopting the Lipinski *et al.* method [3] (Table VI).

Table VI. *Solubility of compounds* **1, 9a-m**

Cpd	X	Y	Z	R_1	R_2	Solubility[a] (μM)
1	C_6H_5	C=O	CH_3	CH_3	3-Cl	**2.3**
9a	C_6H_5	C=O	CH_3	Cl	3-Cl	**2.5**
9b	C_6H_5	C=O	CH_3	OCH_3	3-Cl	**2.2**
9c	C_6H_5	C=O	CH_3	F	3-Cl	**2.5**
9d	C_6H_5	C=O	CH_3	NO_2	3-Cl	***NT***
9e	C_6H_5	C=O	CH_3	CH_3	4-Cl	**2.3**
9f	C_6H_5	C=O	CH_3	Cl	4-Cl	**2.2**
9g	C_6H_5	C=O	CH_3	H	$3-CF_3$	**2.3**
9h	CH_3	C=O	C_6H_5	CH_3	3-Br	**1.4**
9i	$(4-CH_3)-C_6H_4$	C=O	CH_3	CH_3	3-Cl	**1.9**
9j	$(4-OCH_3)-C_6H_4$	C=O	CH_3	CH_3	3-Cl	**2.1**
9k	C_6H_5	C=O	C_6H_5	H	3-Cl	**2.3**
9l	C_6H_5	C=O	CH_3	NH_2	3-Cl	**10.0**
9m	C_6H_5	CHOH	CH_3	CH_3	3-Cl	**2.6**

[a]*Each value is the mean ± SEM (≤ 15%) of three independent determinations (at 1.6 mM and 2.5 mM) performed at 600 and 800 nm.*

Each tested compound was dissolved in DMSO to obtain a 10 mM stock solution; by dilution of the stock solution a 1.6 mM and 2.5 mM solutions were prepared. Then 0.3 microliters (from 1.6 mM solution) or 0.5 microliters (from

2.5 mM solution) at a time were added to 1400 microliters of PBS buffer solution in a 2.5 mL UV cuvette at room temperature. The same volume (0.3 or 0.5 microliters) of DMSO was added to a 1400 microliters of PBS buffer solution in a blank cuvette. The additions of stock solution were spaced 1h apart, until precipitation occurs i.e. solubility limit was achieved. Precipitation was quantified by the absorbance increase due to the light scattering of particulate formed in the cuvette. Increased UV absorbance was measured at 600 and 800 nm to avoid any UV-visible absorption interference in the scattering measurement. The UV measurements were performed on JASCO-V-530 spectrometer supplied with ETC-505T temperature controller.

  The precipitation point was identified as the intersect point of the bilinear curve fitted to the plot of absorbance (at each wavelength) *vs* µL of DMSO. A representative experiment is reported in Figure 3.6 for **9h**.
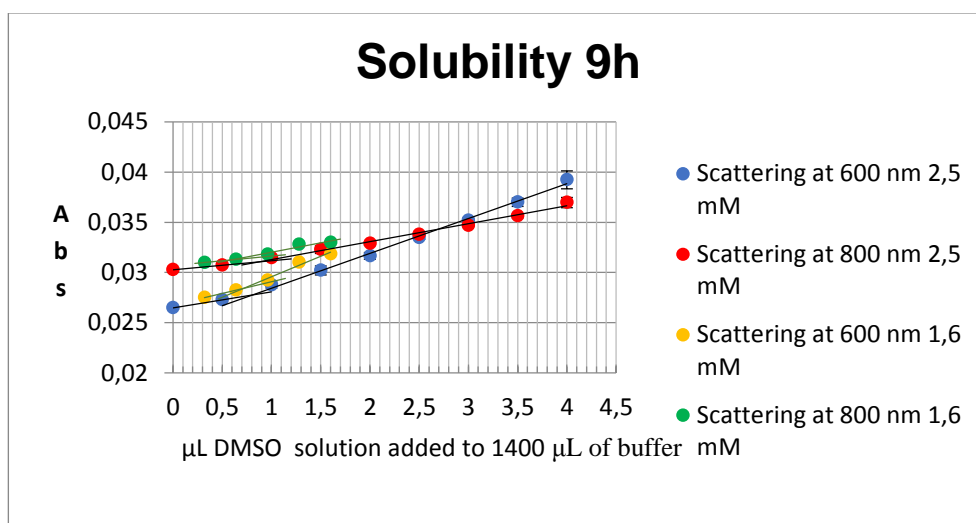

Figure 3.6. *Solubility of* **9h**.

References

[1] Plevin, M. J.; Mills, M. M.; Ikura, M. The LxxLL motif: a multifunctional binding sequence in transcriptional regulation. *Trends Biochem. Sci.* **2005**, *30* (2), 66-9.

[2] Litterst, C. M.; Pfitzner, E. An LXXLL motif in the transactivation domain of STAT6 mediates recruitment of NCoA-1/SRC-1. *J. Biol. Chem.* **2002**, *277* (39), 36052-60.

[3] Lipinski, C. A.; Lombardo, F.; Dominy, B. W.; Feeney, P. J. Experimental and computational approaches to estimate solubility and permeability in drug discovery and development settings. *Adv. Drug Deliv. Rev.* **2001**, *46* (1-3), 3-26.

[4] Veber, D. F.; Johnson, S. R.; Cheng, H. Y.; Smith, B. R.; Ward, K. W.; Kopple, K. D. Molecular properties that influence the oral bioavailability of drug candidates. *J. Med. Chem.* **2002**, *45* (12), 2615-23.

[5] Ribeiro, C. J.; Rodrigues, C. M.; Moreira, R.; Santos, M. M. Chemical Variations on the p53 Reactivation Theme. *Pharmaceuticals* **2016**, *9* (2).

[6] Persico, M.; Ramunno, A.; Maglio, V.; Franceschelli, S.; Esposito, C.; Carotenuto, A.; Brancaccio, D.; De Pasquale, V.; Pavone, L. M.; Varra, M.; Orteca, N.; Novellino, E.; Fattorusso, C. New anticancer agents mimicking protein recognition motifs. *J. Med. Chem.* **2013**, *56* (17), 6666-80.

[7] D'Silva, L.; Ozdowy, P.; Krajewski, M.; Rothweiler, U.; Singh, M.; Holak, T. A. Monitoring the effects of antagonists on protein-protein interactions with NMR spectroscopy. *JACS* **2005**, *127* (38), 13220-6.

[8] Krajewski, M.; Ozdowy, P.; D'Silva, L.; Rothweiler, U.; Holak, T. A. NMR indicates that the small molecule RITA does not block p53-MDM2 binding in vitro. *Nat. Med.* **2005**, *11* (11), 1135-6.

[9] Ferreira, P. M. T.; Maia, H. L. S.; Monteiro, L. S.; Sacramento, J. High yielding synthesis of dehydroamino acid and dehydropeptide derivatives. *J. Chem. Soc., Perkin Trans* **1999**, 1, 3697−3703.

[10] Zhang, J.; Lu, X.; Li, T.; Wang, S.; Zhong, G. Copper-Catalyzed Oxidative Cyclization of 2-Amino-azaarenes with Lignin Models: Synthesis of 3-Phenoxy Imidazo Heterocycles. *J. Org. Chem.* **2017**, *82* (10), 5222-5229.

[11] Reichstein, A.; Vortherms, S.; Bannwitz, S.; Tentrop, J.; Prinz, H.; Muller, K. Synthesis and structure-activity relationships of lapacho analogues. 1. Suppression of human keratinocyte hyperproliferation by 2-substituted naphtho[2,3-b]furan-4,9-diones, activation by enzymatic one- and two-electron reduction, and intracellular generation of superoxide. *J. Med. Chem.* **2012**, *55* (16), 7273-84.

[12] Das, M.; Manna, K. Chalcone scaffold in anticancer armamentarium: a molecular insight. *J. Toxicol.* **2016**, *2016*, 7651047.

[13] Mueller, M. M.; Peter, W.; Mappes, M.; Huelsen, A.; Steinbauer, H.; Boukamp, P.; Vaccariello, M.; Garlick, J.; Fusenig, N. E. Tumor progression of skin carcinoma cells in vivo promoted by clonal selection, mutagenesis, and autocrine growth regulation by granulocyte colony-stimulating factor and granulocyte-macrophage colony-stimulating factor. *Am. J. Pathol.* **2001**, *159* (4), 1567-79.

[14] Grasberger, B. L.; Lu, T.; Schubert, C.; Parks, D. J.; Carver, T. E.; Koblish, H. K.; Cummings, M. D.; LaFrance, L. V.; Milkiewicz, K. L.; Calvo, R. R.; Maguire, D.; Lattanze, J.; Franks, C. F.; Zhao, S.; Ramachandren, K.; Bylebyl, G. R.; Zhang, M.; Manthey, C. L.; Petrella, E. C.; Pantoliano, M. W.; Deckman, I. C.; Spurlino, J. C.; Maroney, A. C.; Tomczuk, B. E.; Molloy, C. J.; Bone, R. F. Discovery and cocrystal structure of benzodiazepinedione HDM2 antagonists that activate p53 in cells. *J. Med. Chem.* **2005**, *48* (4), 909-12.

[15] Dong, L.; Aleem, S.; Fink, C. A. Microwave-accelerated reductive amination between ketones and ammonium acetate. *Tetrahedron Lett.***2010**, 51, 5210-12.

[16] Taylor, J. E.; Jones, M. D.; Williams, J. M.; Bull, S. D. Friedel-Crafts acylation of pyrroles and indoles using 1,5-diazabicyclo[4.3.0]non-5-ene (DBN) as a nucleophilic catalyst. *Org. Lett.* **2010**, *12* (24), 5740-3.

[17] Kwan; Soo, L.; Kee, K. Efficient synthesis of primary amides from carboxylic acids using N,N'-carbonyldiimidazole and ammonium acetate in ionic liquid. *Synthetic Commun.* **2011**, 41 (23), 3497-3500.

[18] Srinivasa, G.R.; Nalina, L.; Abirajand, K.; Gowda, C. Zinc/ammonium formate: a chemoselective and cost- effective protocol for the reduction of azides to ammines. *J. Chem. Res*. **2003**, 10, 603-631.

# Chapter 4
Targeting Microtubules for Anticancer Therapy
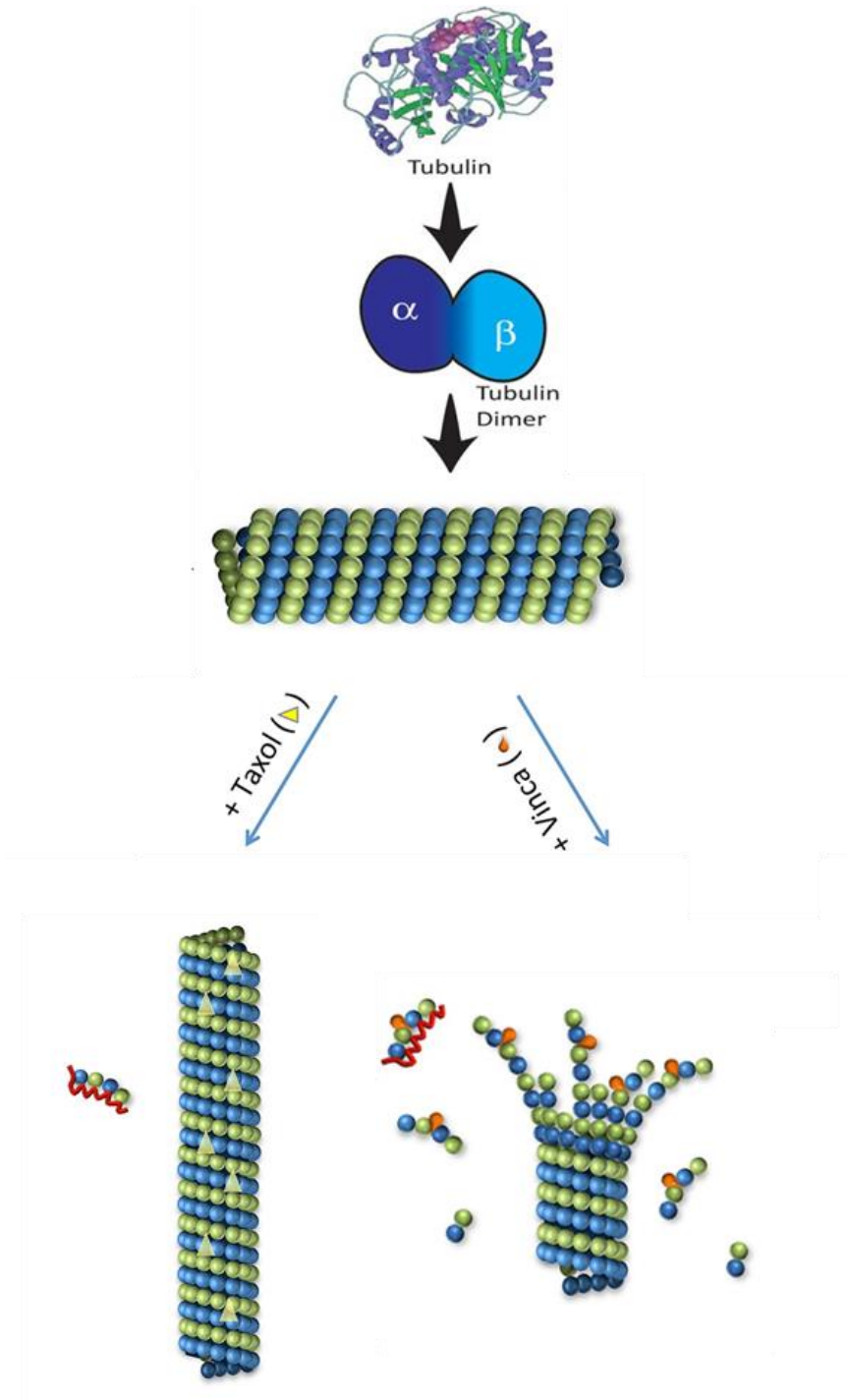
4.1 Structure and function of microtubules

Microtubules (MTs) are crucial for many cellular processes, including cell division, mitotic spindle formation, cell motility, intracellular transport and cell shape maintenance [1, 2].

Structurally, MTs are quite complex: a single microtubule is formed by lateral association of 13 protofilaments, and each protofilament consists of α,β-tubulin heterodimers polymerized in a head-to-tail fashion (Figure 4.1) [3].
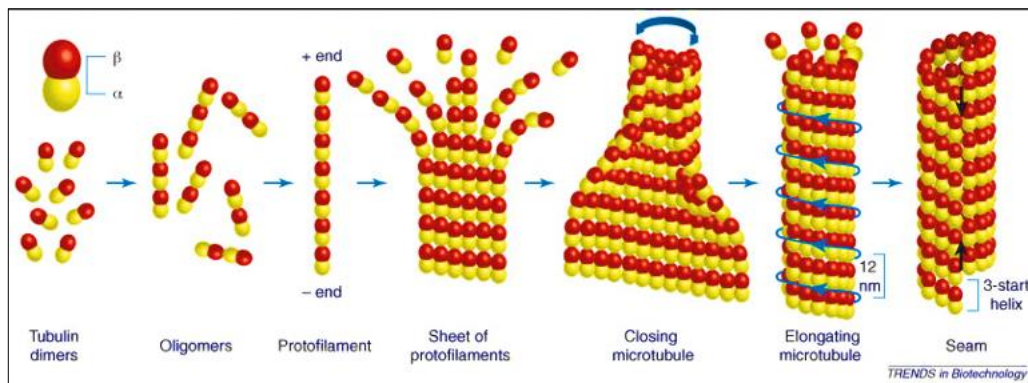
Figure 4.1. *Polymerization of microtubules (from ref. [2])*

Microtubules rapidly switched between periods of polymerization and depolymerization; this highly non-equilibrium behavior, termed *dynamic instability,* is an intrinsic property of microtubules and does not depend on external factors [4].

In vivo, in an interphase cell, microtubules are part of a structural network (the cytoskeleton), and are responsible for transporting substances around the cell. During cell division, this network is completely remodeled to generate a mitotic spindle. At the end of mitosis, the spindle disassembles and the interphase microtubule network reforms.

Notably, all cellular structure (e.g. chromosomes and other organelles) are attached at the ends of microtubules, and as the microtubules grow and shrink, these structures are pushed or pulled around the cell. The two ends of each microtubule seem functionally distinct, because α-tubulin is exposed at one end (the minus end) and is favored for depolymerization, while β-tubulin is exposed at the other end (the plus end) and is favored for polymerization [5].

Dynamic instability is driven by the binding and hydrolysis of GTP by the αβ-tubulin dimer. Many aspects of this process have been elucidated and include the following [5-11] (Figure 4.2):

- both the α- and the β–tubulin monomers bind one molecule of GTP;
- the nucleotide bound to α-tubulin, at the so-called N-site, cannot be exchanged;
- the GTP bound to β-tubulin, at the E-site, can be exchanged with GDP, but only in non-polymerized αβ-tubulin dimers;
- upon polymerization, GTP is hydrolyzed to GDP, that is trapped in the microtubules and can no be exchanged;
- only αβ-tubulin dimer, with GTP at the E site, polymerizes into microtubules at physiological tubulin concentrations; it has high affinity for GTP-bond β-tubulin at the plus end of a growing microtubule;
- GTP hydrolyzes to GDP rapidly after polymerization;
- replacement of GTP by the slowly hydrolysable analogue GMPCPP produces MTs that polymerize normally but depolymerize slowly and don't switch to the depolymerizing state (a transition called *catastrophe*) [10].

In 'GTP-cap' model proposed by Kirschner, a "cap" of GTP-bond β–tubulin at the plus end of growing microtubules is thought to stabilize microtubules itself and promote their further elongation [6, 11].

It has also been reported that although the β-subunit pocket at plus end can bind GTP, it lacks crucial residues necessary for GTP hydrolysis. These residues are donated by the α-subunit in the incoming dimer when it contacts the E-site containing GTP of the terminal β-tubulin subunit [7].

Then, GTP hydrolysis is coupled to polymerization process, as the intrinsic GTP-ase activity of tubulin takes place on the growing microtubules only when the α–subunit in the incoming dimer completes the binding pocket of the exposed β-subunit at plus end [7] (Figure 4.2).

When the GTP-cap is lost (through hydrolysis or other mechanisms), the MT undergoes *catastrophe* (i.e. shifts to depolymerization), whereas regaining the cap is associated with switching back to growth (a transition called *rescue*) [9].

This "GTP-cap" model is supported by experimental evidence and is widely accepted.

However, although significant advances have been made in understanding of the basic structural principles of microtubule dynamic instability, many aspects related to mechanisms that control their assembly and disassembly both *in vitro* and *in vivo* are still unclear and are currently widely investigated [12-17].

In vivo the regulation of microtubules dynamics depends of a complex network of protein protein interactions [18].

Regulator proteins that control microtubule dynamics can be distinguished in: *microtubule-stabilizing* and *microtubule-destabilizing proteins*. The best characterized of these regulatory proteins are the *microtubule-associated proteins* (MAPs) such as tau, MAP2, MAP4, +TIPs (microtubule plus-end tracking proteins), and DCX (doublecortin) [3, 18].
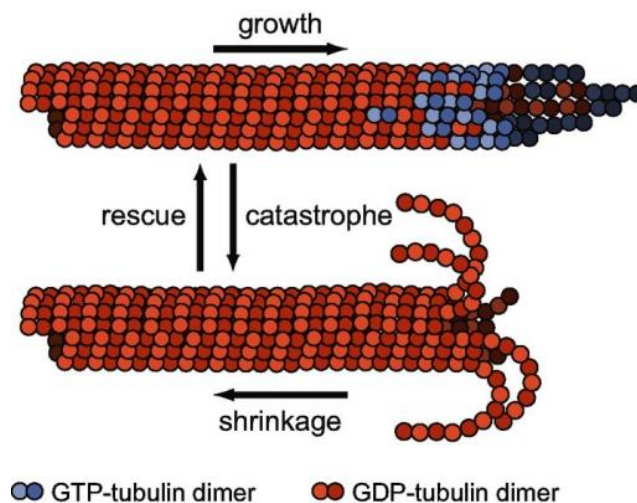
Figure 4.2. *Microtubule dynamic instability (from ref. [17])*

In general, MAPs bind to tubulin at multiple binding sites and stabilize inter-subunit interactions, decreasing catastrophes and/or increasing rescues; moreover, most MAPs identified to date are posttranslationally regulated by phosphorylation [19, 20].

On the contrary, microtubules destabilizing proteins induce *catastrophe*, inhibit polymerization and promote disassembly. The best studied and most potent microtubule depolymerizers are the non motile kinesins from the kinesin-13, kinesin-8 and kinesin-14 family [21-23] and (Op18)/stathmin, a small

protein (19 kDa), originally identified as an oncoprotein [3]. Stathmin physically interacts with tubulin heterodimers forming a ternary tubulin–stathmin complex [24]. Furthermore, this protein is strictly regulated during the cell cycle by transcriptional and posttranscriptional mechanisms. It has been reported that decreased stathmin expression favors microtubule polymerization, whereas increased expression of stathmin reduces microtubule polymer mass [25]. During mitosis, stathmin is inactivated by phosphorylation, thus promoting polymerization and aiding in mitotic spindle assembly [3, 26, 27].

4.2 Tubulin structure

The $\alpha-$ and $\beta-$tubulin share about 40% sequence homology, and exist in several isotype forms and undergo a variety of post-translational modifications [28-30]. In humans, there are six isotypes of α-tubulin and seven isotypes of β-tubulin, and some of them are specifically expressed in specialized cells and tissues [3, 29]. The structure of tubulin has not be elucidated by X-ray for many years because tubulin undergoes easily polymerization, yielding various aggregates of protofilaments that are unsuitable for diffraction studies [31-33].

However, addition of zinc ions and taxol to a purified tubulin give rise to two-dimensional (monolayer) crystals, that can be employed for electron crystallographic analysis. Zinc is used to form sheets, in which the protofilaments are arranged in an antiparallel fashion, while taxol stabilizes the sheets against low-temperature depolymerization and ageing [31, 32]. Then, using low-dose methods, cryo-preservation and image processing, a structure of the tubulin dimer bound to taxol has been obtained at 3.7 Å resolution and subsequently refined at 3.5 Å [32, 33].

The structure of each monomer includes three domains (Figure 4.3):

- an *N-terminal, nucleotide-binding domain*, (aa 1–206), comprising six parallel β-strands (S1- S6) alternating with helices (H1-H6). The loops that connect the β strand with the next helix are directly involved in binding GTP (loops T1 to T6). The *N*-site GTP in α-tubulin is buried at the monomer-monomer interface within the dimer, while the E-site GTP in β-tubulin is exposed on the surface of the dimer;

- *a central domain* (aa 207–384), that is formed by three helices (H8-H10) and a mixed β sheet (S7-S10), and is connected to nucleotide binding domain by helix H7. This domain is involved in hydrolysis, and can thus be considered an essential catalytic subunit of the molecule. In particular, loops T1-T6 and helix H7 from β-tubulin constitute the nucleotide binding domain, whereas loop T7 and Glu254 from α-tubulin are essential for nucleotide hydrolysis;

- a *C-terminal domain* is formed by two antiparallel helices (H11-H12) that cross over the previous two domains. The *C*-terminal tail (i.e. last 10–18 residues) is not visible in the crystal structure, and is the binding site for MAPs.
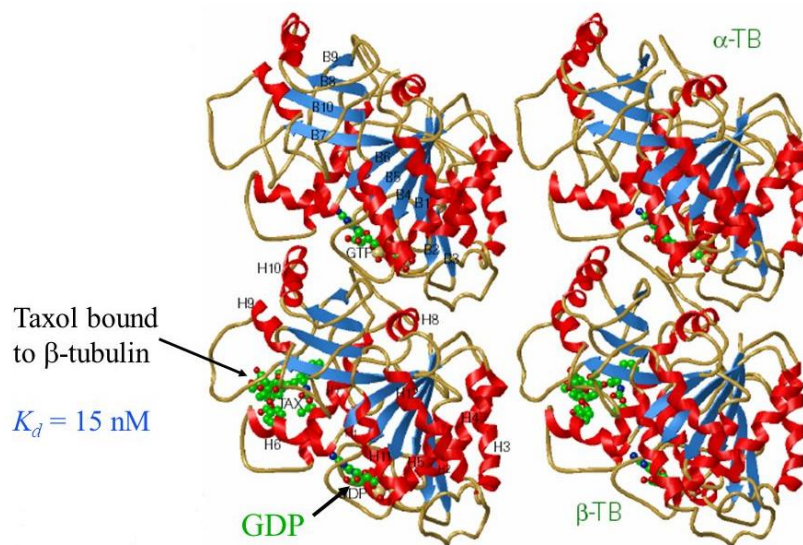
Figure 4.3 *Crystal structure of α and β tubulin (from ref. [32])*

4.3 Antimitotic agents

Microtubules are one of the most investigated anticancer target because of their role in cell division. In clinical there are several compounds that act as antimitotic agents by altering microtubule dynamics. Conventionally, they are classified in two groups, according to their effects at high concentrations on microtubule polymer mass [3].

- *microtubules stabilizers* (e.g. paclitaxel, docetaxel, epothilones, ixabepilone, patupilone, laulimalide, discodermolide) (Figure 4.4);
- *microtubules destabilizers* (e.g. vinblastine, vincristine, vindesine, vinorelbine, vinflunine, colchicine, calcones, combrestatine, 2-methoxyestradiol) (Figure 4.5).

Docetaxel   **Paclitaxel**

Epothilone A: R=H
Epothilone B: R=CH₃   **Ixabepilone**   **Patupilone**

Laulimalide   **Discodermolide**
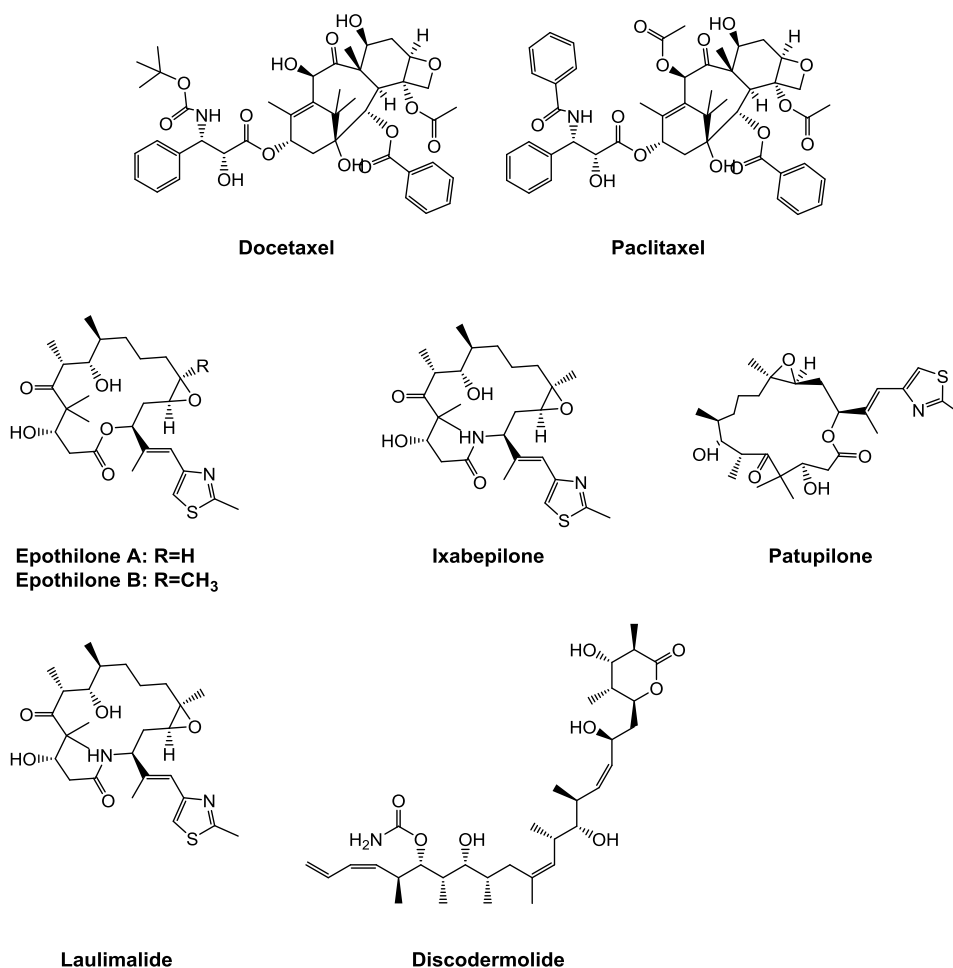
Figure 4.4 *Microtubules stabilizing agents*
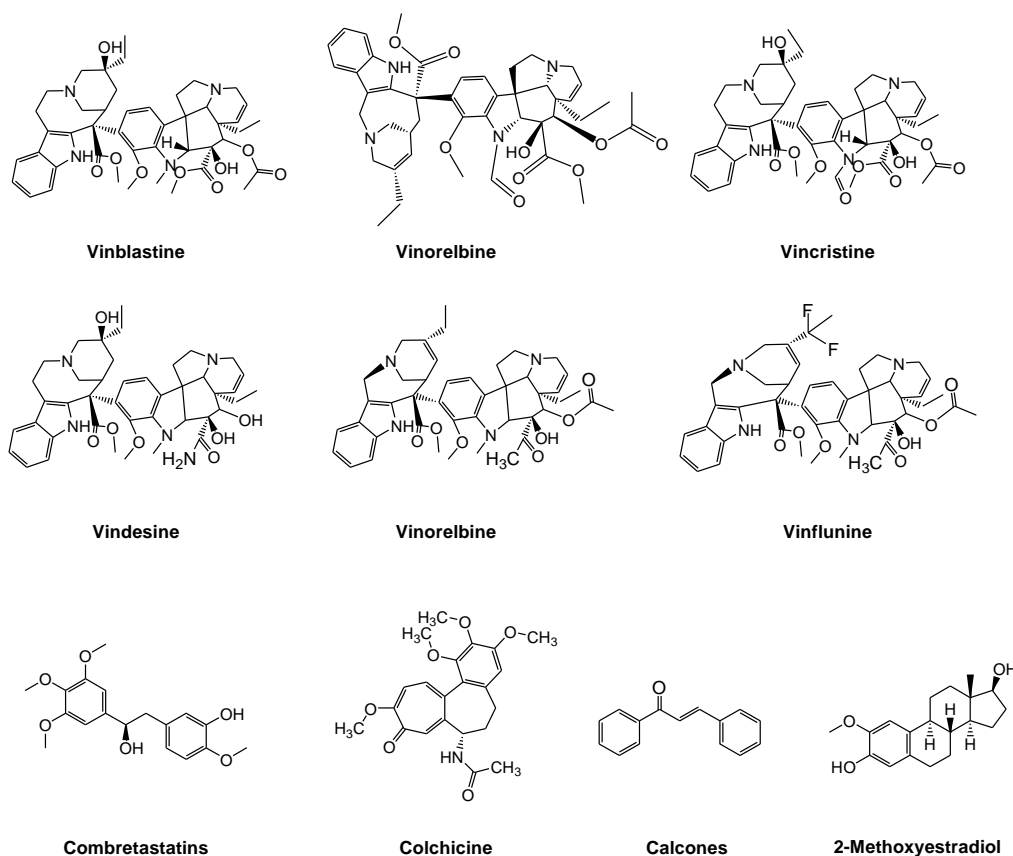
Figure 4.5 *Microtubules destabilizing agents*

However, these drugs potently suppress microtubule dynamics at 10 to 100-fold lower concentrations [3].

At low concentrations, they share a common feature to kinetically stabilize the microtubules without changing the microtubule polymer mass. They block mitosis similarly, altering microtubule dynamics and inducing a loss of tension across sister kinetochores at the metaphase plate. This event activates checkpoint proteins such as Mad2 and BubR1, leading to cell cycle arrest [34-36]. Supporting this common mechanism of action is the finding that stabilizing and destabilizing agents can be combined clinically in chemotherapy regimens with no apparent antagonism [1]. In addition, some combinations (e. g. taxanes with vinblastine) have shown synergism *in vitro*.

The majority of the microtubule targeting agents bind to one of main three binding sites referred as: taxanes, vinca and colchicine binding site (Figure 4.6); however, some compounds bind to tubulin on undefined sites or target microtubules indirectly by altering their posttranslational modifications [3, 37-44].
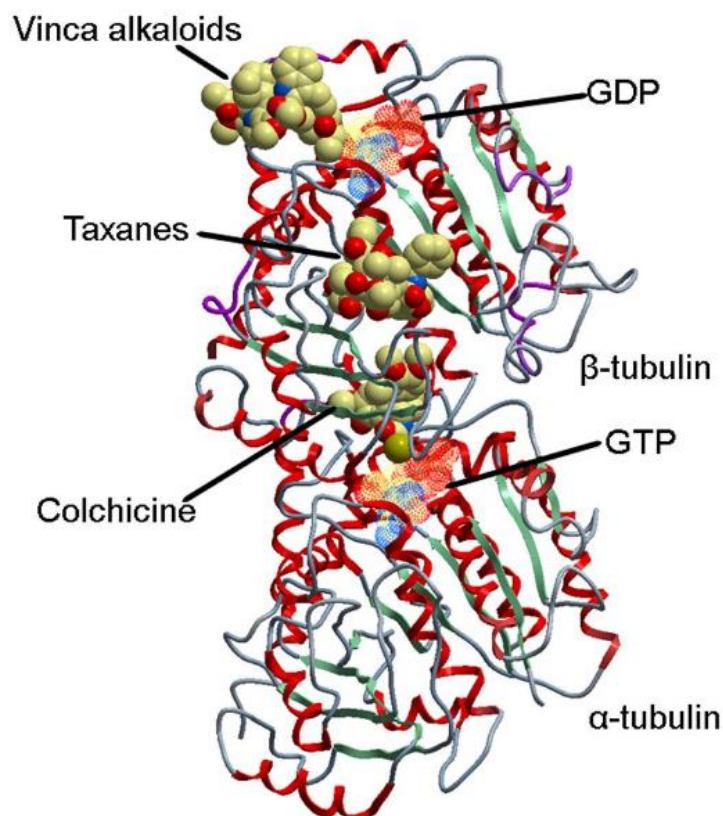
Figure 4.6 *Tubulin binding sites (from ref. [44])*

Taxanes (e.g. paclitaxel, docetaxel) are used primarily for the treatment of a range of solid cancers such as breast, ovarian, gastroesophageal, as well as cancers of the head and neck, and nonsmall cell lung cancer [38-41]. They act by binding to the β–tubulin subunit on the microtubule inner surface, and stabilize protofilaments leading to microtubule over-polymerization (Figure 4.6). Currently available taxanes show a limited intestinal uptake and a poor water solubility, then they are administered intravenously with surfactants such as Cremophor and ethanol, a vehicle associated with severe hypersensitivity reactions [42]. New approaches have been recently developed to improve their oral bioavalibilty or eliminate surfactants from current formulations [42-45].

Vinca domain binders include the *vinca site binders* and *peptide site binders* [3]. The vinca alkaloids, such as vincristine, vinblastine, and vinorelbine, are most often used for haematological malignancies, such as lymphomas and leukemias. They bind near the hydrolyzable GTP site, and alter the dimer conformation,

inhibiting tubulin-dependent GTP hydrolysis and GDP–GTP exchange. At low concentrations, they bind to the plus ends of microtubules, altering their intrinsic dynamics and thus are also referred to as *end poisons* [3].

Peptide site binders (e.g. dolastatins, spongistatins, and cryptophycins) cause microtubule destabilization by inhibiting GTP hydrolysis; their binding site coincide partly with that of vinca alkaloids [3].

Colchicine-site binders (e.g. podophyllotoxin, combretastatins, 2-methoxyestradiol) bind to the intradimeric α-β interface of tubulin heterodimers, contiguous to the GTP-binding domain of the α-tubulin subunit. This leads to the lack of heterodimer formation and prevents the microtubules from extension.

Recently, noscapinoids has been reported as "kinder and gentler" antimitotic agents (Figure 4.7) [46, 47]. These compounds attenuate microtubule dynamics in mitotic cells just enough to engage mitotic checkpoints without perturbing the transport functions of microtubules in postmitotic cells [3].
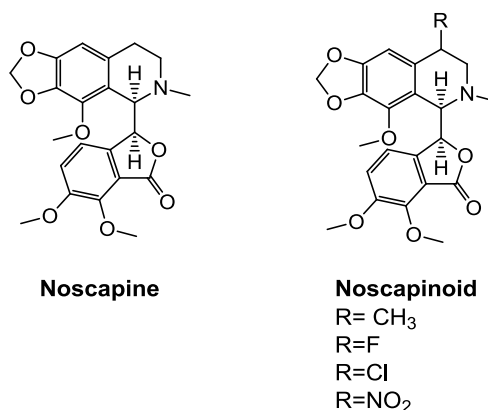
Figure 4.7 *Noscapine and noscapine analogues*

4.4 Mechanisms of drug resistance

The mechanism of drug resistances is a common feature in cancer chemotherapy. Resistance towards microtubule-stabilizing drugs includes above all (Figure 4.8) [1, 48-50]:

- membrane efflux pumps;
- changes in the expression of microtubule-associated proteins (MAPs);
- modifications in β-tubulin isotype composition.

The chemoresistance can also be originate by tubulin mutations, alterations in tubulin post-translational modifications, disorders in the spindle assembly checkpoint (SAC) and dysfunctional regulation of apoptosis.

The most typical efflux pumps in the cell membrane P-glycoprotein (P-gp) is a member of the ATP binding cassette (ABC) superfamily [51]. It is the product of gene amplification of the normal human gene, *mdr1*, and is responsible for the "classical multidrug resistant phenotype". This transporter actively effluxes both vincas and taxanes; in addition, since Pgp is mainly present in the apical membrane of intestinal mucosal membrane, it can lower bioavailability of these drugs by preventing their absorption.
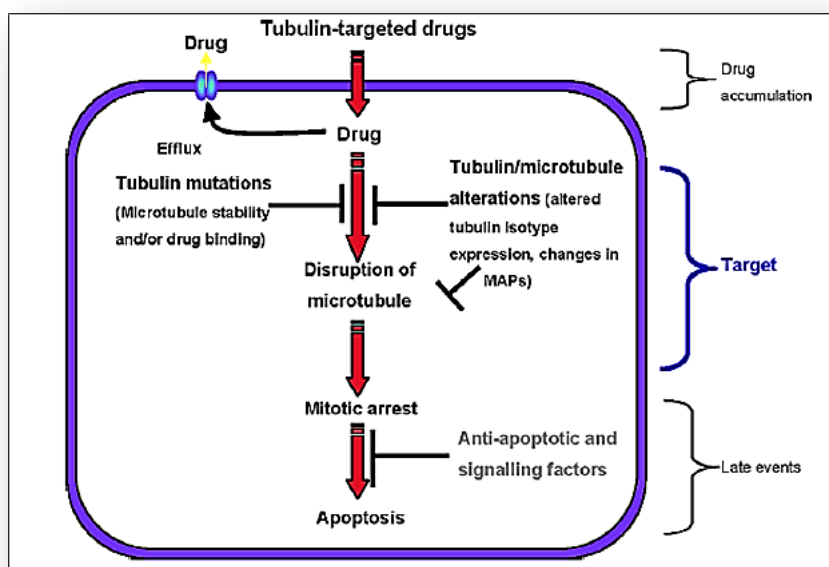
Figure 4.8 *Mechanisms mediating resistance to microtubule targeting agents (from ref. [48])*

Other transporters of the mammalian cell membrane in ABC superfamily are more selective than P-gp, and transport only some types of antitubulin agents. For example, MRP1 protein actively transports vincas, while taxanes are substrates for MRP2 and MRP7, and epothilone B is transported by MRP7 [1].

Moreover, alterations in levels of expression of MAPs correlate with aggressiveness of a variety of human cancers and/or their sensitivity to microtubule-targeting agents [52-54]. For example, overexpression of stathmin

decreases polymerization of microtubules and consequently decreases sensitivity to paclitaxel and, to a lesser extent, to vinblastine [53].

Concerning the mutations of α- and ß- tubulin, the α-tubulin proteins are highly conserved and differ by only a few residues; on the contrary, the β-tubulins differ significantly in their *C*-terminal tail, which is involved in post-translational modifications and in critical interactions with a range of proteins. Based on their C-terminal sequences, β-tubulin isotypes can be assigned to seven distinct classes named βI, βII, βIII, βIVa, βIVb, βV, and βVI. Modifications in ß-tubulin isotype composition have been observed in a range of cancers; analysis of clinical specimens has shown that high expression of tubulin isotypes, βI, βII-, βIII-, βIVa-, and βV-tubulin, correlates with aggressive clinical behaviour, chemotherapy drug resistance and poor patient outcome in many cancers (Table I) [55].

Table I. *Tubulin isotypes and drug resistance (from ref. [54])*

Alteration of Tubulin Isotype	Effect	Tumour Type
High βI-tubulin	Poor response to docetaxel treatment	Breast cancer
Low βII-tubulin expression	Correlates with poor response to taxane treatment or advanced stage disease	Breast and ovarian cancer
High βIII-tubulin expression	Poor survival, poor outcome for surgical resection or MTAs response; Correlates with subtype	Non-small cell lung cancer (NSCLC)
	Correlates with poor survival, poor response to platinum and taxane treatment, advanced stage or aggressive disease	Ovarian cancer
	Favorable response to taxane treatment	Ovarian (Clear cell adeno-carcinoma)
	Poor response to taxane treatment	Breast cancer
	Poor response to taxane/platinum treatment	Uterine serous carcinoma
	Poor response to taxane treatment Advanced disease and early recurrence	Gastric cancer Prostate cancer
High βIV-tubulin expression	Poor response to taxol treatment	Ovarian cancer
High βV-tubulin expression	Favorable response to taxane treatment	NSCLC

References

[1] Dumontet, C.; Jordan, M. A. Microtubule-binding agents: a dynamic field of cancer therapeutics. *Nat. Rev. Drug Disc.* **2010**, *9* (10), 790-803.

[2] Pampaloni, F.; Florin, E. L. Microtubule architecture: inspiration for novel carbon nanotube-based biomimetic materials. *Trends Biotechnol.* **2008**, *26* (6), 302-10.

[3] Stanton, R. A.; Gernert, K. M.; Nettles, J. H.; Aneja, R. Drugs that target dynamic microtubules: a new molecular perspective. *Med. Res. Rev.* **2011**, *31* (3), 443-81.

[4] Horio, T.; Murata, T. The role of dynamic instability in microtubule organization. *Front. Plant. Sci.* **2014**, *5*, 511

[5] Akhmanova, A.; Hoogenraad, C. C. Microtubule minus-end-targeting proteins. *Curr. Biol.* **2015**, *25* (4), R162-71.

[6] Mitchison, T.; Kirschner, M. Dynamic instability of microtubule growth. *Nature* **1984**, *312* (5991), 237-42.

[7] Howard, J.; Hyman, A. A. Dynamics and mechanics of the microtubule plus end. *Nature* **2003**, *422* (6933), 753-8.

[8] Margolin, G.; Gregoretti, I. V.; Cickovski, T. M.; Li, C.; Shi, W.; Alber, M. S.; Goodson, H. V. The mechanisms of microtubule catastrophe and rescue: implications from analysis of a dimer-scale computational model. *Mol. Biol. Cell* **2012**, *23* (4), 642-56.

[9] Nogales, E.; Wang, H. W. Structural intermediates in microtubule assembly and disassembly: how and why? *Curr. Opin. Cell Biol.* **2006**, *18* (2), 179-84.

[10] Hyman, A. A.; Salser, S.; Drechsel, D. N.; Unwin, N.; Mitchison, T. J. Role of GTP hydrolysis in microtubule dynamics: information from a slowly hydrolyzable analogue, GMPCPP. *Mol. Biol. Cell* **1992**, *3* (10), 1155-67.

[11] Drechsel, D. N.; Kirschner, M. W. The minimum GTP cap required to stabilize microtubules. *Curr. Biol.* **1994**, *4* (12), 1053-61.

[12] Bowne-Anderson, H.; Zanic, M.; Kauer, M.; Howard, J. Microtubule dynamic instability: a new model with coupled GTP hydrolysis and multistep catastrophe. *Bioessays* **2013**, *35* (5), 452-61.

[13] Alushin, G. M.; Lander, G. C.; Kellogg, E. H.; Zhang, R.; Baker, D.; Nogales, E. High-resolution microtubule structures reveal the structural transitions in alphabeta-tubulin upon GTP hydrolysis. *Cell* **2014**, *157* (5), 1117-29.

[14] Mitchison, T. J. The engine of microtubule dynamics comes into focus. *Cell* **2014**, *157* (5), 1008-10.

[15] Burbank, K. S.; Mitchison, T. J. Microtubule dynamic instability. *Current Biol.* **2006**, *16* (14), R516-7.

[16] Brun, L.; Rupp, B.; Ward, J. J.; Nedelec, F. A theory of microtubule catastrophes and their regulation. *PNAS* **2009**, *106* (50), 21173-8.

[17] Zelinski, B.; Kierfeld, J. Cooperative dynamics of microtubule ensembles: polymerization forces and rescue-induced oscillations. *Phys. Rev. E Stat. Nonlin. Soft Matter Phys.* **2013**, *87* (1), 012703.

[18] Hughes, J. R.; Meireles, A. M.; Fisher, K. H.; Garcia, A.; Antrobus, P. R.; Wainman, A.; Zitzmann, N.; Deane, C.; Ohkura, H.; Wakefield, J. G. A microtubule interactome: complexes with roles in cell cycle and mitosis. *PLoS Biol.* **2008**, *6* (4), e98.

[19] Drechsel, D. N.; Hyman, A. A.; Cobb, M. H.; Kirschner, M. W. Modulation of the dynamic instability of tubulin assembly by the microtubule-associated protein tau. *Mol. Biol. Cell* **1992**, *3* (10), 1141-54.

[20] Trinczek, B.; Biernat, J.; Baumann, K.; Mandelkow, E. M.; Mandelkow, E. Domains of tau protein, differential phosphorylation, and dynamic instability of microtubules. *Mol. Biol. Cell* **1995**, *6* (12), 1887-902.

[21] Desai, A.; Verma, S.; Mitchison, T. J.; Walczak, C. E. Kin I kinesins are microtubule-destabilizing enzymes. *Cell* **1999**, *96* (1), 69-78.

[22] Gupta, M. L., Jr.; Carvalho, P.; Roof, D. M.; Pellman, D. Plus end-specific depolymerase activity of Kip3, a kinesin-8 protein, explains its role in positioning the yeast mitotic spindle. *Nature Cell Biol.* **2006**, *8* (9), 913-23.

[23] Cai, S.; Weaver, L. N.; Ems-McClung, S. C.; Walczak, C. E. Kinesin-14 family proteins HSET/XCTK2 control spindle length by cross-linking and sliding microtubules. *Mol. Biol. Cell* **2009**, *20* (5), 1348-59.

[24] Steinmetz, M. O. Structure and thermodynamics of the tubulin-stathmin interaction. *J. Struct Biol.* **2007**, *158* (2), 137-47.

[25] Howell, B.; Deacon, H.; Cassimeris, L. Decreasing oncoprotein 18/stathmin levels reduces microtubule catastrophes and increases microtubule polymer in vivo. *J. Cell Sci.* **1999**, *112 (Pt 21)*, 3713-22.

[26] Larsson, N.; Marklund, U.; Gradin, H. M.; Brattsand, G.; Gullberg, M. Control of microtubule dynamics by oncoprotein 18: dissection of the regulatory role of multisite phosphorylation during mitosis. *Mol. Cell. Biol.* **1997**, *17* (9), 5530-9.

[27] Gavet, O.; Ozon, S.; Manceau, V.; Lawler, S.; Curmi, P.; Sobel, A. The stathmin phosphoprotein family: intracellular localization and effects on the microtubule network. *J. Cell Sci.* **1998**, *111 (Pt 22)*, 3333-46.

[28] Nicoletti, M. I.; Valoti, G.; Giannakakou, P.; Zhan, Z.; Kim, J. H.; Lucchini, V.; Landoni, F.; Mayo, J. G.; Giavazzi, R.; Fojo, T. Expression of beta-tubulin isotypes in human ovarian carcinoma xenografts and in a sub-panel of human cancer cell lines from the NCI-Anticancer Drug Screen: correlation with sensitivity to microtubule active agents. *Clin. Cancer Res.* **2001**, *7* (9), 2912-22.

[29] Pascal, V. P.; Burd, B.; Horwitz, S.; Orr, G. A. Quantitative proteomics of α- and β-tubulin isotype expression in human cancer cells. *Proc. Amer. Assoc. Cancer Res.* **2004**, 45.

[30] Song, Y.; Brady, S. T. Post-translational modifications of tubulin: pathways to functional diversity of microtubules. *Trends Cell Biol.* **2015**, *25* (3), 125-36.

[31] Downing, K. H. Structural basis for the interaction of tubulin with proteins and drugs that affect microtubule dynamics. *Annu. Rev. Cell Dev. Biol.* **2000**, *16*, 89-111.

[32] Nogales, E.; Wolf, S. G.; Downing, K. H. Structure of the alpha beta tubulin dimer by electron crystallography. *Nature* **1998**, *391* (6663), 199-203.

[33] Nogales, E.; Whittaker, M.; Milligan, R. A.; Downing, K. H. High-resolution model of the microtubule. *Cell* **1999**, *96* (1), 79-88.

[34] Jordan, M. A.; Toso, R. J.; Thrower, D.; Wilson, L. Mechanism of mitotic block and inhibition of cell proliferation by taxol at low concentrations. *PNAS* **1993**, *90* (20), 9552-6.

[35] Panda, D.; Jordan, M. A.; Chu, K. C.; Wilson, L. Differential effects of vinblastine on polymerization and dynamics at opposite microtubule ends. *J. Biol. Chem.* **1996**, *271* (47), 29807-12.

[36] Fang, G. Checkpoint protein BubR1 acts synergistically with Mad2 to inhibit anaphase-promoting complex. *Mol. Biol. Cell* **2002**, *13* (3), 755-66.

[37] Giannakakou, P.; Villalba, L.; Li, H.; Poruchynsky, M.; Fojo, T. Combinations of paclitaxel and vinblastine and their effects on tubulin polymerization and cellular cytotoxicity: characterization of a synergistic schedule. *Int. J. Cancer* **1998**, *75* (1), 57-63.

[38] Jimenez, P.; Pathak, A.; Phan, A. T. The role of taxanes in the management of gastroesphageal cancer. *J. Gastrointest Oncol.* **2011**, *2* (4), 240-9.

[39] Gradishar, W. J. Taxanes for the treatment of metastatic breast cancer. *Breast Cancer (Auckl)* **2012**, *6*, 159-71.

[40] Chu, Q.; Vincent, M.; Logan, D.; Mackay, J. A.; Evans, W. K. Lung Cancer Disease Site Group of Cancer Care Ontario's Program in Evidence-based, C. Taxanes as first-line therapy for advanced non-small cell lung cancer: a systematic review and practice guideline. *Lung Cancer* **2005**, *50* (3), 355-74.

[41] Misiukiewicz, K.; Gupta, V.; Bakst, R.; Posner, M. Taxanes in cancer of the head and neck. *Anticancer Drugs* **2014**, *25* (5), 561-70.

[42] Wang, H.; Cheng, G.; Du, Y.; Ye, L.; Chen, W.; Zhang, L.; Wang, T.; Tian, J.; Fu, F. Hypersensitivity reaction studies of a polyethoxylated castor oil-free, liposome-based alternative paclitaxel formulation. *Mol. Med. Rep.* **2013**, *7* (3), 947-52.

[43] Yared, J. A.; Tkaczuk K. H. Update on taxane development: new analogs and new formulations. *Drug Des. Devel. Ther.* **2012**, *6*, 371-84.

[44] Xie, S.; Zhou, J. Harnessing Plant Biodiversity for the Discovery of Novel Anticancer Drugs Targeting Microtubules. *Front. Plant Sci.* **2017**, *8*, 720.

[45] Chen, S. M.; Meng, L. H.; Ding, J. New microtubule-inhibiting anticancer agents. *Expert Opin. Investig. Drugs* **2010**, *19* (3), 329-43.

[46] Naik, P. K.; Santoshi, S.; Joshi, H. C. Noscapinoids with anti-cancer activity against human acute lymphoblastic leukemia cells (CEM): a three dimensional chemical space pharmacophore modeling and electronic feature analysis. *J. Mol. Model.* **2012**, *18* (1), 307-18.

[47] Landen, J. W.; Lang, R.; McMahon, S. J.; Rusan, N. M.; Yvon, A. M.; Adams, A. W.; Sorcinelli, M. D.; Campbell, R.; Bonaccorsi, P.; Ansel, J. C.; Archer, D. R.; Wadsworth, P.; Armstrong, C. A.; Joshi, H. C. Noscapine alters microtubule dynamics in living cells and inhibits the progression of melanoma. *Cancer Res.* **2002**, *62* (14), 4109-14.

[48] Kavallaris, M. Discovering novel strategies for antimicrotubule cytotoxic therapy. *EJC Suppl*. **2006**, *4* (7), 3-9

[49] Kavallaris, M. Microtubules and resistance to tubulin-binding agents. *Nat. Rev. Cancer* **2010**, *10* (3), 194-204.

[50] Kavallaris, M.; Annereau, J. P.; Barret, J. M. Potential mechanisms of resistance to microtubule inhibitors. *Semin. Oncol.* **2008**, *35* (3 Suppl 3), S22-7.

[51] Choi, C. H. ABC transporters as multidrug resistance mechanisms and the development of chemosensitizers for their reversal. *Cancer Cell Int.* **2005**, *5*, 30.

[52] Bhat, K. M.; Setaluri, V. Microtubule-associated proteins as targets in cancer chemotherapy. *Clin. Cancer Res.* **2007**, *13* (10), 2849-54.

[53] Mistry, S. J.; Atweh, G. F. Role of stathmin in the regulation of the mitotic spindle: potential applications in cancer therapy. *Mt. Sinai J. Med.* **2002**, *69* (5), 299-304.

[54] Poruchynsky, M. S.; Giannakakou, P.; Ward, Y.; Bulinski, J. C.; Telford, W. G.; Robey, R. W.; Fojo, T. Accompanying protein alterations in malignant cells with a microtubule-polymerizing drug-resistance phenotype and a primary resistance mechanism. *Biochem. Pharmacol.* **2001**, *62* (11), 1469-80.

[55] Parker, A. L.; Teo, W. S.; McCarroll, J. A.; Kavallaris, M. An Emerging Role for Tubulin Isotypes in Modulating Cancer Biology and Chemotherapy Resistance. *Int. J. Mol. Sci.* **2017**, *18* (7).

Chapter 5
Identification of New Microtubules Targeting Agents

1. Targets

β-Tubulin α-Tubulin

PDB ID: 1TUB (1)

4. Biological Evaluation

G1 23%   S 58%

G2m 15%

Sub G1 5%

Count
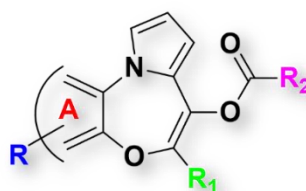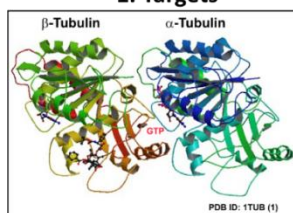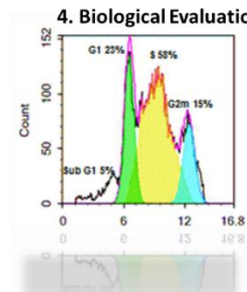
2. Synthesis

3. Characterization

5.1 Background

The pyrrolo-1,5-benzoxazepines (PBOXs) compounds have been described as anticancer agents with IC_{50} values in the micromolar and nanomolar range [1]. The chemical structures of representative anti-proliferative PBOXs (namely PBOX-1, -2, -3, -4, -5, -6, -15, -16 and -21) [2, 3] are reported in Figure 5.1.
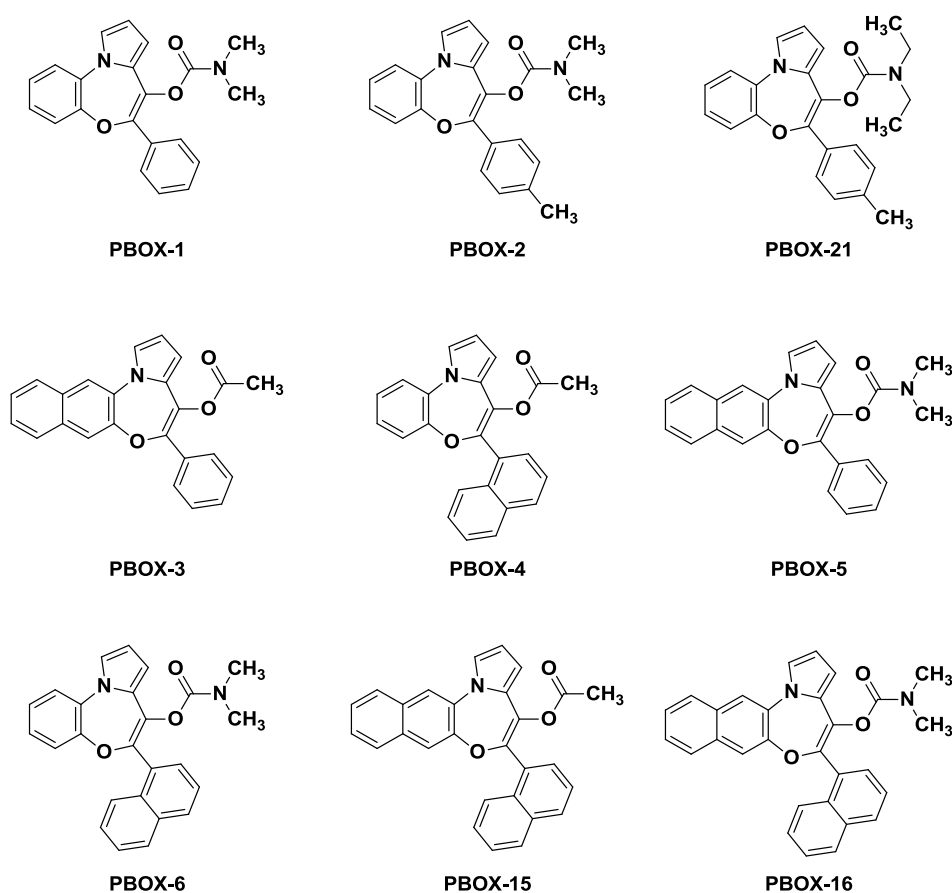
Figure 5.1 *Chemical structure of representative PBOXs*

In general, PBOXs can be classified into two groups, on the basis of their ability to induce or not apoptosis (Figure 5.1); further, the non-apoptotic PBOXs induce a G1 cell cycle arrest, while the pro-apoptotic PBOXs produce a G2/M arrest subsequent to apoptosis [3-6].

Among PBOXs analogues, a more deeper biological investigation was accomplished for PBOX-6 (Figure 5.1). This compound has been investigated against a panel of cancer cell lines including:

- HL-60 (Human promyelocytic leukemia cells), Jurkat (immortalized human T lymphocyte cells), Hut-78 (subcutaneous T-cell lymphoma cells), with a percentage of apoptosis of 45-50% at 10 μM, following 16h treatment [1, 2];

- three chronic myelogenous leukaemia cell line (CML): KYO.1, LAMA 84 and K-562 (an extremely resistant CML cell line), with a percentage of apoptosis of ca 50% at 10 μM, following 16h treatment [3];

- HT29 (colon carcinoma cells, $IC_{50} = 1.9 \pm 0.16$ μM), NCI-H460 (non-small-cell lung cancer cells, $IC_{50} = 1.7 \pm 0.11$ μM), LoVo (colon carcinoma cells, $IC_{50} = 9.2 \pm 0.4$ μM), M109 (murine lung carcinoma, $IC_{50} = 1.8 \pm 0.03$ μM), MesSa (sarcoma cell line, $IC_{50} = 7.1 \pm 0.3$ μM) [2];

- MCF7, with a percentage of apoptosis of 37%, at 25 μM following 72h treatment [4].

It has been reported that PBOX-6 is also capable of inducing apoptosis in drug-resistant HL60-MDR1 cells (expressing P-glycoprotein) and HL60-ABCG2 cells (expressing BCRP), with similar potencies as in parental human promyelocytic leukaemia HL60 cells [5].

Moreover, PBOX-6 did not induce apoptosis in a rat R2C Leydig cell line (at 50 μM following 16h treatment), and showed minimal toxicity to normal peripheral blood mononuclear cells (PBMCs) [1, 6].

PBOX-6 is a microtubule depolymerizing agent; in this regard, indirect immunofluorescence assay evidenced that it causes microtubule depolymerization in MCF-7 cells; furthermore, it also inhibits assembly of purified tubulin *in vitro* and does not bind to either the vinblastine or the colchicine binding site on tubulin, suggesting that it binds to an as-yet uncharacterized novel site on tubulin [6, 7].

It has been reported that PBOX-6 primarily targets tubulin and, as a consequence, promotes different, cell-specific, downstream cellular pathways.

In particular, it was observed that:

- release of cytochrome *c* and activation of caspase-3 are involved in the mechanism by which PBOX-6 induces apoptosis in HL-60 and Jurkat cells [1];

- on the contrary, activation of caspase-3 is not required for PBOX-6-induced apoptosis in CML cells [3];

- apoptosis in chronic myelogenous leukemia (CML) K562 cells as well as in wild-type T leukemia CEM cells (CEM/Neo) and cells overexpressing Bcl-2 (CEM/Bcl-2) depends by time- and dose-dependent phosphorylation and inactivation of anti-apoptotic Bcl-2 and BCL-XL [4];

- caspase-7 (but not caspase-3 and-6) is involved in the mechanism by which PBOX-6 promotes apoptosis in MCF-7 cells [4];

- activation of c-Jun *N*-terminal kinase (c-JNK), which phosphorylates Bcl-2, is essential in the PBOX-6-induced apoptotic pathway in K562 cell; inhibition of JNK activity prevents Bcl-2 phosphorylation and apoptosis, implicating JNK in the upstream signaling pathway leading to Bcl-2 phosphorylation [5, 8];

- in sensitive (SK-N-FI, CHLA-90 and SK-N-BE(2)c) and multidrug resistant neuroblastoma cells (SHSY5Y, Kelly, SK-N-BE(1) PBOX-6 induced cleavage of Bcl-2, a downregulation of MCL-1, and a concomitant increase in BAK and activation of caspase-3, -8 and -9 [9];

- PBOX-6 also evidenced anti-angiogenic activity a property that may augment its antineoplastic properties *in vivo*; in addition, it showed efficacy in an *in vivo* mouse mammary carcinoma model and against resistant chronic myeloid leukaemia cells in *ex vivo* patient samples and *in vivo* [10-12].

However, PBOX-6, despite its promising pharmacological profile, was found to induce protective autophagy in some cancer cell lines [13].

Structure activity relationships (SARs) studies performed on this class of tubulin targeting agents indicated that:

- a 1-naphthyl system on the benzoxazepine ring (R_1, Figure 5.2) leads to potent antiproliferative agents; its replacement with a phenyl, a *p*-MePh, a *p*-OMePh or a 2-naphthyl group decreases the antiproliferative activity leading to analogues with weak-to-negligible activity [2, 14];

- the R_2 substituent (Figure 5.2) can be the alkyl portion of either an ester or a carbamate functional group; in both ester and carbamate series a methyl group is well tolerated, while the introduction of longer alkyl groups results in a complete loss of apoptotic activity [2, 14];

- the presence of a naphtho-fused group (ring A, Figure 5.2) increases the apoptotic activity; furthermore, the introduction of a polar ethoxycarbonyl function at position 3 of the benzo-fused system of PBOX-6 leads to a potent, cell-penetrating apoptotic agent, probing tolerance at the target site. Nevertheless, substitution of the benzo-fused system of PBOX-6 by a pyrido-fused group lowers the apoptotic activity, indicating that a modification of the polarization of π-system might lead to nonoptimal interaction with the target [2, 14].
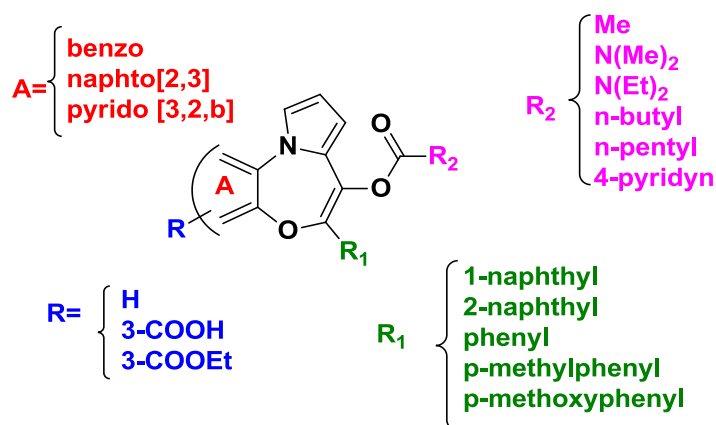
Figure 5.2. *Modifications on the core structure of PBOX-based compounds*

5.2 Aim of the work

This research project was aimed to develop new analogues of PBOX-6 in order to:

- improve its pharmacological and pharmacokinetic profile;

- shed light on structural requirements for interfering with microtubule dynamics and apoptotic activity;

- overcome resistance related to autophagy induction.

To date the benzo-fused ring of PBOX-6 has been substituted only by a naphthyl ring (e.g. PBOX-15, pyrrolobenzoxazepine 4-acetoxy-5-(1-naphthyl)naphtha pyrrolo[1,4]-oxazepine), and by a pyridine ring (Figure 5.1).

Then a first set of compounds bearing substituents with different lipophilic, steric and electronic properties on the benzo-fused ring of PBOX-6 was designed (compounds **17a-h**, Figure 5.3).

Further, it was evaluated also the effect of the removal of the *N*-dimethylcarbamoyl moiety of PBOX-6, and the introduction of a double bond at the 6,7 positions of the pyrrolobenzoxazepine ring (compounds **17i-k**, Figure 5.3).

A second series of putative antiproliferative agents (compounds **17l-n**, Figure 5.4) was generated by ring contraction of the seven membered ring of the pyrrolobenzoxazepine system of PBOX-6 to the six member ring of the benzoxazinone system.

With the exception of **17l**, a *N*-benzyl (**17m**) and a *N*-4-fluorobenzyl (**17n**) were employed as mimetic of the pyrrole-fused system of PBOX-6.

Series I
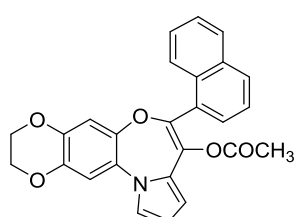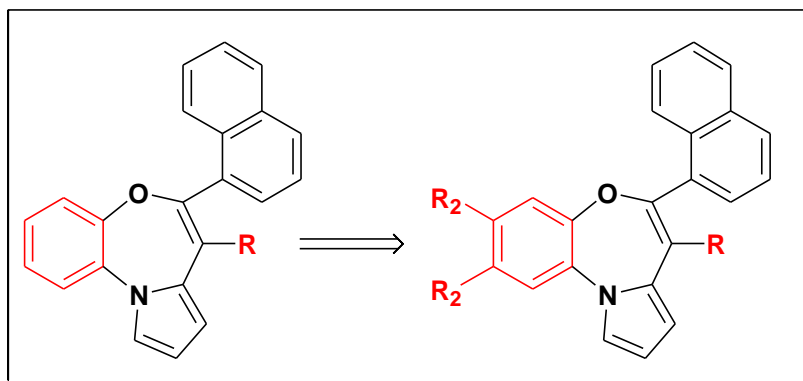
17a
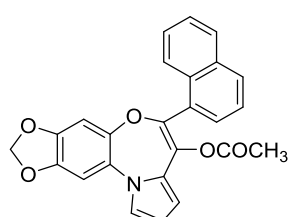
17b
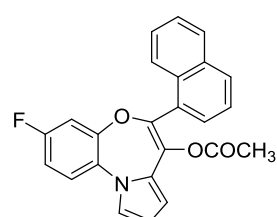
17c
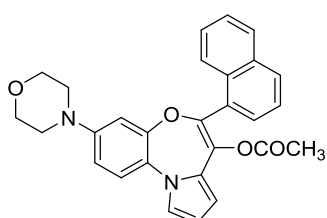
17d
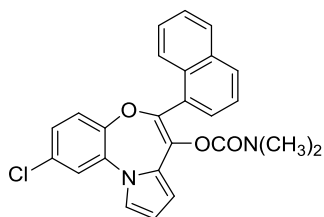
17e
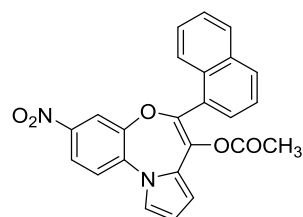
17f
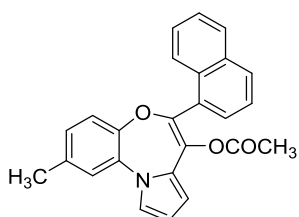
17g
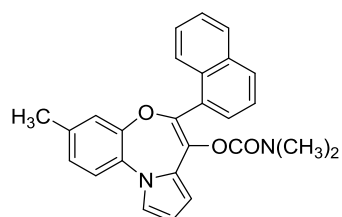
17h
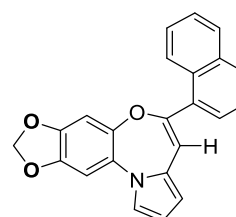
17i
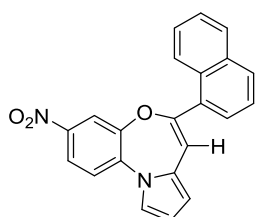
17j
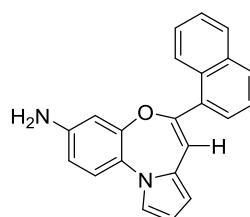
17k

Figure 5.3 *Structure of PBOX analogues **17a-k***

Series II
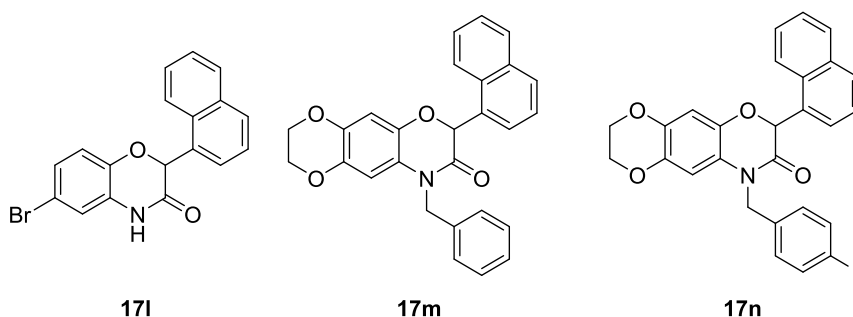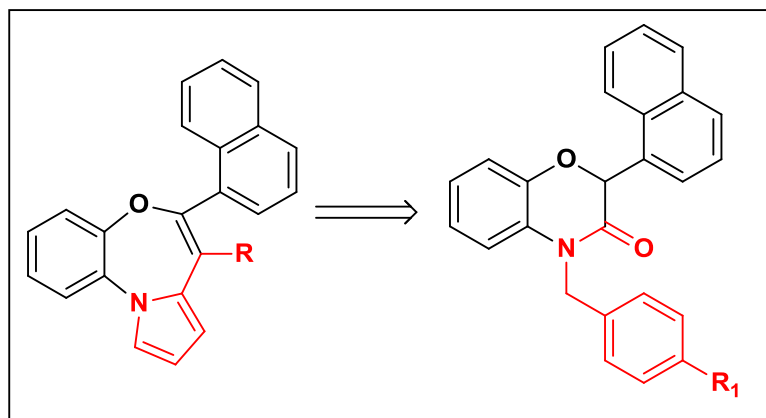
Figure 5.4 *Structure of benzoxazinone derivatives 17l-n*

5.3 Synthesis

In Schemes 5.1-5.4 is described the synthesis of the new PBOX-6 analogues **17a-k**. The 2,3-dihydro-1,4-benzodioxin-6-ol **19a** was not commercially available, and was prepared by reduction of 2,3-dihydrobenzo[δ][1,4]dioxine-6-carbaldehyde **18** with 3-chloroperoxybenzoic acid (*m*CPBA), according to a previously reported procedure with slight modifications (Scheme 5.1) [15]. The intermediate **19a** and its strictly analogue benzo[1,3]dioxol-5-ol **19b** were converted to the corresponding acetyl derivatives **20a,b** [16], which in turn gave the nitro analogues 7-nitro-2,3-dihydro-1,4-benzodioxin-6-yl acetate **21a** and 6-nitro-2H-1,3-benzodioxol-5-yl acetate **21b** respectively in good yields (Scheme 5.1). Then **21a,b** were hydrolyzed with H_2SO_4 (25% v/v) to obtain 7-nitro-2,3-dihydro-1,4-benzodioxin-6-ol **22a** and 6-nitro-2H-1,3-benzodioxol-5-ol **22b** respectively. Commercially available 5-fluoro-2-nitrophenol **22c** was treated with morpholine to give 5-(morpholin-4-yl)-2-nitrophenol **22d** (Scheme 5.1) [17].

Scheme 5.1
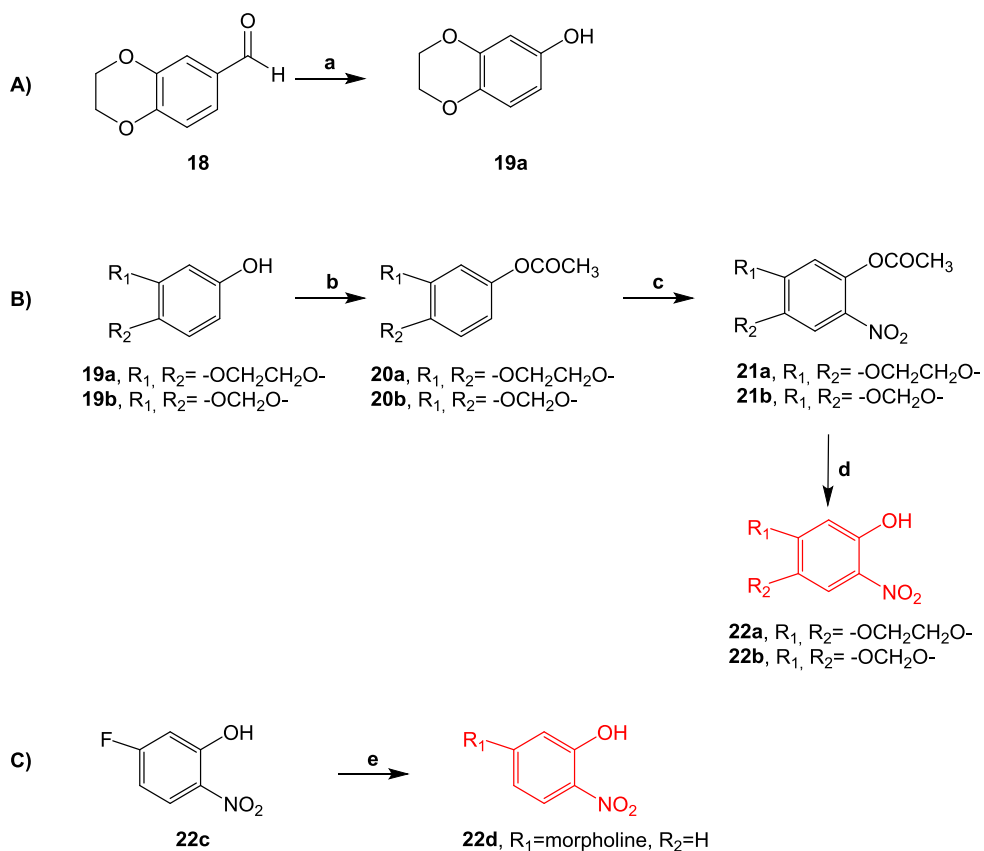
Reagents and conditions: *a) mCPBA, dry DCM, 50 °C, 24h; b) Ac₂O, DCM, rt; c) HNO₃, CH₃COOH, rt, 12h; d) H₂SO₄, 25 %, 90 °C; e) morpholine, DMF, 80 °C.*

   All nitro intermediates **22a-d** were condensed with methanesulfonyl chloride to give **23a-d**, which in turn were reduced to the corresponding amines **24a-d** in the presence of SnCl₂ EtOH (Scheme 5.2). Then the amines **24a-d** were converted by Clauson Kass reaction to the corresponding pyrroles **25a-d**, which after hydrolysis with KOH gave the corresponding derivatives **26a-d**. (Scheme 5.2).

Scheme 5.2

22a, R$_1$, R$_2$= -OCH$_2$CH$_2$O-
22b, R$_1$, R$_2$= -OCH$_2$O-
22c, R$_1$= F, R$_2$= H
22d, R$_1$= morpholine, R$_2$= H

23a, R$_1$, R$_2$= -OCH$_2$CH$_2$O-
23b, R$_1$, R$_2$= -OCH$_2$O-
23c, R$_1$= F, R$_2$= H
23d, R$_1$= morpholine, R$_2$= H

24a, R$_1$, R$_2$= -OCH$_2$CH$_2$O-
24b, R$_1$, R$_2$= -OCH$_2$O-
24c, R$_1$= F, R$_2$= H
24d, R$_1$= morpholine, R$_2$= H

25a, R$_1$, R$_2$= -OCH$_2$CH$_2$O-
25b, R$_1$, R$_2$= -OCH$_2$O-
25c, R$_1$= F, R$_2$= H
25d, R$_1$= morpholine, R$_2$= H

26a, R$_1$, R$_2$= -OCH$_2$CH$_2$O-
26b, R$_1$, R$_2$= -OCH$_2$O-
26c, R$_1$= F, R$_2$= H
26d, R$_1$= morpholine, R$_2$ = H
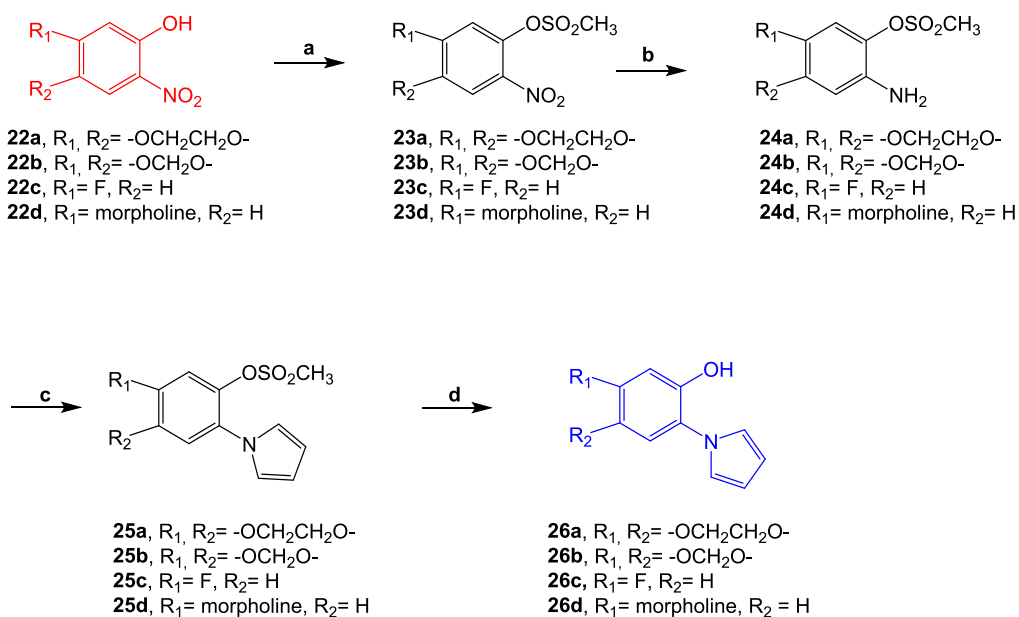
Reagents and conditions: *a) CH$_3$SO$_2$Cl, DCM, rt, 12h; b) SnCl$_2$, EtOH, 70 °C, 12h; c) AcOH, 2,5-dimethoxytetrahydrofuran, 100 °C, 1h; d) KOH, CH$_3$OH, 70 °C, 2h.*

The Clauson Kass reaction was also employed to convert commercially available *orto*-aminophenol **27a-d** to the corresponding pyrroles **28a-d** (Scheme 5.3). Following a previously reported procedure [2], all pyrrole derivatives **26a-d** and **28a-d** were reacted with the methyl ester of α-bromo-1-naphthylacetic acid to give the esters **29a-h**, which after hydrolysis with NaOH 4N and subsequent acidification with 2N HCl provide the acids **30a-h**. The intramolecular Friedel-Crafts cyclization of **30a-h** with PCl$_5$ (1.2 eq)/DCM gave very low yields ($< 15\%$) of the corresponding ketones **31a-h** and/or a complex mixture of by-products. Optimization of this step was achieved with: PCl$_5$ (1.5 eq), ionic liquid ([Bmim] Br) (1-butyl-3-methylimidazole bromide) (1.5 eq) in DCM (final concentration 0.01M), at reflux for 12h. These new reaction conditions improved yields of the ketones **31a-h** (ranging from 45 to 85%), and in all cases not significant formation of by-products was observed. Compound **31f** was reduced to its amino analogue **31i** by SnCl$_2$/EtOH in good yield (Scheme 5.3).

Scheme 5.3

A)

27a, R$_1$= H, R$_2$= Cl
27b, R$_1$= NO$_2$, R$_2$ = H
27c, R$_1$= H, R$_2$= CH$_3$
27d, R$_1$= CH$_3$,R$_2$= H

28a, R$_1$= H, R$_2$= Cl
28b, R$_1$= NO$_2$, R$_2$= H
28c, R$_1$= H, R$_2$= CH$_3$
28d, R$_1$= CH$_3$,R$_2$= H

B)

26a-d, 28a-d

29a, R$_1$,R$_2$= -OCH$_2$CH$_2$O-
29b, R$_1$,R$_2$= -OCH$_2$O-
29c, R$_1$= F, R$_2$= H
29d, R$_1$= morpholine, R$_2$= H
29e, R$_1$= H, R$_2$= Cl
29f, R$_1$= NO$_2$, R$_2$= H
29g, R$_1$= H, R$_2$= CH$_3$
29h, R$_1$= CH$_3$,R$_2$= H

30a, R$_1$,R$_2$= -OCH$_2$CH$_2$O-
30b, R$_1$,R$_2$= -OCH$_2$O-
30c, R$_1$= F, R$_2$= H
30d, R$_1$= morpholine, R$_2$= H
30e, R$_1$= H, R$_2$= Cl
30f, R$_1$= NO$_2$, R$_2$= H
30g, R$_1$= H, R$_2$= CH$_3$
30h, R$_1$= CH$_3$,R$_2$= H

17d, R$_1$= morpholine, R$_2$= H, R$_3$=OCOCH$_3$
17f, R$_1$= NO$_2$, R$_2$= H, R$_3$=OCOCH$_3$

31a, R$_1$,R$_2$= -OCH$_2$CH$_2$O-
31b, R$_1$,R$_2$= -OCH$_2$O-
31c, R$_1$= F, R$_2$= H
31d, R$_1$= morpholine, R$_2$= H
31e, R$_1$= H, R$_2$= Cl
31f, R$_1$= NO$_2$, R$_2$= H
31g, R$_1$= H, R$_2$= CH$_3$
31h, R$_1$= CH$_3$,R$_2$= H
31i, R$_1$= NH$_2$, R$_2$= H

17a, R$_1$,R$_2$= -OCH$_2$CH$_2$O-, R$_3$= OCOCH$_3$
17b, R$_1$,R$_2$= -OCH$_2$O-, R$_3$= OCOCH$_3$
17c, R$_1$= F, R$_2$= H, R$_3$= OCOCH$_3$
17e, R$_1$= H, R$_2$= Cl, R$_3$= OCON(CH$_3$)$_2$
17g, R$_1$= H, R$_2$= CH$_3$, R$_3$= OCOCH$_3$
17h, R$_1$= CH$_3$,R$_2$= H, R$_3$= OCON(CH$_3$)$_2$

Reagents and conditions: *a) AcOH, 2,5-dimethoxytetrahydrofuran, 100 °C, b) K$_2$CO$_3$, methyl 2-bromo-2-(naphtalen-1-yl) acetate; c) NaOH 4N, rt; d) PCl$_5$, [Bmim]Br, DCM, 12h, reflux; e) SnCl$_2$, EtOH, 70 °C, 12h; f) KH, THF, acetyl chloride (for **17a-d**, **17f, g**) or dimethylcarbamoyl chloride, rt, 12h (for **17e**, **17h**).*

Finally, **31a-i** were treated with dimethylcarbamoyl chloride or acetyl chloride in the presence of KH (30% suspension in mineral oil), and only pyrrole derivatives **17a-c**, **17e**, and **17g,h** were isolated.

In Scheme 5.4 is reported the synthesis of the dehydro derivatives **17i-k**. Briefly, **31b** and **31f** were reduced with $NaBH_4$ to **32a** and **32b** respectively. Then reaction with methansulfonyl chloride/TEA gave **17i,j**. Finally, **17j** was converted to its amino analogue **17k** by reduction with $SnCl_2$/EtOH.

Unfortunately, all these dehydro derivatives resulted unstable, giving rise to complex mixtures of by products over time.

Scheme 5.4

31b, 31f

32a, R_1, R_2= -OCH_2O-
32b, R_1= NO_2, R_2= H

17i, R_1, R_2= -OCH_2O-
17j, R_1= NO_2, R_2= H
17k, R_1= NH_2, R_2= H
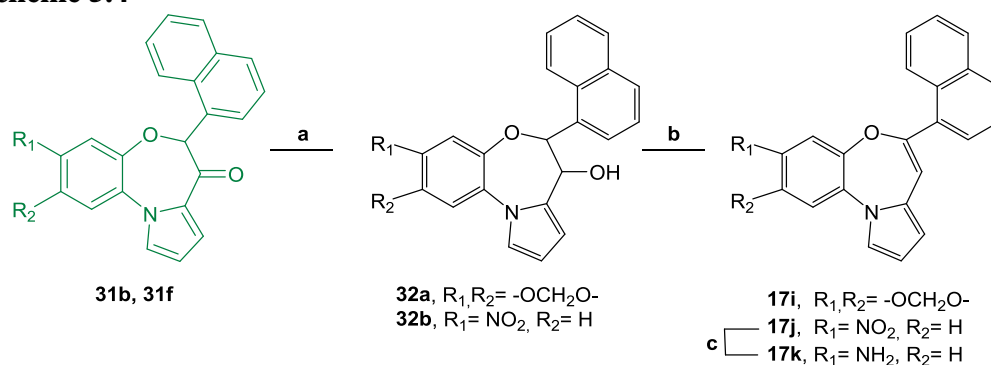
Reagents and conditions: *a) $NaBH_4$, EtOH/H_2O, 70 °C, 12h; b) CH_3SO_2Cl, TEA, DCM, rt; c) $SnCl_2$, EtOH, 70 °C, 12h.*

In Scheme 5.5 is described the synthesis of benzoxazinones **17l-n**. The condensation of 7-amino-2,3-dihydro-benzo[1,4]dioxin-6-ol **22a** and 2-amino-4-bromo-phenol **33** with α-bromonaphthyl methyl ester in the presence of K_2CO_3 gave the benzoxazinone derivatives **34a** and **34b** respectively. Subsequent reduction of **34a,b** with $SnCl_2$/EtOH afforded the corresponding aniline derivatives which spontaneously cyclized to benzoxazinone analogues **35** and **17l** respectively. Finally, **35** was *N*-alkylated with the appropriate benzyl halide to afford final compounds **17m,n**.

Scheme 5.5

22a, R_1, R_2= -OCH$_2$CH$_2$O-
33, R_1= H, R_2= Br

34a, R_1, R_2= -OCH$_2$CH$_2$O-
34b, R_1= H, R_2= Br

35, R_1, R_2= -OCH$_2$CH$_2$O-
17l, R_1= H, R_2= Br

17m, R_1, R_2= -OCH$_2$CH$_2$O-, R_3= H
17n, R_1, R_2= -OCH$_2$CH$_2$O-, R_3= F
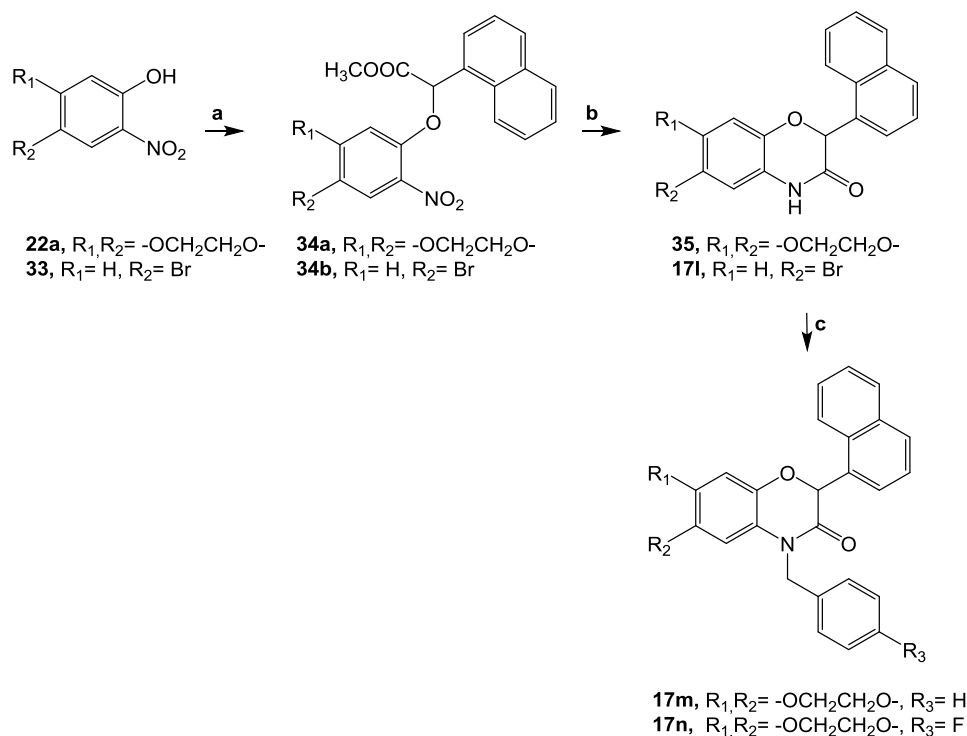
Reagents and conditions: *a) K$_2$CO$_3$, methyl 2-bromo-2-(naphtalen-1-yl)acetate; 12h, rt; b) SnCl$_2$/EtOH/HCl, 80 °C, 12h; c) K$_2$CO$_3$, benzylbromide for **17m** and 4-fluoro-benzylbromide for **17n**, 12h, rt.*

5.4 Biological evaluation

To assess if the newly synthesized PBOX analogues might promote apoptosis, fractional DNA content (sub-G1 assay) was determined by flow cytometry on HL60 (human promyelocytic leukemia) cells (prof. T. Baldari, University of Siena). During apoptosis, genomic DNA is cleaved into smaller fragments, each approximately 180 bp (and multiples of it). This intranucleosomal DNA fragmentation is a specific marker of apoptosis and therefore can be used to quantitate apoptosis using a number of assays. Using flow cytometry, propidium iodide stained cells will stain less intensely and show a peak below the G1 peak (i.e. sub-G1 peak); this assay for measuring apoptosis is easy, reliable, reproducible, and cheap and for these reasons is widely used.

In Figure 5.5 is reported the percentage of cells in subG1 phase for **17a**, **17b**, **17e**, **17g**, **17l-n**, **31a,b** and **31i** at 25 and 10 μM after 24h treatment.

The results show that **17a**, **17b**, **17e**, **17g**, **31a** and **31b** induce a significant enhancement in the percentage of apoptotic cells with values ranging from 51%

(for **17g**) to 64% (for **31a**), compared with vehicle, when tested at 25 μM. A good antiapoptotic activity was also evidenced at 10 μM for compounds **17a**, **17b**, **17e** and **31a** whereas, under the same conditions, compounds **17g** and **31b** were poor active, with percentage in the sub G1 phase of ca 14% and 26% respectively. Finally, compounds **17l-n** and **31i** did not show any significant effect on the cell cycle progression at both tested concentrations of 10 μM and 25 μM.

Although our data are not enough for a comprehensive structure-activity relationships (SARs) analysis, it is possible to postulate that a benzofused 1,4-dioxane system (such as in **17a** and **31a**) may be involved in strong interactions with the target. In this regard, it has to be emphasized that previously reported SARs studies on PBOX series indicated that unsubstituted compounds at the position 7 of the benzoxazepine ring are not active. On the contrary, the introduction of an appropriate enol ester or enol carbamate at this position increased the antiproliferative activity (associated or not to apoptotic pathways), and is consistent with the presence of a lipophilic pocket in receptor binding site that does not tolerate bulky alkyl chains (see Figure 5.2). Surprisingly, the benzofused 1,4-dioxane system associated to removal of enol ester at position 7 (such as in **31a**) retained a good apoptotic activity at 25 μM as well as at 10 μM. Thus, the presence of an enol ester probably it is not strictly required when a strong anchoring group for the binding site is introduced on the benzofused system of PBOX-6 analogues (**17a** *vs* **31a**). Accordingly, the removal of the enol ester group at 7 position together with the introduction of an amino group at position 3 of the benzofused system (such as in **31i**) was detrimental for activity at both tested concentrations, suggesting that an H-bond donor group at this position is not tolerated (**31i** *vs* **31a**). On the other hand, at 25 μM, **17e** and **17g** bearing a chlorine atom and a methyl group respectively at position 2 of the benzofused ring showed a percentage of subG1 of ca 56% and 51% respectively; instead, at 10 μM, only compound **17e** was significantly active indicating that the apoptotic activity is dependent of the electronic state of the pyrrolebenzoxazepine core in forming potential π-stacking interaction(s) with the target molecule (Table 1).

Furthermore, at 10 μM, removal of the enol ester group at the 7 position together with the introduction of a benzofused 1,3-dioxolane system also

decreased the apoptotic activity (**31b** *vs* **17b**, **31a**) indicating a non optimal interaction of the 1,3-dioxolane system with the target.

Overall, these results have also some practical implications from a synthetic point of view. In fact, the introduction of an enol ester or an enol carbamate requires a strong base (such as KH) and a strong acylating agent (such as *N*-dimethylcarbamoyl chloride or acetyl chloride). These reaction conditions are incompatible with sensitive functional groups, which then need to be appropriately protected. On the other hand, enol ester and enol carbamate functional groups are not compatible with various reagents (for example reducing agents). In other words, removal of such groups at 7 position can allow to a more simplified scheme of synthesis, encouraging the introduction of a wider range of substituents on the benzofused ring.

Finally, compounds **17l-n,** lacking pyrrole ring and presenting different substituents on N_1 position were inactive, evidencing a key role played by the pyrrole ring. However, our data are not enough to establish a clear structure-activity correlation. A more deeper investigation of different substituents on N_1 position as well as on the benzoxazinone ring will provide us with more complete evaluation.

*During this PhD experience a small set of benzoxazinone analogues of **17m,n** were synthesized and tested as dual hAK/hGSK-3β allosteric modulators, and results are reported in Chapter 6.*
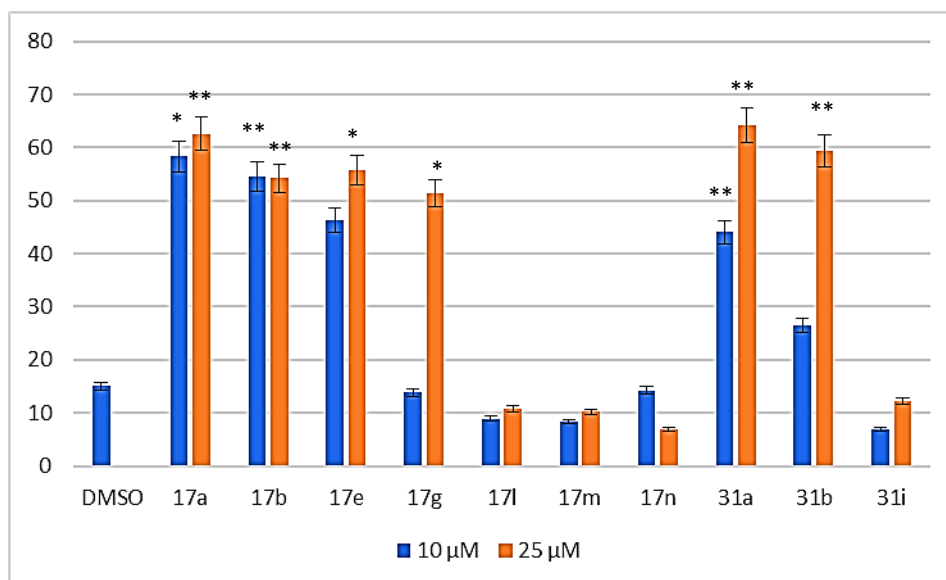
Figure 5.5 *Compounds **17a,b**, **17e**, **17g**, **17l-n**, **31a**, **31b**, **31i** induced apoptosis in HL-60 cells. The bar graphs show the percentage of cells in the sub-G1 phase; data are mean ± SD (n=3); **p< 0.005, *p < 0.001, p < 0.0001.*

Table I. *Efficacy of compounds **17a,b**, **17e**, **17g**, **17l-n**, **31a**, **31b**, **31i** (at 10 μM and 25 μM) on HL-60 cell line as % of apoptosis (sub-G$_1$)*

Cpds	% Sub-G$_1$ (10 μM)	% Sub-G$_1$ (25 μM)
DMSO	15.0	15.0
17a	58.4±16.4	62.6±4.5
17b	54.5±9.08	54.2±9.8
17e	46.2±20.6	55.7±13.7
17g	13.8±11.0	51.3±14.1
17l	8.9±2.1	10.8±2.4
17m	8.3±1.5	10.2±3.5
17n	14.2±4.4	6.9±1.0
31a	44.0±2.6	64.3±7.5
31b	26.5±11.2	59.3±8.5
31i	6.9±2.6	12.2±0.4

5.5 Experimental Section

5.5.1 General

Melting points were taken on a Gallenkamp melting point apparatus. ^{1}H and ^{13}C NMR spectra were recorded at 300 and 75 MHz, respectively, using a Bruker Avance 300 MHz spectrometer. Splitting patterns are described as singlet (s), doublet (d), triplet (t), quartet (q), quintuplet (qt), and broad (br). Mass spectra were obtained by electrospray ionization (ESIMS) using a Thermo Finningan LCQ Deca XP Max ion-trap mass spectrometer equipped with Xcalibur software and an LTQ Orbitrap XL mass spectrometer (Thermo FisherScientific, San Jose, CA, USA) operated in positive ion mode. The Orbitrap mass analyzer was calibrated according to the manufacturer's directions using a mixture of caffeine, methionine, arginine, phenylalanine and alanine-acetate (MRFA), and Ultramark 1621 in a solution of acetonitrile, methanol, and acetic acid. Chromatographic separations were performed on silica gel (Kieselgel 40, 0.040−0.063 mm, Merck). Reactions and product mixtures were routinely monitored by thin-layer chromatography (TLC) on Merck 0.2 mm precoated silica (60 F254) aluminum sheets, with visualization by irradiation with a UV lamp. All starting materials, reagents, and solvents (reagent grade) were purchased from Sigma-Aldrich and used without further purification.

2,3-Dihydro-1,4-benzodioxin-6-ol **19a**
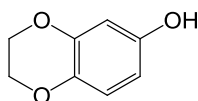
To a stirred solution of 2,3-dihydrobenzo[δ][1,4]dioxine-6-carbaldehyde **18** (1.5 g, 9.1 mmol) in CH_2Cl_2 (16 mL) *m*-CPBA (1.87 g, 1.1 mmol) was added. The suspension was heated at 50 °C for 12h, cooled to room temperature, and then was quenched with a saturated $NaHCO_3$ solution and extracted with CH_2Cl_2. The combined organic phases were concentrated under reduced pressure, and the resulting residue was dissolved in MeOH and 4N NaOH (5 mL) was added. The resulting reaction mixture was stirred at room temperature for 2h, then was acidified with HCl (~ pH= 3). The mixture was extracted with ethyl acetate (3x10 mL), and washed successively with satured solution of $NaHCO_3$ and brine, dried

over anhydrous Na_2SO_4, filtered and solvent was removed under reduced pressure to give 2,3-dihydro-1,4-benzodioxin-6-ol **3a** as a reddish brown oil, that was employed in the next step without further purification.

Yield: 63%.^{1}H NMR (CDCl$_3$) δ: 4.18-4.28 (m, 4H), 6.35 (dt, *J*= 8.7, 1.9 Hz, 1H), 6.41 (d, *J*= 2.8 Hz, 1H), 6.74 (dd, *J*= 8.7, 1.2 Hz, 1H).

5.5.1.1 General Procedure for the Synthesis of **20a,b**

To a stirred solution of phenol **19a,b** (1 eq) in NaOH (10% w/v, 20 mL) at 0 °C, acetic anhydride (1.5 eq) was added at room temperature. Then, when no starting material was detected by TLC (DCM as eluent), the reaction mixture was extracted with DCM. The organic phase was washed with saturated solution of NaHCO$_3$ and brine, then was dried (Na$_2$SO$_4$), filtered, and concentrated under reduced pressure.

2,3-Dihydro-1,4-benzodioxin-6-yl acetate **20a**
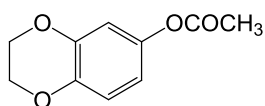
The title compound was obtained as a colorless liquid, and was used in the next step without further purification.

Yield: 97%. ^{1}H NMR (CDCl$_3$) δ: 2.29 (d, *J*= 1.9 Hz, 3H), 4.26 (d, *J*= 1.7 Hz, 4H), 6.58 (dt, *J*= 8.7, 2.3 Hz, 1H), 6.64 (t, *J*= 2.3 Hz, 1H), 6.86 (dd, *J*= 8.7, 1.8 Hz, 1H).

2H-1,3-benzodioxol-5-yl acetate **20b**
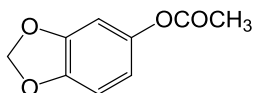
The title compound was obtained as a colorless liquid, and was used in the next step without further purification.

Yield: 98%. ^{1}H NMR (CDCl$_3$): 2.22 (s, 3H), 5.92 (s, 2H) 6.49 (dd, *J*=8.7, 2.4, 1H); 6.59 (d, *J*= 2.4, 1H), 6.74 (d, *J*= 8.7, 1H).

5.5.1.2 General Procedure for the Synthesis of 21a,b

To a solution of the appropriate phenol **20a,b** (1 mmol) in glacial acetic acid (5 mL), a solution of concentrated nitric acid (1.3 mmol, specific gravity 1.42) in glacial acetic acid (3 mL) was added dropwise at room temperature. The resulting mixture was stirred for 3h, and then poured into ice-water. After 1h, a pale-yellow crystalline precipitate was separated by filtration, washed with water, and air-dried. The title compounds **21a,b** were used in the next step without further purification.

7-Nitro-2,3-dihydro-1,4-benzodioxin-6-yl acetate **21a**
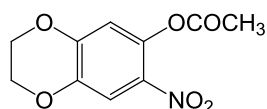
Yield: 98%. ^{1}H NMR (CDCl$_3$) δ:2.38 (s, 3H), 4.29-4.40 (m, 4H), 6.71 (s, 1H), 7.75 (s, 1H)

6-Nitro-2H-1,3-benzodioxol-5-yl acetate **21b**
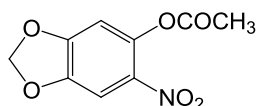
Yield: 75%. ^{1}H NMR (CDCl$_3$) δ: 2.38 (d, *J*= 1.3 Hz, 3H), 6.16 (s, 2H), 6.66 (d, *J*= 1.2 Hz, 1H), 7.61 (d, *J*= 1.2 Hz, 1H).

5.5.1.3 General Procedure for the Synthesis of 22a,b

The appropriate acetyl derivative **21a,b** (1 mmol) was dissolved in H$_2$SO$_4$ (20% v/v, 5 mL), and the resulting mixture was stirred for 3h at 70 °C and then poured into ice-water. After 1h, a pale-yellow crystalline precipitate was separated by filtration, washed with water, and air-dried. The title compounds **22a,b** were used in the next step without further purification.

7-Nitro-2,3-dihydro-1,4-benzodioxin-6-ol **22a**
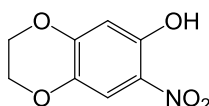
Yield: 78 %. ^{1}H NMR (CDCl$_3$) δ: 4.05-4.56 (m, 4H), 6.59 (s, 1H), 7.64 (s, 1H), 10.59 (s, 1H).

6-Nitro-2H-1,3-benzodioxol-5-ol **22b**
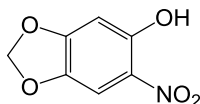
Yield: 98%. ^{1}H NMR (CDCl$_3$) δ: 6.09 (s, 3H), 6.58 (s, 1H), 7.48 (s, 1H), 11.41 (s, 1H).

5-(Morpholin-4-yl)-2-nitrophenol **22d**
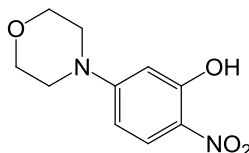
Morpholine (7.96 mmol, 0.69 mL) was added to a solution of 5-fluoro-2-nitrophenol **22c** (0.50 g, 3.18 mmol) in acetonitrile (25 mL), and the resulting mixture was stirred under argon atmosphere at reflux for 2h. Then the reaction mixture was concentrated under reduced pressure and purified by flash chromatography (SiO$_2$, hexane/ethyl acetate 2:1 as eluent) to give **22d** as a yellow solid.

Yield 97%. ^{1}H NMR (CDCl$_3$) δ: 3.42 (td, *J*= 4.9, 1.7 Hz, 4H), 3.85 (td, *J*= 4.9, 1.7 Hz, 4H), 6.33 (t, *J*= 2.2 Hz, 1H), 6.45 (dt, *J*= 9.7, 2.2 Hz, 1H), 7.97 (dd, *J*= 9.6, 1.6 Hz, 1H), 11.20 (s, 1H).

5.5.1.4 General Procedure for the Synthesis of **23a-d**

To a solution of the appropriate alcohol **22a-d** (1 mmol) in DCM (10 mL) stirred at °0 C, a solution of methanesulfonyl chloride (1.3 mmol) and TEA (1.5 mmol) in DCM (10 mL) was added dropwise. The reaction mixture was stirred at room temperature overnight, then was diluted with DCM, washed with 1M NaHCO$_3$, brine, dried (MgSO$_4$) and filtered. The solvent was removed in vacuo, and the

resulting residue was purified by flash chromatography (SiO$_2$, EtOAc/petroleum ether, 40-60 °C, 7:3 as eluent) to give the title compounds **23a-d** in good yields.

7-Nitro-2,3-dihydro-1,4-benzodioxin-6-yl methanesulfonate **23a**
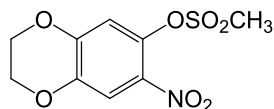
Yield: 88%. ^{1}H NMR (CDCl$_3$) δ: 3.35 (d, *J*= 1.6 Hz, 3H), 4.29-4.45 (m, 4H), 7.04 (d, *J*= 1.6 Hz, 1H), 7.71 (d, *J*= 1.6 Hz, 1H).

6-Nitro-2H-1,3-benzodioxol-5-yl methanesulfonate **23b**
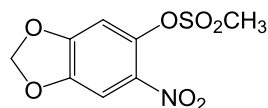
Yield: 80%. ^{1}H NMR (CDCl$_3$) δ: 3.36 (d, *J*= 1.7 Hz, 3H), 6.19 (d, *J*= 1.7 Hz, 2H), 6.98 (d, *J*= 1.7 Hz, 1H), 7.55 (d, *J*= 1.8 Hz, 1H).

5-(Fluoro-4-yl)-2-nitrophenyl methanesulfonate **23c**
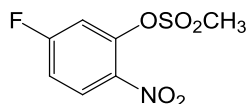
Yield: 71%. ^{1}H NMR (CDCl$_3$) δ: 3.39 (d, *J*= 3.0 Hz, 3H), 7.21 (t, *J*= 8.4 Hz, 1H), 7.32 (d, *J*= 8.3 Hz, 1H), 8.15 (t, *J*= 8.8, 4.0 Hz, 1H). ^{13}C NMR (CDCl$_3$) δ: 39.2, 113.2, 113.5, 114.8, 115.1, 128.1, 128.3, 138.5, 138.6, 142.5, 142.7, 163.0, 166.5.

5-(Morpholin-4-yl)-2-nitrophenyl methanesulfonate **23d**
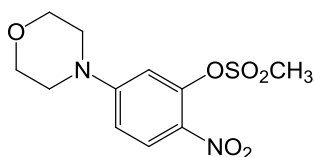
Yield: 76%. ^{1}H NMR (CDCl$_3$) δ: 3.37-3.44 (m, 7H), 3.87 (t, *J*= 5.0 Hz, 4H), 6.65-6.88 (m, 2H), 8.06-8.21 (m, 1H).

5.5.1.5 General Procedure for the Synthesis of **24a-d**

A mixture of the appropriate nitro derivative **23a-d** (1 mmol) and tin (II) chloride (5 mmol) in ethanol (10 mL) was heated at 80 °C under nitrogen. After 12h, the starting material disappeared, and the solution was allowed to cool to room temperature and then poured into ice-water. The pH was made slightly basic (pH= 8), by addition of 5% $NaHCO_3$, and the mixture was extracted with ethyl acetate. The organic phase was washed with brine, dried over $MgSO_4$ and filtered. The organic solvent was removed under vacuum, and the resulting residue was purified by flash chromatography (SiO_2, EtOAc/petroleum ether, 40−60 °C, 5:5 as eluent) to afford the title compounds **24a-d** in good yields.

7-Amino-2,3-dihydro-1,4-benzodioxin-6-yl methanesulfonate **24a**
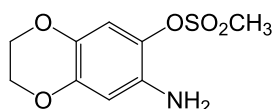
The title compound was obtained as a brown solid.

Yield: 78%. ^{1}H NMR ($CDCl_3$) δ: 3.18 (s, 3H), 4.14-4.28 (m, 4H), 6.35 (s, 1H), 6.80 (s, 1H).

6-Amino-2H-1,3-benzodioxol-5-yl methanesulfonate **24b**
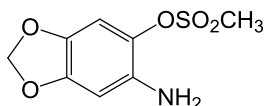
The title compound was obtained as a brown solid.

Yield: 70%. ^{1}H NMR ($CDCl_3$) δ: 3.18 (d, = 1.4 Hz, 3H), 3.77 (s, 1H), 5.92-5.97 (m, 2H), 6.38 (s, 1H), 6.78 (s, 1H).

2-Amino-5-fluorophenyl methanesulfonate **24c**
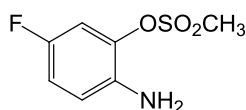
The title compound was obtained as a colourless solid.

Yield: 77%. ^{1}H NMR (CDCl$_3$) δ: 3.22 (s, 3H), 3.85 (s, 2H), 6.78 (t, J = 9.0, 5.6 Hz, 1H), 6.89 (t, 1H), 7.03 (d, J = 8.7, 2.6 Hz, 1H). ^{13}C NMR (CDCl$_3$) δ: 110.6, 110.9, 114.9, 115.2, 117.4, 117.6, 123.9, 135.8 (2C), 135.9, 153.4, 156.6.

2-Amino-5-(morpholin-4-yl)phenyl methanesulfonate **24d**
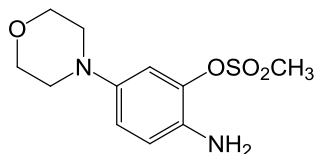
The title compound was obtained as a white solid.

Yield: 95%. ^{1}H NMR (CDCl$_3$) δ: 3.00-3.10 (m, 4H), 3.19 (d, J = 2.6 Hz, 3H), 3.85 (dt, J = 7.7, 2.8 Hz, 4H), 6.75-6.80 (m, 3H), 6.85 (d, J = 2.2 Hz, 1H).

5.5.1.6 General Procedure for the Synthesis of Pyrrole Derivatives **25a-d** *and* **28a-d**

To a stirred solution of the appropriate aminophenyl derivative **24a-d**, **27a-d** (1 mmol) in acetic acid (10 mL) 2,5-dimethoxytetrahydrofuran (1.1 mmol) was added dropwise. The resulting solution was stirred at 100 °C until the starting material was not detected by TLC (DCM as eluent). Then acetic acid was evaporated, and the residue was diluted with ethyl acetate and washed with 10% Na$_2$CO$_3$ solution and brine. The organic phase was dried over Na$_2$SO$_4$, filtered, and concentrated in *vacuo*. Then purification by flash column chromatography (SiO$_2$, EtOAc/petroleum ether, 40−60 °C, 7:3 as eluent) afforded the title products **25a-d, 28a-d** in good yields.

7-(1H-pyrrol-1-yl)-2,3-dihydro-1,4-benzodioxin-6-yl methanesulfonate **25a**
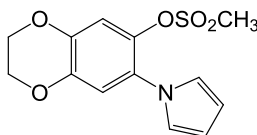
The title compound was obtained as a white solid.

Yield: 90%. ^{1}H NMR (CDCl$_3$) δ: 2.52 (s, 3H), 4.32 (s, 4H), 6.33 (t, J= 2.2 Hz, 2H), 6.91 (t, J= 2.2 Hz, 2H), 6.94 (s, 1H), 7.01 (s, 1H).

6-(1H-pyrrol-1-yl)-2H-1,3-benzodioxol-5-yl **25b**
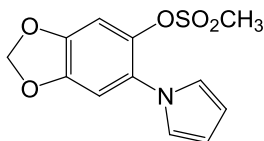
The title compound has been obtained following the general procedure as a white solid.

Yield: 60%. ^{1}H NMR (CDCl$_3$) δ: 2.52 (s, 3H), 6.09 (d, *J*= 1.0 Hz, 2H), 6.29-6.36 (m, 2H), 6.87 (s, 1H), 6.91 (t, *J*= 2.2 Hz, 2H), 6.95 (d, *J*= 0.9 Hz, 1H).

5-Fluoro-2-(1H-pyrrol-1-yl)phenyl methanesulfonate **25c**
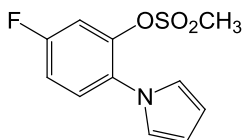
The title compound was obtained as a white solid.

Yield: 96%. ^{1}H NMR (CDCl$_3$) δ: 2.61 (s, 3H), 6.37 (q, *J*= 2.3 Hz, 2H), 6.94 (q, *J*= 2.3 Hz, 2H), 7.15 (ddt, *J*= 8.8, 7.4, 2.6 Hz, 1H), 7.22-7.31 (m, 1H), 7.43 (ddd, *J*= 8.5, 5.6, 2.3 Hz, 1H). ^{13}C NMR (CDCl$_3$) δ: 37.0, 110.5, 112.9, 113.2, 115.2, 115.5, 121.9, 127.3, 127.4, 130.3 (2C), 143.1, 143.2, 159.1, 162.4.

5-(Morpholin-4-yl)-2-(1H-pyrrol-1-yl)phenyl methanesulfonate **25d**
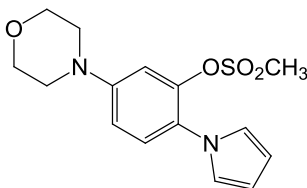
The title compound was obtained as a white solid.

Yield:85%. ^{1}H NMR (CDCl$_3$) δ: 2.54 (s, 3H), 3.23 (dd, *J*= 5.8, 3.8 Hz, 4H), 3.77-3.93 (m, 4H), 6.33 (t, *J*= 2.1 Hz, 2H), 6.84-6.98 (m, 4H), 7.31 (d, *J*= 8.7 Hz, 1H).

4-Chloro-2-(1H-pyrrol-1-yl) phenol **28a**
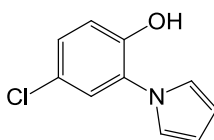
The title compound was obtained as a pale-yellow oil.

Yield: 85%. ^{1}H NMR (CDCl$_3$) δ: 5.50 (s, 1H), 6.42 (t, *J*= 2.2 Hz, 2H), 6.87 (t, *J*= 2.3 Hz, 2H), 6.99 (d, *J*= 8.5 Hz, 1H), 7.21-7.31 (m, 2H).

5-Nitro-2-(1H-pyrrol-1-yl)phenol **28b**
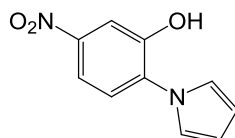
The title compound was obtained as a yellow solid.

Yield: 70%. ^{1}H NMR (CDCl$_3$) δ: 5.90 (s, 1H), 6.44-6.53 (m, 2H), 6.94-7.02 (m, 2H), 7.42 (d, *J*= 8.6 Hz, 1H), 7.85-7.99 (m, 2H).

4-Methyl-2-(1H-pyrrol-1-yl)phenol **28c**
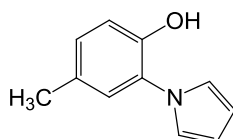
The title compound was obtained as a colourless oil.

Yield: 61%. ^{1}H NMR (CDCl$_3$) δ: 2.33 (s, 3H), 6.41 (t, *J*= 2.1 Hz, 2H), 6.88 (t, *J*= 2.1 Hz, 2H), 6.91-7.00 (m, 1H), 7.06-7.11 (m, 2H).

5-Methyl-2-(1H-pyrrol-1-yl)phenol **28d**
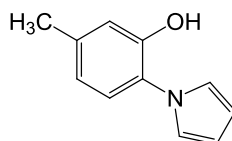
The title compound was obtained as a colourless solid.

Yield: 85%. ^{1}H NMR (CDCl$_3$) δ: 2.38 (s, 4H), 5.23 (s, 1H), 6.40 (t, *J*= 2.1 Hz, 2H), 6.80 (dd, *J*= 7.9, 1.9 Hz, 1H), 6.81-6.94 (m, 3H), 7.14 (d, *J*= 7.9 Hz, 1H).

5.5.1.7 General Procedure for the Synthesis of Pyrrole Derivatives **26a-d**

To a solution of the mesyl derivatives **25a-d** (1.5 mmol) in methanol (10 mL) was added KOH (3 mmol), and the resulting mixture was refluxed until no starting material was detected by TLC (DCM as eluent). The solvent was removed under

reduced pressure, and the resulting residue was acidified with 2M HCl (pH~3) and extracted with EtOAc. The organic phase was dried (Na_2SO_4), filtered, and the solvent was removed under vacuum. The resulting residue was purified by flash chromatography (SiO_2, DCM as eluent).

7-(1H-Pyrrol-1-yl)-2,3-dihydro-1,4-benzodioxin-6-ol **26a**
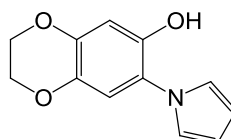
The title compound was obtained as a white solid.

Yield: 82%. [^1]H NMR (CDCl$_3$) δ: 4.21-4.36 (m, 4H), 6.38 (t, *J*= 2.6 Hz, 2H), 6.59 (d, *J*= 1.9 Hz, 1H), 6.81 (t, *J*= 4.7, 2.3 Hz, 3H).

6-(1H-Pyrrol-1-yl)-2H-1,3-benzodioxol-5-ol **26b**
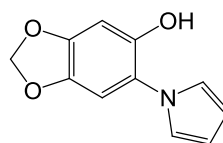
The title compound was obtained as a white solid.

Yield: 70%. [^1]H NMR (CDCl$_3$) δ: 5.98 (s, 2H), 6.36-6.41 (m, 2H), 6.60 (s, 1H), 6.73 (s, 1H), 6.79 (t, *J*= 2.2 Hz, 2H).

5-Fluoro-2-(1H-pyrrol-1-yl)phenol **26c**
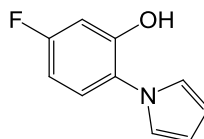
The title compound was obtained as a colourless oil.

Yield: 90%. [^1]H NMR (CDCl$_3$) δ: 6.42 (t, *J*= 2.1 Hz, 2H), 6.70 (td, *J*= 8.3, 2.8 Hz, 1H), 6.77-6.81 (m, 1H), 6.82 (t, *J*= 2.2 Hz, 2H), 7.21 (dd, *J*= 8.7, 5.9 Hz, 1H). [^13]C NMR (CDCl$_3$) δ: 103.8, 104.1, 107.5, 107.8, 110.7, 121.9, 124.3, 124.4, 127.6, 127.8, 151.7, 151.8, 160.9, 164.1.

5-(Morpholin-4-yl)-2-(1H-pyrrol-1-yl)phenol **26d**
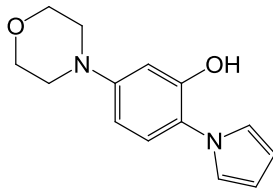
The title compound was obtained following as a white solid.

Yield: 95%. ^{1}H NMR (CDCl$_3$) δ: 3.19 (t, 4H), 3.88 (t, 4H), 6.38 (t, *J*= 2.2 Hz, 2H), 6.52 (dd, *J*= 8.6, 2.7 Hz, 1H), 6.58 (d, *J*= 2.7 Hz, 1H), 6.82 (t, *J*= 2.2 Hz, 2H), 7.15 (d, *J*= 8.6 Hz, 1H).

5.5.1.8 General Procedure for the Preparation of **29a-h**.

K$_2$CO$_3$ (1.5 mmol) was added to a solution of pyrrole derivatives **26a-d, 28a-d** (1 mmol) in anhydrous DMF (20 mL) at room temperature. The reaction mixture was stirred for 10 min at room temperature, and then a solution of methyl 2-bromo-2-(naphthalen-1-yl)acetate (1.2 mmol) in anhydrous DMF (5 mL) was added dropwise. After 12h at room temperature, the solvent was removed in *vacuo,* and the residue was taken up in dichloromethane. The organic layer was washed with brine, dried, and evaporated. The residue was purified by flash chromatography (AcOEt/ *n*-hexane 1:9 as eluent) to afford the title compounds **29a-h** in good yields.

Methyl 2-(naphthalen-1-yl)-2-{[7-(1H-pyrrol-1-yl)-2,3-dihydro-1,4-benzodioxin-6-yl]oxy}acetate **29a**
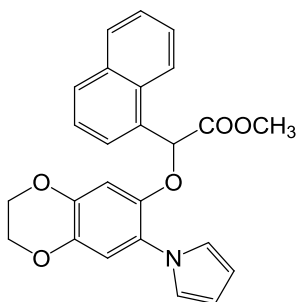
The title compound **29a** was obtained as a white solid.

Yield: 80%. ^{1}H NMR (CDCl$_3$) δ: 3.65 (d, *J*= 1.9 Hz, 3H), 4.19-4.27 (m, 4H), 5.78 (s, 1H), 5.88 (d, *J*= 1.9 Hz, 1H), 6.29 (q, *J*= 2.2 Hz, 2H), 6.60 (d, *J*= 2.0 Hz, 1H),

6.86 (d, *J*= 1.4 Hz, 1H), 7.00 (dd, 2H), 7.34-7.66 (m, 5H), 7.71-7.92 (m, 2H), 8.17 (d, *J*= 8.0 Hz, 1H), 8.30 (d, *J*= 8.3 Hz, 1H).
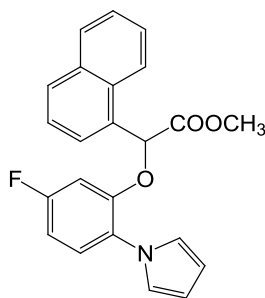
Methyl 2-(naphthalen-1-yl)-2-{[6-(1H-pyrrol-1-yl)-2H-1,3-benzodioxol-5-yl]oxy}acetate **29b**
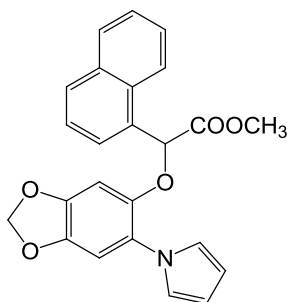
The title compound **29b** was obtained as a colourless oil.

Yield: 92%. ^{1}H NMR (CDCl$_3$) δ: 3.63 (s, 3H), 5.69 (s, 1H), 5.94 (q, *J*= 1.3 Hz, 2H), 6.30 (t, *J*= 2.2 Hz, 2H), 6.63 (s, 1H), 6.81 (s, 1H), 6.98 (t, *J*= 2.2 Hz, 2H), 7.42 (dd, *J*= 8.1, 7.2 Hz, 1H), 7.48-7.56 (m, 3H), 7.85 (ddt, *J*= 9.3, 8.3, 1.2 Hz, 2H), 8.16 (dt, *J*= 7.6, 1.3 Hz, 1H).

Methyl 2-[5-fluoro-2-(1H-pyrrol-1-yl)phenoxy]-2-(naphthalen-1-yl)acetate **29c**

The title compound **29c** was obtained as a colourless amorphous solid.

Yield: 82%. ^{1}H NMR (CDCl$_3$) δ: 3.68 (s, 3H), 6.11 (s, 1H), 6.33 (q, *J*= 2.1 Hz, 3H), 6.72-6.83 (m, 3H), 7.04 (q, *J*= 2.1 Hz, 3H), 7.25-7.33 (m, 3H), 7.46 (t, 1H), 7.55 (dt, *J*= 6.0, 2.7 Hz, 2H), 7.61 (d, 1H), 7.84-7.94 (m, 3H), 8.18 (d, 2H).

Methyl 2-[5-(morpholin-4-yl)-2-(1H-pyrrol-1-yl)phenoxy]-2-(naphthalen-1-yl)acetate. **29d**
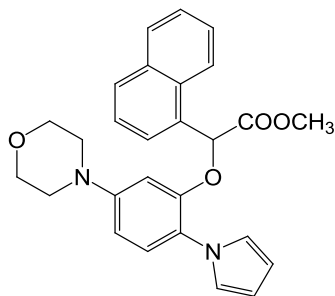
The title compound **29d** was obtained as a colourless amorphous solid.

Yield: 92%. ^{1}H NMR (CDCl₃) δ: 3.00 (t, *J*= 4.9 Hz, 4H), 3.66 (s, 3H), 3.81 (t, *J*= 4.8 Hz, 4H), 6.01 (s, 1H), 6.31 (q, *J*= 3.1, 2.6 Hz, 2H), 6.56 (q, *J*= 3.6 Hz, 2H), 6.95 (dt, *J*= 18.0, 2.1 Hz, 1H), 7.03 (t, *J*= 2.1 Hz, 2H), 7.22 (d, *J*= 9.4 Hz, 1H), 7.44 (t, *J*= 7.7 Hz, 1H), 7.48-7.60 (m, 1H), 7.61 (d, *J*= 7.3 Hz, 1H), 7.87 (dd, *J*= 9.8, 7.7 Hz, 2H), 8.23 (d, *J*= 8.2 Hz, 1H).

(4-Chloro-2-pyrrol-1-yl-phenoxy)-naphthalen-1-yl-acetic acid methyl ester **29e**
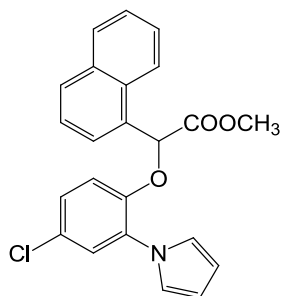
The title compound **29e** was obtained as a pale-yellow oil.

Yield: 89%. ^{1}H NMR (CDCl₃) δ: 3.67 (d, *J*= 2.7 Hz, 3H), 6.06 (s, 1H), 6.34 (t, *J*= 2.4 Hz, 2H), 6.96 (d, *J*= 8.9 Hz, 1H), 7.11 (dt, *J*= 7.1, 2.4 Hz, 3H), 7.34 (d, *J*= 2.6 Hz, 1H), 7.44 (t, 1H), 7.50-7.63 (m, 3H), 7.83-7.91 (m, 2H), 8.20 (d, 1H).
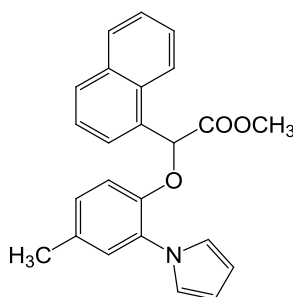
Methyl 2-(naphthalen-1-yl)-2-[5-nitro-2-(1H-pyrrol-1-yl)phenoxy]acetate **29f**
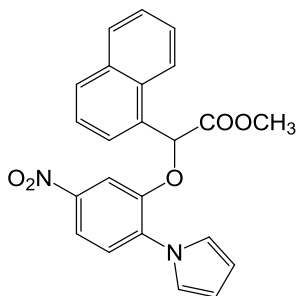
The title compound **29f** was obtained as a pale-yellow oil.

Yield: 85%.^{1}H NMR (CDCl$_3$) δ: 3.73 (s, 3H), 6.38 (dd, *J*= 4.0, 1.8 Hz, 3H), 7.25 (t, *J*= 2.2 Hz, 2H), 7.41-7.62 (m, 4H), 7.70 (d, *J*= 7.2, 1.2 Hz, 1H), 7.86-8.01 (m, 4H), 8.23 (d, 1H).
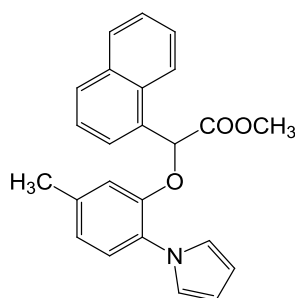
Methyl 2-[4-methyl-2-(1H-pyrrol-1-yl)phenoxy]-2-(naphthalen-1-yl)acetate **29g**

The title compound **29g** was obtained as a colourless oil.

Yield: 88%. ^{1}H NMR (CDCl$_3$) δ: 2.31 (s, 3H), 3.66 (s, 3H), 6.04 (s, 1H), 6.32 (t, *J*= 2.2 Hz, 2H), 6.94 (s, 2H), 7.07-7.18 (m, 3H), 7.44 (t, *J*= 7.7 Hz, 1H), 7.54 (tt, *J*= 7.2, 5.2 Hz, 2H), 7.62 (d, *J*= 7.1 Hz, 1H), 7.87 (t, *J*= 8.7 Hz, 2H), 8.22 (d, *J*= 7.7 Hz, 1H).

*Methyl 2-[5-methyl-2-(1H-pyrrol-1-yl)phenoxy]-2-(naphthalen-1-yl)acetate* **29h**

The title compound **29h** was obtained as a colourless oil.

Yield: 95%. ^{1}H NMR (CDCl$_3$) δ: 2.31 (s, 3H), 3.66 (s, 3H), 6.14 (s, 1H), 6.41 (t, *J*=4.2 Hz, 1H), 6.89 (s, 1H), 7.07 (t, *J*=4.2 Hz, 1H), 7.22 (d, *J*= 7.7 Hz, 1H), 7.43-7.58 (m, 5H); 7.65 (d, *J*=7, 1H); 7.845-7.90 (m, 3H); 8.23(d, *J*=1.3 Hz, 1H).

5.5.1.9 General Procedure for the Preparation of Compounds **30a-h.**

The appropriate ester **29a-h** (1 mmol) was dissolved in 20 mL of MeOH, and 4N NaOH (10 mL) was slowly added. The reaction mixture was stirred at room temperature for 3h, the organic solvent was removed under vacuum, and the residue was acidified with 4N HCl until pH 3-4. The suspension was extracted with EtOAc, and the organic phase was washed with brine, dried, filtered and solvent was removed under reduced pressure. The residue was purified by flash chromatography (EtOAc as eluent) to afford the title compounds **30a-h** in good yields.
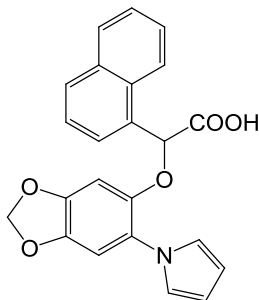
2-(Naphthalen-1-yl)-2-{[7-(1H-pyrrol-1-yl)-2,3-dihydro-1,4-benzodioxin-6-yl]oxy}acetic acid **30a**
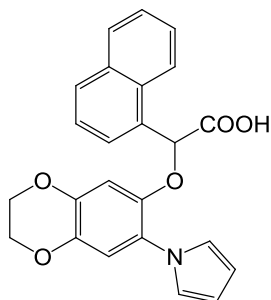
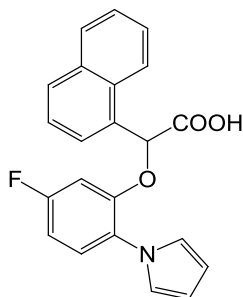The title compound **30a** was obtained as a white solid.

Yield: 98%. ^{1}H NMR (CDCl$_3$) δ: 5.88 (s, 1H), 6.30 (dt, *J*= 4.7, 2.2 Hz, 3H), 6.54 (d, *J*= 1.9 Hz, 2H), 6.86 (d, *J*= 2.0 Hz, 1H), 6.96 (d, *J*= 2.3 Hz, 1H), 6.98 (t, *J*= 2.3 Hz, 2H), 7.51-7.62 (m, 4H), 7.82-7.91 (m, 2H), 8.03 (s, 1H), 8.13-8.20 (m, 2H).

2-(Naphthalen-1-yl)-2-{[6-(1H-pyrrol-1-yl)-2H-1,3-benzodioxol-5-yl]oxy}acetic acid **30b**
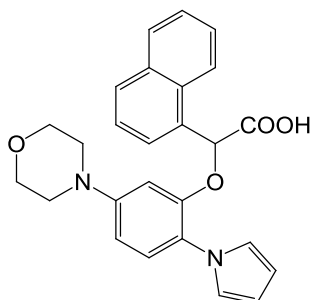

The title compound **30b** was obtained as a white solid.

Yield: 98%. ^{1}H NMR (CDCl$_3$) δ: 5.69 (s, 1H), 5.92 (s, 2H), 6.32 (t, *J*= 2.3 Hz, 2H), 6.49 (s, 1H), 6.80 (s, 1H), 6.94 (t, *J*= 2.2 Hz, 2H), 7.35-7.57 (m, 5H), 7.86 (t, *J*= 7.4 Hz, 2H), 8.11 (d, *J*= 7.8 Hz, 1H).

2-[5-Fluoro-2-(1H-pyrrol-1-yl)phenoxy]-2-(naphthalen-1-yl)acetic acid **30c**
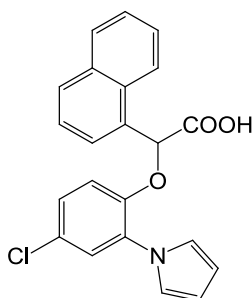

The title compound **30c** was obtained as a white solid.

Yield: 98%. ^{1}H NMR (CDCl$_3$) δ: 6.10 (s, 1H), 6.34 (t, *J*= 2.3 Hz, 2H), 6.72-6.82 (m, 2H), 7.01 (t, *J*= 2.2 Hz, 2H), 7.29 (d, 1H), 7.44 (t, *J*= 7.7 Hz, 1H), 7.54 (d, 2H), 7.61 (d, *J*= 7.1 Hz, 1H), 7.84-7.93 (m, 2H), 8.17 (d, *J*= 3.5 Hz, 1H).

2-[5-(Morpholin-4-yl)-2-(1H-pyrrol-1-yl)phenoxy]-2-(naphthalen-1-yl)acetic acid **30d**

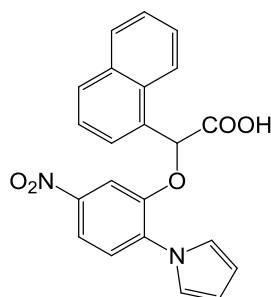The title compound **30d** was obtained as a white solid.

Yield: 98%. ^{1}H NMR (CDCl$_3$) δ 2.85-2.93 (m, 4H), 3.73 (t, *J*= 4.9 Hz, 4H), 6.04 (s, 1H), 6.33 (s, 2H), 6.47 (d, *J*= 2.7 Hz, 1H), 6.55 (s, 1H), 6.98 (s, 2H), 7.21 (d, *J*= 8.4 Hz, 1H), 7.43 (t, *J*= 7.9 Hz, 1H), 7.49-7.65 (m, 3H), 7.87 (t, *J*= 9.9 Hz, 2H), 8.20 (d, *J*= 8.1 Hz, 1H).

2-[4-Chloro-2-(1H-pyrrol-1-yl)phenoxy]-2-(naphthalen-1-yl)acetic acid **30e**

The title compound **30e** was obtained as a colourless prisms.

Yield: 95%. ^{1}H NMR (CDCl$_3$) δ: 6.07 (s, 1H), 6.34 (t, *J*= 2.2 Hz, 2H), 6.93 (d, *J*= 8.8 Hz, 1H), 7.05-7.12 (m, 3H), 7.33 (d, *J*= 2.6 Hz, 1H), 7.40-7.47 (m, 1H), 7.51-7.56 (m, 2H), 7.60 (d, *J*= 7.2, 1.2 Hz, 1H), 7.85-7.92 (m, 2H), 8.12-8.22 (m, 1H).
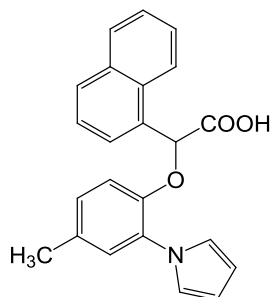
2-(Naphthalen-1-yl)-2-[5-nitro-2-(1H-pyrrol-1-yl)phenoxy]acetic acid **30f**

The title compound **30f** was obtained as a pale yellow solid.

Yield: 98%. ^{1}H NMR (CDCl$_3$) δ: 4.73 (s, 4H), 6.38 (dd, *J*= 4.7, 2.5 Hz, 4H), 7.20 (t, *J*= 2.2 Hz, 2H), 7.42-7.51 (m, 2H), 7.51-7.59 (m, 2H), 7.69 (dd, *J*= 7.3, 1.2 Hz, 1H), 7.87-7.97 (m, 5H), 8.15-8.24 (m, 1H).
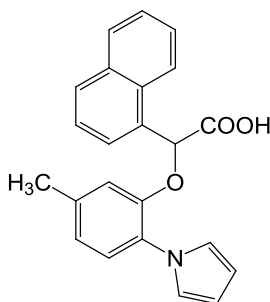
2-[4-Methyl-2-(1H-pyrrol-1-yl)phenoxy]-2-(naphthalen-1-yl)acetic acid **30g**

The title compound **30g** was obtained as a white solid.

Yield: 93%. ^{1}H NMR (CDCl$_3$) δ 2.29 (s, 3H), 6.04 (s, 1H), 6.33 (t, *J*= 2.1 Hz, 2H), 6.80-6.99 (m, 2H), 7.06 (t, *J*= 2.2 Hz, 2H), 7.14 (d, *J*= 1.9 Hz, 1H), 7.44 (d, *J*= 7.7 Hz, 1H), 7.47-7.64 (m, 3H), 7.87 (dd, *J*= 8.7, 6.4 Hz, 2H), 8.14-8.22 (m, 1H).

2-[5-Methyl-2-(1H-pyrrol-1-yl)phenoxy]-2-(naphthalen-1-yl)acetic acid **30h**

The title compound **30h** was obtained as a white solid.

Yield: 93%. ^{1}H NMR (CDCl$_3$) δ: 8.24 (d, *J*= 8.9 Hz, 1H) 7.89 (t, *J*= 7.3Hz, 3H) 7.65 (d, *J*= 6.8 Hz, 1H), 7.44-7.58 (m, 5H), 7.22 (d, *J*=7.7, 1H), 7.07 (s, 1H), 6.86 (s, 1H), 6.31 (s, 1H), 6.14 (s, 1H), 2.3 (s, 3H).

5.5.1.10 General Procedure for the Preparation of Compounds **31a-h.**

The appropriate acid **30a-h** (1.0 mmol) was added to a solution of phosphorus pentachloride (1.2 mmol) and 1-butyl-3-methylimidazolium bromide (1.5 mmol) in dry dichloromethane (50 mL) over a period of 2h. The reaction mixture was stirred at 55 °C for 12h and then was poured into crushed ice, basified with 10% NaOH solution, and extracted with chloroform. The organic layers were washed with brine, dried over Na$_2$SO$_4$, and evaporated. The residue was purified by flash column chromatography (DCM as eluent) and recrystallized (EtOAc/*n*-hexane) to afford the pure compounds **31a-h** in good yield.

5-(Naphthalen-1-yl)-9,10-dihydro [1,4]dioxino[2',3':4,5]benzo[1,2-b]pyrrolo[1,2-d][1,4]oxazepin-4(5H)-one **31a**
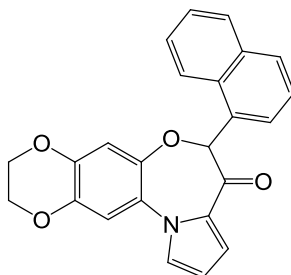
The title compound **31a** was obtained as a white solid.

Yield: 94%, mp: 182-184 °C. ^{1}H NMR (CDCl$_3$) δ: 4.04-4.27 (m, 4H), 6.18 (s, 1H), 6.39 (s, 1H), 6.54 (dd, *J*= 4.0, 2.8 Hz, 1H), 6.93 (s, 1H), 7.28 (q, *J*= 3.6, 2.2

Hz, 2H), 7.35 (t, *J*= 7.6 Hz, 1H), 7.42 (dd, *J*= 4.0, 1.7 Hz, 1H), 7.50-7.62 (m, 2H), 7.87 (dd, 2H), 8.20 (d, *J*= 8.2 Hz, 1H). ^{13}C NMR (CDCl$_3$) δ: 64.2, 88.9, 110.3, 111.7, 111.8, 120.8, 124.4, 124.8, 125.9, 126.4, 126.7, 127.2, 127.5, 128.8, 129.8, 131.5, 132.1, 133.4, 133.9, 140.9, 141.9, 189.9. HRMS (ESI) *m/z* 384.1236 [M+H]$^+$ (calc. for [C$_{25}$H$_{17}$NO$_4$]$^+$ 384.1236).

5-(Naphthalen-1-yl)-[1,3]dioxolo[4',5':4,5]benzo[1,2-b]pyrrolo[1,2-d][1,4]oxazepin-4(5H)-one **31b**
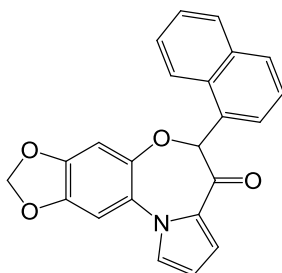
The title compound **31b** was obtained as a white solid.

Yield: 90%. ^{1}H NMR (CDCl$_3$) δ: 5.92 (d, *J*= 9.1 Hz, 2H), 6.25 (s, 2H), 6.55 (t, *J*= 4.0, 2.7 Hz, 1H), 6.88 (s, 1H), 7.21-7.30 (m, 2H), 7.33 (t, *J*= 7.6 Hz, 1H), 7.42 (dd, *J*= 4.1, 1.8 Hz, 1H), 7.50-7.70 (m, 2H), 7.88 (dd, 2H), 8.21 (d, *J*= 8.2 Hz, 1H); ^{13}C NMR (CDCl$_3$) δ 88.9, 102.0, 102.3, 104.4, 111.7, 120.8, 124.3, 124.8, 126.0, 126.5, 126.6, 126.8, 127.1, 127.5, 128.8, 130.0, 131.6, 133.5, 133.9, 145.3, 145.9, 189.9. HRMS (ESI) *m/z* 392.0885 [M+Na]$^+$ (calc. for [C$_{23}$H$_{16}$NO$_4$Na]$^+$ 392.0899).

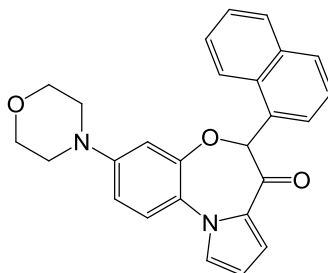*(±)3-Fluoro-6-(naphthalen-1-yl)benzo[b]pyrrolo[1,2-d][1,4]oxazepin-7(6H)-one* **31c**
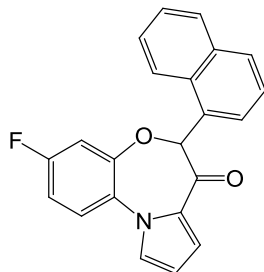
The title compound **31c** was obtained as a white solid.

Yield: 45%. ^{1}H NMR (CDCl$_3$) δ: 6.35 (s, 1H), 6.45 (s, 1H), 6.58 (t, *J*= 3.6 Hz, 1H), 6.88 (t, *J*= 8.5 Hz, 1H), 7.19 (d, *J*= 6.8 Hz, 1H), 7.24-7.41 (m, 3H), 7.48 (d,

J= 2.8 Hz, 1H), 7.60 (dt, *J*= 20.1, 7.3 Hz, 2H), 7.87 (dd, *J*= 20.2, 8.1 Hz, 2H), 8.23 (d, *J*= 8.3 Hz, 1H).
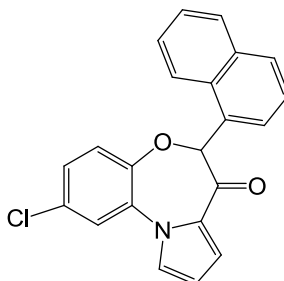
(±)3-Morpholino-6-(naphthalen-1-yl)benzo[b]pyrrolo[1,2-d][1,4]oxazepin-7(6H)-one **31d**

The title compound **31d** was obtained as a white solid.

Yield: 45%. ¹H NMR (CDCl₃) δ: 2.81 (d, *J*= 19.6 Hz, 4H), 3.75 (s, 4H), 6.28 (s, 1H), 6.55 (dd, *J*= 4.1, 2.7 Hz, 1H), 6.77 (s, 1H), 7.19-7.36 (m, 5H), 7.46 (dt, *J*= 5.8, 2.9 Hz, 1H), 7.50-7.69 (m, 2H), 7.75-7.95 (m, 2H), 8.25 (d, *J*= 8.5 Hz, 1H).

(±)-2-Chloro-6-(naphthalen-1-yl)benzo[b]pyrrolo[1,2-d][1,4]oxazepin-7(6H)-one **31e**

The title compound **31e** was obtained as colorless prisms.

Yield: 60%. ¹H NMR (CDCl₃) δ: 6.34 (s, 1H), 6.60 (dd, *J*=4.0, 2.7 Hz, 1H), 6.64 (d, *J*=8.7 Hz, 1H), 6.89 (dd, *J*=8.9, 2.4 Hz, 1H), 7.18 (d, *J*=7.1 Hz, 1H), 7.25-7.32 (m, 1H), 7.34 (t, *J*= 2.9, 1.8 Hz, 1H), 7.40 (d, *J*= 2.5 Hz, 1H), 7.51 (dd, *J* = 4.0, 1.8 Hz, 1H), 7.53-7.66 (m, 2H), 7.79-7.93 (m, 2H), 8.25 (d, *J*= 8.4 Hz, 1H).

(±)6-(Naphthalen-1-yl)-3-nitrobenzo[b]pyrrolo[1,2-d][1,4]oxazepin-7(6H)-one
31f

The title compound **31f** was obtained as a pale-yellow solid.

Yield: 91%. ^{1}H NMR (CDCl$_3$) δ: 6.43 (s, 1H), 6.68 (t, *J*= 3.4 Hz, 1H), 7.17 (d, *J*= 7.0 Hz, 1H), 7.22-7.31 (m, 1H), 7.42 (d, *J*= 2.3 Hz, 1H), 7.50-7.63 (m, 4H), 7.69 (t, 1H), 7.86 (dd, *J*= 21.0, 8.1 Hz, 2H), 8.01 (dd, *J*= 9.0, 2.6 Hz, 1H), 8.25 (d, *J*= 8.4 Hz, 1H); ^{13}C NMR (CDCl$_3$) δ: 88.0, 113.3, 119.9, 121.0, 121.9, 122.9, 123.1, 124.6, 126.4, 126.8, 127.3, 129.0, 130.2, 130.6, 131.4, 133.7, 133.8, 138.8, 145.4, 147.5, 188.3.
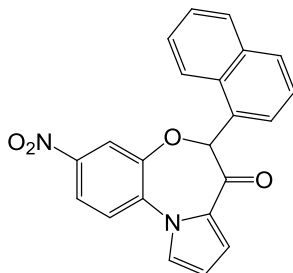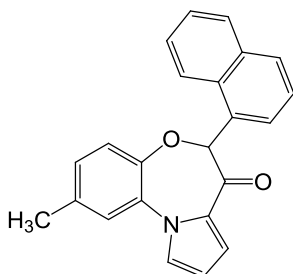
2-Methyl-6-(naphthalen-1-yl)benzo[b]pyrrolo[1,2-d][1,4]oxazepin-7(6H)-one
31g

The title compound **31g** was obtained as a white solid.

Yield: 62%. ^{1}H NMR (CDCl$_3$) δ: 2.33 (s, 3H), 6.23 (d, *J*= 5.7 Hz, 1H), 6.56 (d, *J*= 6.1 Hz, 1H), 6.78 (td, *J*= 25.8, 23.6, 8.7 Hz, 1H), 7.16-7.49 (m, 5H), 7.57 (dq, *J*= 14.8, 7.3 Hz, 2H), 7.75-7.97 (m, 3H), 8.23 (t, *J* =9.1 Hz, 1H); ^{13}C NMR (CDCl$_3$) δ: 21.0, 88.4, 111.8, 121.1, 122.4, 123.4, 124.5, 124.8, 126.0, 126.6, 126.7, 127.4, 127.9, 128.7, 129.8, 131.6, 132.0, 133.1, 133.5, 133.8, 135.6, 190.1.
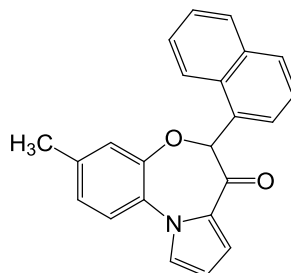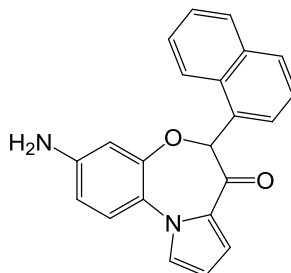
(±)3-Methyl-6-(naphthalen-1-yl)benzo[b]pyrrolo[1,2-d][1,4]oxazepin-7(6H)-one
31h

The title compound **31h** was obtained as a white solid.

Yield: 59%. ^{1}H NMR (CDCl$_3$) δ: 2.16 (s, 3H), 6.18 (s, 1H), 6.56 (t, *J*= 3.5 Hz, 1H), 6.68 (s, 1H), 6.98 (d, *J*= 8.2 Hz, 1H), 7.25-7.39 (m,4H), 7.44 (d, *J*= 4.0 Hz, 1H), 7.56 (p, *J*= 7.0 Hz, 2H), 7.86 (dd, *J*= 16.3, 7.8 Hz, 2H), 8.20 (d, *J*= 8.1 Hz, 1H).

(±)3-Amino-6-(naphthalen-1-yl)benzo[b]pyrrolo[1,2-d][1,4]oxazepin-7(6H)-one
31i

A mixture of **31f** (0.230 g, 6.21 mmol) and tin (II) chloride (0.6993 g, 3.1 mmol) in ethanol (30 mL) was heated at 80 °C under argon. After 12h, the starting material disappeared, and the solution was allowed to cool to room temperature and then poured into ice-water. The pH was made slightly basic (pH= 8), by addition of 5% NaHCO$_3$, and the resulting mixture was extracted with ethyl acetate. The organic phase was washed with brine, dried over MgSO$_4$ and filtered. The organic solvent was removed under reduced pressure, and the resulting residue was purified by column chromatography (SiO$_2$, EtOAc/petroleum ether, 40−60 °C, 5:5 as eluent) to give **31i** as a colourless solid.

Yield: 90%, mp:130-133 °C. ^{1}H NMR (300 MHz, CDCl$_3$) δ: 3.57 (s, 2H), 6.16 (d, *J*= 20.3 Hz, 2H), 6.46 (dd, *J*= 8.6, 2.6 Hz, 1H), 6.52 (dd, *J*= 4.0, 2.7 Hz, 1H), 7.20 (d, *J*= 8.5 Hz, 1H), 7.24-7.37 (m, 3H), 7.41 (dd, *J*= 4.1, 1.8 Hz, 1H), 7.50-7.61 (m, 2H), 7.81-7.95 (m, 2H), 8.20 (d, *J*= 8.2 Hz, 1H); ^{13}C NMR (CDCl$_3$) δ: 88.6, 109.4, 111.4, 112.1, 120.4, 122.8, 124.5, 124.8, 125.2, 125.9, 126.3, 126.6, 127.5,

128.7, 129.8, 131.5, 132.2, 133.1, 133.9, 145.7, 189.8. HRMS (ESI) *m/z* 341.1279 $[M+ H^+]^+$ (calc. for $[C_{22}H_{17}N_2O_2]^+$ 341.1290).

5.5.1.11 General Procedure for the Preparation of Compounds **17a-c, 17e, 17g,h**

To a suspension of potassium hydride (1.2 mmol) in anhydrous THF (5 mL) was added a solution of the appropriate ketone **31a-c, 31e, 31g-h** (1 mmol) dissolved in anhydrous THF (2 mL). The reaction mixture was stirred at room temperature for 2h, and then dimethylcarbamoyl chloride (2 mmol) (for **17a-c**, **17g**) or acetyl chloride (2 mmol) (for **17e**, **17h**) was slowly added. After stirring for 12h at room temperature, the solvent was removed in *vacuo* and the residue was taken up in EtOAc. The organic layer was washed with brine, dried, filtered and concentrated under reduced pressure. The residue was purified by flash chromatography (SiO₂, dichloromethane/hexane 1:1 as eluent) and recrystallized (EtOAc/hexane) to give the title compounds **17a-c, 17e, 17g, h** in good yields.

5-(Naphthalen-1-yl)-9,10-dihydro-[1,4]dioxino[2',3':4,5]benzo[1,2-b]pyrrolo[1,2-d][1,4]oxazepin-4-yl acetate **17a**
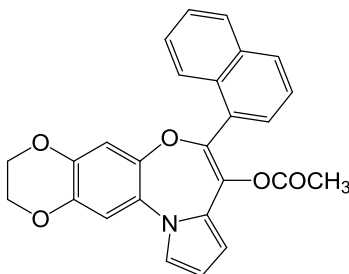
The title compound **17a** was obtained as colorless prisms.

Yield: 45%, mp: 226-228 °C. ¹H NMR (CDCl₃) δ: 1.86 (s, 3H), 4.17-4.35 (m, 4H), 6.42 (d, *J*= 2.3 Hz, 2H), 6.48 (s, 1H), 6.95 (s, 1H), 7.14 (t, *J*= 2.4 Hz, 1H), 7.42-7.58 (m, 4H), 7.90 (d, 2H), 8.11 (dt, *J*= 8.5, 2.8 Hz, 1H); ¹³C NMR (CDCl₃) δ: 20.5, 64.3, 109.7, 110.4, 110.8, 110.9, 121.5, 125.0, 126.1, 126.4 (2C), 126.8, 127.0, 127.1, 128.1, 129.6, 130.8, 131.2, 133.6, 133.9, 141.0, 141.7, 145.5, 146.0, 168.8. HRMS (ESI) *m/z* 448.1143 $[M+ Na]^+$ (calc. for $[C_{26}H_{19}NO_5Na]^+$ 448.1161).
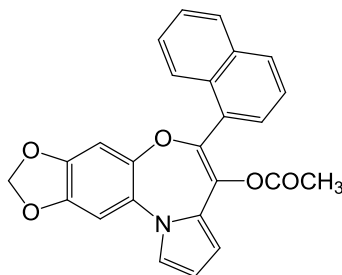
5-(Naphthalen-1-yl)-[1,3]dioxolo[4',5':4,5]benzo[1,2-b]pyrrolo[1,2-d][1,4]oxazepin-4-yl acetate **17b**

The title compound **17b** was obtained as colorless prisms.

Yield: 38%, mp: 157-159 °C. ^{1}H NMR (CDCl$_3$) δ: 1.88 (s, 3H), 6.00 (s, 2H), 6.38-6.47 (m, 3H), 6.93 (s, 1H), 7.15 (t, *J*= 2.3 Hz, 1H), 7.43-7.51 (m, 2H), 7.53 (t, 2H), 7.85-7.96 (m, 2H), 8.07-8.16 (m, 1H); ^{13}C NMR (CDCl$_3$) δ: 20.5, 102.0, 103.0, 103.6, 109.5, 110.4, 121.5, 125.0, 126.1, 126.3, 126.4, 126.8, 126.9, 127.1, 128.1, 129.7, 130.5, 131.2, 133.7, 134.2, 145.1, 145.9, 146.1, 146.2, 168.8. HRMS (ESI) *m/z* 412.1186 [M+ H^{+}][+] (calc. for [C$_{25}$H$_{18}$NO$_5$][+] 412.1185).

3-Fluoro-6-(naphthalen-1-yl)benzo[b]pyrrolo[1,2-d][1,4]oxazepin-7-yl acetate **17c**
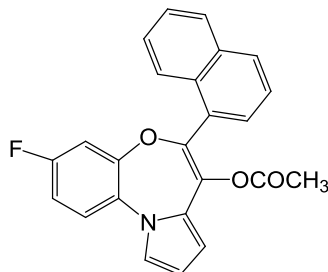
The title compound **17c** was obtained as colorless prisms.

Yield: 30%, mp: 65-67 °C. ^{1}H NMR (CDCl$_3$) δ: 1.88 (d, *J*= 1.1 Hz, 3H), 6.46 (t, *J*= 1.6 Hz, 2H), 6.69 (dt, *J*= 8.6, 1.9 Hz, 1H), 6.95-7.06 (m, 1H), 7.19 (q, *J*= 2.3, 1.8 Hz, 1H), 7.41 (ddd, *J*= 8.9, 6.0, 1.5 Hz, 1H), 7.45-7.50 (m, 2H), 7.51-7.59 (m, 2H), 7.88-7.98 (m, 2H), 8.03-8.15 (m, 1H); ^{13}C NMR (CDCl$_3$) δ: 20.5, 110.1, 110.2, 110.5, 110.8, 112.6, 112.9, 121.6, 121.7, 123.1, 123.2, 125.0, 126.2 (2C), 126.5, 126.9, 127.1, 128.2, 129.7, 129.8, 130.3, 131.1, 133.7, 134.1, 145.7, 152.1, 152.2, 159.1, 162.4, 168.8. HRMS (ESI) *m/z* 408.1001 [M+ Na][+] (calc. for [C$_{24}$H$_{16}$FNO$_3$Na][+] 408.1012).

2-Chloro-6-(naphthalen-1-yl)benzo[b]pyrrolo[1,2-d][1,4]oxazepin-7-yl-dimethyl carbamate **17e**

The title compound **17e** was obtained as a colorless solid.

Yield: 71%. ^{1}H NMR (300 MHz, CDCl$_3$) δ: 2.65 (s, 3H), 2.76 (s, 3H), 6.48 (s, 2H), 6.86 (dd, *J*=8.6, 2.2 Hz, 1H), 7.09 (d, *J*= 8.3 Hz, 1H), 7.20 (s, 1H), 7.52 (ddd, *J*= 28.2, 15.7, 8.2 Hz, 5H), 7.91 (d, *J*= 8.0 Hz, 2H), 8.09-8.18 (m, 1H); ^{13}C NMR (CDCl$_3$) δ: 36.1, 36.6, 110.4, 111.3, 121.3, 122.8, 123.5, 125.1, 126.0, 126.3, 126.4, 126.6, 127.4, 128.0, 128.1, 129.5, 130.6, 130.7, 131.4, 133.6, 134.1, 134.5, 145.9, 150.4, 154.0. ESIMS *m/z* 453.0963 [M+Na]$^{+}$.
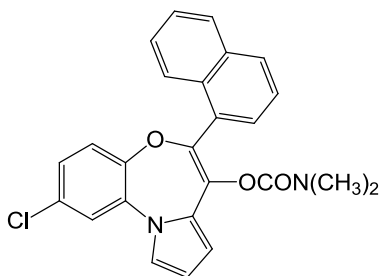
2-Methyl-6-(naphthalen-1-yl)benzo[b]pyrrolo[1,2-d][1,4]oxazepin-7-yl acetate **17g**

The title compound **17g** was obtained as colorless prisms.

Yield: 50%. ^{1}H NMR (CDCl$_3$) δ: 1.87 (s, 3H), 2.41 (d, *J*= 2.9 Hz, 3H), 6.44 (d, *J*= 2.4 Hz, 2H), 6.80 (d, *J*= 8.2 Hz, 1H), 6.95 (d, *J* = 8.5 Hz, 1H), 7.24 (d, *J*= 2.2 Hz, 2H), 7.38-7.60 (m, 4H), 7.85-7.97 (m, 2H), 8.11 (dd, *J*= 6.3, 3.3 Hz, 1H). ^{13}C NMR (CDCl$_3$) δ: 20.57, 21.0, 109.9, 110.6, 121.5, 122.2, 123.3, 125.0, 126.1, 126.4, 127.0, 127.2, 127.6, 128.1, 129.6, 130.9, 131.2, 132.7, 133.7, 133.9, 135.7, 146.0, 149.7, 168.9. ESIMS *m/z* 404.1250 [M+Na]$^{+}$.
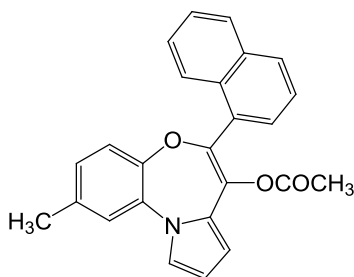
3-Methyl-6-(naphthalen-1-yl)benzo[b]pyrrolo[1,2-d][1,4]oxazepin-7-yl-dimethylcarbamate **17h**
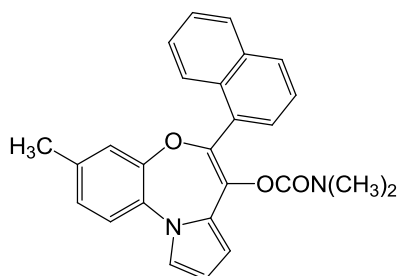
The title compound **17h** was obtained as colorless prisms.

Yield: 47%. ^{1}H NMR (CDCl$_3$) δ: 2.25 (s, 3H), 2.64 (s, 3H), 2.75 (s, 3H), 6.44 (t, *J*= 2.5 Hz, 2H), 6.74 (d, *J*= 1.8 Hz, 1H), 7.03 (d, *J*= 8.1 Hz, 1H), 7.20 (d, *J*= 2.4 Hz, 1H), 7.31 (d, *J*= 8.1 Hz, 1H), 7.41-7.57 (m, 3H), 7.60 (d, *J*= 7.0 Hz, 1H), 7.90 (d, *J*= 8.0 Hz, 2H), 8.13-8.23 (m, 1H). HRMS (ESI) *m/z* 411.1693 [M+ H$^+$]$^+$ (calc. for [C$_{25}$H$_{18}$NO$_5$]$^+$ 411,1709).

5.5.1.12 General Procedure for the Preparation of **32a,b**

A mixture of ketone **31b** or **31f** (1 mmol) and NaBH$_4$ (1.2 mmol) in ethanol and water (4:1 mL) was heated at 50 °C under argon. After 12h, the starting material disappeared and solvent was evaporated *in vacuo*. The residue was solubilized in ethyl acetate, and the organic phase was washed with brine, dried over MgSO$_4$ and filtered. The solvent was removed under vacuum and the resulting residue was used in the next step without any further purification.

5-(Naphthalen-1-yl)-4,5-dihydro-[1,3]dioxolo[4',5':4,5]benzo[1,2-b]pyrrolo[1,2-d][1,4]oxazepin-4-ol **32a**
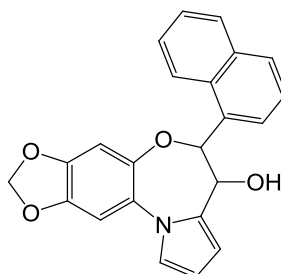
The title compound **32a** was obtained as a white solid.

Yield: 90%. ^{1}H NMR (CDCl$_3$) δ: 5.35 (t, *J*= 7.1 Hz, 1H), 5.92 (d, *J*= 9.0 Hz, 1H), 6.06 (s, 2H), 6.34 (t, *J*= 3.2 Hz, 1H), 6.54 (d, *J*= 5.7 Hz, 1H), 6.88 (d, *J*= 1.7 Hz,

1H), 6.96 (s, 1H), 7.05 (dd, *J*= 2.9, 1.7 Hz, 1H), 7.40-7.59 (m, 3H), 7.91 (dd, *J*= 9.9, 7.4 Hz, 3H), 8.12 (d, *J*= 8.1 Hz, 1H).

6-(Naphthalen-1-yl)-3-nitro-6,7-dihydrobenzo[b]pyrrolo[1,2-d][1,4]oxazepin-7-ol **32b**
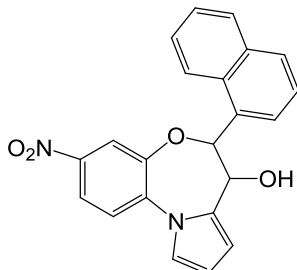
The title compound **32b** was obtained as a pale yellow solid.

Yield: 90%. ^{1}H NMR (CDCl₃) δ: 5.36 (d, *J*= 5.7 Hz, 1H), 6.35 (dd, *J*= 3.5, 1.8 Hz, 1H), 6.45 (q, *J*= 2.6, 2.0 Hz, 1H), 6.60 (d, *J*= 3.2 Hz, 1H), 7.21 (t, *J*= 3.1, 1.7 Hz, 1H), 7.49-7.69 (m, 5H), 7.76 (d, *J*= 7.4 Hz, 1H), 7.96 (q, *J*= 8.3, 7.8 Hz, 3H), 8.11 (dd, *J*= 8.9, 2.5 Hz, 1H), 8.25 (d, *J*= 2.4 Hz, 1H).

5.5.1.13 General Procedure for the Synthesis of **17i**, **j**

To a solution of the appropriate alcohol **32a,b** (1 mmol) in DCM (20 mL) stirred at 0 °C, a solution of methanesulfonyl chloride (1.3 mmol) and TEA (1.5 mmol) in DCM (10 mL) was added dropwise. After 12h, the starting material disappeared, and the reaction mixture was diluted with DCM, washed with 1M NaHCO₃, brine, dried (MgSO₄), and the solvent was removed in *vacuo*. Purification by flash chromatography (SiO₂, EtOAc/petroleum ether,(40−60 °C), 7:3 as eluent) afforded **17i,j** as solids. All compounds were recrystallized (EtOAc/hexane) as colorless prisms.

5-(Naphthalen-1-yl)-[1,3]dioxolo[4',5':4,5]benzo[1,2-b]pyrrolo[1,2-d][1,4]oxazepine **17i**
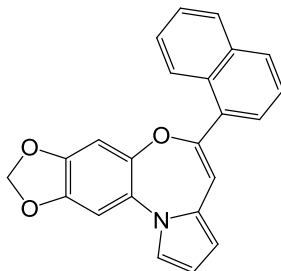
The title compound **17i** was obtained a white solid.

Yield: 87%. ^{1}H NMR (CDCl$_3$) δ: 5.99 (d, *J*= 1.0 Hz, 2H), 6.32 (d, *J*= 3.6 Hz, 1H), 6.40-6.45 (m, 1H), 6.46 (s, 1H), 6.52 (d, *J*= 1.0 Hz, 1H), 6.88 (d, *J* = 1.0 Hz, 1H), 7.11 (t, 1H), 7.47 (d, *J*= 7.6 Hz, 1H), 7.49-7.57 (m, 2H), 7.64 (d, *J*= 7.2 Hz, 1H), 7.90 (dd, *J*= 8.8, 5.5 Hz, 2H), 8.27-8.41 (m, 1H).

6-(Naphthalen-1-yl)-3-nitrobenzo[b]pyrrolo[1,2-d][1,4]oxazepine **17j**
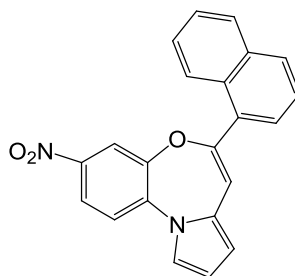
The title compound **17j** was obtained as a pale yellow solid.

Yield: 64%. ^{1}H NMR (CDCl$_3$) δ: 6.41 (d, *J*= 3.7 Hz, 1H), 6.51 (d, *J*= 3.4 Hz, 2H), 7.22 (d, *J*= 3.0 Hz, 1H), 7.53 (ddd, *J*= 14.7, 8.6, 5.1 Hz, 4H), 7.65 (d, *J*= 7.3 Hz, 1H), 7.89-7.96 (m, 3H), 8.13 (dd, *J*= 8.9, 2.5 Hz, 1H), 8.24-8.36 (m, 1H).

6-(Naphthalen-1-yl)benzo[b]pyrrolo[1,2-d][1,4]oxazepin-3-amine **17k**
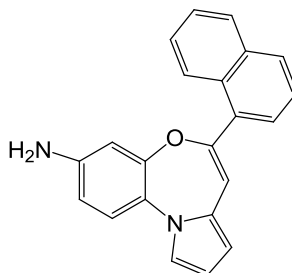
A mixture of **17j** (0.200 g, 0.56 mmol) and tin (II) chloride (0.533 g, 2.8 mmol) in ethanol (30 mL) was heated at 80 °C under argon. After 12h, the starting material disappeared and the solution was allowed to cool to room temperature. The pH was made slightly basic (pH= 8), by addition of 5% NaHCO$_3$, and the mixture was extracted with ethyl acetate. The organic phase was washed with brine, dried over MgSO$_4$ and filtered. The solvent was removed under vacuum, and the

resulting residue was purified by flash chromatography (SiO$_2$, EtOAc/petroleum ether, 40−60 °C, 5:5 as eluent) to afford **17k** as a white solid.

Yield: 95%. ^{1}H NMR (CDCl$_3$) δ: 6.30 (d, *J*= 3.7 Hz, 1H), 6.48 (d, *J*= 3.4 Hz, 2H), 7.20 (d, *J*= 3.0 Hz, 1H), 7.35-7.40 (m, 4H), 7.60 (d, *J*= 7.3 Hz, 1H), 7.90-7.95 (m, 3H), 7.96 (dd, *J*= 8.9, 2.5 Hz, 1H), 8.06-8.10 (m, 1H); ^{13}C NMR (CDCl$_3$) δ: 109.0, 109.6, 110.3, 110.8, 111.8, 120.7, 123.3, 125.0, 125.9, 126.2, 126.5, 126.7(2C), 128.3, 128.9, 129.1, 131.1, 133.7, 134.4, 145.7, 152.2, 152.9.

7-Amino-2,3-dihydro-benzo[1,4]dioxin-6-yloxy)-naphthalen-1-yl-acetic acid methyl ester **34a**
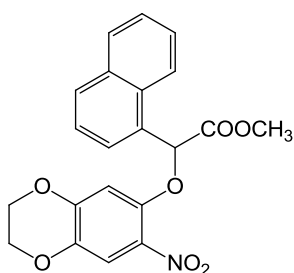
K$_2$CO$_3$ (1.072 g, 7.7 mmol) was added to a solution of **22a** (0.383, 1.94 mmol) in anhydrous DMF (50 mL) at room temperature. The reaction mixture was stirred for 10 min at room temperature, and then a solution of methyl 2-bromo-2-(naphthalen-1-yl)acetate (0.7021 g, 2.52 mmol) in anhydrous DMF (10 mL) was added dropwise. After 12h at room temperature, the solvent was removed in *vacuo* and the residue was taken up in dichloromethane. The organic layer was washed with brine, dried, filtered and evaporated. The residue was purified by flash chromatography (SiO$_2$, ethyl acetate: *n*-hexane:DCM 3:7:1 as a eluent) to afford **34a** as a yellow solid.

Yield: 91%. ^{1}H NMR (CDCl$_3$) δ: 3.72 (d, *J*= 2.8 Hz, 3H), 4.24 (d, *J*= 13.3 Hz, 4H), 6.28 (d, *J*= 3.2 Hz, 1H), 6.53 (d, *J*= 2.9 Hz, 1H), 7.44-7.74 (m, 4H), 7.89 (t, 3H), 8.29-8.47 (m, 1H).

(4-Bromo-2-nitro-phenoxy)-naphthalen-1-yl-acetic acid methyl ester **34b**
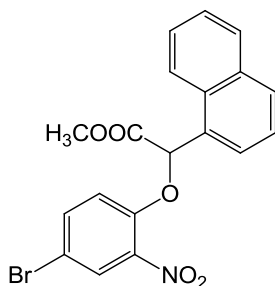
The title compound was obtained according to the procedure described for **33a**, as a yellow solid.

Yield: 57%. ^{1}H NMR (CDCl$_3$) δ: 3.73 (d, *J*= 2.0 Hz, 3H), 6.38 (d, *J*= 2.1 Hz, 1H), 6.93 (dd, *J*= 8.9, 2.1 Hz, 1H), 7.49-7.68 (m, 4H), 7.82 (d, *J*= 7.2 Hz, 1H), 7.90-7.95 (m, 2H), 8.03 (d, *J*= 2.4 Hz, 1H), 8.32 (d, *J*= 8.4 Hz, 1H).

*6-Naphthalen-1-yl-2,3-dihydro-8H-1,4,5-trioxa-8-aza-anthracen-7-one* **35**
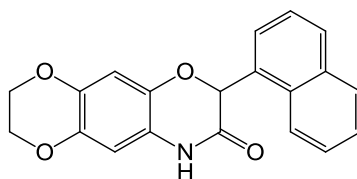
A mixture of **34a** (0.6159, 1.50 mmol) and tin (II) chloride (1.69 g, 7.52 mmol) in ethanol (10 mL) was heated at 80 °C under argon. After 12h, the solvent was evaporated *in vacuo* and the resulting residue was dissolved in ethyl acetate. Then, the organic phase was washed with brine, dried over MgSO$_4$, filtered and solvent was removed under vacuum. The residue was purified by flash chromatography (SiO$_2$, ethyl acetate/*n*-hexane 1:1 as eluent) to afford **35** as a yellow solid.

Yield: 75%. ^{1}H NMR (DMSO-*d$_6$*) δ: 4.15 (s, 4H), 6.26 (s, 1H), 6.39 (d, *J*= 3.8 Hz, 1H), 6.51 (d, *J*= 4.0 Hz, 1H), 7.41-7.51 (m, 2H), 7.58 (dq, *J*= 6.1, 3.7, 2.2 Hz, 2H), 7.84-8.03 (m, 2H), 8.10-8.33 (m, 1H), 10.85 (s, 1H).

6-Bromo-2-naphthalen-1-yl-4H-benzo[1,4]oxazin-3-one **17l**
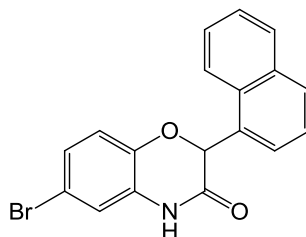
The title compound **17l** was obtained according to the procedure described for **35** as a white solid.

Yield: 42%. ^{1}H NMR (DMSO) δ: 6.69 (s, 1H), 6.86 (d, *J*= 8.3 Hz, 1H), 7.13 (dd, *J*= 8.4, 2.3 Hz, 1H), 7.40-7.53 (m, 3H), 7.59 (qd, *J*= 7.0, 5.5, 3.3 Hz, 2H), 7.95-8.05 (m, 2H), 8.21 (d, *J*= 7.7 Hz, 1H); ^{13}C NMR (DMSO) δ: 78.1, 114.5, 115.7,

118.9, 124.7, 125.4, 126.6, 126.7, 127.1, 127.3, 129.1, 130.6, 131.0, 131.3, 131.6, 134.0, 142.2, 161.5.

Benzyl-6-naphthalen-1-yl-2,3-dihydro-8H-1,4,5-trioxa-8-aza-anthracen-7-one

17m
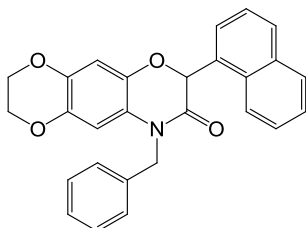
Cs_2CO_3 (0.8851g, 2.6 mmol) was added to a solution of benzoxazinone derivative **35** (0.3, 8.99 mmol) in anhydrous DMF (50 mL) at room temperature. After 10 min a solution of benzyl bromide (0.200 g, 1.17 mmol) in anhydrous DMF (10 mL) was added dropwise. The reaction mixture was stirred at room temperature overnight, then the solvent was removed in *vacuo* and the resulting residue was taken up in dichloromethane. The organic layer was washed with HCl 1N, brine, dried, filtered and evaporated. The residue was purified by flash chromatography (SiO$_2$, ethyl acetate/*n*-hexane 3:7 as eluent) to afford **17m** as a white solid.

Yield: 92%, mp: 136-138 °C. ^{1}H NMR (CDCl$_3$) δ: 4.14 (s, 4H), 5.25 (d, *J*= 2.3 Hz, 2H), 6.34 (s, 1H), 6.42 (s, 1H), 6.59 (s, 1H), 7.23-7.47 (m, 6H), 7.57 (ddd, *J*= 15.5, 10.9, 6.6 Hz, 2H), 7.88 (t, *J*= 7.5 Hz, 2H), 8.30 (d, *J*= 8.3 Hz, 1H); ^{13}C NMR (CDCl$_3$) δ: 45.7, 64.2, 104.5, 106.5, 123.0, 124.3, 124.8, 125.9, 126.2, 126.6, 127.3, 127.6, 128.8, 128.9, 130.1, 130.5, 131.5, 134.1, 136.3, 138.4, 138.7, 139.3, 165.3. HRMS (ESI) *m/z* 446.1347 [M+ Na]$^+$ (calc. for [C$_{27}$H$_{21}$NO$_4$]$^+$ 446.1368).

8-(4-Fluoro-benzyl)-6-naphthalen-1-yl-2,3-dihydro-8H-1,4,5-trioxa-8-aza-anthracen-7-one **17n**
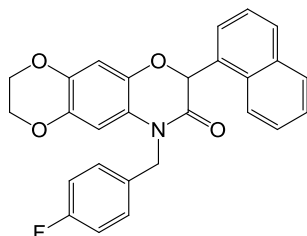
The title compound was obtained according to the procedure described for **17m** as a white solid.

Yield: 80%, mp: 165-167 °C. ^{1}H NMR (CDCl$_3$) δ: 4.15 (d, *J*= 2.0 Hz, 4H), 5.13-5.28 (m, 2H), 6.32 (d, *J*= 1.8 Hz, 1H), 6.42 (d, *J*= 1.8 Hz, 1H), 6.57 (d, *J*= 1.7 Hz, 1H), 7.07 (td, *J*= 8.6, 2.0 Hz, 2H), 7.28 (d, *J*= 1.9 Hz, 1H), 7.34-7.45 (m, 4H), 7.57 (p, *J*= 7.1 Hz, 2H), 7.76-7.95 (m, 2H), 8.27 (d, *J*= 8.2 Hz, 1H); ^{13}C NMR (CDCl$_3$) δ: 45.0, 64.2, 104.2, 106.6, 115.6, 115.9, 122.7, 124.2, 124.7, 126.0, 126.1, 126.6, 128.8, 129.0, 129.1, 130.2, 130.4, 131.5, 132.0, 132.0, 134.1, 138.4, 138.7, 139.4, 160.5, 163.8, 165.3. HRMS (ESI) *m/z* 464.1258 [M+Na]$^+$ (calc. for [C$_{27}$H$_{21}$NO$_4$]$^+$ 464.1274).

5.5.2 Biological assay

Human promyelocytic leukemia cells HL60 (ECACC) were maintained at a density between 200,000e1,000,000 cell/mL at 37 °C with 5% CO$_2$ in RPMI-1640 media with GlutaMAX™ supplemented with 10% fetal bovine serum, 50 U/mL penicillin and 50 mg/mL streptomycin (Invitrogen, Carlsbad, CA, USA).

Cells (10^6 /sample) were treated with 10 and 25 μM of **17a, 17b, 17e, 17g, 17l-n, 31a,b, 31i** for 24h. Control samples were treated with vehicle (0.1% DMSO). Apoptosis was assessed by measuring "sub-G0/G1" DNA content using flow cytometry. Flow cytometry was carried out using a FACScan flow cytometer (BectoneDickinson, San Jose, CA, USA) equipped with a 15-mW 488 nm argon ion laser. The green (FL1) and red (FL2) fluorescence data were collected through a 530/30 and a 585/42 band pass filter, respectively. Data acquisition was performed using CellQuest software. Data were analyzed and plotted using Flowjo. Cell cycle distribution was quantified by flow cytometric analysis of propidium iodide (PI Invitrogen UK) stained cells. Briefly, treated cells were fixed and permeabilized with 70% ethanol overnight at 4 °C and incubated with 100 mg RNAse and 20 mg/mL PI (Sigma) for 30 min. Samples were analyzed in a FACScan flow cytometer (Becton Dickinson, San Jose, CA) using CellQuest software. Doublets were excluded and 20.000 events were acquired for each sample.

References

[1] Zisterer, D. M.; Campiani, G.; Nacci, V.; Williams, D. C. Pyrrolo-1,5-benzoxazepines induce apoptosis in HL-60, Jurkat, and Hut-78 cells: a new class of apoptotic agents. *J. Pharmacol. Exp. Ther.* **2000**, *293* (1), 48-59.

[2] Mc Gee, M. M.; Gemma, S.; Butini, S.; Ramunno, A.; Zisterer, D. M.; Fattorusso, C.; Catalanotti, B.; Kukreja, G.; Fiorini, I.; Pisano, C.; Cucco, C.; Novellino, E.; Nacci, V.; Williams, D. C.; Campiani, G. Pyrrolo[1,5]benzoxa-(thia)zepines as a new class of potent apoptotic agents. Biological studies and identification of an intracellular location of their drug target. *J. Med. Chem.* **2005**, *48* (13), 4367-77.

[3] Mc Gee, M. M.; Campiani, G.; Ramunno, A.; Fattorusso, C.; Nacci, V.; Lawler, M.; Williams, D. C.; Zisterer, D. M. Pyrrolo-1,5-benzoxazepines induce apoptosis in chronic yelogenousleukemia (CML) cells by bypassing the apoptotic suppressor bcrabl. *J. Pharmacol. Exp. Ther.* **2001**, *296*, 31-40.

[4] Mc Gee, M. M.; Hyland, E.; Campiani, G.; Ramunno, A.; Nacci, V.; Zisterer, D. M. Caspase-3 is not essential for DNA fragmentation in MCF-7 cells during apoptosis induced by the pyrrolo-1,5-benzoxazepine, PBOX-6. *FEBS Lett.* **2002**, *515*, 66-70.

[5] M.; Greene, L. M.; Ledwidge, S.; Campiani, G.; Nacci, V.; Lawler, M.; Williams, D. C.; Zisterer, D. M. Selective induction of apoptosis by the pyrrolo-1,5-benzoxazepine 7-[[dimethylcarbamoyl]oxy]-6-(2-naphthyl)pyrrolo-[2,1-d](1,5)-benzoxazepine (PBOX-6) in Leukemia cells occurs via the c-Jun NH2-terminal kinase-dependent phosphorylation and inactivation of Bcl-2 and Bcl-XL. *J. Pharmacol. Exp. Ther.* **2004**, *310* (3), 1084-95.

[6] Nathwani, S. M.; Butler, S.; Fayne, D.; McGovern, N. N.; Sarkadi, B.; Meegan, M. J.; Lloyd, D. G.; Campiani, G.; Lawler, M.; Williams, D. C.; Zisterer, D. M. Novel microtubule-targeting agents, pyrrolo-1,5-benzoxazepines, induce apoptosis in multi-drug-resistant cancer cells. *Cancer Chemother. Pharmacol.* **2010**, *66* (3), 585-96.

[7] Mulligan, J. M.; Greene, L. M.; Cloonan, S.; Mc Gee, M. M.; Onnis, V.; Campiani, G.; Fattorusso, C.; Lawler, M.; Williams, D. C.; Zisterer, D. M. Identification of tubulin as the molecular target of proapoptotic pyrrolo-1,5-benzoxazepines. *Mol. Pharmacol.* **2006**, *70* (1), 60-70.

[8] Mc Gee, M. M.; Campiani, G.; Ramunno, A.; Nacci, V.; Lawler, M.; Williams, D. C.; Zisterer, D. M. Activation of the c-Jun *N*-terminal kinase (JNK) signaling pathway is essential during PBOX-6-induced apoptosis in chronic myelogenous leukemia (CML) cells. *J. Biol. Chem.* **2002**, *277*, 18383-18398.

[9] Lennon, J. C.; Bright, S. A.; Carroll, E.; Butini, S.; Campiani, G.; O'Meara, A.; Williams, D. C.; Zisterer, D. M. The novel pyrrolo-1,5-benzoxazepine, PBOX-6,

synergistically enhances the apoptotic effects of carboplatin in drug sensitive and multidrug resistant neuroblastoma cells. *Biochem. Pharmacol.* **2014**, *87* (4), 611-24.

[10] Greene, L. M.; Fleeton, M.; Mulligan, J.; Gowda, C.; Sheahan, B.J.; Atkins, G.J.; Campiani, G.; Nacci. V.; Lawler, M.; Williams, D. C.; Zisterer, D. M. The pyrrolo-1,5-benzoxazepine, PBOX-6, inhibits the growth of breast cancer cells in vitro independent of estrogen receptor status and inhibits breast tumour growth in vivo. *Oncol. Rep.* **2005**, *14*, 1357-1363.

[11] Bright, S. A.; McElligott, A. M.; O'Connell, J. W.; O'Connor, L.; Carroll, P.; Campiani, G.; Deininger, M. W.; Conneally, E.; Lawler, M.; Williams, D. C.; Zisterer, D. M. Novel pyrrolo-1,5-benzoxazepine compounds display significant activity against resistant chronic myeloid leukaemia cells in vitro, in ex vivo patient samples and in vivo. *Br. J. Cancer* **2010**, *102* (10), 1474-82.

[12] Nathwani, S. M.; Butler, S.; Meegan, M. J.; Campiani, G.; Lawler, M.; Clive, W.; Zisterer, D. M. Dual targeting of tumour cells and host endothelial cells by novel microtubule-targeting agents, pyrrolo-1,5-benzoxazepines. *Cancer Chemother. Pharmacol.* **2010**, *66*, 289-300.

[13] Greene, L. M.; Nolan, D. P.; Regan-Komito, D.; Campiani, G.; Williams, D. C.; Zisterer, D. M. Inhibition of late-stage autophagy synergistically enhances pyrrolo-1,5-benzoxazepine-6-induced apoptotic cell death in human colon cancer cells. *Int. J. Oncol.* **2013**, *43* (3), 927-35.

[14] Greene, L. M.; Butini, S.; Campiani, G.; Williams, D. C.; Zisterer, D. M. Pre-clinical evaluation of a novel class of anti-cancer agents, the Pyrrolo-1, 5-benzoxazepines. *J. Cancer* **2016**, *7* (15), 2367-2377.

[15] Engelbrecht, I.; Petzer, J. P.; Petzer, A. The synthesis and evaluation of sesamol and benzodioxane derivatives as inhibitors of monoamine oxidase. *Bioorg. Med. Chem. Lett.* **2015**, *25* (9), 1896-900.

[16] Ying, Z.; Desikan, R.; Xu, X.; Maiseyeu, A.; Liu, C.; Sun, Q.; Ziouzenkova, O.; Parthasarathy, S.; Rajagopalan, S. Modified methylenedioxyphenol analogs lower LDL cholesterol through induction of LDL receptor expression. *J. Lipid Res.* **2012**, *53* (5), 879-87.

[17] Rynearson, K. D.; Charrette, B.; Gabriel, C.; Moreno, J.; Boerneke, M. A.; Dibrov, S. M.; Hermann, T. 2-Aminobenzoxazole ligands of the hepatitis C virus internal ribosome entry site. *Bioorg. Med. Chem. Lett.* **2014**, *24* (15), 3521-5.

Chapter 6
Development of Dual *h*AK/*h*GSK-3β Inhibitors
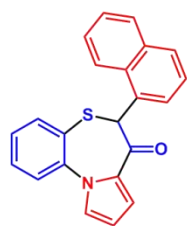
39
IC$_{50}$ *h*AK > 50 mM
IC$_{50}$ *h*GSK-3b=16 mM

40a-s

ATP binding site

Ado binding site

Allosteric binding site previously identified for compound NSD438

*During this PhD experience, some benzoxazinone derivatives (analogues of compounds **17m,n**, see Chapter 5) have been synthesized and tested as dual hAK/hGSK-3β inhibitors with potential neuroprotective properties. The next sections provides a brief description of this research project. For more details, see: Brogi, S.; Ramunno, A. et al Eur. J. of Med Chem **2017**, 138, 438-457 [1].*

6.1 Introduction

Current therapy of neurodegenerative diseases (such Alzheimer's, Parkinson's, Huntington's diseases, and amyotrophic lateral sclerosis) involves neuroprotective agents able only to alleviate the symptoms of the specific pathology and/or slow down its progression without stopping it. Recently, multi-target-directed ligand (MTDL) approach has emerged as a promising strategy for treatment of such disorders [2, 3].

This pharmaceutical approach consists in having a single molecular entity able to hit multiple targets involved in the same pathology, overcoming the disadvantages associated to the administration of drug cocktails [4].
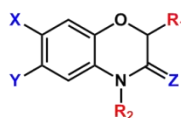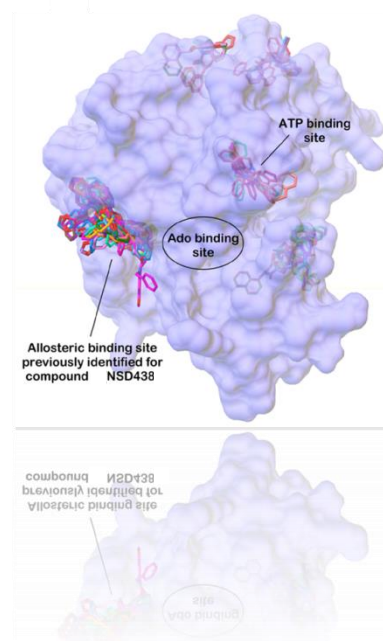
Human adenosine kinase (*h*AK, EC.2.7.1.20) and *human* glycogen synthase-3β (*h*GSK-3β, EC 2.7.11.26) are involved in neurodegenerative disorders.

*h*AK catalyzes the phosphorylation of adenosine to AMP, using ATP as the phosphate donor: Adenosine + ATP = AMP + ADP [5]. This enzyme is one of the most abundant nucleoside kinases in mammalian tissues, and is the first enzyme in the anabolic pathway of adenosine utilization. Its abnormal activity has been associated with some brain and neurodegenerative disorders such as schizophrenia, bipolar disorder, Alzheimer's and Parkinson's diseases [6].

*h*GSK-3β is a serine/threonine protein kinase that mediates the addition of phosphate molecules onto serine and threonine amino acid residues [7]. It has been reported that *h*GSK-3β plays a critical role in abnormal tau phosphorylation, a process thought to cause neurofibrillary tangles in Alzheimer's disease [8]. More recently, it was found that *h*GSK-3β is also involved in different mechanisms of Parkinson's disease, including the accumulation of α-synuclein aggregates, oxidative stress (OS) and mitochondrial dysfunction [9].

6.2 Rational design of dual *h*AK/*h*GSK-3β allosteric modulators

Aiming at developing *h*AK/*h*GSK-3β dual inhibitors with potential neuroprotective properties, the chemical structure of known allosteric inhibitors of *h*AK or *h*GSK-3β exemplified by NSD438 (**36**) [10], VP0.7(**37**) [11], and benzothiazinone (**38**) [12] was investigated to retrieve the common structural determinants for allosteric inhibition of both enzymes (Figure 6.1).
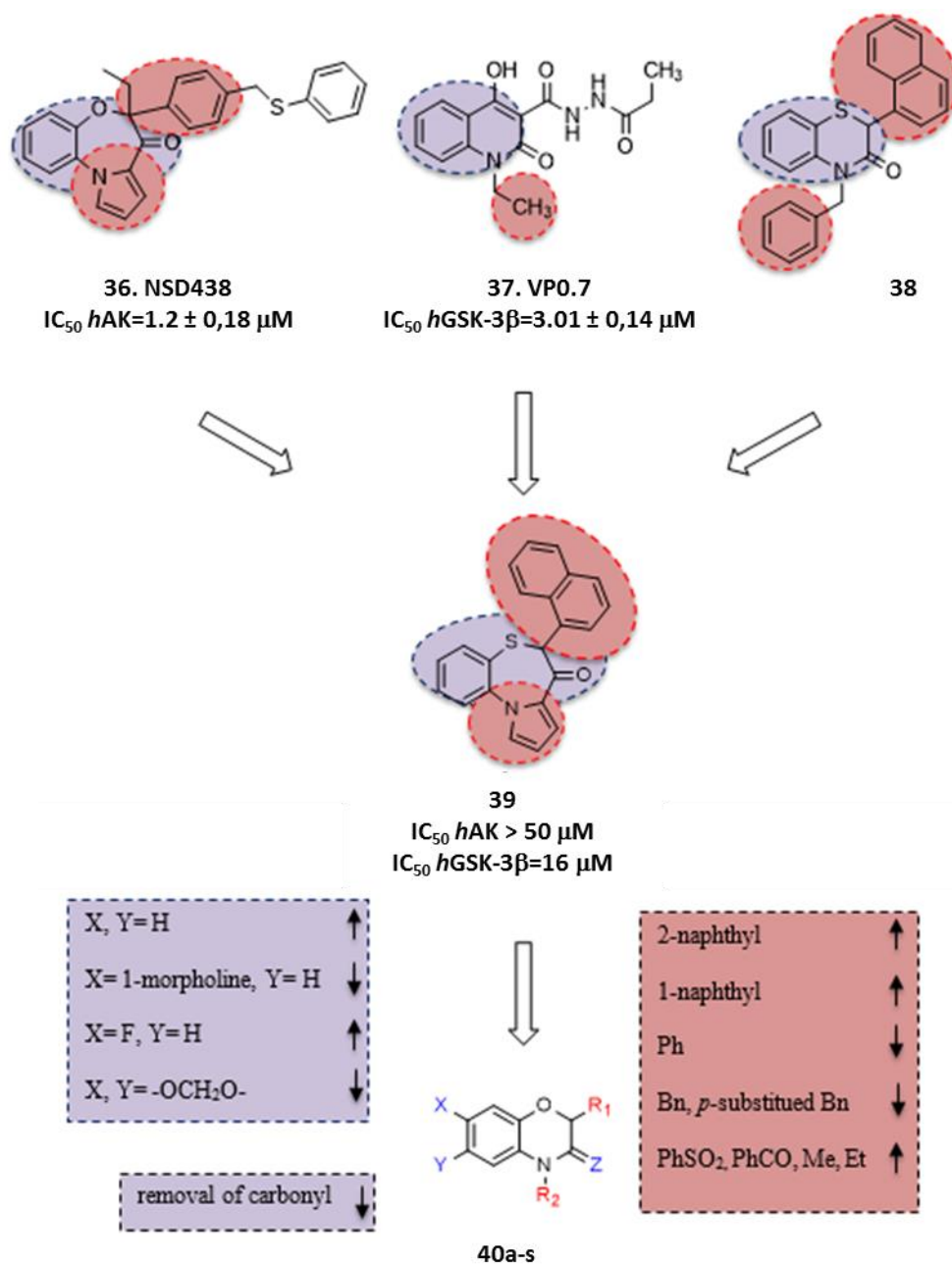
Figure 6.1 *Outline of the rational design of hAK/hGSK-3β dual allosteric inhibitors **40a-s***

A preliminary biological test allowed to select compound **39** [13] (Figure 6.1) as a 16 μM *h*GSK-3β inhibitor. Then, a bicyclic scaffold that mimics that of compound **36** was designed on the basis of the bioisosteric ring contraction of the seven membered ring of the pyrrolobenzoxazepine system of **36**, and the transformation of the keto group of **36** in the lactamic functional group of the benzoxazinones **40a-s** (Table I). An aromatic system attached to the lactam nitrogen, mainly represented by an *N*-benzyl-substituted system as in **38**, was employed as mimetic of the pyrrole-fused system of **36**.

All the developed compounds were investigated as dual inhibitors of *h*AK and *h*GSK-3β (Table I).

Table I. *Inhibitory activity of compounds* **36**, **39** (±)-**40a-s** *against hAK and hGSK-3β (IC$_{50}$, μM).*

40a-s

Cpd	R$_1$	R$_2$	X	Y	Z	*h*AK IC$_{50}$ (μM)[a] (%)[b]	*h*GSK-3β IC$_{50}$ (μM)[a] (%)[b]
36	-	-	-	-	-	1.2[c]	NT[d]
39	-	-	-	-	-	> 50	16
(±)-**40a**		benzyl				NT[d]	> 50
(±)-**40b**		4-CH$_3$-benzyl				NT[d]	50
(±)-**40c**	1-methylnaphthyl	4-F-benzyl	H	H	O	40	5.4
(±)-**40d**		4-Cl-benzyl				NT[d]	> 50
(±)-**40e**		4-NO$_2$-benzyl				NT[d]	> 50

Cpd	R₁	R₂	X	Y	Z	*h*AK IC$_{50}$ (μM)[a] (%)[b]	*h*GSK-3β IC$_{50}$ (μM)[a] (%)[b]
(±)-40f		(OCH₃)				31.6	8.1±1.8
(±)-40g		(F)	H	H	O	32.2	8.7±1.8
(±)-40h		(ketone)	H	H	H,H	NT[d]	> 50
(±)-40i		(sulfonyl)				57.4	4.1±0.3
(±)-40j		(F)	F	H	O	24.7	21.2±6.3
(±)-40k		(F)	(morpholine)	H	O	> 50	10.1±2.8
(±)-40l			-OCH₂O-		O	13.6	6.4±0.96
(±)-40m		(F)				> 50	8.1±0.8
(±)-40n	Me					> 50	> 50
(±)-40o	Et					> 50	25.6
(±)-40p			-OCH₂O-		O	13.7	6.9±1.5
(±)-40q						> 50	50
(±)-40r	Me		-OCH₂O-		O	> 50	> 50
(±)-40s	Et					> 50	> 50

a) Each value is the mean of at least three determinations, standard error of the mean is 15%; b) inhibition % when tested at 50μM; c) from ref [10]; d) NT, not tested.

For the most representative compounds of this series, **40c** and **40l**, a blind docking calculation was carried out, employing AutoDock software and considering *h*AK in its closed form (PDB ID: 1BX4) [14]. The data analysis clearly evidenced that the most plausible binding site on *h*AK enzyme for the lower energy poses of both enantiomers of **40c** and **40l** is the allosteric site previously identified for compound **36** [10]. A molecular docking study was performed for all synthesized compounds **40a-s** into this allosteric site and results were consistent with the biochemical data. Furthermore, in order to establish the mechanism of action also on *h*GSK-3β, kinetic experiments were performed varying both [^{33}P]-ATP and **40c/40l** concentrations. Then, it was found that the compounds inhibit the enzyme by a non-competitive mechanism, interacting with either the enzyme or the enzyme-substrate complex, decreasing the rate of the enzyme catalytic activity, without modification of the dissociation constant for the substrate/enzyme complex. Moreover, taking into account the pharmacophore similarity of **40a-s** with **37** and **38**, it was postulated that the new compounds bind the allosteric site targeted by compound **37** [11] on *h*GSK- 3β. Molecular docking studies into this postulated allosteric site were performed and also in this case results were consistent with the biochemical results.

Finally, since oxidative stress is one of the main causes of neurodegeneration, the potential antioxidant profile of **40c,l** was assessed in human neuroblastoma cell lines (IMR 32, undifferentiated and neuronal differentiated). In particular, it was evaluate the ability of selected compounds to counteract ROS production induced by 50 μM of H_2O_2, which is the highest dose that did not affect dramatically cells morphology and viability. Results indicated that **40c,l** have potent antioxidant activity, even at the lower doses. In addition, they did not show any cytotoxic effect, determined by the LDH release, at the concentration range evaluated (from 0.1 to 50 μM) (Figure 6.2).
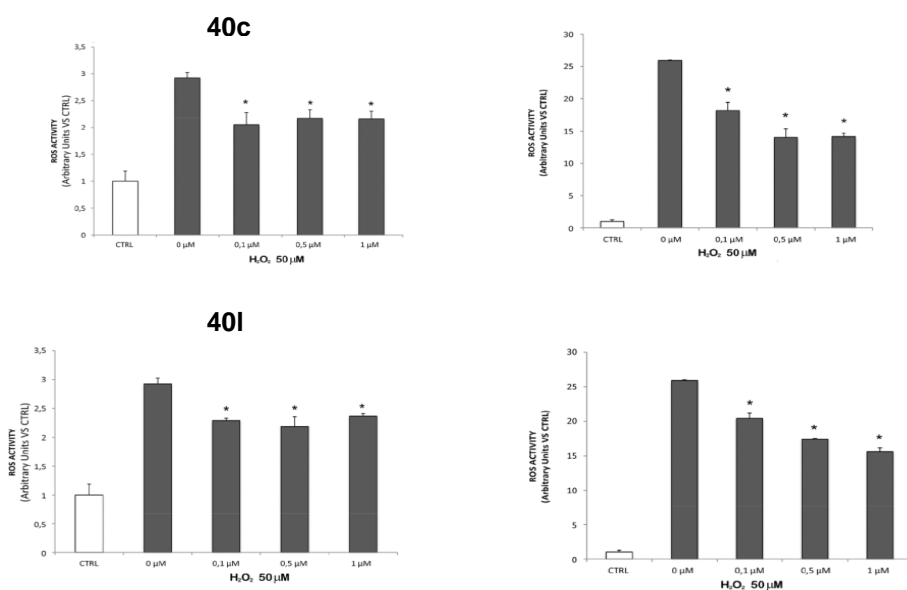
Figure 6.2 *Prevention of ROS formation by the selected compounds (**40c,l**). Values represent average ± SD for three experiments in triplicate. *p < 0.05 versus untreated sample (0 μM).*

6.3 Synthesis

Compounds **40a-s** were synthesized as described in Schemes 6.1-6.3. Briefly, condensation of 2-aminophenol **41** with α-bromonaphthyl ester **42a** or **42b** in the presence of K_2CO_3 gave the benzoxazinone derivatives **43a,b** that were N-alkylated with the appropriate benzyl bromide to afford compounds **40a-g** (Scheme 6.1, Table I). Reduction of **43a** with BH_3SMe_2 in THF gave the corresponding benzoxazine **44**, which was reacted with benzoyl chloride or benzenesulfonyl chloride to obtain **40h** and **40i** respectively (Scheme 6.1). The benzoxazinones **46a-e** were prepared from O-alkylation of appropriate 2-nitrophenol derivatives **22b-d** (*see Chapter 5, Scheme 5.1*) with α-bromonaphthyl ester **42a** or **42b** or α-bromophenyl ester **42c** to provide the corresponding intermediates **45a-e** (Scheme 6.2). Subsequent reduction of **45a-e** afforded the corresponding aniline derivatives which spontaneously cyclized to benzoxazinone analogues **46a-e**. Finally, **46a-e** were N-alkylated with the appropriate benzyl/alkyl halides to furnish the title compounds **40j-s**.

Scheme 6.1
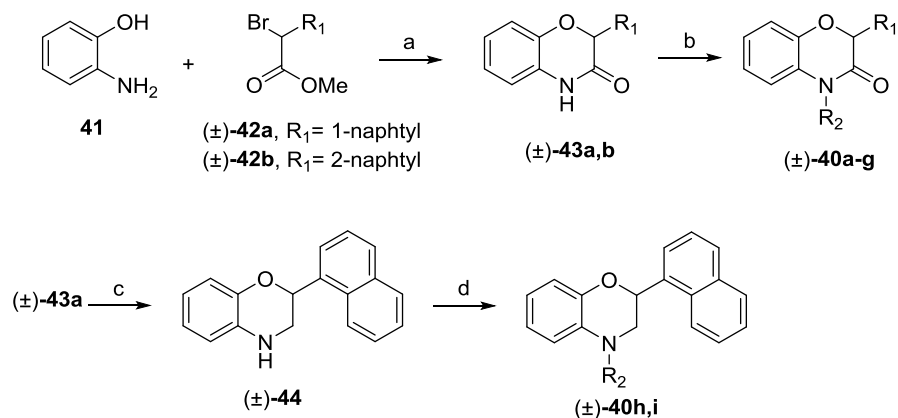
Reagents and conditions: *a) K$_2$CO$_3$, dry DMF, 100°C; b) Cs$_2$CO$_3$, dry DMF, rt, R$_2$Br; c) BH$_3$SMe$_2$, dry THF, rt, 12 h; d) benzoyl chloride (for **40h**) or benzenesulfonyl chloride (for **40i**), TEA, dry DCM, rt, 12 h.*

Scheme 6.2

22b, X,Y= -OCH$_2$O$^-$
22c, X= F, Y= H
22d, X= 1-morpholine, Y= H

(±)-**42a**, R$_1$= 1-naphtyl
(±)-**42b**, R$_1$= 2-naphtyl
(±)-**42c**, R$_1$= phenyl

(±)-**45a**, X,Y= -OCH$_2$O-, R$_1$= 1-naphtyl
(±)-**45b**, X,Y= -OCH$_2$O-, R$_1$= 2-naphtyl
(±)-**45c**, X,Y= -OCH$_2$O-, R$_1$= phenyl
(±)-**45d**, X= F, Y = H, R$_1$= 1-naphtyl
(±)-**45e**, X= 1-morpholine, Y = H, R$_1$= 1-naphtyl
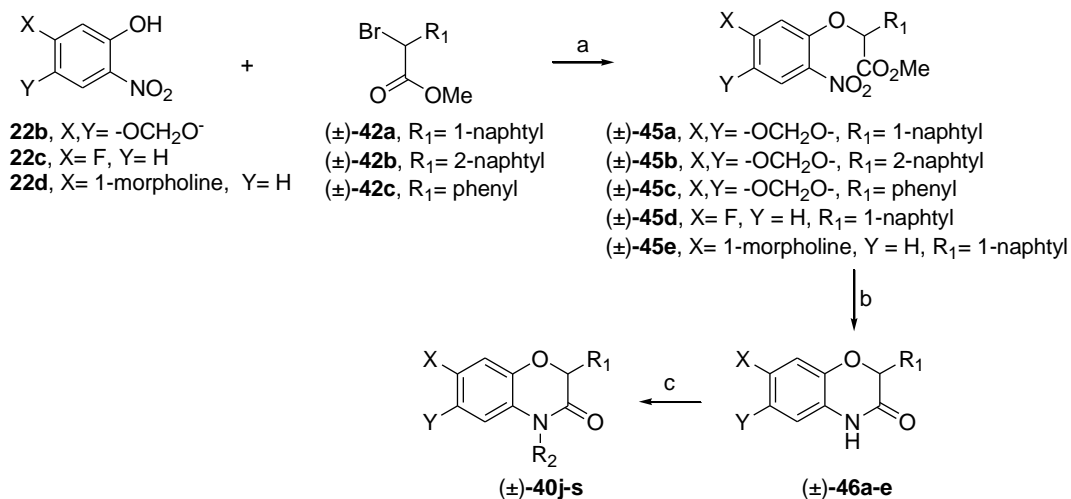
Reagents and conditions: *a) K$_2$CO$_3$, dry DMF, rt, 12 h; b) Fe/NH$_4$Cl/THF/H$_2$O, 100°C (for **46a,b**) and SnCl$_2$/EtOH, 80°C (for **46c-e**); c) Cs$_2$CO$_3$, dry DMF, appropriately p-substituted benzylbromide, rt.*

References

[1] Brogi, S.; Ramunno, A.; Savi, L.; Chemi, G.; Alfano, G.; Pecorelli, A.; Pambianchi, E.; Galatello, P.; Compagnoni, G.; Focher, F.; Biamonti, G.; Valacchi, G.; Butini, S.; Gemma, S.; Campiani, G.; Brindisi, M. First dual AK/GSK-3beta inhibitors endowed with antioxidant properties as multifunctional, potential neuroprotective agents. *Eur. J. Med. Chem.* **2017**, *138*, 438-457.

[2] Cavalli, A.; Bolognesi, M. L.; Minarini, A.; Rosini, M.; Tumiatti, V.; Recanatini, M.; Melchiorre, C. Multi-target-directed ligands to combat neurodegenerative diseases. *J. Med. Chem.* **2008**, *51* (3), 347-72.

[3] Agis-Torres, A.; Solhuber, M.; Fernandez, M.; Sanchez-Montero, J. M. Multi-Target-Directed Ligands and other Therapeutic Strategies in the Search of a Real Solution for Alzheimer's Disease. *Curr. Neuropharmacol.* **2014**, *12* (1), 2-36.

[4] Espinoza-Fonseca, L. M. The benefits of the multi-target approach in drug design and discovery. *Bioorg. Med. Chem.* **2006**, *14* (4), 896-7.

[5] Boison, D. Adenosine kinase: exploitation for therapeutic gain. *Pharmacol. Rev.* **2013**, *65* (3), 906-43.

[6] Boison, D.; Chen, J. F.; Fredholm, B. B. Adenosine signaling and function in glial cells. *Cell Death Differ.* **2010**, *17* (7), 1071-82.

[7] Beurel, E.; Grieco, S. F.; Jope, R. S. Glycogen synthase kinase-3 (GSK3): regulation, actions, and diseases. *Pharmacol. Ther.* **2015**, *148*, 114-31.

[8] Avila, J.; Wandosell, F.; Hernandez, F. Role of glycogen synthase kinase-3 in Alzheimer's disease pathogenesis and glycogen synthase kinase-3 inhibitors. *Expert. Rev. Neurother.* **2010**, *10* (5), 703-10.

[9] Credle, J. J.; George, J. L.; Wills, J.; Duka, V.; Shah, K.; Lee, Y. C.; Rodriguez, O.; Simkins, T.; Winter, M.; Moechars, D.; Steckler, T.; Goudreau, J.; Finkelstein, D. I.; Sidhu, A. GSK-3beta dysregulation contributes to parkinson's-like pathophysiology with associated region-specific phosphorylation and accumulation of tau and alpha-synuclein. *Cell Death Differ* **2015**, *22* (5), 838-51.

[10] Savi, L.; Brindisi, M.; Alfano, G.; Butini, S.; La Pietra, V.; Novellino, E.; Marinelli, L.; Lossani, A.; Focher, F.; Cavella, C.; Campiani, G.; Gemma, S. Site-directed Mutagenesis of Key Residues Unveiled a Novel Allosteric Site on Human Adenosine Kinase for Pyrrolobenzoxa(thia)zepinone Non-Nucleoside Inhibitors. *Chem. Biol. Drug. Des.* **2016**, *87* (1), 112-20.

[11] Palomo, V.; Soteras, I.; Perez, D. I.; Perez, C.; Gil, C.; Campillo, N. E.; Martinez, A. Exploring the binding sites of glycogen synthase kinase 3. Identification and characterization of allosteric modulation cavities. *J. Med. Chem.* **2011**, *54* (24), 8461-70.

[12] Zhang, P.; Li, S.; Gao, Y.; Lu, W.; Huang, K.; Ye, D.; Li, X.; Chu, Y. Novel benzothiazinones (BTOs) as allosteric modulator or substrate competitive inhibitor of glycogen synthase kinase 3beta (GSK-3beta) with cellular activity of promoting glucose uptake. *Bioorg. Med. Chem. Lett.* **2014**, *24* (24), 5639-5643.

[13] Mc Gee, M. M.; Gemma, S.; Butini, S.; Ramunno, A.; Zisterer, D. M.; Fattorusso, C.; Catalanotti, B.; Kukreja, G.; Fiorini, I.; Pisano, C.; Cucco, C.; Novellino, E.; Nacci, V.; Williams, D. C.; Campiani, G. Pyrrolo[1,5]benzoxa(thia)zepines as a new class of potent apoptotic agents. Biological studies and identification of an intracellular location of their drug target. *J. Med. Chem.* **2005**, *48* (13), 4367-77.

[14] Morris, G. M.; Huey, R.; Lindstrom, W.; Sanner, M. F.; Belew, R. K.; Goodsell, D. S.; Olson, A. J. AutoDock4 and AutoDockTools4: Automated docking with selective receptor flexibility. *J. Comput. Chem.* **2009**, *30* (16), 2785-91.

CONCLUSIONS

In this thesis the development of putative new inhibitors of the p53/MDM2/MDM4 interactions and new modulators of the tubulin polymerization has been described.

Previously reported biological and molecular modeling studies carried out on compound **1** (namely 4-benzoyl-5-methyl-1-(4-methylbenzylbenzyl)-1H-pyrrole-2 carboxylic acid 3-chlorobenzylamide), evidenced the involvement of p53/MDM2/MDM4 axis in its anticancer mechanism of action. Then, compound **1** was chosen as lead compound for the design and synthesis of a new set of pyrrole derivatives (**9a-k**) aimed at improving its pharmacological profile.

Two of them **9a** and **9k** were evaluated against the NCI-60 human cancer cell line panel (NHI/NCI, Bethesda, USA). Compound **9a** at 10 μM (48h treatment) showed a good antiproliferative activity on a prostate tumor cell line (PC-3), and on two colon cancer lines (HCT-116 and HCT-15), with percent growth (*PG*) of treated cells of 25.20%, 32.47%, and 34.06% respectively, while compound **9k** significant was less active on PC-3 cell line (*PG*= 44.66%), and ineffective on HCT-116 and HCT-15 cell lines. In addition, **9k** reported a percent growth on HOP-92 (non-small cell lung cancer), and NCI-H522 (non-small cell lung cancer) of 54.45%, 52.85% respectively.

All synthesized compounds **1**, **9a-m** were investigated on three cell lines (MTT assay) including: HCT-116 (colon cancer), A375 (melanoma) and HaCat (immortalized human keratinocytes), using nutlin-3a as reference anticancer molecule. Compound **9l** (1-(4-aminobenzyl)-4-benzoyl-5-methyl-1H-pyrrole-2-carboxylic acid 3-chloro-benzylamide) was found to be the most active pyrrole derivative with IC_{50} values of ca 10 μM on A375 and HaCat cell lines. Further, a second set of pyrrole derivatives (**11a-n**) bearing a polar/protonable group in position 2 of the pyrrole ring was synthesized, with the aim to improve water solubility of this class of compounds and mimic a further interaction of p53 with MDM2 engaging Leu22 (p53) and Gln72 (MDM2). Biological screening of **11a-n** is currently in progress on various tumor cell lines for a better definition of their pharmacological profile.

PBOX-6 (namely 7-[(dimethylcarbamoyl) oxy]-6-(2-naphthyl)pyrrolo-[2,1-*d*][1,5]benzoxazepine) was the lead compound of new microtubulin targeting

agents developed during this PhD experience. In particular, a first set of compounds bearing substituents with different lipophilic, steric and electronic properties on the benzo-fused ring of PBOX-6 was synthesized (compounds **17a-h**). In order to extend SAR studies of this class, the introduction of a double bond at 6,7 positions of the benzoxazepine ring (compounds **17i-k**) was evaluated; unfortunately, this modification gave unstable derivatives. Finally, some benzoxazinone derivatives (**17l-n**) were synthesized as simplified structures coming from ring contraction of the seven membered ring of the pyrrolobenzoxazepine system of PBOX-6.

The ability of PBOX-6 analogues to affect the cell cycle and induce apoptosis was assessed by flow cytometric analysis on HL60 (human promyelocytic leukemia) cells at 10 μM and 25 μM.

At 25 μM compounds **17a**, 17**b**, **17e**, **17g**, **31a,b** induced increase in the pre-Gl peak, due to apoptotic cell death, with percentage in the sub-G1 phase in a range of 51-64%; at 10 μM only compounds **17a**, **17b**, **17e** and **31a** showed a significant effect on the cell cycle progression, with percentage in the sub-G1 phase in a range of 44-58%. Interestingly, the removal of enol function at position 7 of the benzoxazepine ring associated to the introduction of a benzofused 1,4-dioxane system such as in **31a** retained the apoptotic activity at both tested concentrations of 25μM and 10 μM.

Overall, our results extend the SAR studies carried out so far on this class of derivatives and encourage a further process of lead optimization.

.